Fatigue Life Prediction and Strength Degradation of Wind Turbine Rotor Blade Composites

R.P.L. Nijssen

ABSTRACT

Wind turbine rotor blades are subjected to a large number of highly variable loads, but life predictions are typically based on constant amplitude fatigue behaviour. Therefore, it is important to determine how service life under variable amplitude fatigue can be estimated from constant amplitude fatigue behaviour. A life prediction contains different elements: the counting method, formulations for describing S-N curves, constant life diagrams, and damage rules. For the description of damage, two models were investigated and compared, the Miner's sum method and strength-based life prediction. In the Miner's sum method, the results of a counting method and constant amplitude fatigue behaviour description are converted into a damage parameter, 'Miner's sum'. Potential effects of load order are not taken into account and the value of the damage parameter only indicates whether or not failure occurred: it does not relate to a physically quantifiable damage. In the strength-based method, life is predicted by calculating the effect of each load cycle on strength, until the load exceeds the remaining strength. An expected advantage of this cycle-by-cycle method is, that sequence effects can be implicitly included. Moreover, the damage parameter is at all times related to a physically quantifiable parameter (viz. strength). The successful application of the strength-based method requires a description of the post-fatigue strength, which entails considerable experimental effort. In addition, a strength-based life prediction is much more computationally intensive than Miner's sum and can not always utilise the same counting methods. The experimental research involved a considerable amount of material tests, which give a detailed image of static strength, constant and variable amplitude fatigue behaviour as well as strength degradation for different glass-fibre reinforced laminates. Block-test experiments confirm the existence of sequence effects on life. Residual strength tests show the strength degradation after fatigue for a range of fatigue load conditions. The significance of an adequate description of the constant amplitude behaviour is evident from the various life predictions. Commonly used simplifications, such as the Linear Goodman Diagram, result in highly non-conservative predictions. The residual strength model yields more conservative predictions than Miner's sum for the investigated tension-dominated load sequences. The experimental effort required for the determination of the strength degradation, and the computational effort do not justify this relatively small advantage. For future research, it is recommended to further improve the description of the constant life diagram.

This report is based on a dissertation, publicly defended by the author on November 27th, 2006 at Delft University of Technology, at 15:00 in the 'Senaatszaal' of the Aula, Mekelweg 5, in Delft, the Netherlands.

It was approved by the committee:

Cover: Wind turbine in Wieringermeerpolder, the Netherlands, and constant life diagram of MD2 material

Summary

Fatigue life prediction and strength degradation of wind turbine rotor blade composites

Wind turbine rotor blades are subjected to a large number of highly variable loads, but life predictions are typically based on constant amplitude fatigue behaviour. Therefore, it is important to determine how service life under variable amplitude fatigue can be estimated from constant amplitude fatigue behaviour.

A life prediction contains different, partly independent, elements:
- the counting method, used for describing variable amplitude signals as a collection of constant amplitude cycles
- formulations for describing S-N curves which relate the stresses to the number of cycles to failure
- constant life diagrams which are made up of S-N curves for different stress ratios
- damage rules, which relate the life expectancy of a specimen to the stress history

For the description of damage, two models were investigated and compared, viz. the Miner's sum method and strength-based life prediction.
In the Miner's sum method, the results of a counting method and constant amplitude fatigue behaviour description are converted into a damage parameter, 'Miner's sum'. Potential effects of load order are not taken into account. Moreover, the value of the damage parameter only indicates whether or not failure occurred: it does not relate to a physically quantifiable damage. These are limitations to the model which suspectedly might cause inaccurate predictions.
In the strength-based method, life is predicted by calculating the effect of each load cycle on strength, until the load exceeds the remaining strength. An expected advantage of this cycle-by-cycle method is, that sequence effects can be implicitly included. Moreover, the damage parameter is at all times related to a physically quantifiable parameter (viz. strength). The successful application of the strength-based method requires a description of the post-fatigue strength, which entails considerable experimental effort. In addition, a strength-based life

prediction is much more computationally intensive than Miner's sum and can not always utilise the same counting methods.

In the comparison of the Miner's sum and the strength-based method, the influence and significance of the other life prediction elements, such as counting methods and description of constant amplitude fatigue behaviour on life prediction are included.

The experimental research involved a considerable amount of material tests. The material tests give a detailed image of static strength, constant and variable amplitude fatigue behaviour (both block tests and (variants of) the WISPER spectrum were used), as well as strength degradation for different glass-fibre reinforced laminates. By selecting a single coupon geometry for all material tests on a single material, and the definition and use of standard test conditions, a consistent database was created.

The block-test experiments confirm the existence of sequence effects on life, although more data are required to fully quantify them.

The residual strength tests show the strength degradation after fatigue for a range of fatigue load conditions. Significant tensile strength degradation is observed in R=0.1 and R=-1 fatigue experiments. Generally, compressive strength remains within the boundaries of the initial static strength distribution. This behaviour was observed for different laminates.

The significance of an adequate description of the constant amplitude behaviour is evident from the various life predictions. Commonly used simplifications, such as the Linear Goodman Diagram, result in highly non-conservative predictions. The residual strength model yields more conservative predictions than Miner's sum for the investigated tension-dominated load sequences. The experimental effort required for the determination of the strength degradation, and the computational effort do not justify this relatively small advantage. For future research, it is recommended to further improve the description of the constant life diagram.

This work is focussed on fatigue of composites for wind turbine rotor blades. Nevertheless, the results are relevant for other composite structures as well.

Notation

Abbreviations

(S)LGD	(Shifted) Linear Goodman Diagram
ABG	Anti-Buckling Guide
AGARD	Advisory Group for Aerospace Research and Development
ASTM	American Society for Testing and Manufacturing
BT	Block Test
C	Compression (or R=10 block in block test)
C/G(F)(R)P	see G/C(F)(R)P
CA, VA	Constant, Variable Amplitude
Carlos	CAR component LOading Standard
CG	clip-gauge extensometer
CLD	Constant Life Diagram
CLT	Classical Laminate Theory
CRES	Centre for Renewable Energy Research
CSM	Chopped Strand Mat
DIN	Deutsches Institut für Normung e.V.
DLR	German Aerospace Centre
DNV	Det Norske Veritas (certification institute)
DOE	Department of Energy
EC, EU	European Commission, European Union
ENSTAFF	ENvironmental FALSTAFF
FACT	FAtigue of wind turbine ComposiTes (database)
FALSTAFF	Fighter Aircraft Loading STAndard For Fatigue evaluation
G/C(F)(R)P	Glass/Carbon Fibre(-Reinforced) Plastic/Polymer/Polyester
GL	Germanischer Lloyd (certification institute)
H	H (block test)
IEC	International Electrotechnical Committee
ISO	International Standardisation Organisation
K-S	Kolmogorov-Smirnoff
L	Low (block test)
LGD	see (S)LGD
LVDT	Linear Variable Displacement Transducer
MD(2)	Multi Directional; MD2 is standard MD material used in OPTIMAT
MEKP	Methyl Ethyl Ketone Peroxide (accelerator for polymerisation)
MIL	Composite Materials Handbook MIL-17
MSU	Montana State University
N	Neutral: zero mean stress; R=-1 (block test)
NLR	Nationaal Luchtvaart-en Ruimtevaartlaboratorium (National Aerospace Laboratory, the Netherlands)
OptiDAT	Database for the OPTIMAT project
OPTIMAT	Acronym for OPTIMAT BLADES, 'OPTImal use of MATerials for

	wind turbine rotor BLADES
PEEK	PolyEtherEtherKetone (thermoplastic matrix material)
PRODETO	PRObabilistic DEsign TOol
PROFAR	PRObabilistic distribution of FAtigue strength of Rotor blades
R, R-value	Ratio of minimum to maximum stress or strain
RSD	Residual Strength Degradation
RAL	Rutherford-Appleton Laboratory
RF	RainFlow
RFERM	RainFlow-Equivalent Range-Mean
RISØ	National Research Institute of Denmark
RM	Range-Mean
RTM	Resin Transfer Moulding
SD	Strength Degradation
SEM	Scanning Electron Microscopy
SG	Strain Gauge
SLERA	Strength-Life-Equal-Rank Assumption
SMC	Sheet Moulding Compound
ST(T/C)	Static Test (Compression/Tension)
T	Tension (or R=0.1 block in block test)
TURBISTAN (cold and hot)	gas TURBIne engine STANdard
TWIST	Transport WIng STandard
U(T, C)S	Ultimate (Tensile/Compressive) Stress (failure stress)
UD(2)	Uni Directional; UD2 is standard UD material used in OPTIMAT
UP	University of Patras, Greece
VA (, CA)	Variable Amplitude (Constant Amplitude) fatigue
VARTM	Vacuum Assisted Resin Transfer Moulding
VTT	Technical Research Centre of Finland
VUB	Free University Brussels
WASH	Wave Action Standard History
WISPER (WISPERX, NEW WISPER, Reversed WISPER)	Wind turbine Reference Spectra
WMC	Knowledge Center Wind turbine Materials and Constructions

Greek and Roman Symbols

ψ	factor for R-value dependence
θ	dominant fibre angle
γ	strength degradation parameter
σ	stress
ε	strain
σ, μ	see μ, σ
μ, σ	mean, standard deviation (Normal distribution)
α, β	shape, scale parameters (Weibull distribution)
β, α	see α, β
a, b, c, d, A, B, C, D, x, K, m	S-N curve or stiffness degradation parameters
C	strength degradation parameter, Confidence
D	Damage
E	modulus

f	frequency, or fractional life
J	cost function
K	multiplier for tolerance bounds
n or N	generic life (cycles/time/sequences). Typically, N is used for nominal or average life, n for fractional life.
P	Probability
s or S	generic load (stress/strain/displacement/load)
T/Z/U	student's T/ Normal/Uniform distribution

Sub/superscripts

∞	infinity
0	initial
1	first cycle
amp	amplitude
eq	equivalent
i	'initial' or refers to cycle type (bin)
L, S	large, small
mean	mean
min, max	
r	residual
S, L	small, large

Table of Contents

List of Tables

List of Figures

Chapter 1

Introduction

This chapter gives a general overview of wind turbine rotor blade fatigue, and addresses several general issues of composites and composite fatigue, before motivating this dissertation.

1.1 Background

Modern wind turbine rotor blades have two striking characteristics. First, the loads they are subjected to are extreme in terms of number of load cycles and variability. Second, they are large, intricately shaped, composite structures. In this chapter, the nature of fatigue loads, typical rotor blade materials, and fatigue in general, is explored. The objectives, approach and constraints of the research are briefly discussed.

1.2 Typical rotor blade fatigue loads

The loads on rotor blades are in two ways extreme. This is illustrated in Figure 1, which shows engineering applications of composites (from left to right: bicycle, car, aeroplane, helicopter, bridge, wind turbine), with on the abscissa the number of significant load cycles experienced during the structure's life, and on the ordinate the degree of variation in the load cycles.
Wind turbine rotor blades are subjected to a high number of loads during their targeted economical lifetime of 20 years. Estimates of the number of load cycles are up to 10^8 or 10^9 load cycles (Mandell[181], 1992; van Delft[69], 1997).

Second, these loads show high variability. The variability of loads on a rotor blade is a consequence of the stochastic nature of the wind. This is notwithstanding the fact, that there are indeed some regular components of fatigue loading. These deterministic and non-deterministic components of the fatigue loads have been studied by Sutherland[310] [1996]. In regions of the load-
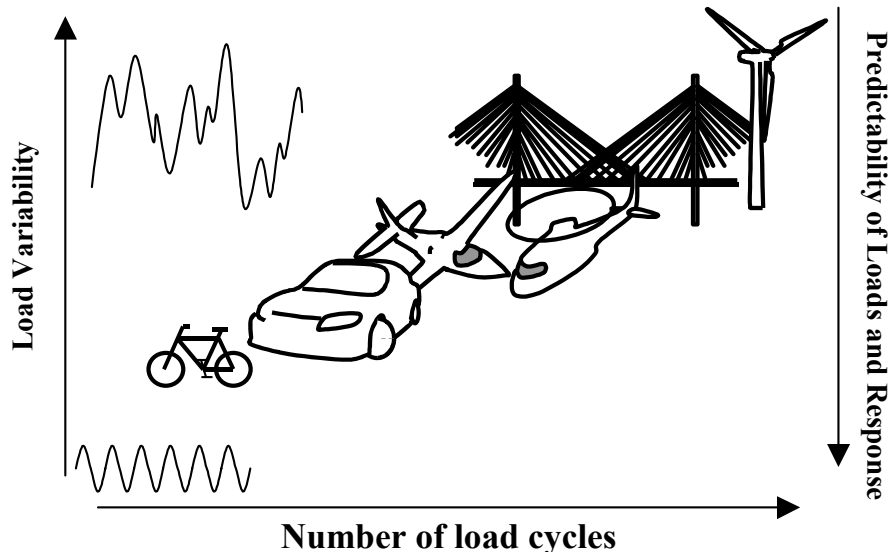
Figure 1: Wind turbine loading regime

bearing structure toward the trailing and leading edge of the wing structure, the stresses and strains are dominated by the gravity loading of the blade in the rotor plane, causing an alternating stress in the structure with mean load close to zero. Furthermore, the vertical velocity profile of the wind causes regular load fluctuations. Nevertheless, most of these regular load components are dependent on rotor speed, and thus on wind speed, which is, by nature, largely irregular (this is not true for constant speed machines).

A wind turbine rotor blade is loaded in flap-wise and edgewise direction (Figure 2). Despite ongoing efforts to integrate structural and aerodynamic optimisation, the current rotor blade geometry can be divided in load carrying components, and parts, that are geometrically optimised for aerodynamic performance. The flapwise loads are carried by the main spar, the edgewise loads by the spar, and
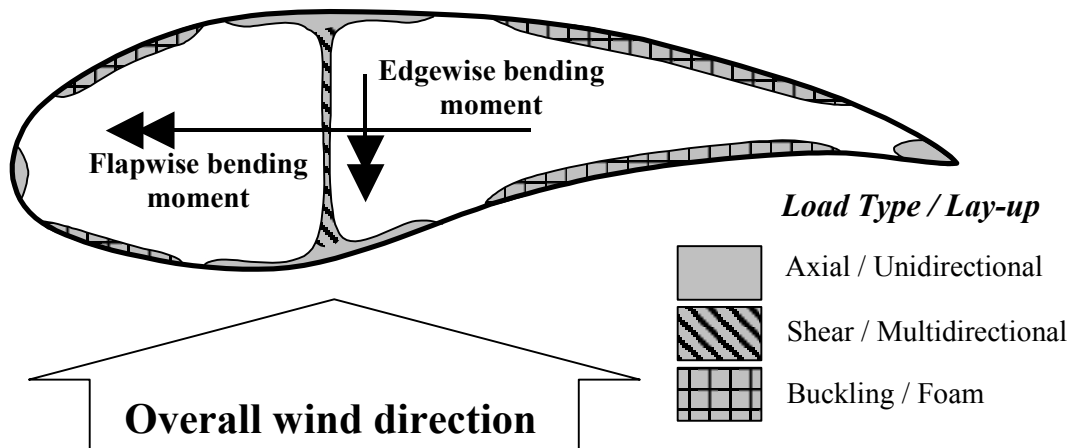
Figure 2: Typical rotor blade cross-section

by reinforcement, which may be present in the leading and trailing edges of the blade. The remainder of the blade is generally constructed of multi-axial skin material and a sandwich structure, ensuring aerodynamic geometry, resistance to torsion, low weight and high buckling resistance. Figure 2 indicates, what the main loads are, for different areas in the load-bearing structure.

The flapwise-loads originate mainly from the wind load, acting perpendicularly on the rotor plane. These loads vary strongly in amplitude and mean. Edgewise loads originate mainly from the fact that the blade is loaded by its own weight, and by the torque loads that actually drive the turbine. The loading direction for edgewise loads changes twice during each revolution. These loads are more regular. Sutherland[311] [1999] shows, that the edgewise blade root bending moment frequency distribution from a small turbine contains two peaks; one originating from the wind loading, the other a result of the blade being loaded by its own weight. Caprile et al.[45] [1996] present histograms of mid-size wind turbine blade edgewise and flapwise bladeroot moments, showing the same peak for the edgewise loading. For larger rotor blades, the edgewise gravity fatigue loading becomes increasingly relevant for life prediction. Kensche[151] [1990] gives typical root bending moments from measurements on wind turbine blades, both in flap and edgewise direction.

Fatigue loads in wind turbine blades have a certain degree of statistical variability. Among material variability and other uncertainties, the actual varying load is an important source of scatter, as e.g. Svensson[316] [1997] acknowledged. Lange[168] [1996] found fatigue reliability to be significantly affected by the type of model chosen for the loads data. He noted an increasing spread in failure probabilities for a given turbine life for flatter S-N curves. Riziotis et al.[271] [2000] have, based on numerical modelling of wind and wind turbines of the 0.5 MW class with different control strategies, identified the turbulence intensity as the most significant influence on fatigue load contribution. In related research, Mouzakis et al.[205] [1999] have quantified the additional fatigue loading due to terrain complexity to be ca. 30%. They include measured bending moment data in their publication.

1.3 Terminology

A note should be included on terminology. A variable amplitude load signal, such as the blade load, can be referred to as either 'spectrum' or 'load sequence'. Although both are used, it can be argued that 'spectrum' implies a description in terms of spectral content (disregarding order of load cycles), and that 'load sequence' refers to the order of load cycles, not so much to spectral content. Using the techniques discussed later, a load sequence can be reduced to

its spectral content with loss of cycle order information. Conversely, different load sequences might result from an identical spectral description. In practice, this distinction is not generally made, and in this thesis 'spectrum' and 'load sequence' will both be used for the same signal types.

1.4 Rotor blade materials

Typically, rotor blades are constructed from fibre reinforced polymers. The reason for this is the high stiffness, high stiffness-to-density ratio, and good fracture toughness (Brøndsted[40], 2005). Typically, continuous glass-fibre composites are used, although designers are moving towards employing carbon fibres because these stiffer fibres are slowly becoming affordable for the wind industry. In both cases, the material grade used in wind turbines, relative to aerospace composites, is characterised by relatively coarsely woven laminates. The fibres are embedded in a polymer matrix, which provides some resistance to compression loads, but mainly serves to align and fix the fibres geometrically. A large percentage of current blades is manufactured from polyester, but epoxy is also widely used. The density is very similar, but better fatigue performance is attributed to composites with epoxy matrices, enabling lighter design. Moreover, the absence of toxic styrene vapours during production is an advantage of epoxies. Essentially all blades are made with thermoset resins.

Indicated in Figure 1 is the degree in which life estimates are reliable. Basically, the predictability of the loads and response is inversely proportional to the variability of the loads – the more strongly the loads vary, the less predictable they are, and the more difficult it is to calculate the response (dynamic, fatigue) of the materials and structure. However, the reproducability of the structure is also a factor. Small, mass-produced articles of homogeneous material are more easily made to comply with the original design, hence their behaviour can be predicted better. In terms of manufacturing, wind turbine rotor blades are today among the largest composite structures that are made in series production, and e.g. blade-to-blade variation has been characterised only to a limited extent. These are not topics of this dissertation, although some information can be found in the following paragraphs.

1.5 Fatigue of composites

1.5.1 General

Before the fatigue of composites is treated in general, first a brief introduction to the fatigue terminology should be given. A fatigue load is generally represented

by a cyclic, typically sinusoidal, waveform. The characteristics of this waveform are given in Figure 3, in terms of the generic quantities *S* and *N*. For
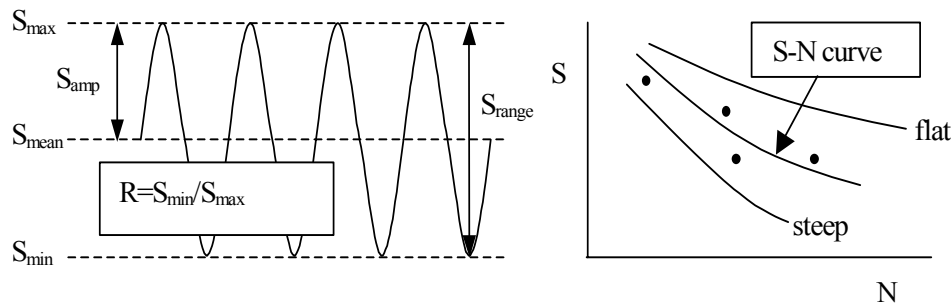
Figure 3: General fatigue terminology

S, stress, load (per unit of width or thickness), strain, or displacement can be used. Typically, stress is used for homogeneous materials, and strain is preferred for composites. For *N*, the number of cycles to failure is typically used. Also, half cycles to failure, number of load sequences to failure, or number of cycles to a pre-defined stiffness degradation, can be used.

The results of fatigue experiments are mostly plotted in an S-N diagram, showing *S* versus *N*. An example is shown in Figure 3. In general, fatigue properties are determined mainly by the slope of the S-N curves, as indicated in the figure. A 'flat' S-N curve (small slope) is often considered to represent superior fatigue properties over a 'steep' S-N curve. The appraisal of fatigue behaviour depends also on the location of the intercept with the abscissa. The treatment of S-N data will be more extensively discussed in Chapter 2.

For determining static strength and modulus, many standards are available. These prescribe standard test conditions, specimen geometry for optimal performance and report format. For fatigue testing of composites, there is, to date, only a limited amount of fatigue test prescriptions available. ASTM[7] [1996] has published a standard for tension-tension testing of composites; ISO[134] [2003] have a general fatigue testing standard.

Some general observations on fatigue of composites can be made. First, fatigue properties are found to be superior to those of many other materials, by virtue of their 'flat' S-N curve. S-N curve slope is generally used as a descriptor of the fatigue resistance, the slope is very low in composite fatigue. This can be typified as 'good' fatigue behaviour, since sensitivity to fatigue loads drops significantly as the load range drops. Arguably so; this also means, that a small increase in load results in substantial fatigue life shortening.

Moreover, scatter in fatigue life is typically higher than for metals, and can only partly be explained by variations in test conditions. See section 2.3.6. The combination of a flat S-N curve and large scatter hampers predictability of fatigue life.

Second, the composite S-N curve is characterised by the absence of a fatigue limit. No cyclic load amplitude has been found below which fatigue life is infinite. This is further investigated in section 2.3.3.

Where composite materials are generally known for their poor resistance to compression loads, compressive fatigue properties can be considered quite superior to the tensile fatigue properties. This is considering the slope of the S-N curve, and strength degradation. In compression-compression fatigue the S-N curve is typically very 'flat'. Another 'good' property in compression fatigue is the conservation of strength. As the strength degradation experiments show, strength degradation in compressive fatigue is insignificant (see Chapter 4).

Fatigue of composites has presented researchers and designers with considerable modeling difficulties. Modelling delamination of a composite can be accomplished using existing single-crack type approaches, but these do not necessarily work with all composite laminate geometries. The damage induced by fatigue often results in multiple, distinctly different, interacting damage types, which hampers modelling.

The flexibility in laminate design is the main strength of composite materials. Variation of the fibre direction, type and content, and of other parameters, such as matrix, matrix fillers, fibre sizing, stacking sequence, etc., allow for extensive tailoring of the product to its application. This comes at the price of their elusive characterisation, notably with respect to fatigue properties. First, a composite product represents a convolution of manufacturing processes, micro- and macro-geometry, structural loading and component properties and interactions. No two composite structures are the same, and evaluation of a design is subject to many uncertainties, like fibre orientation, fibre-matrix adhesion, presence of residual strains.

1.5.2   Literature

Much has been written on composites in general, and fatigue of composites in particular. The particular application of composites in wind turbine rotor blades has not been extensively documented to date, but considerable research efforts have already been expended at universities, and in the industry. Given the increase in wind power plants, and the associated risk, research funds aimed to improve fatigue reliability and design accuracy of rotor blades are well-invested. A brief overview of some of the relevant literature is provided.

Overviews of wind energy technology

General overviews were recently provided by Milborrow et al.[200] [1999], and Milborrow[201] [2000]. A newer version of the first reference was produced by Gardner[105] et al. [2004]. An EC communication[90] [1997] describes the targets for the future application of wind power. General literature on wind turbine design includes the rather accessible work by Quarton[264] [1998].

Blade materials

Currently, the reinforcement material of choice for rotor blades is glass-fibres. Increasing rotor dimensions result in blade deflection issues. Moreover, they bring about a near-cubic weight increase, leading to gravity load issues. These issues have initiated investigations into using carbon fibre in rotor blade designs (e.g. Griffin[108], 2001; Griffin et al.[109], 2003), apart from geometrical/aerodynamic design improvements (e.g. TPI composites[322], 2002). Other considerations are use of thermoplastic materials for use in rotor blades, although, despite their potential in e.g. recyclable, or self-repairing structures, their basic fatigue performance has been reported to be worse than equivalent thermoset-based laminates, e.g. Gamstedt and Talreja[97] [1999].

Composite fatigue

Boller[36] [1969, pp. 340] provides an early review of composite fatigue. A quote:

> *'The variables in a composites evaluation seem to be astronomical, but when properly understood they really are not. Each variable must be considered separately and weighed according to how it affects service life. Because of the complexity of the behavior of composite materials under dynamic stress, there is a serious need for data generated according to basic principles and reported precisely'*

Over thirty years after Boller wrote these words, his assertions still have not lost much of their validity.

Early observations on damage modes, life and strength prediction were documented for various composites by Hahn[113] [1978].

Historically, fatigue life prediction methodologies were often taken directly from metal fatigue. In the survey by Fatemi and Yang[92] [1998], several cumulative damage models are seen, that were later adopted to describe composite fatigue. An example is the Marco-Starkey[190] [1954] concept of non-linear damage accumulation, which was later used by Adam et al.[3] [1994] and Gamstedt and Sjögren[99] [2002] in load sequence experiments on carbon/epoxy composite specimens and featured in an overview of cumulative damage methods for fibrous composites by van Paepegem[247] [2002], who based his description of the model on the abovementioned work of Adam et al. Müller and Michaeli[206] [1990] augmented this model with a Weibull description of probability of failure for implementation into a finite element package.

Another historical aspect of fatigue of composites is its strong aerospace connotation. Although fatigue has long been considered irrelevant as a design driver, most early publications deal with fatigue of aerospace grade composites, containing predominantly carbon fibres. Och[234] [1983] has presented aspects of fatigue strength in the frame of an AGARD panel on helicopter (fatigue) design. A general overview of fatigue mechanisms in rotating structures, such as rotor blades, flywheels and paper machine rolls, is presented by Gamstedt et al.[98] [2001]. Reifsnider and co-workers have produced a considerable number of

papers spanning several decades of fatigue research, and focussing on the relation between damage and fatigue strength in composite laminates (Reifsnider[266], 1980; Miller et al.[202], 1984; Reifsnider et al.[269], 2000). A modern account of the basic issues in aerospace-driven composite fatigue research is given by Curtis and Davies[57] [2000].

An enumeration of selected authorities should furthermore include Schütz[289] [1996], who provides an extensive overview of fatigue research efforts. Even though this article is, to say the least, not exclusively dedicated to fatigue in composites, and puts special emphasis on local research efforts in Germany between 1920 and the end of the second World War, this is a comprehensive document, assessing the literature between 1838 an 1996. Schijve, to whom this document was dedicated, has condensed some decades of fatigue experience and research into an educational book (Schijve[283], 2001), and has produced several works on variable amplitude fatigue in aerospace materials (Schijve[279-284], 1972-2001).

Marissen[191] [2002] identified improved strength prediction as one of the requirements for more successful implementation of composites in general, and indicated in particular that long-term (compressive) durability should be subject of more research.

Wind turbine blade material fatigue
Fatigue in the particular application of wind turbine rotor blades is discussed by Kensche[155] [2004]. Sutherland[311-315], Mandell, and Samborsky et al.[181-189, 275-277] have a long record of rotor blade material fatigue research [1992-2005].

Joosse and van Delft[146] [1996] expressed their concern on excluding fatigue as a research subject and reviewed research performed in the Netherlands between 1984 and 1996.

Wahl[328] has provided valuable data and analysis, which are most relevant to the current work, notably the experimental work done on the DD16 material, see 4.3.

1.5.3   Damage characterisation and failure definition

Mandell[179] [1981] gives a summary of what is seen from the literature:

'Fatigue crack growth in fiber composites occurs by such complex modes as to frustrate efforts at developing comprehensive theories and models, despite its obvious importance. Under certain loading conditions and with certain types of reinforcement, simpler modes of fatigue crack growth are observed. These modes are more amenable to modelling efforts, and the fatigue crack growth rate can be predicted in some cases.'

For all materials, fatigue life prediction for constant, or variable amplitude fatigue, can be roughly classified into 3 categories:

- Cumulative/Progressive damage
- Phenomenological/empirical
- (Micro-)Mechanics

Cumulative/Progressive damage

The term 'damage' is generally used for all kinds of physical deterioration of the material, notwithstanding its effects on material performance. In Miner's sum (section 3.3), which is said to describe linear accumulation of 'damage', the nature of this damage is not specified, neither is its effect on material performance, such as stiffness or strength. In practice, 'damage' should be application-related. In pressure vessels, a useful damage parameter would be matrix cracks causing leakage. Also, damage can be expressed in terms of stiffness degradation (see section 1.5.4). For reliability driven design, a probability of failure can be used as a failure or damage definition. Ryder and Walker[273] [1976] noted, that in tension-compression fatigue the first occurrence of delamination was related to the onset of final failure, and could be used as a failure criterion. For tensile fatigue, they proposed coupon breakage as definition of failure. They described the residual strength at a probability of survival in fatigue equal to 90%. Owen[241] [1974], in a review of his research, showed that prior to failure by specimen separation, there were two other distinct failure mechanisms, occurring much earlier in life. First, debonding of fibres from the resin occurred, and second, resin cracks formed. When plotted in the S-N diagram, the onset of debonding and resin cracking may be described using S-N curve type formulations.

In this work, 'failure' is defined as the instance when the specimen can no longer bear the intended load. In practice, this leads to considerable damage to the specimen, or to complete separation of parts of the specimen. In the frame of this research, which is aimed mainly at comparing materials and investigating various influences on material performance, this is an appropriate failure definition.

Miller et al.[202] [1984] described 'damage' in terms of matrix and fibre cracking sequences, and in terms of the resulting strength degradation. They investigated constant amplitude fatigue at different R-values, and simple load spectra. They asserted, that damage, strength, stiffness, and life are interrelated.

Miner's sum and variants employing semi-empirical additional parameters, such as the model by Owen and Howe[240] [1972] have in common, that any potential sequence effects are neglected. The order of the load cycles is not taken into account in the fatigue life prediction. Another characteristic is, that the damage parameter is dimensionless, and often open to interpretation. Usually, failure is related to a value of the damage parameter of '1'.

In the model by Marco and Starkey[190] [1954], the damage parameter is again abstract and not related to a physical characteristic of the material, but the order of the cycles is taken into account.

Phenomenological/Empirical
Phenomenological models have in common that a physically measureable parameter is tracked during fatigue loading. Typically, these models describe strength or stiffness degradation during constant amplitude fatigue and use these descriptions in spectrum load fatigue life predictions. A major drawback of this category is, that extensive experimental data is required to describe the models and no veritable guarantee is given that model parameters that are appropriate for one composite apply to accurate life prediction for another.

Meso/Micromechanics
Finally, advocates of the micromechanical models attempt to describe composite degradation due to fatigue from the basic material and basic ply properties. Usually, these models are characterised by considerable detail in the modelling of the constituents, and implementation of rather complicated models describing different, progressively developing and interacting, failure modes.

For quasi-static loading of composites, failure prediction methodologies based on classical laminate theory were summarised and compared in detail by Soden et al.[301] [1998] and Hinton et al.[123] [2002]. Detailed models describing damage accumulation and stiffness degradation are under development, e.g. Joffe[143] [1999], Megnis et al.[196-199] [2004], whose models are to be expanded for fatigue and extreme conditions, such as high temperature or exposure to salt water.
Varna et al.[324, 325] [2001, 2004] have combined meso-scale and microscale modelling to efficiently describe stiffness as a function of (static) strain in cross-ply glass-fibre/epoxy laminates, incorporating damage evolution.

For fatigue, implementation of micromechanics modelling for fatigue life prediction is still in its exploratory phase. Reifsnider and co-workers have a long record of investigations attempting to link micro-mechanical modelling to long term fatigue behaviour of composite, e.g. Reifsnider et al.[267] [1983].
The success of micro-mechanical approaches for fatigue to date is limited to single failure modes.
For compression fatigue, Slaughter and Fleck[297] [1993] suggest, that microbuckling can be a dominant fatigue failure mode in some cases. They developed a model capable of predicting fatigue microbuckling in metal-matrix composites, but experimental data to validate their efforts on polymer matrix composites, or to evaluate under what conditions microbuckling is a dominant failure mode, is lacking.
More work pertaining to single failure mode was published by Petermann and Plumtree[250] [2001]. They formulated a unified fatigue failure criterion for unidirectional laminates, taking into account both the normal and shear strains.

They used the fibre direction as a critical plane, which 'guides' the crack growth. This method requires numerical calculation of the relation between applied load and microstresses and –strains. Using their own data and data from literature, they validated their 'unified fatigue parameter', which they claimed to be –within a scatter band of 2 decades– fibre angle independent. From their results, the method seems to work best for larger off-axis angles.

Recently, Subramanian et al.[308] [1995] claimed a successful attempt to model the influence of fibre-matrix influence on tensile fatigue behaviour of a composite laminate. Krasnikovs and Megnis[160] [2005] investigated fibre breakage in a unidirectional laminate under R=0.1 tension fatigue loading.

Many of these efforts are not free of empiricism, as e.g. the work by Akshantala and Talreja[4] demonstrates [2000]. Nyman[230] [1996], suggests, that interlaminar shear stresses are the reason there is little hope for ply-based micromechanics methods to accurately describe failure of multi-axial laminates. For fatigue failure, among other assumptions, he asserted that the distinction between first-ply-failure and last-ply-failure is negligible in terms of number of cycles to failure.

Van Paepegem[245] [2001] has implemented a fatigue damage model based on displacement-driven bending fatigue experiments into a finite-element method.

There is a thin line between phenomenological and micromechanical modelling. Miller et al.[202] [1984] have published a report on cumulative damage modelling, where they introduced and explored the concept of dividing a laminate in 'subcritical' and 'critical' elements. The 'subcritical' elements do not lead to composite failure, but their damage initiation and progression significantly affect the fatigue behaviour of the laminate, and ultimate failure of the 'critical' elements. Their method was based on a mechanistic approach regarding the failure mechanisms in the subcritical element, whereas they utilised phenomenological models to describe failure of the critical elements. Their approach can be described as a mixture of phenomenological and mechanistic. They note, (pp. 154) that:

> '...mechanistic models are only as good as our understanding of the damage events induced by fatigue loading in composite laminates...'.

Jen et al.[137-138] [1998] describe a method to predict fatigue life of carbon/PEEK using existing methods. They combined experimental S-N curves with Classical Lamination Theory (CLT), a modified Tsai-Hill failure criterion, and a ply-by-ply Miner summation, and compared their predictions to experimental data describing tensile fatigue of laminates containing fibres at different orientations. They obtained acceptable agreement, except for laminates with only ±45° layers. This is an example of a ply-level analysis. A laminate optimization in
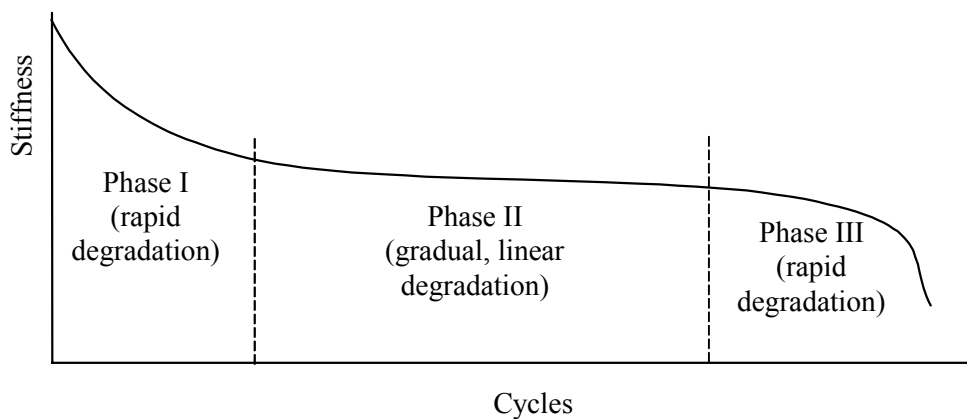
Figure 4: Typical stiffness degradation in composites (schematic)

terms of fibre volume, ply thickness, and fibre orientation, was carried out by Adali[1] [1985] using a similar approach.

1.5.4 Stiffness degradation

Stiffness is potentially an interesting measure of the laminate's condition and resistance to (fatigue) loading, which is quantifiable non-destructively. It may be useful in lifetime predictions, or for ranking residual strength data. In the following paragraphs, some general observations from the literature are discussed.

In general, stiffness degradation in fatigue follows the pattern shown in Figure 4. Stiffness degradation occurs in three stages. At the beginning and near the end of fatigue life, stiffness degradation is rapid, but for most of the fatigue life, stiffness degradation is gradual and linear with fatigue life. The severity of each stage, and total amount of stiffness degradation depends on laminate composition and material properties, as well as type of fatigue loading. Stiffness can be measured using adhesively bonded strain gauges or clip-on type extensometers. Sometimes, stiffness is derived from displacement data. Provided that the measurement equipment has sufficient resolution, this can give an accurate description of stiffness. However, damage of the coupon in the grip may suggest larger strains than are experienced in reality. From experience in the OPTIMAT programme (see 4.2), for example, the tab would progressively debond from the coupon, resulting in increasing displacements, whereas the stiffness, measured by extensometers, would not decrease or decrease more slowly. Moreover, stiffness degradation is matrix-driven. Stiffness degradation in the glass-fibres is relatively small. Therefore, stiffness degradation is more pronounced for off-axis laminates than for laminates with a considerable amount of fibres in loading direction.

Glass

Figure 5 shows 10% stiffness degradation life for various laminates. These data are from the FACT database (De Smet and Bach[71], 1994).
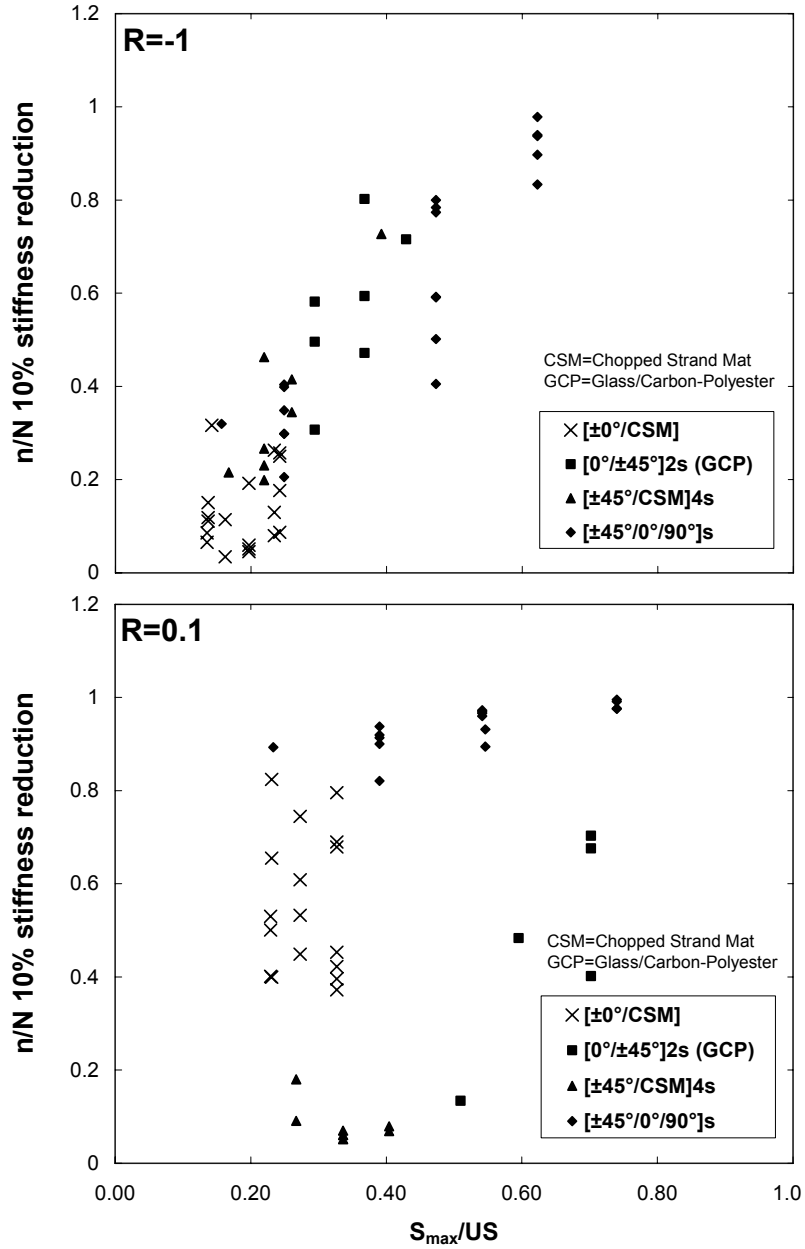
Figure 5: 10% stiffness degradation life from FACT database

Data are shown for R=0.1 (for R-value definition, see Figure 3) and R=-1 fatigue of various glass/polyester and one hybrid glass/carbon/polyester lay-ups. These data suggest, that, for R=-1 fatigue of laminates containing off-axis

layers, there is a linear correlation between normalised maximum stress and stiffness degradation; 10% relative stiffness reduction is achieved earlier for lower stresses. For unidirectional (UD) material, stiffness reduction seems to occur at the same life fraction, independent of cyclic stress. This is also true for R=0.1 of UD material. For laminates containing 0° layers, 10% relative stiffness reduction is reached in a later stage of fatigue life for R=0.1 than in R=-1, except for the laminate containing carbon fibres. For the ±45°/CSM laminate, the stiffness reduction threshold is reached much earlier in R=0.1 than in R=-1. For R=0.5, 0.1, and -1 tests on glass-fibre/polyester dogbone-shaped UD specimens relevant to wind turbine applications, Bach[21, 22] [1990, 1991] published stiffness degradation and related it to macroscopic damage observed during the tests. He noted, that initial stiffness degradation was larger for R=-1 than for R=0.1, and attributed this to microbuckling in regions of the material where voids were present. In Bach[22] [1991], 10% stiffness reduction occurs in a much earlier stage of fatigue life for R=-1 than for R=0.1, see Figure 5. Further stiffness degradation was related to initiation and development of delaminations. From his description, it can be deduced, that part of the stiffness degradation may have been driven by the dogbone geometry, which is sensitive to axial delamination from the gripping area in this UD (with CSM) material. Reported stiffness degradation was in the order of 20 to 25% prior to final failure. Samborsky[276] [1999] and Mandell and Samborsky[183] [1997] tabulated changes in longitudinal modulus for laminates containing 0° and +/- 45° layers, in the order of 10-20% for both coupons and beam substructures, in early phases of fatigue life (n/N<0.5). Stiffness change was smallest for laminates containing significant 0° layers, as the change in modulus was attributable to matrix cracking in the off-axis layers. They quoted De Smet and Bach[71] [1994] in stating that stiffness degradation in actual blade structures would be governed by delaminations and adhesive failures in structural details, rather than by overall stiffness degradation of the material.

For glass-fibre/epoxy, Foley et al.[94] [1983] observed total modulus degradation of ca. 50% for multidirectional, and approximately 10-20% for a cross-ply laminate in tensile fatigue. Modulus in tensile tests was measured with an extensometer. In fatigue, the hysteresis loops were recorded at predetermined intervals. They indicated that the modulus degradation was accurately reproduced from specimen to specimen, and from their data, it is observed that life fraction can be estimated to an accuracy of 10-20% from measured stiffness degradation.

Stiffness degradation was mentioned as a measure of microdamage by Joneja[139] [1986] in a resin comparison study. The modulus degradation observed in the filament wound specimens was insignificant in tougher resin specimens, even up to 75% of the life fraction. Some modulus degradation was observed in a very ductile resin system, this was attributed to microdamage.

Philippidis and Vassilopoulos[253] [2000] have discussed a wealth of stiffness degradation data obtained from a multidirectional laminate. A total of 17 S-N curves were determined at R-values of –1, 0.1, 0.5, and 10, and for different cut-angles of the laminate. Data for R=0.1, suggest that stiffness degradation is roughly independent of off-axis angle. From their locally weighted average stiffness degradation lines, no clear trend is discernible between stress level (nominal lifetime) and stiffness degradation, although there is a tendency for less stiffness degradation for higher stresses in a 75° off-axis laminate. The scatter in E_n/E_i is in the order of 10%. In the analysis of R=-1 stiffness degradation data from the same test programme, Philippidis and Vassilopoulos[252] [1999] obtained a generally smaller scatter, at ca. 5% for both the same MD material and a unidirectional material. It is not mentioned explicitly how stiffness is measured, but it is suspected that this was done using grip displacement, as the coupon surfaces were covered by an anti-buckling jig, which would hamper stiffness measurement using clip-gauges or strain gauges.

Ellyin and Kujawski[85] [1995] report a normalised modulus degradation of ca. 40% for a [±45°] glass-fibre epoxy in R=0.05 tensile fatigue, which seems to be independent of the stress range measured. They related this to the cyclic creep accumulation. Strain was measured using a clip-on type extensometer.

Naeem[208] [1989] investigated the relation between propagation of single-mode damage induced by a notch and specimen compliance. He used unidirectional and cross-ply glass/polyester laminates. From a comparison of these two laminates and two notch sizes, he found that compliance was proportional to damage extent and independent of notch size or shape. Compliance was deduced from overall extension of the specimen; strain measurements were not included in the experimental programme.

Echtermeyer[82] [1994] recorded stiffness degradation of different wind turbine materials under R=-1 fatigue, using an extensometer attached to the specimen edge. For a laminate with 45% of the fibres in loading direction, the stiffness degradation was much more gradual than for a laminate with 98% of the fibres in the loading direction. Both laminates showed a precipitous stiffness drop very close to failure.

El Kadi and Ellyin[84] [1994] found no stiffness loss up to a high fraction of life, regardless of stress level, for off-axis glass/epoxy laminates of 19°, 45°, 71°, and 90° off-axis angles subjected to R=0 fatigue.

Diao et al.[72] [1995] observe from the literature, that normalised stiffness degradation is independent of stress level (they quoted the group of Yang, Jones, and Whitworth). They formulate normalised stiffness in their experiment on glass/epoxy:

$$\frac{E}{E_i} = a \cdot e^{-b\frac{n}{N}} + c \tag{1}$$

with $a=0.26$, $b=8.5$, and $c=0.76$ in their case. The parameter c represents the final value of normalised stiffness, a governs the start point of the curve, and a larger value of b leads to a steeper stiffness degradation during phase I.

Andersen and Lilholt[11, 12] [1988] have performed extensive constant amplitude fatigue testing of 'wingblade' materials. They describe damage and stiffness degradation of various off-axis laminates, and give a predefined stiffness reduction during fatigue as a possible design limit.
Andersen et al.[13] [1996] have formulated and validated a stiffness criterion for generating fatigue design curves:

$$\frac{E}{E_1} = 1 - K \left(\frac{\sigma_a}{E_0} \right)^c N \tag{2}$$

Philippidis and Vassilopoulos[253] [2000] used this later for deriving fatigue design allowables.

Carbon
Published modulus degradation data are predominantly for carbon fibre composites, and in tension-tension fatigue ($0<R<0.2$). Moreover, the carbon fibre publications discussed below predominantly describe aerospace grade composites, which are different (thinner laminae, thinner laminates, finer tows and weaves, generally more expensive) from carbon laminates considered for wind turbines.
Jones and Whitworth[140] [1984], and Wevers et al.[338] [1987] observed stiffness degradation patterns for tension-tension fatigue of carbon reinforced epoxy, where Young's modulus degrades linearly up to a high fraction of life, followed by a higher degradation rate. Total stiffness degradation was in the order of 15% to 20%. Wevers et al. augmented the information on damage development that could be deduced from stiffness degradation with Acoustic Emission readings (AE), to identify the development of different damage modes. As O'Brien[232] [1978] had noted, the cumulative number of acoustic emissions is a measure for the accumulated stiffness degradation. A comprehensive review and appraisal of acoustic emission techniques and their application in qualifying and quantifying damage in composites up to 20 years ago is provided by Hamstad[114] [1986]. A recent feasibility study of acoustic methods in rotor blades is presented by Blanch et al.[30] [2002].
Yang and Jones[355] [1978] found (shear) modulus degradation of 10-15% for $[\pm35°]_{2s}$ graphite/epoxy laminates. This was measured using two extensometers at right angles.

Schulte, Nowack et al.[287] [1985] identified as the most appropriate damage parameter the modulus at the end of the linear part of the stiffness degradation curve, but before the precipitous stiffness decrease prior to final failure. They noted a stiffness decrease of some 10% prior to final failure, for two load levels in R=0.1 fatigue of a cross ply graphite/epoxy specimen. The load levels were 800 and 900 MPa, resulting in about a decade difference in nominal lifetime. Stiffness was measured using a clip gauge. The stiffness degradation was very similar, suggesting similar damage modes. Some initial analysis of two-block simple load spectra suggested, that life prediction by means of following damage accumulation in terms of stiffness reduction yielded non-conservative results. They suggested, that other processes, not included in stiffness models, led to additional damage and shorter experimental lives than the stiffness-based predictions.

Whereas the abovementioned work suggests monotonous degradation of Young's Modulus with expended fatigue life, Ganczakowski et al.[100] [1987] observed stiffening, both in quasi-static tensile loading and in the early fatigue life of R=0.1 fatigue in cross-ply Kevlar/epoxy laminates. This was attributed to fibre straightening. The stiffening effect was more pronounced for higher cyclic stress levels. In fact, for the cross-ply material they distinguished four alternating regions, the first and third of which were dominated by stiffening, the other two by modulus degradation due to matrix cracking in the 90° layers. Stiffening and cracking in cross-plies are competing mechanisms. Accordingly, in unidirectional material, no modulus degradation was seen, and the modulus degradation was more pronounced in thicker laminates. Daniel et al.[58, 59] [1987, 1998] also investigated stiffness during monotonic and cyclic tensile loading of cross-ply graphite/epoxy and noted initial stiffening in the stress-strain curves of the first cycles beyond the second cycle for stresses exceeding that of the static characteristic damage state level. Final modulus degradation was constant according to their observations, but initial drop in modulus was related to the cyclic stress level (larger initial reduction for higher stress level).

Awerbuch and Hahn[20] [1977] were surprised at an unexplained increase in tensile modulus after tensile fatigue of graphite/epoxy specimens. The modulus was measured before and after fatigue using an extensometer, occasionally backed up by strain gauges.

Stiffness degradation in life estimates

The first authors to suggest stiffness degradation as a damage accumulation parameter were Wang and Chim[331] [1983]. They found a power-law relationship between the rate of damage development number of fatigue loading cycles. Although the work of Wang and Chim clearly states, that the change in material properties was more significant in the random short-fibre SMC material than in continuous filamentary composite laminates in general, stiffness degradation has been used in combination with a strain failure criterion by various authors. Hwang and Han[124, 125] [1986] introduced the fatigue modulus concept (essentially, this is applied stress divided by resultant strain in fatigue) and used
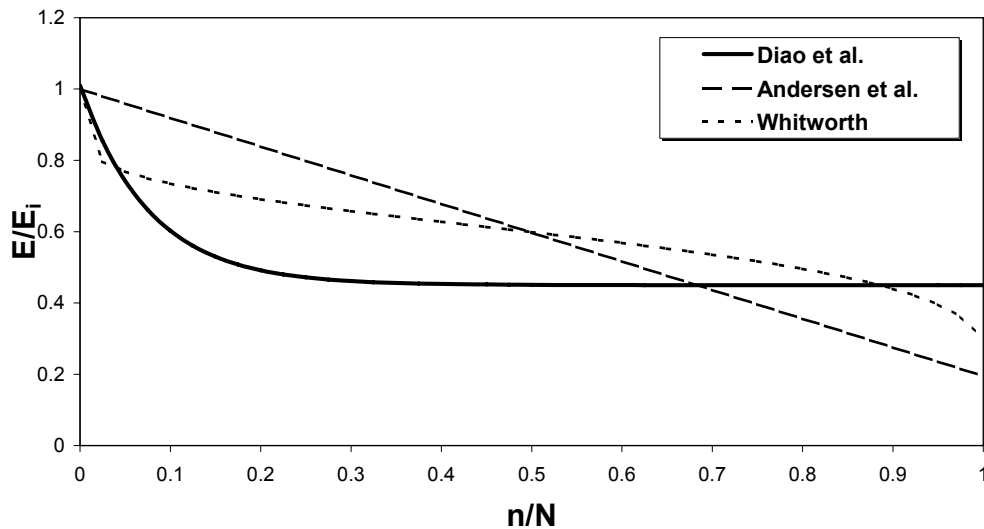
Figure 6: Different stiffness degradation models

a power law equation to describe fatigue modulus degradation. Hahn and Kim[111, 112] [1975, 1976] suggested, that fatigue failure occurs, when the modulus in fatigue decreases to within the scatter of the modulus distribution in a quasi-static test. This 'secant modulus criterion' was evaluated by O'Brien[232] [1978], and his experimental work on Boron/Epoxy laminates of four different lay-ups indicated, that it was a useable concept, except for UD material, since no significant modulus degradation could be measured for that laminate. He describes the 'extreme' stiffness degradation in his tests on transverse, cross-ply, and multi-directional laminates as a result of homogeneous, isotropic matrix damage.

Zhang and Hartwig[361] [2002] proposed recording damping (related to energy loss) as a better damage metric than stiffness degradation. They compared the fatigue behaviour of epoxy-based unidirectional specimens with that of a thermoplastic-based carbon material. According to their observations, the degree of damping was influenced by the nature of the damage evolution.

Petermann and Schulte[249] [2002] demonstrated for R=0.5 fatigue on a carbon reinforced epoxy [±45°] laminate, that mean strain gave a better description of fatigue damage than stiffness, but this was not applicable to reverse or R=0.1 fatigue loading.

Whitworth[344] [1998] investigated stiffness degradation in [±35°]$_s$ graphite/epoxy laminates under R=0.1 fatigue, using data from earlier test campaigns. Stiffness measurements were done using stiffness measurements from the test system LVDT and a clip-on type strain transducer. These results were used to demonstrate the validity of a model that predicts stiffness degradation. The model is based on the premise that failure occurs once the strain in fatigue reaches ultimate failure strain. Later, this model was used in a description of residual strength after fatigue (Whitworth[345], 2000).

Some of the models discussed above are shown in Figure 6.

Summarising, stiffness is a useful parameter to assess a laminate's condition non-destructively. Theoretically, it can be used for life prediction in combination with a strain criterion. For analysis of residual strength tests, it could be used to improve the estimate of fatigue life fraction. Numerous authors have investigated and modelled stiffness degradation. In general, stiffness degrades in two or three distinct stages. Rapid degradation occurs in the first and last section of the stiffness degradation curve, as depicted in Figure 4, whereas the majority of the degradation curve is well described by a linear, slowly decreasing segment.

Fibre dominated laminates:
- 10-25% Stiffness degradation, at a life fraction independent of stress level for R=0.1
- For R=-1 ~10% Stiffness degradation, life fraction is smaller for R=0.1 than for R=-1
- Stiffening is possible due to fibre straightening in an initially wavy laminate

Matrix dominated (off-axis) laminates:
- Stiffness degradation is attributed to matrix damage
- Total stiffness degradation 25-45%

1.5.5 *Fibre*

Most rotor blades are mainly constructed using glass-fibre reinforcement. Carbon fibres have the potential of creating lighter blades because their stiffness is much higher than that of glass-fibres. Also, the S-N curves are flatter.

Joosse et al.[148, 149] [2002] have analysed the cost-effectiveness and static and fatigue behaviour of candidate carbon fibre laminates for use in load carrying sections of rotor blades. It was concluded, that total cost of the turbine could be reduced by 4-5% by replacing glass-fibres with carbon fibres in heavily loaded parts of the blade structure.

Griffin et al.[108] [2002] investigates the influence of blade material, and manufacturing processes, on the maximum rotor blade length. For larger blades, fundamental changes in the material systems may be required according to this study.

Bach[23] [1992] has compared fatigue lives of a glass/carbon hybrid laminate to an equivalent glass laminate. For R=0.1, he noted an improvement in fatigue behaviour for the hybrid material, which also reflected in comparative tests using the predominantly tensile WISPER spectrum (for a description of this spectrum, see 3.1). However, for R=-1, the increase in fatigue performance did not match his expectations, when compared on a load basis.

The influence of fibre volume on composite fatigue behaviour is schematically shown in Figure 7 (note, that in practice, composites contain between ~30% to ~75% fibre). At low fibre volumes, the performance is determined primarily by the matrix material, which does not generally have structural properties comparable to those of the fibres. Tension strength is low, compressive strength somewhat higher. Tensile strength is proportional to the fibre content. Compression strength is also proportional, but at very high fibre volumes, the amount of matrix material is insufficient to bond the fibres together.

At high fibre volume fractions, different authors have shown that fatigue performance degrades. Boller[33] [1964] performed extensive testing on various lay-ups and mean (tensile) stresses on waisted glass/epoxy specimens and found that 33% (by weight) of resin gave the best fatigue strength at 10 million cycles. Mandell et al.[185] [1999] have done studies where they advertently raised or lowered local resin content and presented knock-down factors for both fatigue and static performance. They noted that locally increasing fibre volume improved static performance, but could be detrimental for fatigue performance. In another study by the same group, it was demonstrated that for some fibre architectures, fatigue performance dropped as the fibre volume exceeded a certain value (Samborsky[276], 1999). He demonstrated, that for tensile R-values, the slope of the S-N curves increased for higher fibre volume fractions. If the variations in fibre volume fractions are within narrow ranges, some correlation may exist between static strength and fibre volume fraction, but fibre volume fraction does not seem to be the dominant factor for scatter in fatigue life at a specific load level, Nijssen[224] [2006].
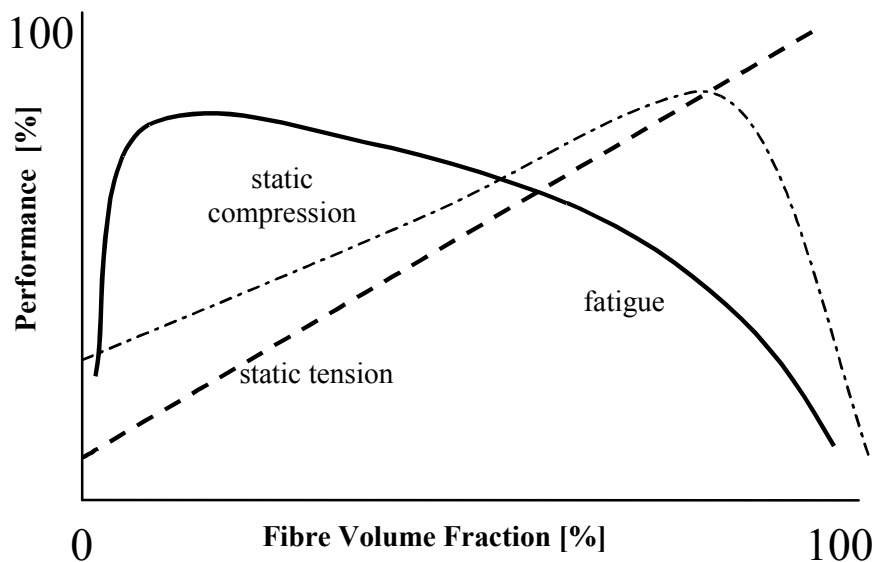
Figure 7: Influence of fibre volume fraction on performance

(not to scale, schematic)

1.5.6 Resin

Thermosets

Traditionally, polyester and epoxies are used as resin material in wind turbine blades, the latter being preferred mainly because of health/environment issues during production and because of smaller slope of the S-N curve in the GL recommendations[101, 102] [1999, 2003].

Comparisons of polyester and vinylester matrix materials, demonstrate that vinylester and polyester for wind applications tend to have comparable fatigue characteristics, e.g. publications by Graham and Mohamadian et al.[107, 204] [1989, 1990]. Also, for toughened resins, no influence of matrix material was seen in comparing axial fatigue of epoxy, vinylester, and polyesters at R=-1, R=0.1 and R=10, so cost would be the driving factor for matrix selection, Mandell et al.[183, 186] [1997, 2000]. Other studies by Mandell et al.[181, 182, 186] [1992, 1994, 2002] show, that influence of the matrix is negligible.

Filis et al.[93] [2004] suggest, that glass-fibre composites are matrix dominated in their fatigue behaviour, because of higher fibre strains, as opposed to carbon fibre composites. This would imply an influence of matrix on fatigue life.

Guemes et al.[110] [1989] have also compared polyester, vinylester, and epoxies on plain and notched specimens. Despite differences in fracture characteristics, they did not find any difference in static and fatigue performance, and they assert that matrix sensitivity might exist for CRP, but not for GRP.

Thermoplastics

The use of thermoplastics in wind turbine rotor blades is in its early stages. The potential, in terms of sustainability, is the recyclability of the thermoplastic materials. Although the viscosity does not seem to make separation of fibre and resin feasible, laminates can be more easily chopped up and remodeled into short-fibre products or filler material than thermosets. Connection methods such as welding, and repair methods, also offer potential advantages over e.g. epoxies.

In terms of basic material properties, most properties are comparable to epoxy, but thermoplastics have been seen to exhibit superior fracture toughness, see e.g. Donaldson[76] [1985] for a detailed comparison between epoxy and polyetheretherketone (PEEK). Performance in static tests can be improved by using PEEK, as reported by Maekawa et al.[177] [1994]. However, before the resin can be considered for use in wind turbine rotor blades, the fatigue behaviour must be comparable to that of thermoset laminates. Moreover, PEEK is relatively expensive.

Static flexure and flexure S-N curves and a description of failure modes of graphite-thermoplast and graphite-epoxy were discussed by Croman[55] [1987]. The fatigue behaviour was worse for the thermoplastic, an amorphous polyamide (J-Polymer), which showed far less delamination than the thermoset.

This is in agreement with the damage initiation delay reported by Henaff-Gardin and Lafarie-Frenot[121] [1992].

Cinquin et al.[48] [1990] have described fatigue behaviour of a thermoplastic composite and deliver a detailed account of the influence of constituents and fibre surface treatment on e.g. the fatigue behaviour.

Buggy and Dillon[42] [1991] noted from flexural fatigue on graphite composites, that epoxy laminates performed better only in the case of cross-plied or unidirectional lay-ups, and that for angle plies, the performance was similar. They also noted a increase in slope of the S-N curve at low stress levels.

For carbon fibre constrained laminates, Henaff-Gardin and Lafarie-Frenot[121] [1992] have compared the quasi-static and tensile fatigue behaviour of a thermoplastic and thermoset composite. They report equivalent performance for the static case, but with fatigue lives one or two decades below that of the thermoset. In addition, damage development in the thermoplastic was negligible, and final fracture modes was ductile, as opposed to brittle in the thermoset resin. Their work indicates, that fatigue behaviour of thermoplastics is worse than thermosets.

Gamstedt[96] [1997] has noted that the static properties for carbon reinforced PEEK were superior to those of carbon reinforced epoxy, but in fatigue the epoxy showed better performance. These observations were done exclusively for fully tensile conditions.

Zhang and Hartwig[361] [2002] corroborated Gamstedts observation, and, for tension-tension fatigue of AS4/PEEK and AS4/Epoxy described the difference in fatigue mechanisms and the effect on damping (which can be related to energy dissipation).

Song and Otani[306] [1998], however, reported better fatigue performance of CF/PEEK compared to CF/epoxy in similar circumstances. They observed a clear difference in damage progression, where the epoxy matrix showed significant transverse cracking prior to fracture of the longitudinal fibres, whereas the PEEK laminate did not display as much matrix damage but had more extensive longitudinal fibre fracture in early fatigue life. They managed to quantify the susceptibility of the laminate to transverse matrix cracking and longitudinal fibre fracture by describing the material in terms of matrix shear strength, stresses in the transverse layers, match of E-modulus and fibre volume fraction.

For bending fatigue of thermoplastic composites containing randomly oriented continuous glass-fibres, Caprino and d'Amore[46] [1998] concluded, that the presence of an inherently ductile thermoplastic matrix did not sensibly affect fatigue life. This was contrary to their expectations, and they attributed this to the constraining action of the reinforcement.

Thermoplastic dogboned specimens tested by Mandell and Samborsky[189] [2005] in tensile fatigue showed worse compressive static strengths and strains, better tensile strengths and strains, and worse fatigue behaviour with respect to epoxy or vinylester specimens with equal fibre content.

Prior to application of thermoplastics in wind turbine blades, the fatigue behaviour has to be investigated in detail, as stated by van Rijswijk, Joncas et al.[270] [2005]. They present a simplified comparison of epoxy-based and PA-6 based composites for rotor blades, resulting in a marginal preference for PA-6 based on static properties and material bulk cost. Their comparison lacks a sensitivity analysis showing the influence of their assumptions concerning basic material properties.

Overall, the above materials research suggests, that thermoplastics have worse fatigue behaviour than thermoset resins, both in carbon and glass-based composites. Seemingly contradictory, this is due to their higher toughness, which might be an impediment to stress redistribution. From a fatigue point of view, as a first step towards application in wind turbines, an extensive comparative material's testing programme should be carried out on dedicated wind turbine composites.

1.5.7 Coupon versus structure

Improving the knowledge of a material's fatigue behaviour is only part of describing full scale blade characteristics. With regards to the current research, this is especially true, since only uni-axial, in-plane loading of balanced and symmetrical, relatively thin laminates is considered, which are only remotely representative for blade structures.

In experimental work, aimed at observation of fatigue behaviour for representative materials, laminates are typically used with either uni-directional, shear-dominated, or quasi-isotropic lay-ups. Referring to wind turbine rotor blades, these represent the spar flanges, or shear webs.

In full-scale blades (for blade testing see e.g. van Delft et al.[60, 63, 66, 67] [1988, 1993, 1994, 1996]), multi-axial loading conditions are present in the entire blade, and particularly significant in design details and in thick laminates. Limited research was done on coupons or substructures reflecting these stress states.

Useful research has been performed on the influence of ply-drops and on the behavior of substructures in static and fatigue conditions in relation to simple coupon tests, but the microscopical stress state was not investigated, Mandell[185, 187] [1999, 2002]. Test results on composite rotor blade spar beams are reviewed in Kensche et al.[154] [1996]. Also, biaxial specimens can be used. These can be tubes under pressure (see e.g. Soden et al.[302] [2002]), tubes subjected to simultaneous axial loading and torsion (e.g. Whitney et al.[340] [1971], Lee et al.[172] [1999]), or cruciform specimens. Especially the design of a cruciform test specimen for a composite is difficult, since it has to meet a number of stringent requirements (uniform stress distribution in measurement/failure area, repeatable results, large range of tests possible) see e.g. Welsh and Adams[336]

[2002], van Wingerde and van Delft[348] [2002], van Hemelrijck and Smits[120] [2003].

Extreme conditions

This work does not address material behaviour in 'extreme conditions' relevant to placement of wind turbines in deserts, arctic regions and in offshore climate.

For wind energy composites, specific knowledge of the material degradation due to temperature influences and influence of humidity until now is limited to a few scattered investigations. Generally, previous work shows, that moisture absorption degrades the static properties of rotor blade composites. A literature survey on the effect of moisture concludes that static properties are affected most by moisture and that effects on fatigue diminish in the high cycle range, Bulder and Bach[43] [1991]. No moisture influence on fatigue could be identified in Kensche[152] [1993]. The potential of hybrid composites in terms of lower moisture sensitivity was found. This is confirmed by recent research, which shows that the addition of carbon fibres may improve a glass-fibre composite's fatigue properties in wet conditions, Shan et al.[294] [2002]. Some results on composite strength and modulus in dry and wet conditions, at temperatures ranging between –20°C and 70°C can be found in Mandell et al.[186] [2000]. Effects of humidity were investigated in the OPTIMAT project, showing a shorter fatigue life for tests performed at 100% relative humidity. Static properties decreased with increase in temperature, notably shear dominated properties. Also, fatigue at elevated temperature resulted in shorter lifetimes DNV[75] [2006].

Coupon geometry

Coupon geometries are prescribed for different test types in e.g. ISO[132-134], ASTM[7-8]. Sometimes, however, there are reasons to deviate from e.g. parallel-sided (rectangular) coupons and use dogbone (waisted) coupons.

Curtis et al.[56] [1988] have reported no influence of using waisted (dogbone) or parallel-sided specimens for a multidirectional or ±45° laminate. In this publication, they also address issues of wave shape and frequency. For a laminate containing predominantly 0° layers, test specimen geometry is more significant, as illustrated by the work of Henaff-Gardin and Lafarie-Frenot[121] [1992].

The significance of the 0° layers is corroborated to some extent by the fact that the OPTIMAT standard geometry is rectangular (section 4.2.3), whereas the MSU tests (section 4.3.3) are done on dogbone coupons. As described in Mandell and Samborsky [2006], the failure mode in waisted coupons depends on the relative amount of 0° fibres.

Waviness

Piggot[263] [1995] discussed various effects of fibre waviness, observed from controlled introduced waviness in unidirectional composite coupons. Waviness influences composite compressive resistance, as well as fatigue resistance. He quoted Mandell[181] [1992] in asserting, that even in tensile fatigue, waviness

could adversely affect fatigue life, due to fretting of adjacent fibres. Shear strength and delamination resistance were seen to increase for wavy fibres.

Size effect/failure modes

Wisnom[352] [1999] concludes from a review of various composite static strength studies on carbon and glass-fibre/epoxy, that a significant size effect exists, where strength decreases with increasing coupon volume (this is keeping geometry constant; the effects of different geometries on failure strength/life was not investigated explicitly). This effect is strongest for matrix-dominated failure. Indications are noted, that size effect does decrease with increasing scale, but nevertheless, it is pointed out that the possibility of a size effect on strength should be taken into account when designing large structures using data obtained from small coupons.

Griffin et al.[108] [2001] conducted scaling studies, attempting to push the limits of using contemporary materials in future designs and suggesting use of alternative materials. They hypothesise that size of the blade may either offset fatigue characteristics towards shorter lives because of the larger probability of resin-rich areas, areas of increased porosity, resin cure variations, etc., or towards longer lives because damage arrest may occur in blades (e.g. when stress concentrations are diminished by delaminations, which is less likely in smaller coupons).

In this light the work of van Leeuwen et al.[173] [2002] and Och[233] [1980] should be mentioned, who confirmed that there is a reasonable agreement between coupon tests and (model) blade tests. They compared blade tests in flap- and edgewise direction for a small model rotor blade to coupon tests and demonstrated, that both the slope of the fatigue curve, the actual fatigue stress levels, and the scatter compared reasonably well after they corrected for mechanisms that occurred exclusively in the blades. Mandell et al.[184] [1998] found 'no major contradictions' in validating the behaviour of a model substructure in terms of predicted strength, stiffness, failure mode, and lifetime. At the same time, they emphasised the sigificance of design details.

van Wingerde et al.[350] [2006] performed tests on extremely large rectangular glass-fibre/epoxy coupons, to investigate the influence of size effect. A considerable effect on strength and fatigue life was seen, but the load introduction of the large coupon was suspected to be at least a partial cause for the difference in performance.

1.6 Problem

Current life prediction methods for composite rotor blade structures have been demonstrated to be potentially non-conservative. Van Delft et al.[69] [1997] presented experimental results from glass-fibre-reinforced coupons subjected to two different standardised variable amplitude loading sequences, WISPER, and its shortened variant WISPERX. They compared these data to predictions made

using the GL standards[101] [1993]. They made two important observations. First of all, the life predicted using a linear Goodman diagram and log-log S-N curves was highly non-conservative and exceeded the experimentally determined fatigue lives by up to a factor of 100. Second, the effect of small load amplitudes in the WISPER sequence did not result in significantly shorter fatigue lives in the life estimate, but had a clear influence in the experiments, reducing the number of WISPER sequences compared to the number of WISPERX sequences by a factor of approximately 2. They attributed the discrepancy between experiment and model to the well-known fact, that the approach used for variable amplitude life estimates employs 'Miner's Rule'. This method does not take into account sequence effects. This means, that the order of the load cycles does not have any influence on the amount of life that is expended in the structure. Furthermore, they questioned the assumption, that small load cycles have negligible damaging influence. This assumption was made in the derivation of the WISPERX sequence, and corroborated by the prediction method. Among others, Nijssen et al.[211-213] [2001, 2002] attempted to improve life predictions using modified formulations for the S-N curve and constant life diagrams. However, this approach still does not take into account the potential effect of loading sequence.

In aeronautical composite fatigue research, strength degradation models have been extensively formulated. These models take into account the order of load cycles, by quantifying the strength degradation in a cycle-by-cycle analysis. Comparing the instantaneous strength to the instantaneous load, these models are used as life prediction methods. Incorporating the static and fatigue scatter in the analysis creates a probabilistic life prediction estimate. Wahl[328] [2001] proposed to use residual strength analysis for wind turbine composites, and validated a non-linear model using repeated block tests and single R-value modifications of WISPER. Andersons and Korsgaard[14-16] [1997, 1999] collected tensile residual strength data for input in the model. The experimental basis for the various strength degradation models which have been developed in the past, is very limited, especially for wind turbine rotor blade composites. The amount and duration of fatigue tests involved in creating a representative database for predictive purposes is a limiting factor.

In general, the absence of a consistent and detailed description of the fatigue behaviour and strength degradation of wind turbine rotor blade composites hampers insight into the actual response to spectral loading, and hinders the development and implementation of an accurate and reliable life estimation model. In addition, the blade loading itself is poorly predictable compared to e.g. aerospace applications, where the sequence and magnitude of loads is relatively well-known in advance.

1.7 Objectives

The objective of the research is to improve life estimates of wind turbine rotor blade composites under variable amplitude loading. Ultimately, the research aims to contribute to improved life prediction guidelines, which can be incorporated in the standards. In practice, this means that, through decreasing the uncertainty in a fatigue calculation, the safety factors, that deal with the uncertainties could be decreased.

1.8 Approach

Classical fatigue analysis is performed, using the Palmgren-Miner approach and various degrees of detail in the input data in terms of counting method, S-N curves and constant life diagram. In addition, a strength degradation model for life and strength prediction is implemented. As an example, the WISPER spectrum and derivatives from this spectrum are used for the predictions. A considerable amount of experimental work is required. The Montana State University (MSU) database as well as the EU OptiDAT database were extended with two separate datasets, both comprising a few hundred static, fatigue, residual strength, and spectrum tests. These data were used to develop and evaluate various models. The need for interconsistency of the data is emphasised.

1.9 Scope

The focus of the experimental programme is on a special class of composite materials, viz. wind turbine rotor blade composites. Nevertheless, the semi-empirical approach and findings are likely to be useful for other composites structures.

The major constraints on the research are the fact, that research is on coupon level, the models derived from the observations are phenomenological, and based on uni-axial experiments. Microscopic damage assessment is limited. Macroscopic damage modes that may be induced by structural details are not included. Thus, transitions from shear web to flanges, laminate tapering, panel buckling, macroscopic cracks in the blade skin -which are known to cause major damage in practical applications-, are not modeled, nor is their influence on blade life qualified. Multi-axiality of the ply stress state, which is inherent in most multi-axial laminates and probably in thick uni-axial laminates, and near geometrical discontinuities, is not explicitly taken into account, although most of the research was performed on multi-axial laminates. Laminate details such as fibre waviness, resin content, fibre volume fraction, thickness tapering, are

not explicitly taken into account, although some are well-described for the coupons.

Mainly fibre-dominated lay-ups are considered, in a limited number of different ply configurations. Micro-damage assessment and resulting models are not considered explicitly due to the fact that at this moment, a unified approach, combining micro-damage models to explain the macro-behaviour of the material, is not fully developed.

The prediction of the actual loads is not discussed here. The discussion is limited to the material side of the blade.

1.10 Structure of the report

In Chapter 2, the reader can find in some detail the aspects of constant amplitude fatigue behaviour and its descriptors of mainly glass-fibre composites. Typical fatigue behaviour characteristics are assessed in terms of types of S-N curves that are appropriate, and summary of the fatigue behaviour in the constant life diagrams. Constant amplitude fatigue behaviour is at the basis of both classical fatigue analysis and residual strength degradation models and is therefore described in detail.

In the following chapter, spectrum life prediction methods are discussed. The main focus is on the classical fatigue analysis and strength degradation models, and the influence of varying model parameters on the life prediction is investigated.

Chapter 4 reports the experimental efforts. Two projects serve as a source of input data. The OPTIMAT blades project is a large European cooperative research project, in which numerous fatigue, static, residual strength, and spectrum tests have been carried out, the results of which can be of use for modeling and validation purposes. The results of this project are summarised in the OptiDAT database. A similar, separate project was carried out at Montana State University (MSU). The similarities and differences in test procedure, equipment, and results are reported in detail.

The influences of various components on the life prediction, are discussed in Chapter 5. In the final chapter, conclusions and recommendations for future research are made.

The relevant literature is discussed and compared to the findings in the appropriate chapters, rather than in a separate literature survey. The references can be found in alphabetical order after the last chapter. The data used for this report, and the results of many other relevant experiments on comparable laminates and materials can also be found in the OptiDAT database, and in the DOE/MSU databases.

Summary of this chapter

Chapter 1 motivates the subject of the dissertation. Life predictions for load spectra have been problematic in previous publications. Inaccuracies were generally attributed to Miner's summation, and sometimes to formulation of the S-N curve and constant life diagrams (CLDs). This thesis will investigate S-N formulation, counting methods, CLD formulation, as well as Miner's sum and strength degradation in an attempt to identify the most appropriate life prediction methodology for wind turbine rotor blade composites.

Furthermore, this chapter gives a general introduction to fatigue terminology, and to fatigue of composites, describing loads, materials, relevant literature and some composite fatigue issues which should be mentioned for general interest, but are not necessarily applicable to life prediction, nor will they be significantly further elaborated in this thesis.

- *The fatigue terminology is described*
- *Loads in a rotor blade structure are dominated by highly variable flapwise wind loading, and more deterministic edgewise gravity loading.*
- *Various damage characterisation approaches from the literature are outlined, describing damage at different scales*
- *Stiffness degradation in glass and carbon fibre composites is discussed, and its potential use in life prediction*
- *Influence of fibre and resin on composite performance is outlined*
- *Part of the discussion is given on the relevance of coupon tests for description of a full structure*

The next chapter is devoted to constant amplitude fatigue, and focusses on the issues that are relevant for life prediction.

Chapter 2

Constant amplitude fatigue

This chapter starts with a detailed description of the 'building blocks' of prediction methodologies for variable amplitude fatigue. These building blocks describe the constant amplitude fatigue behaviour, and include several formulations of S-N curves, and the Constant Life Diagram. Some issues relevant to the determination and description of constant amplitude fatigue behaviour, such as scatter, are described at the end of the chapter.

2.1 The S-N diagram

As was briefly discussed in 1.5.1, fatigue data are represented in the S-N diagram, recall Figure 3. This diagram includes results of fatigue tests in terms of their S and N characteristics. S and N represent load (maximum stress, or strain amplitude, or displacement range, etc.) and life (time, number of load cycles to failure, etc.), respectively. Below, unless otherwise stated, it is assumed, that the S-N curve is plotted for a constant R-value. Other ways to set up the fatigue test are also possible, such as varying amplitude around a constant mean.

Various methods exist to analytically describe the data in an S-N diagram. This description is called the 'S-N curve', and is needed for life prediction. The most common S-N curve formulations are discussed below, including methods to derive the S-N curves from experimental data.

2.1.1   Common S-N formulations

Note, that, although N is the dependent variable, it is commonly plotted on the abscissa instead of the ordinate. This tradition will be followed here for graphical representation of S-N curves, but in S-N curve analysis, fatigue life should be (and, in this work, will be) treated as the dependent variable.

Fatigue tests, that were taken out of the machine prior to fatigue failure are called 'run-outs'. In general, these are included in the S-N diagram and indicated with an arrow pointing diagonally upward. They can be in-/excluded from the S-N curve definition.

Results of static tests may be in-/excluded from the S-N diagram or S-N curve definition at will. This is further discussed in 2.3.4.

Classically, the logarithm of constant amplitude fatigue life N is assumed to be linearly dependent on the governing stress/strain S, or its logarithm.

These two formulations of the S-N curve are:

$$log\,N = a + b \cdot log\,S \tag{3}$$

or:

$$log\,N = c + d \cdot S \tag{4}$$

where

N	=	Generic term describing lifetime
S	=	Generic term describing stress- or strain
a – d	=	Constants which depend on fatigue stress state

or, equivalently:

$$N = CS^b \tag{5}$$

where C is equal to 10^a. The former is commonly called a log-log or power law formulation, and the latter a lin-log or exponential formulation. There is no apparent convention in literature as to whether maximum stress, stress amplitude, stress range, or the equivalent strain quantities should be used. Since none of these parameters completely defines the constant amplitude waveform, the *S-N* diagram is not complete without at least a mention of either another of the *S*-parameters, or the R-value.

The R-value is defined as the ratio of minimum to maximum stress:

$$R = \frac{S_{min}}{S_{max}} \tag{6}$$

It is common practice to define the S-N diagram for constant R-value. As a result, the parameters of the S-N curve are different for different R-values. Also, for other S-N formulations (section 2.1.2), one should bear in mind, that strong dependence on R-value may exist, and the parameters of the S-N curve should be explicitly associated with an R-value.
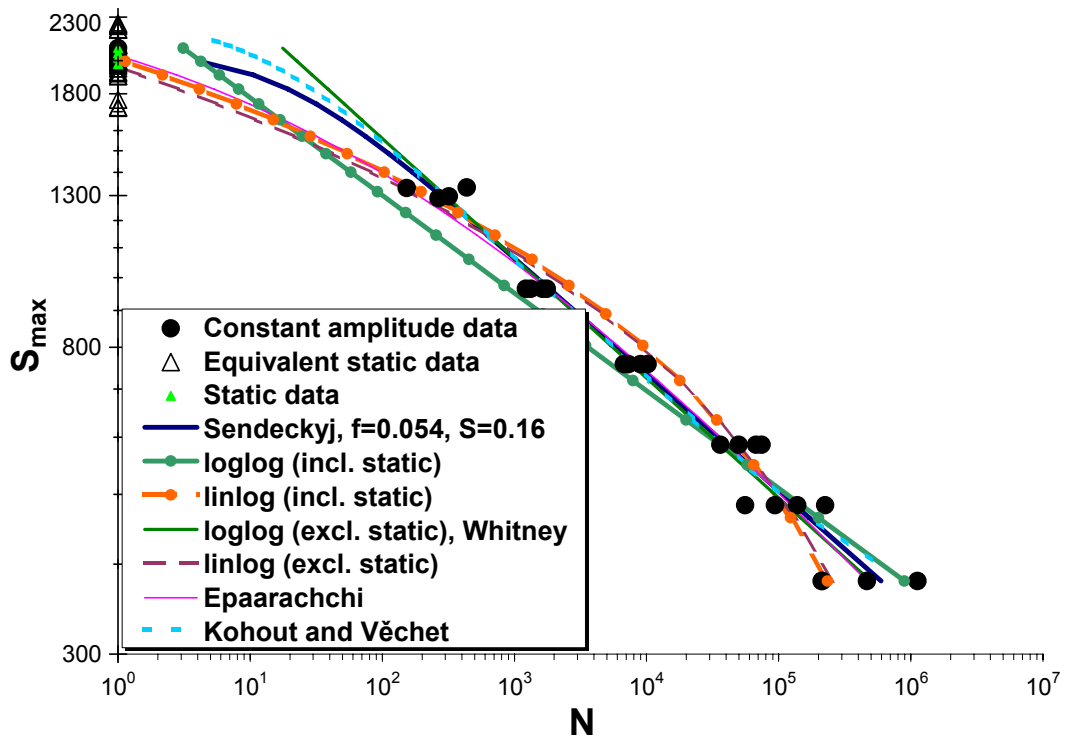
Figure 8: Various constant amplitude S-N curve fits

(0°)₈ glass/epoxy, R=0.1

In Figure 8, typical S-N curve fits are shown for both the power law and exponential formulation, using typical data (from Sendeckyj[291], 1979). Note, that the effect of including or excluding static strength will be discussed in section 2.3.4.

Historically, eq. 3 is generally referred to as the Basquin relation (coined by Basquin in 1910), eq. 4 is known as the Wöhler curve (d.d. 1870).

Spindel and Haibach[307] [1981] tabulate more (semi-)logarithmic expressions and their date of origin for the S-N curves, that were used predominantly in steels.

Echtermeyer[82] [1994] gave the parameters of a standard R=-1 strain-life log-log S-N curve, for mainly [0°, 90°, CSM] lay-ups of polyester and vinylester-glass laminates, and some criteria for its use. It seemed appropriate for laminates with more than 2% of the fibres in loading direction.

Mandell et al.[181] [1992] note, that in many cases it is difficult to distinguish which of the two expressions is the more representative form. Composites with well-aligned fibres either parallel to the (uni-axial) load direction, or at some orientation to the load direction, tend to follow eq. 4 closely, as do composites with multidirectional reinforcement, that have a life-dominating layer. More complex cases, such as woven fabrics, and chopped strand composites tend to have somewhat nonlinear S-N curves on a semi-log plot, and the most

appropriate curve fit is unclear. Woven fabric reinforcements show an even more nonlinear trend on a semi-log plot.

Bach[23] [1992] noted that a log-log expression fits 0/±45° glass-fibre reinforced data best.

Wharmby et al.[339] [2003] observed, that the stress-life relationship was best described by the lin-log expression. Interestingly, they suggested that occurrences of damage concomitant to ultimate fatigue failure of their specimens, viz. crack initiation and onset of delamination, were also described by this expression.

In the case of the existence of a fatigue limit, eq. 3 is sometimes formulated as:

$$S = S_\infty + \frac{B}{N^x} \tag{7}$$

where S_∞ is the fatigue or endurance limit stress, see Och[234] [1983].

The formulation of an S-N curve has an important influence on blade design, as was pointed out, for example, in van Delft et al.[61] [1990]. They found a design mass difference of 30% when extrapolating data to low strains using a log-log instead of a lin-log representation of the design S-N curve, and keeping all other variables constant. In a realistic design, such a mass difference would be compensated by geometrical optimisation. In a fatigue life prediction, the influence of the S-N formulation may also depend on the other parts of the prediction method. Nevertheless, their work does point out the potential significance in S-N formulation.

2.1.2 Other S-N formulations

Apart from the (semi-)logarithmical formulations described above, numerous other S-N formulations exist, some of which are described here and exemplified in Figure 8. Sims and Brogdon[296] [1977] used a modified power law relationship to fit various datasets. The formulation contains parameters that include R-value dependency. Parameters were found by minimisation of a least squares formulation, which, they noted, was not recommended outside the data range, given the large amount of fitting parameters.

$$N = \left[b \Big/ \left(S - a + cA^{-y} \right) \right]^{\frac{1}{x}} \tag{8}$$

where $A=(1-R)/(1+R)$, and a, b, x, and y are fitting parameters.

Caprino and co-workers[46, 47] [1998, 1999] formulated a two-parameter S-N formulation from a strength degradation equation, combined with the notion,

from experimental data, that the slope of the S-N curve became smaller as the R-value increased, for R>0:

$$US - S_{max} = aS_{max}(1-R)\left(N^c - 1\right)$$ (9)

The parameters a and c are coupled in the original formulation. Epaarachchi and Clausen[89] [2003] have recently expanded this to a three-parameter S-N formulation, which takes into account the dependency of stress ratio influence on dominant fibre angle, and frequency effects:

$$US - S_{max} = aS_{max}(1-\psi)^{1.6-\psi|sin\theta|}\left[\frac{S_{max}}{US}\right]^{0.6-\psi|sin\theta|}\frac{1}{f^c}\left(N^c - 1\right)$$ (10)

The parameters ψ, θ, and f quantify the R-value dependence, dominant fibre angle, and frequency, respectively.
Sutherland et al.[315] (e.g. [2005]) have adopted this formulation for the description of their detailed constant life diagram, where they reduced the R-value and frequency parameters to fitting parameters, leading to more accurate description of both static and fatigue strength in a single S-N curve, at the expense of numerical simplicity.
Kohout and Věchet[158] [2001] have described an S-N formulation, consisting of three regions. Their work clearly has a steel-connotation, the rightmost horizontal part of the curve is related to the fatigue limit. The curve basically consists of a log-log S-N curve which is bounded by two horizontal sections, with a smooth transition in between. In full, the description of the curve is:

$$\sigma = a\left[\frac{(N+B)C}{N+C}\right]^b$$ (11)

B and C are parameters describing the bounding lifetimes. The horizontal asymptotic sections require constraints on the σ-axis if the expression is to be rewritten with N as a dependent variable.
Harik et al.[115] [2002] noted, that a transition exists between low cycle fatigue and high cycle fatigue of unidirectional glass/epoxy prepregs. The 'engineering S-N curve', in their case a lin-log expression, did not fit the data suitably. The data seemed to exhibit a transitional change in slope, or 'knee'. They formulated a bi-linear semi-logarithmic S-N curve. Although the idea of physically describing the observed transition in damage mechanics is attractive, in this case a log-log S-N curve might solve part of the data fitting error.

In general, the above methods contain an assumed form of R-value dependency and should only be used with care where this dependency is not experimentally verified.

2.1.3 S-N-P curves

In most cases, the mean S-N curve is used to describe fatigue data. However, for certification purposes it may be worthwhile to describe the S-N data in terms of percentiles other than this 50% survivability line. In that case, the percentile is included in the S-N formulation, as exemplified by e.g. Och[234] [1983], or -more recently and pertaining to wind turbine materials- Kensche[153] [1994] or Sutherland[314] [2004]. Kensche used a two-parameter ε-N curve, which is essentially a log-log S-N curve with a superimposed Weibull distribution:

$$\varepsilon = \beta \frac{\left(-\ln P(N)\right)^{\frac{1}{\alpha}}}{\left((N-A)C\right)^S} \qquad (12)$$

where α and β are the Weibull parameters, and P is the percentile of interest. A and C are the slope and intercept of the log-log S-N curve. He compared predictions using 95% survivability curves to experimental data of WISPER and WISPERX-loaded coupons.

For more detailed analysis or reliable design, the probability bounds should be replaced by tolerance bounds, see section 2.3.7.

2.1.4 S-N curve parameter estimation

Linear regression
Linear regression is a common feature in most graphing software, and can be used to find the constants *a-d* in eq. 3 and 4, and some of the other S-N models.

If an automated linear regression algorithm is used, it should be certain that *(log)N* is treated as the dependent variable and that *(log)S* is treated as the independent variable, although some publications use *S* as the dependent variable, cf. Och[234] [1983]. Incorrect treatment of the data leads to a (usually small) rotation of the regression line around the mean.

The accuracy of the regression is often expressed in terms of the R^2-value. More details on linear regression can be found in any textbook on statistics. Figure 8 shows an example of typical fatigue data, fit with eq. 3 and 4 using linear regression.

Whitney
Whitney[341] [1981] fitted a log-log (power law) S-N curve to a set of fatigue data. However, he does not use 'Normal statistics' linear regression, but Weibull statistics. His procedure for data reduction consists of three distinct phases:

- Finding the Weibull shape parameter, α, and the scale parameter *N*, per stress level
- Pooling the data, assuming that the Weibull parameters are independent of stress level
- Finding the Weibull parameters for the complete fatigue dataset

Using the Whitney method requires an iterative routine to find the most appropriate shape parameter per level, before and after pooling of the data.

By definition, Whitney does not include static data. Also, at least two datapoints per stress level are needed for the algorithm to work. Preferably, more data points are needed, the pooling scheme helps to 'enlarge' the database from which the Weibull parameters are found.

Catering for run-outs, Whitney includes a correction on the pooling scheme for 'type I censoring'. This means that the tests are terminated at a predefined number of cyles. As a consequence, if one stress level contains only two points, of which one is a run-out, and run-outs are discarded, this level is discarded altogether in the process of finding α. The reason is, that it is not possible to derive an α or *N* for a single point, hence data cannot be normalised at this level and used to find the overall α and *N*.

Sendeckyj
Sendeckyj's[291] [1979] method of describing S-N data is fundamentally different from linear regression and Whitney's method in the sense that it makes use of the SLERA (Strength-Life-Equal-Rank-Assumption, section 3.4.4), thus assuming that fatigue life is uniquely related to initial static strength and residual strength. Sendeckyj's method consequently also allows using residual strength data for determining constant amplitude behaviour.

In this paper, Sendeckyj describes an iterative method to find the best fit of his wearout model to a dataset containing fatigue data, static data, and residual strength data. This procedure, which amounts to maximising the shape parameter of a Weibull describing equivalent static data, can be extended to other S-N formulations. Figure 8 also shows data, fit with Sendeckyj's expression.

Comparison of S-N parameter estimation methods
In Nijssen et al.[218] [2004], different methods of S-N formulations were compared, viz. linear regression, 'Whitney', and 'Sendeckyj'. One of the conclusions was, that the approach suggested by Sendeckyj's method can lead to different values of especially the *C* (location-) parameter when comparing results between laboratories. This depends on the type and settings of the optimisation algorithms used in parameter determination. The shape parameter and the slope at longer lifetime of the S-N curve turned out to be virtually identical for all labs, per investigated dataset. An important feature of the

method by Sendeckyj[291] [1979], viz. its potential in dealing with residual strength data, however, was not included in the analysis in this report.

A similar conclusion was reached in an earlier study, by Joosse et al.[144-145] [1993, 1994]. He preferred linear regression to the Sendeckyj method because of its relative simplicity, and because the results were very similar in the range where *log(N)>3*.

Another aspect of S-N formulation, which is not so obvious from the description of the mean S-N curve, is the statistical treatment of the data. Linear regression implies the use of a Normal distribution, whereas Whitney and Sendeckyj use Weibull distributions. These distribution types give slightly different locations of the confidence bounds.

2.2 Constant Life Diagrams
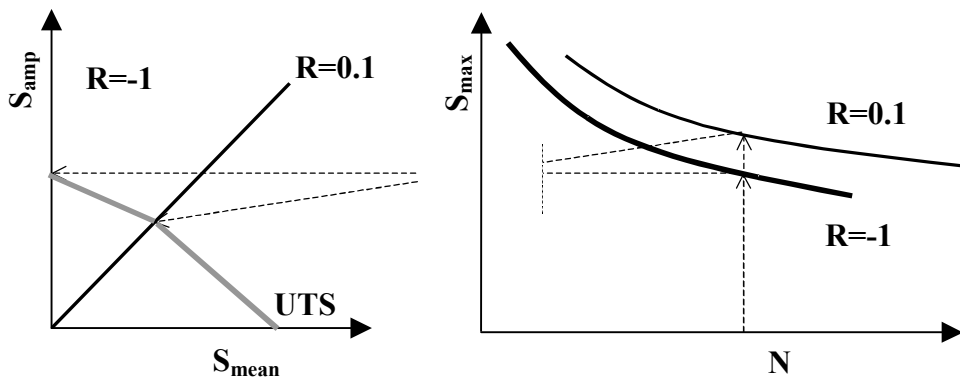
Figure 9: Construction of a constant life line from two S-N curves

The Constant Life Diagram, or CLD, is a representation of S-N data. The constant-life lines in the CLD connect points with the same estimated lifetime, as a function of the mean stress and stress amplitude. A simple example is shown in Figure 9, where the maximum stresses are read from S-N curves at R=-1 and R=0.1. These maximum stresses are converted to amplitude and mean stresses based on the R-value (in this case, S_{amp} is equal to S_{max} for R=-1, and S_{amp}=0.45 S_{max}, S_{mean}=0.55 S_{max} for R=0.1). The two points in the S_{mean}, S_{amp} plane can be connected by a straight line, and to UTS; thus a constant life line is created based upon multiple R-values (see 2.2.3).

The CLD can be seen as the projection of the constant amplitude fatigue data on a plane perpendicular to the life axis, at the N=1 mark. Figure 10 illustrates this. A three-dimensional representation of a group of S-N curves is seen, and lines connecting identical lifetimes. Each S-N curve is determined at a fixed R-value, and is therefore in a flat plane, at an angle to the horizontal plane. The different
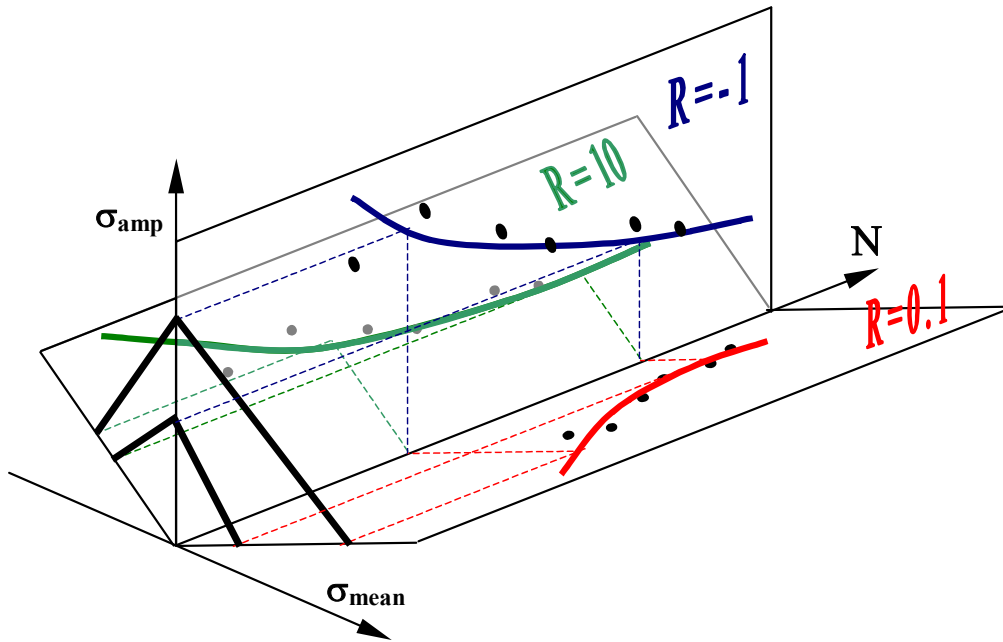
Figure 10: Schematic of relation between S-N curves and CLD

'S-N planes' all intersect with a straight line representing zero stress. This line is also the life axis.

Straight lines from the origin are lines of constant R-value, since mean stress and stress amplitude are directly proportional to each other. The ordinate is therefore co-located with the R=-1 line (zero-mean stress line).

The highest alternating stress value for N=1 (the 'top' of the CLD) is usually assumed to be on, or very near to, the ordinate.

In metals, the CLD is typically symmetric if static strength in tension and compression are the same, because fatigue mechanisms in the tensile and compressive R-value regions.

In composites, the CLD is typically not symmetric. The static strengths in tension and compression are typically not equal. In fatigue, there are different damage and failure mechanisms in tension and compression. In tension the composite is governed by fibre (in a fibre-dominated lay-up). In compression, the composite's properties are mostly determined by the matrix and matrix-fibre interaction. Sometimes, the top of the CLD lies slightly towards the tensile region for short lives, and moves towards compressive mean stresses for longer lives.

The CLD is a very useful tool for the engineer who wants to set up a lifetime prediction. In this sense, it is an indispensable summary of the material fatigue behaviour. On the other hand, one might argue that any CLD provides a very poor description of the fatigue characteristics. There are a few drawbacks in the CLD:

- Constant life lines denote mean fatigue life. The link to the actual data (which can not (easily) be plotted in the CLD) is lost, and information on scatter in the S-N curves is lost.
- The fact that the CLD, besides describing fatigue, includes regions pertaining to creep and static failure is not explicitly clear
- The CLD contains a singularity in the R-value

The first problem can be somewhat mitigated by plotting both the mean lives and some percentile or tolerance bound on life. In fact, it may be useful to use a CLD constructed from e.g. 95%/95% tolerance bounds as a basis for life prediction, see e.g. Sutherland and Mandell[314, 315] [2004, 2005].

As for the second problem, the abscissa represents the R=1 line. This seems misplaced in a diagram describing fatigue, for R=1 is a constant creep load rather than a fatigue load. Extending constant life lines to the abscissa is questionable. For how is a lifetime in terms of number of cycles related to a lifetime expressed in units of time? In practice, when limited information in the all-tension or all-compression régime is available, all constant lifelines are assumed to converge to the ultimate tensile or compressive strength on the abscissa. The detailed CLD by Mandell et al.[188] [2003], including 'creep failure', was created by relating number of cycles to failure to time to failure via a constant frequency.

Also, the N=1 line, which is often included in the CLD, represents static failure. As seen in 2.3.4, static failure might be related to the low-cycle fatigue behaviour, and as such should be included in the S-N curve and the CLD. On the other hand, questions exist about including static data in the S-N curve, discussed in 2.3.4.

Finally, a singularity occurs travelling from the all-compressive region of the CLD to the tensile-compressive region. Here, the R-value jumps from $+\infty$ to $-\infty$. In the case of numerical implementation of the CLD, this singularity should be taken into account.

Finally, the CLD typically includes the N=1 constant life line (static). However, the very low cycle fatigue region (up to 10^3 cycles) is not relevant for most load spectra, and including these life lines in the CLD can lead to distortions of the diagram. It is recommended to plot only constant life lines from around 10^3 cycles.

Boller[36] [1969] plotted the constant life diagram differently, in a way slightly more intuitive with regards to the position of compressive and tensile regions. This form of the CLD was also used by other authors, such as Berkovits and Fang[29] [1993].

Sutherland[311] [1999] observes, that constant life diagrams for metals are symmetric, whereas for composites they are distinctly not, although the degree

of non-symmetry depends on the method of compressive fatigue testing (anti-buckling guide). In a summary of fatigue performance of wood and polymer matrix composites by Ansell et al.[17] [1993], they note, that the shape of CLDs for wood and polymer matrix composites is similar. Most of the fatigue data are offset to the tensile side of the CLD, and the maximum occurs close to the R-value R=UCS/UTS.

Below, several formulations for the CLD are discussed in detail. These will be used in the predictions of Chapter 5.

2.2.1 Linear Goodman diagram

The classical Linear Goodman diagram is the most commonly used CLD because of its simplicity. For any cycle type with mean stress s_{mean} and stress amplitude s_{amp}, an equivalent stress amplitude s_{eq} at R=-1 is derived according to:

$$s_{eq} = \frac{s_{amp} \cdot UTS}{UTS - s_{mean}} \qquad (13)$$

$$s_{eq} = \frac{s_{amp} \cdot UCS}{UCS - s_{mean}} \qquad (14)$$

These formulas follow from Figure 11. In this figure, the abscissa represents both s_{mean} and R=1. The ordinate represents the R=-1 line. The other lines are lines that connect points in the s_{mean}, s_{amp}-space with equal lifetime. As a
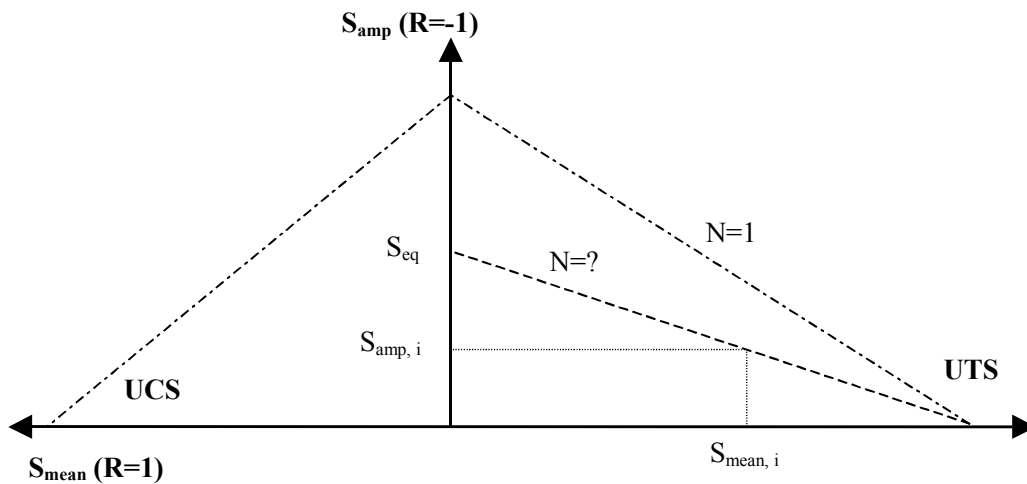
Figure 11: Linear Goodman Diagram

bounding constant life line, the N=1 line is included in the figure.
The equivalent stress, found from these formulations, is input in any S-N definition describing the S-N curve at R=-1, and the allowable number of cycles N_i for this particular cycle type results from this.

In his historical review, Sendeckyj[292] [2001] points out, that the name Goodman is unjustly connected to this form of the constant life diagram, as not Goodman, but Haigh was, apparently, the first to plot stress amplitude versus mean stress. Moreover, Fidler was the first to propose a theory called 'dynamic theory' for the design of bridge members, which Goodman later processed into his popular engineering book, and was credited for by later authors. Thus, it would be more correct to refer to 'the Haigh representation of the constant life diagram, showing a linear formulation of the dynamic theory'. In keeping with common practice and for purposes of readability, the terms 'constant life diagram' and 'Linear Goodman diagram' or 'Linear Goodman Formulation' will be used here, with the above note as a reminder of the incorrectness of this terminology.

2.2.2 Shifted Goodman diagram

In the most recent design requirements by Germanischer Lloyd[102] [2004] (GL), the linear Goodman diagram (GL[101], 1993) was replaced with a 'shifted' version from a Dutch pre-standard[210] [1999]. Compared to the classical Goodman diagram the top has moved to the right, to the geometric mean of UTS and UCS, and for N=1, the amplitude is equal to the average of UTS and UCS, see Figure 12.

As in the Linear Goodman diagram, all mean and amplitude stresses are converted to an equivalent amplitude. The allowable number of cycles is related
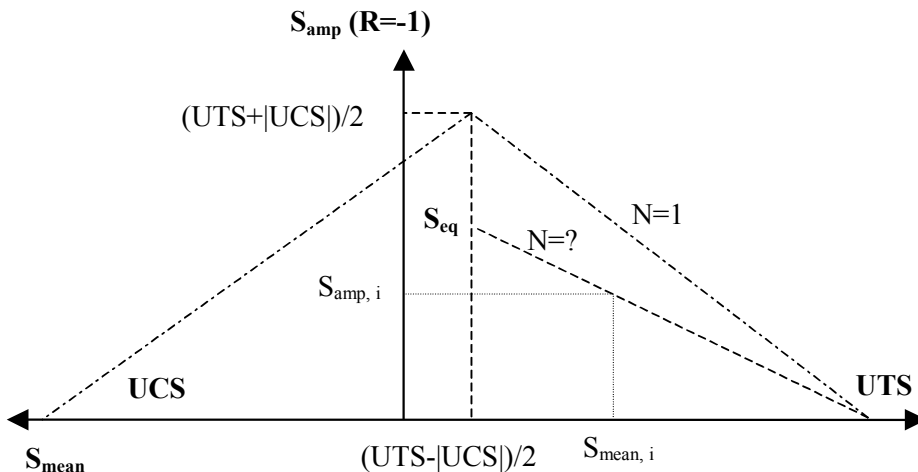
Figure 12: Shifted Linear Goodman Diagram

to this amplitude via experimental data at R=-1 (without GL's partial safety, static, and fatigue reduction factors):

$$N = \left[\frac{UTS + |UCS| - \left|2 \cdot s_{mean} - UTS + |UCS|\right|}{2 \cdot s_{amp}} \right]^{\frac{-1}{d}} \quad (15)$$

This formulation of the Goodman aims to reflect the asymmetry in the CLD that is evident from detailed experiments, while maintaining the simplicity that is an attractive feature of the Linear Goodman diagram. An important simplification is evident from Figure 12: the R=-1 line does not radiate from the origin, but it is parallel to the ordinate.

2.2.3 Multiple R-value CLD

The linear Goodman diagram and the shifted linear Goodman diagrams are both based on the availability of R=-1 experimental S-N data only. If more S-N curves are available, these can be incorporated into the CLD. This means, however, that simplified mean stress formulations, as given in equations 13-15, are no longer applicable. Instead, the CLD needs to be interpolated between R-values. Usually, this is done by straight lines connecting equal lives, see Figure 13. Depending on the type of S-N formulation, this interpolation can be done analytically, or needs some regression or optimisation algorithm, such as the one proposed by Philippidis and Vassilopoulos[258] [2004].

In order to avoid or mitigate multiple R-value experiments, while at the same time having an accurate description of the CLD, simplified analytical formulations have been proposed. An example is the multi-parameter semi-empirical fatigue model that was proposed to describe the CLD by Bond[37] [1999]. Harris et al. (cf. Ansell[17] [1993]) have proposed a parabolic expression
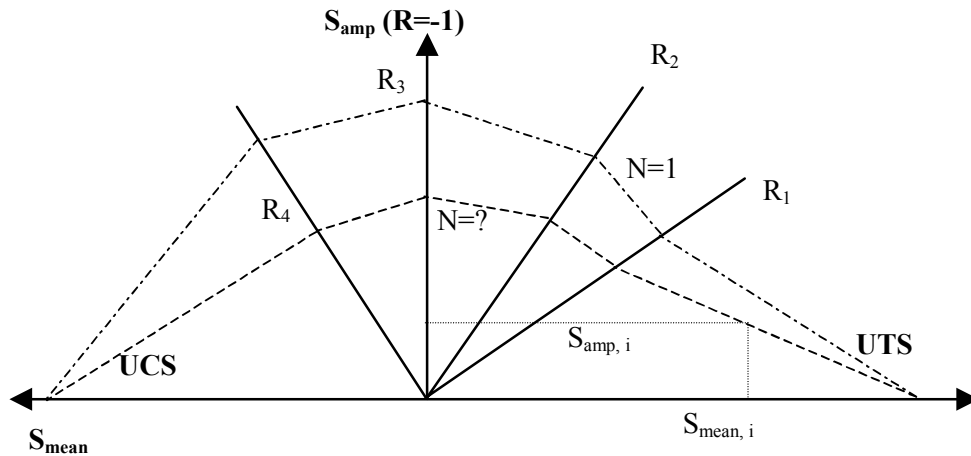
Figure 13: Multiple R-value CLD

to fit data in the CLD from their work on carbon fibre composites:

$$\frac{s_{amp}}{UTS} = f\left(1 - \frac{s_{mean}}{UTS}\right)\left(UCS/UTS + \frac{s_{mean}}{UTS}\right) \tag{16}$$

This was later developed into (Adam[2], 1986, Beheshty[27] 1999) augmented this to:

$$\frac{s_{amp}}{UTS} = f\left(1 - \frac{s_{mean}}{UTS}\right)^u \left(UCS/UTS + \frac{s_{mean}}{UTS}\right)^v \tag{17}$$

where f, u and v are fitting parameters. Basically, f can be used to scale the basic parabola to fit different median lives, and u and v are slope parameters in the tensile and compressive mean stress regions, respectively.

A multislope formulation of the CLD was proposed by Boerstra[32] [2005], with essentially the same functionality. The formulation originally abandons the classification in R-values. However, it can be modified to follow the traditional terminology.
A noteworthy aspect of the associated methods used to obtain the model parameters, is the fact that they utilise all fatigue data for developing the constant life lines. Thus, the constant life description at any R-value is determined not only from the data at that R-value, but using the data at all other R-values. This potentially allows for detailed CLD-formulation at minimum experimental effort. However, this depends on the actual complexity of the CLD and the formulation and regression method needs to be validated for the material in question.

2.2.4 *Equivalent stress level*

A life prediction method that seems to work well for some experiments, and is very useful in design practice to compare the severity of load spectra and failure of different designs to one another, is the translation of a load spectrum into an equivalent constant amplitude load.
A method, sensitive only to ranges, was proposed by Dover[77] [1979], introduced for composites by Amijima et al.[9] [1982], and applied to rotor blades by Brøndsted[39, 40] [1997, 2005]. It was also used in determining the load spectrum test specification for the OPTIMAT project (Krause[161], [2005]). To account for the effect of mean stress, the equivalent load is related to constant amplitude fatigue load at a predefined R-value, which leads to the same number of fatigue cycles as the number of cycles in the variable amplitude spectrum. The equivalent stress method is derived from basic log-log S-N curve formulation, a standard equivalent load method, and Miner's summation. The most important

assumption is, that for each load cycle type *i*, the parameters *C* and *m* are equal (the expression $N \cdot S^m = C$ is used). The R-value chosen influences the predictions via *m*. In the case of regular spectra, i.e. with small variations in constituent load characteristics, the equivalent load can be useful in estimating fatigue life. Since it is derived from Miner's summation, it does not take account of sequence effect. Because use is made of a reference R-value, changes in failure mode, that may occur in a spectrum containing both tensile and compressive loads, are not taken into account.
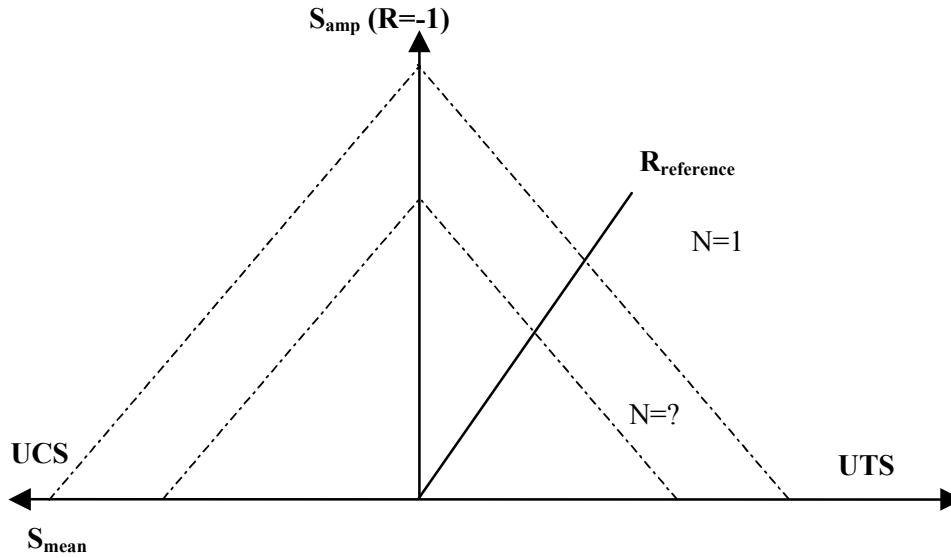
Figure 14: Equivalent load method CLD

The full derivation is given in Brøndsted[39, 40] [1997, 2005]. The equivalent stress level is defined by:

$$S_{eq} = \left(\frac{\sum n_i S_i^m}{\sum n_i} \right)^{\frac{1}{m}} \left(\frac{1}{M} \right)^{\frac{1}{m}} \tag{18}$$

where

S_{eq}	=	Equivalent maximum stress at selected R-value
S_i	=	Maximum stress at cycle *i*
n_i	=	Number of cycles with S_i
M	=	Value of Miner's sum at failure (usually 1)
m	=	Slope of the S-N curve at selected R-value

Because of the main assumption in this method (C_i and m_i equal to *C* and *m* for the reference R-value for all cycle types), it can be seen as a different

formulation of the constant life diagram, rather than as a formulation of the damage accumulation rule. The constant life diagram, which results from equal S-N curve parameters consists of lines at a 45° angle through the reference S-N curve, and is symmetric with respect to R=-1. The constant life diagram arising from the equivalent load method is shown in Figure 14.

Thus, instead of using equation 18, this alternative constant life diagram in combination with Miner's sum can also be used, with identical prediction results. Life estimates with the equivalent stress method are also included in the predictions of Chapter 5.

This formulation assumes, that the failure mode for tension and compression fatigue is equal, as long as the load amplitude is equal. For composites, this is an unrealistic assumption.

van Delft et al.[68, 69] [1996, 1997] have calculated WISPER(X) life predictions using a modification of the linear Goodman diagram using parallel lines instead of lines converging at the mean stress axis. This was elaborated in Nijssen et al.[211-213] [2001, 2002], and although the modification was not based on physical considerations, this seemed to give satisfactory results. Later work from a different laboratory and on a different material did seem to indicate a tendency for CLD lines to be parallel near the mean stress axis, albeit with a convenient transformation of creep data to fatigue lives (Sutherland[314], 2004).

2.3 S-N curve and CLD issues

2.3.1 Stress versus strain, and control mode

When composing his construction from individual layers, the designer would like to have design rules that are based on strains rather than stresses. Strains are equal for all layers (in the structural reference frame of a uniformly, uni-axially loaded laminate).

However, the data that the experimenter provides are usually expressed in terms of loads or stresses. This is a consequence of the constraints on most common fatigue equipment, which favours either load controlled or displacement controlled experiments. This means that the controller maintains either a constant cyclic load, or a constant cyclic displacement. Typically, fatigue damage increases in the specimen, and stiffness decreases. As a result, strain increases in the load controlled test, and, inversely, the load decreases in the displacement controlled test. Theoretically, if a strain measuring device is mounted to the structure, strain-controlled testing is feasible, but in practice it is hardly ever used. Early failure of strain gauges, and the susceptibility of clip-on type extensometers to slip or detach from the specimen might lead to significant distortions or discontinuities in their output signal, potentially causing the test to fail or become unreliable when using strain-controlled testing, and hampering

long-term strain measurements. The load cell or displacement sensor are less susceptible to these errors and are therefore much more commonly used to give feedback to the control equipment.

Most constant amplitude fatigue tests are load controlled, so that the stress characteristics (mean and amplitude) remain constant throughout the test. The strain and grip displacement is prone to changes, with two main causes:

- decrease of the modulus
- wear of the specimen-grip interface

Ryder and Walker[273] [1976, p. 208] asserted, that the difference in mechanical response (fatigue) might be more easily correlated on the basis of strain to failure, than ultimate stress. This conclusion was drawn from a comparison of two laminates, which had distinctly different stress-strain curves (linear vs non-linear).

Joosse and van Delft[145] [1994] analysed data from the FACT database, and noted, that when presented on a stress-based normalisation, the data showed less scatter than when plotted on strain-base. In another publication[144] [1993], they considered the analysis of FACT data in more detail, and stated that normalisation by stress was debatable, since the static failure mode is different from that at high-cycle fatigue. Furthermore, the normalisation method should take into account differences in test specimen shape and test speed for static tests compared to fatigue tests. Normalisation with compressive strength was observed to be especially sensitive to these effects, and, from a practical point of view, less feasible because compressive static data are generally less abundant than tensile data. They concluded, that normalisation generated less problems, when strain data are used.

In this work, due to the fact, that load-control was used in the fatigue tests, normalisation is best done using 'initial strain'. In practice, normalising with stress was found to be equally appropriate. Mandell and co-workers use normalised (by static strength) S-N diagrams extensively to compare materials, e.g. [189].

2.3.2 *Anti-buckling guide*

An anti-buckling device may be required to obtain the compressive properties if Euler buckling is suspected or observed in compression testing of some coupon geometries. Using a simple anti-buckling guide was not sufficient to increase the compressive static performance of the OPTIMAT coupons, and was not recommended[333]. Previous European projects have made use of an anti-buckling guide (ABG) for compressive (fatigue) tests (Kensche[154], 1996). Note, that Sutherland[311] [1999], from a comparison of European and US fatigue data in a constant life diagram, has theorised that an anti-buckling guide is likely to affect

the symmetry of the constant life diagram. In the current work, an anti-buckling guide was not used.

2.3.3 Fatigue limit

Despite the fact, that the existence of a fatigue limit is 'limited' to ferrous steels and titanium in constant amplitude fatigue, many researchers have attempted to find the fatigue limit in composite materials. Especially early research is characterised by a general tendency to treat the novel advanced composites as metallic materials. Historically, this is no surprise, as materials research laboratories shifted their attention from metals to composites.

To date, the existence of a fatigue limit has not yet been established in composite materials. Thus, every load cycle should be considered as damaging, although, due to the high initial strength and low slope of typical composite S-N curves, fatigue life at low loads can be extremely long, which hampers the detection of a fatigue limit.

Hypothetically, the non-existence of a fatigue limit in composite material is sensible. In steel, a certain force is needed to initiate slippage in the internal crystal structure. Below a certain load, no fatigue occurs. Thus, for the virgin material, one assumes a fatigue limit, but for a structure one assumes the absence of a fatigue limit. Since composite materials can be regarded as structures rather than materials, the absence of a fatigue limit makes sense.

In addition, the crack initiation mechanisms in composites are, due to their general structure and processing techniques, likely to occur before completion of the composite part, i.e. in the mould, due to residual stresses that are a result of the manufacturing process and differences in thermal expansion coefficient of the composite's constituents, see e.g. Kiasat[156] [2000].

Interesting data are provided by Boller[33] [1964]. He tested glass/epoxy, using three different resin systems and a [±5°] and [0°,90°] lay-up, for R=-1 fatigue performance. The slope of his S-N curves is comparable to those found in the OPTIMAT project (chapter 4.2). His data show a flattening of the S-N curve near 25% of the static strength (even on a log-log plot), suggesting a fatigue limit (see Figure 15; the data at and beyond 1 million cycles are run-outs).

Oldyrev[237] [1972] related the 'fatigue strength' to the inflection point in the static stress-strain diagram of the laminate. He used a pseudo-fatigue limit, i.e. the stress at which a coupon reaches a predefined number of cycles, in the case of Oldyrev 10 million.

Ryder and Walker[273] [1976] tested two laminates in tension-tension, and tension-compression fatigue, and although they noted that it was not definitely proven, a fatigue life endurance limit appeared to exist.

Chou et al.[53] [1980] speculate, on limited available data, that no fatigue limit exists for composite materials. They recommend, that a pseudo-fatigue limit be used.
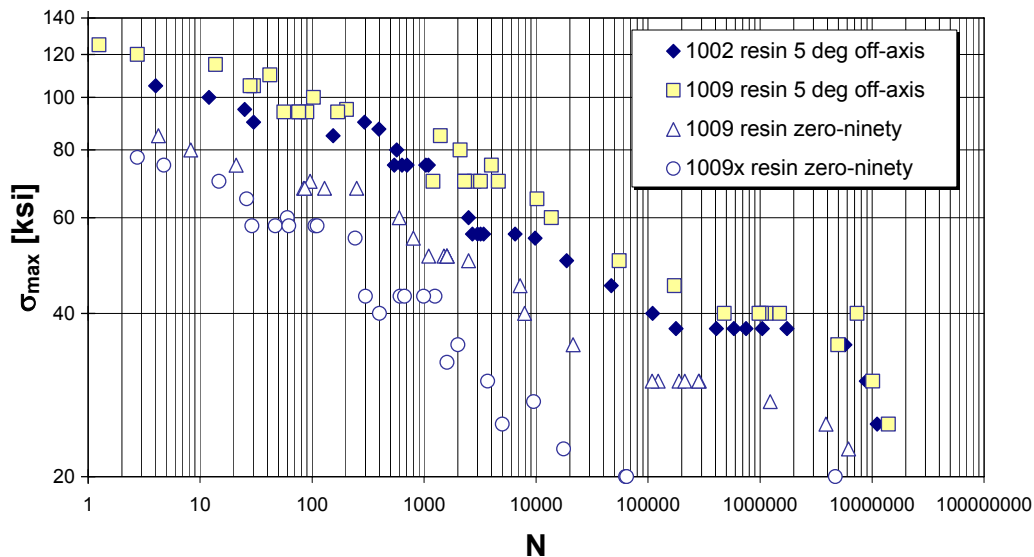
Figure 15: Early composite fatigue data from Boller[33] [1964]

Wang and Chim[331] [1983] did not find a 'cyclic stable state' in random short fibre SMC composite coupons; loaded in tensile fatigue.

Talreja[317-320] [1981-1985] speculated extensively on damage mechanisms and resulting fatigue behaviour of various composites and corroborated his theories with data. He discussed unidirectional, off-axis, and angle ply laminates, and, among other aspects of the S-N diagram, discussed fatigue limits. Basically, he assumed the existence of a fatigue limit, albeit at a low strain level. For unidirectional materials, he theorised, that the fatigue limit of a laminate would be determined by the fatigue limit of the matrix material, and that, for off-axis materials, the fatigue limit of the material would consequently be lower (since the fibre would more and more be seen as a 'crack'). In practice, most composites, even the unidirectional laminates, have some off-axis material to keep the dry fabric intact during handling/manufacturing. Thus, based on the hypothesis of Talreja, it might be argued that, since the presence of 'pre-cracks', e.g. formed by stitching or voids, is virtually unavoidable, the fatigue limit will be low. He took a value of 0.1% as the limiting value of strain for fibre debonding from the matrix. He noted, that Owen[241] [1974] had demonstrated a value of 0.12% as a safe strain limit to avoid the debonding of short fibre composites (i.e. matrix dominated) up to 1 million cycles. He added, that if avoidance of debonding were to be part of the design criteria, this would impose serious limitations.

Apart from unidirectional and off-axis materials Talreja[317] [1981] also discusses angle-plied laminates, which are sensitive to delamination. He also provided tentative strain values for matrix cracking (determining the fatigue limit in unidirectional materials), fibre debonding (which governs the onset of fatigue damage in cross-plies), and delamination (which may correlate with the fatigue limit in angle-ply laminates). The strain values were 0.6%, 0.1%, and 0.46%, respectively.

Foley et al.[94] [1983] noted, that the existence of a fatigue limit was uncertain, but for angle ply laminates, there was a tendency for the S-N curve to flatten out.

Och[234] [1983] presents estimates for the fatigue limits of several materials relevant to aerospace and helicopter engineering, among which the bending fatigue limit and interlaminar shear fatigue limits of unidirectional glass and carbon laminates.

Mandell[180] [1990] warns about misinterpretation of S-N data tested at frequencies that are too high. When testing at a fixed frequency, the high-load data may reach temperatures (due to hysteretic heating), which cause the coupon to fail thermally, rather than in fatigue. When a significant increase in fatigue life is seen at lower load levels, this gives the impression of a fatigue limit, whereas it is rather a result of the shift from thermal failures to fatigue failure.
Limited data are available for high-cycle fatigue (~10^8 cycles), although Mandell et al.[187] [2002] have performed single strand high frequency tests up to 10^{10} cycles using modified subwoofers as testing equipment. Van Delft et al.[62, 64, 65] [1993] and Mandell agree on the uncertainty of the existence of a fatigue limit.

Bach[21] [1990] suggested, from constant amplitude fatigue tests on rotor blade composites, that any potential fatigue limit would be in the very high cycle range (>10^9) and low load (<0.15 UTS). More specifically, for R=0.1 the fatigue limit could be expected at 0.3% strain, and at 0.2% strain for R=-1 in the case of unidirectional laminates. For diagonally reinforced laminates, the fatigue limit was expected to be 0.1% lower for both R-values. In a later report, he noted no indication of a fatigue limit in 0°/±45° GFRP.

Summarising, from more than 30 years of research by various scientists on various different composite laminates, no fatigue limit has been proven to exist. The existence of a fatigue limits seems unlikely in composite materials, or irrelevant in the range of cycles encountered in practical applications. This implies, that every load cycle has a potential damaging effect on a composite structure, and should be taken into account in life prediction calculations.

2.3.4 Inclusion of static data

An ongoing discussion concerns whether or not to include static data in the S-N diagram. It seems, that neither the inclusion of static data, nor their exclusion can be justified. An enumeration of the arguments pro and con:

Pro:

- Static data are fatigue specimens which failed in the first load cycle
- Including static data in the linear regression diminishes inconsistencies in low-cycle region
- S-N formulations that describe both static and fatigue have the potential of simplifying experimental programmes and life prediction, since fatigue behaviour can be described by static strength and a slope parameter

Con:

- Static strength is usually not obtained at strain rates congruent with fatigue strain rates
- Including static data might cause the fatigue life to be poorly represented for certain ranges of cycles
- Static and fatigue failure modes are often distinctly different
- Models which include the static strength require more parameters to model the material's behaviour

Strictly speaking one might consider static data as fatigue data which have failed within the first fatigue cycle, with maximum peak equal to the ultimate stress. As such, a static test can be included in the S-N diagram at N=1, or at N=0.25, assuming the fatigue load follows a sine wave signal and fails in the tensile part.

If the S-N curve parameters are derived from fatigue data in the range, say, 10^3-10^6, the resulting S-N curve might intercept the S_{max}-axis at values different from ultimate strength. For example, the ordinate-intercept could be above UTS for R=-1 and below UTS for R=0.1. This is obviously not realistic and is likely to distort the constant life diagram. Inclusion of static data diminishes such inconsistencies. On the other hand, it can cause the S-N formulation to accurately represent static data, but poorly predict fatigue life for certain cycle ranges. This is seen in Figure 8. Compare the log-log and lin-log fits, which are plotted either including or excluding static data. Especially for the log-log formulation, the fit completely misses the static data if these were excluded from the linear regression, or poorly matches the fatigue data if the static data were included in the fit.

If both static- and fatigue behaviour could be described by a unique linear expression, this would greatly simplify the life prediction formulations and

minimise experimental effort. Such an expression would allow the fatigue life to be described by the static strength and slope parameters of the S-N curve formulation. Germanischer Lloyd recommends this, if no detailed data are available, GL[102] [2003].

Due to the strain rate sensitivity of some materials, it is recommended to allow inclusion of static strength data only in cases, where the static strengths have been obtained at strain rates comparable to the strain rates seen in fatigue. Often, S-N curves are obtained at fixed frequencies in the order of ~10 Hz, yielding strain rates that are an order of magnitude above the strain rates in static test recommendations (~1 mm/min). Then, any strain rate effect may complicate plotting static and fatigue data in a single diagram. In situations where strain rate is lower, for higher maximum strain level, as is the case in the OPTIMAT project, the comparison of fatigue strain rate to static strain rate is more justified.

Typically, no S-N formulation describes both the static and fatigue data with a single expression and is numerically robust (see 2.1.4). Linear regression is a simple and straightforward method, but examples show, that static data and fatigue data are usually not connected by a single line, even when static data are collected at 'fatigue' strain rates. Models would be needed, that employ more parameters to facilitate inclusion of static data, such as the wearout model described by Sendeckyj, but the model parameters are sensitive to convergence criteria.

A practical argument against the advantages of including static data, is the fact that in most fatigue calculations, low-cycle fatigue is of little or no interest, given the long design fatigue lives. In some cases, it is fully justified to disregard low-cycle fatigue altogether and use a constant life diagram which starts at 10^3 cycles. On the other hand, in variable amplitude fatigue some high load cycles (e.g. 50 year gusts) might need to be accounted for.

A fundamental argument against inclusion of static data is, that a static failure cannot be compared to a fatigue failure, due to the different failure mechanisms. There are, in fact, several examples in the literature where modifications of a laminate proved deleterious for the fatigue performance, with little or no loss in static strength. Mandell et al.[185] [1999] have done studies where they advertently raised or lowered local resin content and presented knock-down factors for both fatigue and static performance. They noted that locally increasing fibre volume improved static performance, but could be detrimental for fatigue performance. Similarly, Konur and Matthews[159] [1989] concluded from their review that composites with improved constituents, such as high strain fibres and matrices, do not necessarily show an improvement in fatigue life. These examples indicate, that it seems incorrect to describe both fatigue and static failure by a single line.

Static and fatigue failure mode may be more consistent for matrix dominated composites than for fibre dominated composites, and the difference in failure

mechanisms also depends on the type of fatigue test. Including static tensile strength in an R~-1 S-N diagram is less valid than including it in an R=0.1 S-N diagram, since in the first case, failure is more likely to be induced by delamination.

Wahl[328] [2001] shows some constant life diagrams for which both Wöhler (power law) and Basquin (exponential) relations have been used, in- and excluding static data. No conclusions as to which method is more appropriate is drawn from his data.

Mandell[180] [1990] did note a dependency of slope on static strength. The higher the initial strength, the higher the slope of the S-N curve (log-log fit, see 2.1.1).

Echtermeyer[82] [1994] excludes static data from the formulation of his standard ε-N curves, because failure mechanisms at high strains are not relevant to long lifetimes.

Summarising, although inclusion of static data can help interpolation of the S-N formulation in the low-cycle region, there are both fundamental and practical obstacles preventing the inclusion of static data. It is therefore recommended not to include static data in the S-N curve derivation. This implies, that low-cycle fatigue can also be excluded from plots of constant life diagrams.

2.3.5   Effect of rate

A topic, which is related to section 2.3.4, is strain rate of the static and fatigue tests. The residual strength tests of the OPTIMAT and MSU test campaigns (sections 4.2.5, 4.3.5) are all carried out at static loading rates. The literature suggests, that, at higher loading rates, static strength may be higher. Therefore, the residual strength degradation model is potentially conservative, since the residual strengths from the test programme are likely to be lower than the residual strength that might be measured in a variable amplitude operational loading condition. In order to validate the strength degradation model in life predictions, some influence of loading rate should be taken into account in the spectrum life prediction with the residual strength model. The magnitude of this loading rate correction, as estimated in the literature, and established for the standard OB specimens, is the subject of the following paragraphs.

Static strain rate

Kujawski and Ellyin[167] [1995] stated, that fibre dominated failure modes are not sensitive to rate or frequency dependence in fibreglass/epoxy laminates. For matrix dominated failure modes, they expected rate or frequency dependence due to the viscous nature of the resin, and they found rate and frequency effects for ±45° fibreglass/epoxy laminates. They did not test a fibre dominated material. Shah Khan et al.[293] [2000] subjected woven glass-fibre reinforced composites to increasing compressive strain rates. They found increasing maximum stress for strain rates up to 1/s. For higher strain rates, they found a decrease in maximum stress which they found difficult to explain. For short

fibre composites, the relationship between logarithm of the strain rate and maximum stress was linear for polyester and vinylester. Okoli and Smith[235] [2000] investigated the influence of strain rate on Poisson's ratio and found none. In the same article, increase in maximum stress of roughly 10% per decade increase in strain rates are reported. Okoli[236] [2001] has observed increased failure energy for tensile tests at high strain rates. For tensile failure energy, he measured an increase of 17% per decade increase in the log of strain rate.

Over a comparable range of strain rates, for the OPTIMAT standard specimens, Nijssen[219] [2004] has observed increased maximum stress and strain in static tests done in tension and compression, at a loading rate of ca. 700 times higher than for the standard static test procedure (at ISO-compatible loading rate). The MD and UD materials showed similar behaviour at high strain rates. He visualised trends, indicating, that static strengths increased for higher loading rates. No significant influence on the modulus was measured. Similar findings for the DOE/MSU materials were recorded by Samborsky[276] [1999], who describes strain rate sensitivity of different materials using a linear relationship between maximum tensile stress and the logarithm of the strain rate:

$$US = US_0 + a \cdot log\left(\frac{d\varepsilon}{dt}\right) \tag{19}$$

where US_0 is the intercept with the ordinate, and a is a regression constant. This is consistent with Eyring's[91] [1936] model of viscosity, which suggests that yield stress varies linearly with the logarithm of strain rate.

Samborsky[276] also provides data for compressive strength, and noted similar strain rate effects as for the tensile case, i.e. increasing stresses and strains for increasing loading rates. In practice, the increase in static strength was in the order of 5-15% per decade of strain rate.

No relevant data were found in the FACT database.

Fatigue strain rate

In fatigue, the effect of frequency seems to be the result of whichever phenomenon is most influential; time at load, or temperature rise due to heating of the coupon.

For cyclic loading at a given amplitude, the temperature depends on the loading frequency, due to mechanical energy dissipation and heating from grip friction. A higher frequency will lead to shorter fatigue lives if heat cannot be dissipated adequately through external cooling, and internal heating raises the temperature of the test article to inappropriate levels. In the OPTIMAT project, a significant frequency effect was encountered, where high frequencies for high load amplitudes led to unacceptably short fatigue lives. This was attributed to the temperature rise in the coupon (section 4.2.4). James et al.[136] [1968] found a

sensitivity of glass/epoxy to frequency, which was most pronounced in the high-stress-low-cycle region (flexural fatigue), and diminished at lower strain ranges. They do not discuss if this is caused by time at load (creep) or internal heating, but the latter seems to be the most relevant, since full-reversal loads were applied, and higher frequency led to a lower lifetime. This suspicion is reinforced by the fact, that fatigue lives converged at lower strains. Sensitivity to frequency has been reported for tensile fatigue of different graphite lay-ups by Curtis et al.[56] [1988], who reported considerable frequency sensitivity of carbon-PEEK, which they noted resulted in shorter fatigue lives with larger temperature rise in the laminate.

For non-zero mean loadings, however, frequency sensitivity may also be related to creep sensitivity. The higher the frequency, the shorter the time-at-load, the longer the fatigue life is in terms of number of cycles, when time-at-load is dominant. It is assumed that additional effects, such as stress corrosion in the glass-fibres as described by Kim and Ebert[157] [1979], can be excluded. Creep is matrix dominated; in glass-fibre dominated lay-ups, the creep sensitivity is expected to be negligible.

Amijima et al.[9] [1982] found, that for a glass-fibre/polyester coupon tested at R=-1, between 0.1 and 20 Hz, lower frequency yielded longer fatigue lives, but the S-N curves converged around 10^7 cycles (when extrapolated with a log-log S-N curve).

Saff[274] [1983] showed for tension fatigue on $[\pm 45°]_{2s}$ laminates, and for R=-1 fatigue on a fibre dominated and a matrix dominated laminate (all graphite/epoxy), that lower frequency resulted in shorter lifetimes, which was slightly more pronounced for the matrix dominated laminate. He showed a positive correlation between the ratio of cycles at high frequency to the cycles at low frequency, and the ratio of calculated shear stress versus axial stress.

Ellyin and Kujawski[85] [1995] noted, that for matrix-dominated lay-ups, a time-at-load type frequency effect exists. Fibre-dominated materials do not exhibit rate or frequency sensitivity. They investigated the effect of frequency for $[\pm 45°]$ laminates, and found, that at low stresses, the cyclic creep rate increased with lower frequency, resulting in shorter fatigue lives. At high stresses, this trend was opposite, and they indicated, that at higher loads, the influence of temperature would be more pronounced. Later, El Kadi and Ellyin[84] [1994] found no frequency effect in off-axis 45° laminates.

Summarising, the effect of static strain rate is an increase in apparent strength. The static strain rate should therefore be specified if static data are plotted in an S-N diagram or in a residual strength plot.

Higher fatigue frequency or strain rate leads to lower lifetimes in OPTIMAT glass coupons investigated in this work, which was suspected to be a heating issue. Other authors have seen various influences of fatigue frequency.

The static and fatigue frequency are an important part of the S-N description given their influence on strength and lifetime.

2.3.6   Scatter

Variation in fatigue life and static strength is unavoidable for populations consisting of multiple coupons. The following paragraphs discuss *scatter* in terms of:

- typical scatter in strength and life
- potential sources of scatter
- characterisation of scatter; best descriptors of distributed data

Typical scatter values

Typical values of static scatter in glass-resin composites are generally within ±10% of the mean value. The degree of scatter is related to failure mode. Tensile tests tend to have less scatter than compressive tests. This could be attributed to the variations in bending or buckling between the individual tests. Partially, scatter is also inherent to the material production.

In the OPTIMAT programme, extensive static data were collected, allowing for an assessment of scatter in wind turbine rotor blade composites. The test characteristics and results are discussed in chapter 4.2. Two exemplary probability plots are shown in Figure 16.

This plot displays the cumulative failure probability versus static load. In addition, it contains information on the parameters of Normal distribution (mean μ and standard deviation σ) and a two-parameter Weibull distribution (scale and shape parameters α and β), fit through the data using linear regression in a transformed probability plot. In addition, the corresponding cumulative distribution functions are plotted, as well as the lognormal distribution function. For each distribution function, the goodness-of-fit is expressed in terms of the Kolmogorov-Smirnoff (K-S-)distance parameter (see e.g. NIST[228], 2005). Essentially, this is the largest difference between the data and the distribution function fit. The values of the K-S parameter are given in the legend, between brackets.

For fatigue, a typical value of scatter in glass/epoxy are, roughly, one decade. Ryder and Walker[273] [1976] tested two different laminate in tensile, tension-compression fatigue, and in tensile and compressive (residual) strength. They noted, that there was considerable difference in the scatter in the two laminates.

Chou et al.[53] [1980] give typical fatigue scatter of three decades for graphite/epoxies, with a Weibull shape factor of about 1-2 for general laminates, and even lower for unidirectional laminates ~0.4.
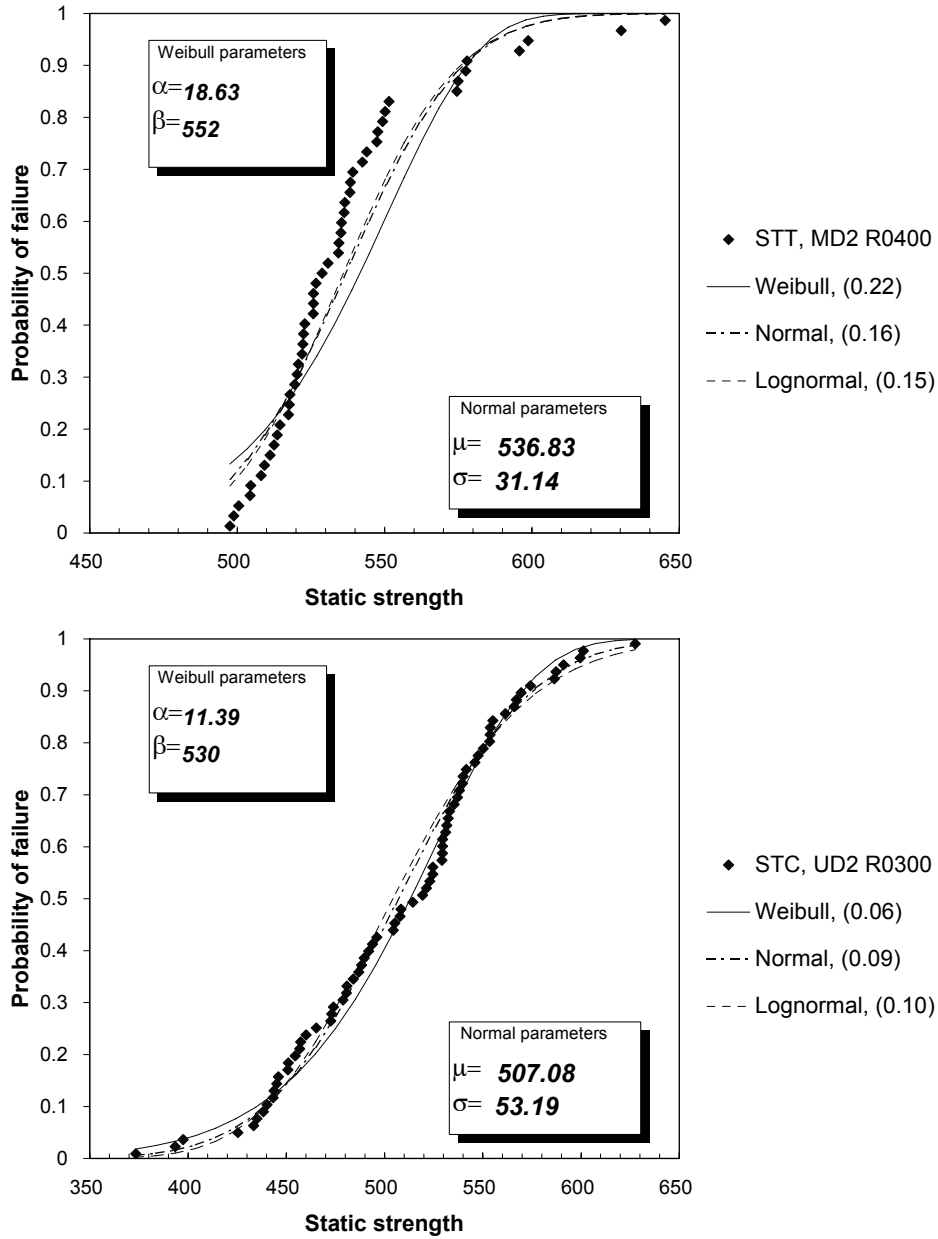
Figure 16: Sample probability plots indicating typical static scatter

Sources of scatter

Barnard et al.[25] [1985] performed tensile static and fatigue tests on glass-fibre epoxy. From this, they noted two sources of scatter in fatigue data, i.e. scatter due to a failure mode change at a certain stress level (dependent on material properties), and scatter due to variation in the static strengths of the material. They derived scatter in fatigue from the static scatter, and postulated that the strength-life-equal-rank-assumption (SLERA) was supported by their data since the range of fatigue data at each stress level was predicted by their method to derive equivalent fatigue data from static data.

Croman[55] [1987] reported worse fatigue behaviour for a thermoplastic flexure specimen than for a thermoset, with a slightly steeper S-N curve showing less scatter in the results.

Henaff-Gardin and Lafarie-Frenot[121] [1992] noted, that for the same material, a dogbone shaped specimen gave better fatigue life than a parallel-sided specimen, but the scatter was higher.

Lee[171] et al. [1997] highlighted the large scatter in their sample datasets, leading them to question the validity of life predictions based on median S-N curves.

Bach's[22] data [1991] suggest decrease in scatter with increasing life. This is in accordance with the 'fatigue life diagram' philosophy of Talreja and others, where fatigue behaviour is characterised by three regions.

A commonly accepted assumption is, that the scatter in fatigue life is independent of stress levels, or fatigue data are homoscedastic. This means, that fatigue data can be pooled and the statistical properties can be calculated from the pooled dataset, e.g. Trantina[323] [1981], Sutherland[312] [2000]. Typically, the fatigue data at a single stress level fall within a single decade in terms of fatigue cycles to failure. The OPTIMAT data support this assumption, see chapter 4.2.

From tests on the MSU specimens, a dependence is found of specimen shape on fatigue life scatter. For a dogbone-shaped specimen, R=10 fatigue exhibited two to three decades of scatter. When the same tests were repeated with a parallel-sided specimen, the fatigue life scatter decreased to about a single decade (with the same mean fatigue lives, although the dogbone seems to go to larger lives in the lower stress region).

An interesting hypothesis would be, that scatter in static strength can be somehow related to scatter in fatigue strength. Caprino and d'Amore[46] [1998] derived a strength degradation model, which allowed the scatter in static strength to be derived from the scatter in fatigue life. They obtained good correlation with experimental data. As mentioned above, Barnard et al.[25] also correlated strength with life.

Summarising, it can be stated, that both scatter in fatigue lives and in static strengths represents the inherent variability in material quality from coupon to coupon. In general, outside the strain range of static tests, fatigue lives are

spread over approximately one decade, independent of strain level. Static test results generally are within 10% of their mean value. The degree of scatter, however, depends on a large number of (mostly interdependent) parameters.

- Variations in fibre and matrix properties
- Manufacturing conditions
- Test coupon geometry, size, and pre-treatment
- Stress/strain level and R-value
- Test set-up (including plate-to-plate, lab-to-lab, machine-to-machine variation)

As an important example, R=10 fatigue is sensitive to specimen shape and pre-treatment. It was observed, that for a given pre-treatment or geometry, the scatter can be unexpectedly large.

Characterisation of scatter

For more detailed characterisation of scattered data, it would be useful to know how to describe static and fatigue distributions. Following Weibull[334] [1951], it is recommended to do preliminary analysis of the data by means of plotting a histogram. Then, one may decide, whether data are best described by a (Log)Normal or Weibull distribution. Table 1 shows a qualitative comparison between distribution types.

Table 1: Comparison of distribution types for fatigue life description

LogNormal	Normal	Weibull
log-symmetric	symmetric	non-symmetric
$0 < N < \infty$	$-\infty < N < \infty$	$0 =< N < \infty$
2 parameter	2 parameter	2/3 parameter
		analytically simpler distribution function
robust parameter estimation	robust parameter estimation	parameter estimation more sensitive to numerical techniques

The (log)Normal distribution is useful for describing symmetrical distributions. For additional freedom in the description of failure distributions, the Weibull-distribution, introduced by Wallodi Weibull[334] [1951], is most appropriate. The (cumulative) distribution function is described explicitly, which facilitates analytical treatment, although the estimation of the distribution parameters is less straightforward than for the Normal distribution.

Using Monte Carlo simulation, Liu[176] [1997] took samples from a Weibull distribution, and fitted them to Lognormal and Weibull distribution functions. He did the same for samples from Lognormal distributions. He argued, that the

failure mechanism should be taken into account when choosing a distribution. Weibull is most appropriate to physical mechanisms where failure follows a weakest-link model. The Lognormal distribution is suitable for proportional growth, for example crack growth is randomly proportional to the size of the crack. The lognormal model is therefore also suitable for fatigue degradation. Nevertheless, based on his Monte Carlo experiments, he concluded, that fitting the data to a Weibull distribution was safer for engineering practice than using a Lognormal distribution.

In some cases, the distribution of fatigue life has been seen to exhibit distinct peaks, corresponding presumably to different failure modes. Weibull advocated a preliminary analysis of the data and showed, that in some datasets a synthesis of two different Weibull distributions was preferable. Chou et al.[51] [1979] later described a method to estimate the parameters of such a 'bi-modal' fatigue life distribution, which they applied to data from literature, among which the Bofors steel example from Weibull's original paper. For some of the examples in his paper, Weibull was able to describe physical grounds for the bi-modality.
For small populations of fatigue data, it may be difficult to distinguish between the distribution types. In these cases, the opinion of Whitney[342, 343] [1982, 1983] is commemorated, who states:

'...the lognormal distribution and the two-parameter Weibull distribution usually provide equally adequate, or equally inadequate, fit to data on composite strength and fatigue life.'

Hwang and Han[126] [1987] plotted static, constant amplitude fatigue, and two-stress level fatigue results in a probability plot and fitted a Normal, Lognormal, and Weibull distribution to the experimental data. They observed, that for their static strength dataset, any of the three distributions was appropriate. For the fatigue results, the Normal distribution clearly did not give a satisfactory fit. They concluded, that the Weibull distribution is most appropriate for fatigue results, whereas the log-Normal distribution will be most applicable in cases of extreme scattering.

Whitney[342, 343] [1982, 1983] advocated the use of the lognormal distribution over the Weibull distribution, and pointed out several advantages of this distribution type (except for the case of censored data, where numerical techniques were required). His main argument was that his version of the lognormal distribution is useful from an engineering viewpoint.

For the OPTIMAT and the MSU data, (log)Normal and two-parameter Weibull distributions have been fit through the static and fatigue data. No consistent superiority of either of the distribution forms over the others was evident from these extensive data, see e.g. section 4.2.4.

In practice, the Weibull distribution is popular, because it can be easily manipulated analytically, due to its straightforward algebraic form. On the other hand, for the calculation of tolerance bounds on fatigue life data, it seems to be less practical, see section 2.3.7.

2.3.7 Tolerance bounds

Characterisation of the scatter in fatigue data, as described above, is the first step to deriving design data from experimental fatigue results. Typically, the designer utilises values of fatigue life, which are characterised by a probability of failure, and a confidence value.
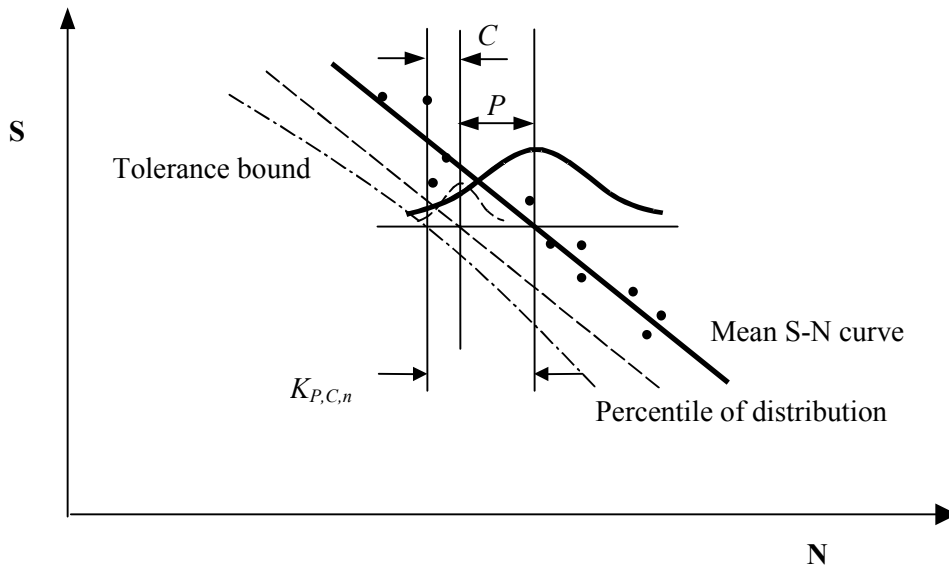
Figure 17: Schematic of tolerance bounds

The probability of failure is the value for the entire population, above which *x%* of the specimens will fail. The confidence level is a measure of how accurate the probability of failure can be obtained from a sample of the population. A combination of failure probability and confidence is a *confidence bound*, or *tolerance bound*. In other words, a tolerance bound is the probabilistic formulation of a percentile. A schematic of tolerance bounds is displayed in Figure 17.

The calculation of confidence intervals with respect to the me(di)an value or standard deviation of an assumed distribution is not discussed here. For information on this subject, the reader is referred to Little[175] [1981], or to the relevant standards (ASTM[6], 1998; DIN[73, 74] 1983, 1987; ISO[131] 1980). Also, an important assumption is, that the fatigue data can be described by a Normal distribution.

One-dimensional data

Tolerance bounds are defined for one-dimensional data (e.g. static strengths):

$$X^* = \bar{x} - K_{P,C,n} \cdot s \qquad (20)$$

X^* = lower, one-sided tolerance limit
$\bar{x}$ = sample mean
K = multiplier for a specific level of P, and C and n
P = probability of survival, P<1
C = confidence level, C≤1
n = number of test results in a sample (sample size)
s = sample standard deviation

Analytically, finding $K_{P, C, n}$ amounts to establishing the Cth quantile of the noncentral t-distribution with non-centrality parameter $U_P \cdot \sqrt{n}$ with number of data points n and degrees of freedom f (Owen[238], 1968; MIL[193], 1997):

$$P\left[T_f(\delta) \leq K_{P,C,n} \sqrt{n} \mid \delta = U_P \sqrt{n}\right] = C \qquad (21)$$

The non-central t-distribution is written as:

$$T_f(\delta) = \frac{Z + \delta}{\sqrt{\dfrac{\chi^2}{f}}} \qquad (22)$$

where Z is a standard normal distribution.
For certain commonly used tolerance bounds, the multiplier $K_{P, C, n}$ has been pre-calculated for general use, e.g. by Lieberman[174] [1958], and Owen[239] [1968], and can be read from a look-up table. Several tables with $K_{P, C, n}$ have been published and some are reproduced in Nijssen[216] [2004]. By comparing the various tables of tolerance bound factors from the literature, it is demonstrated, that the values of $K_{P, C, n}$ for different sample sizes which Natrella[209] [1963] reproduced from Lieberman[174] [1958], are identical to the values found in DIN[74] [1987] and in the MIL[193] handbook [1997] for the A-basis values (*C;P=95;99*)-tolerance limits. For combinations of P, C and n that are not tabulated, Natrella refers to a Sandia Corporation Monograph by D.B. Owen[239] [1958], and also gives a formula to approximate $K_{P, C, n}$:

$$K_{P,C,n} = \frac{U_P + \sqrt{U_P^2 - ab}}{a} \qquad (23)$$

$$a = 1 - \frac{U_C^2}{2(n-1)} \qquad (24)$$

$$b = U_P^2 - \frac{U_C^2}{n} \qquad (25)$$

U_i = i^{th} percentile of the standard normal distribution

The resulting $K_{P,\,C,\,n}$s are slightly lower than the tabulated values in the tables. This and other approximations are surveyed in Owen[239] [1968]. The MIL-handbook[193] also gives approximations of the tabulated values by an algebraic expression:

$$k_A = 2.326 + e^{\left(1.34 - 0.522\, ln(n) + \frac{3.87}{n}\right)} \qquad (26)$$

$$k_B = 1.282 + e^{\left(0.958 - 0.520\, ln(n) + \frac{3.19}{n}\right)} \qquad (27)$$

The resulting values are within 0.2% of the tabulated values for $n>16$.

Echtermeyer[82] [1994] prescribes to subtract two times the standard deviation (in log ε) from a mean ε -N curve to obtain the boundary of the 95% confidence interval (recall from section 2.1 that he provided a 'standard' ε-N curve). Note that he implies here, that strain is the dependent variable, whereas generally, confidence bounds would be expected to be formulated in terms of life.
Sutherland[313] [2000], who also provides a discussion of tolerance bounds tailored to fatigue data, uses the one-dimensional method following e.g. Natrella.
The Germanischer Lloyd regulations[102] give a formula, taken from DIN[74] [1987], to find the characteristic values in terms of stresses or strains as a function of the percentile of the population and the desired confidence limit. A variation coefficient of 0.15% (i.e. standard deviation is 15 % of the mean) may be used without verification. The low value for this coefficient suggests, that eq. 28 is specifically meant for static data.

$$R_k(P,C,0.15,n) = X^* = \bar{x}\left(1 - 0.15\left[U_P + \frac{U_C}{\sqrt{n}}\right]\right) \qquad (28)$$

R_k = characteristic value
U_i = i^{th} percentile of the standard normal distribution

This means that $K_{P, C, n}$ from equation 28 is represented by the term between straight brackets:

$$K_{P,C,n} = \left[U_P + \frac{U_C}{\sqrt{n}} \right]$$
(29)

Two-dimensional data

None of the methods detailed in the previous section takes into account the two-dimensional nature of fatigue data, and consequently the tolerance bounds are parallel to the mean S-N curves. If a tolerance limit would be calculated for fatigue data, one would expect the confidence band to be bounded by hyperbolic tolerance limits, as is the case for the confidence band for the me(di)an in ASTM[6] [1998]. In other words, the factor $K_{P,C,n}$ is a function of stress range or fatigue life, or:

$$X^* = \bar{x} - K_{P,C,n}(s) \cdot s$$
(30)

Owen[238, 241] [1968] published a thorough survey of properties of the t-distribution, containing a statistically correct expression for the $K_{P, C, n}$ in two-dimensional data, as was reproduced here in equations 21 and 22. Because the relative importance in determination of a percentile is smaller as datapoints are farther away, $K_{P, C, n}$ should become larger at the edges of the sample space. Although references on this topic date back from as far back as 1939 (see Owen[238, 241], 1968), it has apparently not become common practice to calculate the exact tolerance limit. Owen has reviewed and extended an existing approximation, which Shen[295] [1996] has used to develop design curves for engineering purposes with a linear approximation to the hyperbolic tolerance bounds. This is called the 'approximate Owen limit'. The level of confidence is not uniform across the sample space and is most accurate at the average of the data, as was also pointed out by Ronold[272] et al. [1996]. Recently, Williams et al.[346] [2003] adopted this method for statistical analysis of fatigue data.

The 95/95 tolerance bounds are compared in Figure 18. Clearly, Natrella [1963] and DIN 55303-5 [1983] give identical values for KP, C, n. For the A- and B-basis values, DIN 55303-5 and the MIL-handbook [1997] give identical results (not shown here), so it can be expected that a table of 95/95 tolerance bounds would also be identical to the one in Natrella or DIN 55303-5. This expectation is corroborated by the fact that all three refer to Owen.
The highest (most conservative) K-factors are given by the approximate Owen limit. Note that Germanischer Lloyd[101] [1993] gives the lowest $K_{P, C, n}$, but these are relevant for static strengths.
Thus for 95/95 tolerance bounds, Germanischer Lloyd gives the least conservative results, the Owen approximation the most conservative and DIN
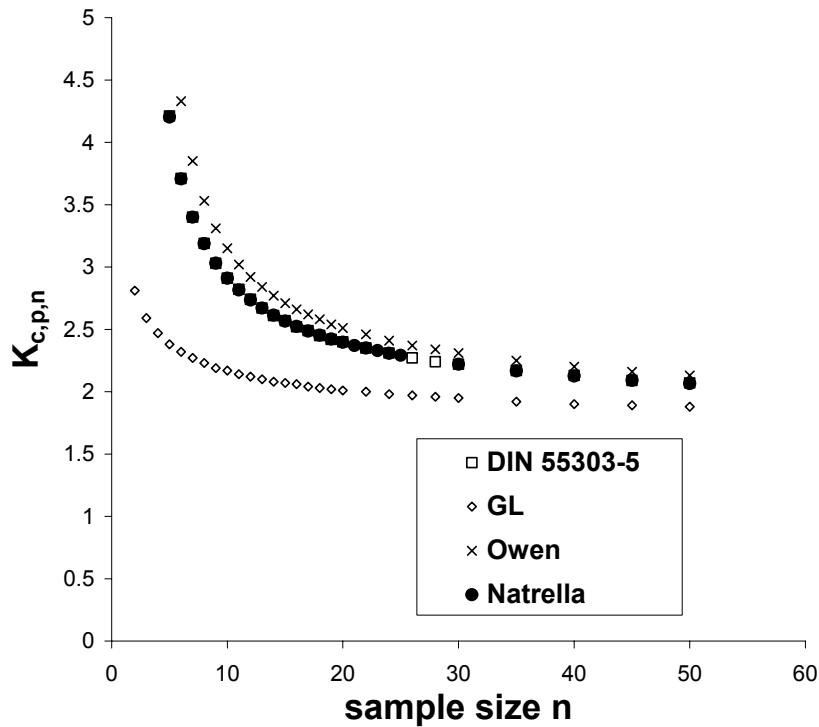
Figure 18: Comparison of tolerance bound factors from literature

55303-5, the MIL-handbook and Natrella are in between. This ranking is also valid for C=95% and P=90%, see Nijssen[216] [2004].

Extrapolation of tolerance bounds

For determination of confidence bounds outside the data range, Ronold and Echtermeyer have developed the following empirical formula for the particular case of C=P=95%:

$$K_{0.95, 0.95, n \geq 10} = 1.645 + 2.567(n-2)^{-0.71} + \frac{5.588}{\sqrt{n-2}} \cdot \frac{\Delta x}{L_x} \qquad (31)$$

with

Δx	=	distance between current value of independent variable and mean of data range
L_x	=	data range = $x_{max} - x_{min}$
$\Delta x / L_x$	=	larger than 1.0

For other *C* and *P*, the values of the coefficients are different.

An important note to be made here, is that fatigue lives can be expressed both in terms of the Normal and Log-Normal distribution. In the case of the latter

distribution type, the procedure for determining the mean S-N curves and tolerance bounds is identical, save for the fact that fatigue life is expressed in log(N) rather than N.

The difference in result from the two formulations is, that the tolerance bounds based on the assumption of a Normal distribution are more conservative than those calculated for a Log-Normal distribution.

Summarising, for samples (fatigue data) that stem from populations with a Normal distribution, the lower tolerance bound is found by subtracting $K_{P, C, n}$ times the sample standard deviation from the sample mean. Classically, for common tolerance bounds, calculations for engineering purposes are facilitated by look-up tables for $K_{P, C, n}$.

When $K_{P, C, n}$-values from different sources are compared, it is found that the approximate Owen limit gives the most conservative results and Germanischer Lloyd gives the least conservative one-sided tolerance limits. The reason for this may be, that the GL-confidence limit definition is specifically meant for static data (instead of fatigue data).

Determination of mathematically correct (two-dimensional) tolerance bounds for fatigue data is not common practice for engineering purposes. Although the knowledge on how to obtain statistically correct tolerance bounds on fatigue data has been available for at least several decades, it seems not to have been incorporated in design guidelines for wind turbines yet. Ultimately, a method to determine rotor blade reliability should include similar procedures for the loads. Veldkamp[326] [2006] has looked at both the load and fatigue data side for the probabilistic design of wind turbines.

2.3.8   Interpolation anomaly

For interpolation of the CLD built from R=-1 data, the linear Goodman formulation can be used. For interpolation of a multi-R-value CLD, several methods exist. The simplest is suggested by DNV[75] [2006]. For interpolation of the CLD, a method was devised by Philippidis and Vassilopoulos[258] [2004], which works for both exponential and power law S-N curves.

The S-N curves generated by the Linear Goodman Diagram, are only described by a power law expression for R=-1. For other R-values, the S-N curves, derived from the LGD, are slightly non-linear, and this nonlinearity is proportional to the angle with the S_{amp}-axis. This is called the 'interpolation anomaly'.

Figure 19 illustrates this. It shows the right-hand side of the CLD, described by a realistic R=-1 S-N curve. A green radial line in the LGD indicates the R-value of the derived S-N curve. This S-N curve is obtained by plotting the amplitudes corresponding to the intersections of the radial with the constant life lines in the

LGD. The derived S-N curve is non-linear in the log-log S-N diagram. To emphasise this, it is fitted with a straight line (continuous). In addition, a curve is plotted, which shows the ratio of fatigue life predicted by the derived curve, and that of the linear fit.
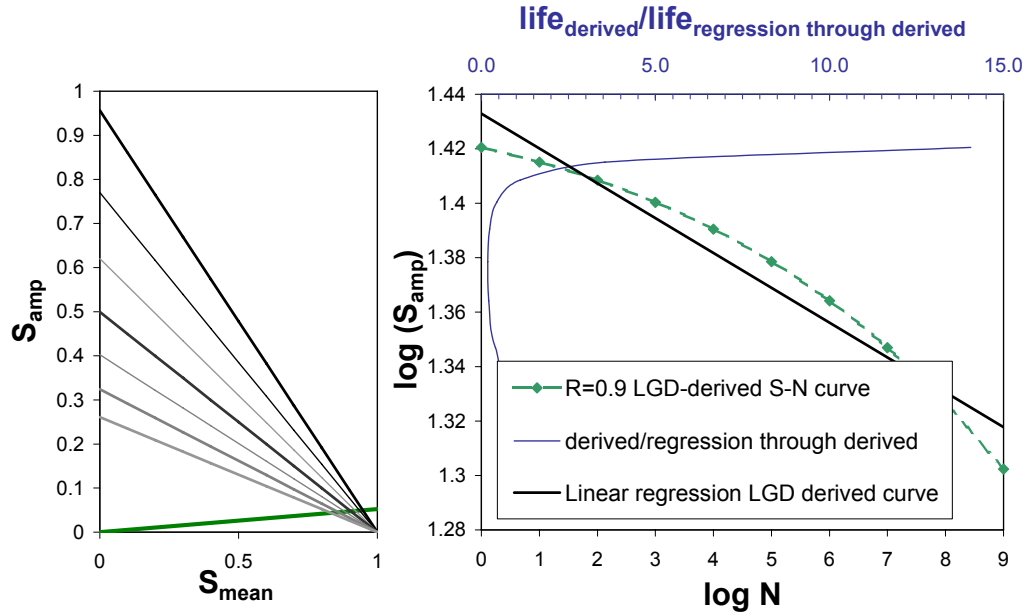
Figure 19: Interpolation anomaly example

Summarising, the LGD generates S-N curves at R<>-1, which do not follow the log-log formulation. The formulation by e.g. Philippidis and Vassilopoulos does generate log-log S-N curves and therefore can be regarded as in better agreement with the experimental data. Comparison of life predictions using the Linear Goodman Diagram (log-log S-N curve only at R=-1) and e.g. the method by Philippidis and Vassilopoulos (log-log S-N curves in a large part of the CLD) may therefore not be completely justified. However, the resulting life predictions are not expected to be very different.

Summary of this chapter

Chapter 2 describes constant amplitude fatigue as the basis for spectrum fatigue predictions.

- *The log-log and lin-log S-N diagrams are described, as well as other formulations and parameter estimation methods, such as linear regression or the methods by Whitney and Sendeckyj*
- *A description of the most commonly used constant life diagrams (Linear Goodman, shifted Linear Goodman, Multiple R-value, Equivalent Load Method) is given; these will all be used in the spectrum life predictions of this dissertation*
- *Various issues that were encountered during this work and in the literature are discussed. Although the influence on life prediction of some of the issues cannot be unequivocally resolved or quantified, they are all relevant to this work. It is demonstrated, that a fatigue limit most likely does not exist; that static data should be excluded from an S-N parameter estimation; the importance of static and fatigue rate is illustrated by examples; general trends in static and fatigue scatter and the formulation of tolerance bounds is discussed.*

The next chapter uses the constant amplitude formulations from Chapter 2 as part of the method to predict life in spectral fatigue.

Chapter 3

Spectrum fatigue

This chapter describes Miner-based and strength-based spectrum fatigue analysis and life prediction. The chapter starts with a description of standardised loading spectra. Then, counting methods are discussed, that facilitate reducing the spectrum load sequence to its constituents. Miner's sum is discussed as the prime example of sequence-insensitive fatigue life prediction. Residual strength degradation is described as a means of residual property analysis and life prediction for load spectra.

3.1 Complex spectra

In the following paragraphs, a review is provided of the principle and application of standardised loading sequences. The WISPER wind turbine standardised test sequence, and variations, are described in some detail, because these are used in the tests and predictions of Chapter 4 and Chapter 5.

3.1.1   Overview of standardised loading sequences

Spectrum loading tests provide a way to simulate in a laboratory, what the material experiences in realistic operating conditions, while allowing other influences, such as temperature or moisture, to be controlled.

As was mentioned in 1.2, variable amplitude loading can be described either in terms of stochastic content, or as fixed sequences. In order to be reproducable in a laboratory environment, the load sequence is usually fixed. Typically, the load sequence is scalable.

In order to rank materials in terms of variable amplitude fatigue performance, standardised load sequences have been defined, which are representative for a range of applications. None of them should be used as design spectra, but they do reflect the type and number of fatigue cycles that can be encountered in the particular application. A brief description of various examples is given below.

WISPER, and its derivatives (NEW) WISPER(X), will be described more extensively, as they are most relevant for the current research.

After the first loading spectrum ever by Gassner (see Schütz[290], 1989; Berger et al.[28], 2002), several standardised fixed loading sequences have been developed over the past 3 decades. They are application-based, so they are representative for a specific engineering application, operating in a specific environment. Examples of such spectrum loads are:

- Load and speed collectives for dimensioning of tractor travel drives (Renius[265], 1976)

, or the spectra described by Schütz[290] [1989], such as:

- GAUSS, by Heuler and Seeger[122] [1986]
- WASH, Wave Action Standard History, a standardised stress-time history for North Sea offshore structures, see Solin[304] [1990]
- Walz (steel mill drive loading standard)
- Carlos (CAR component LOading Standard)

The National Aerospace Laboratory of the Netherlands (NLR) has been involved in the development of a considerable number of aerospace-related standardised load sequences for fatigue analysis and testing. An online overview of the spectra is available (NLR homepage[229]), and an extensive description, and the loading spectra themselves can be obtained from NLR. These loading spectra are enumerated here:

- FALSTAFF, Fighter Aircraft Loading STAndard For Fatigue evaluation, developed in 1975, represents the load history of the wing root of a fighter aircraft. A cycle truncated, shorter, version (developed to reduce testing time by CEAT in Toulouse, France) is available under the acronym miniFALSTAFF, or short FALSTAFF
- ENSTAFF (= ENvironmental falSTAFF), published in 1987, is the same as FALSTAFF, but has been augmented with environmental condition information, i.e. temperature and moisture, related to the structural loading
- TWIST, The Transport WIng STandard load programme, from 1973, and its shortened version MINITWIST, are standardised load sequences representative of the load history of the wing root of a transport aircraft
- Cold, and Hot TURBISTAN (gas TURBIne engine STANdard), developed around 1985, represent the loading in the cold- and hot-sections of gas turbine engine disks

- Helix and Felix, and their shortened versions Helix/32 and Felix/28, were published in 1984. These standard loading sequences apply to either articulated or semi-rigid main rotors of helicopters

An overview of loading spectra, the rationale behind them, and possible applications of standardised sequences, is treated in detail by Schijve[281] [1985], Schütz[290] [1989] and by ten Have[118] [1989].

Most of the load spectra are encountered in the literature as the focus of variable amplitude investigations, e.g. on the effects of truncation (limiting the cycle ranges or maxima), and omission (eliminating particular cycle types from the loading spectrum) on composite lifetime. Often, the original load sequence needed to be modified to suit the objective of the investigation.

Lee, Fu and Yang[170] [1996] used a modification of the spectrum representing the loads experienced by a fighter plane's horizontal tail during 596 flights. They simplified the 98 blocks of constant amplitude (amounting to a total of 19440 cycles) to 20 blocks with similar probabilistic characteristics. A residual stiffness model was validated using these test results.

Schaff and Davidson[278] [1997] used FALSTAFF, and two very similar spectra to test the predictive powers of their residual strength model (the similarity of the spectra to FALSTAFF stems from the fact that these Schütz and Gerharz Fighter (SGF) spectra were developed by (and named after) two scientists who were closely involved in the definition of FALSTAFF, Schütz and Gerharz[288] [1977].

TWIST, and truncated variations of this spectrum, have been used by Phillips[251] [1981].

Philippidis and Vassilopoulos[258] [2004] used a modification called MWISPER to validate their fatigue failure criterion. For this modification, the zero stress-level was offset downward, to the smallest integer (1), so that the complete spectrum consists of tension-tension cycles. They also used a spectrum called EPET573, which is a simulated load history, derived by means of aeroelastic calculations for a 14 m wind turbine rotor blade and it is representative of flap bending moment fluctuations on a cross-section of the blade located 2.414 m from the root. The load case definition stems from (IEC[127], 1998), and the result is a 10 minute spectrum of 3893 loading reversals or 1946 load cycles. When the time series is normalised with respect to its minimum value and rounded to integer numbers, it has a maximum value of 157, a minimum of 1, while the mean value is 71.47.

Wahl[328] [2001] replaced all valleys in WISPERX by values, such that constant R-value half cycles remained. He created R=0.1 and R=0.5 modified versions of WISPERX. Strictly speaking, a Rainflow count of this signal does not yield a constant R-value counting result, since Rainflow cycles will be extracted that do

not consist of valleys and their preceding peaks, but for the purpose of his method (where he did not use Rainflow counting, but rather evaluated the strength degradation due to subsequent ranges), it is justified to call it a 'constant R-value spectrum'.

Badaliance et al.[24] [1982] investigated the effects of modifications of an F15 fighter (predominantly compressive) spectrum on the fatigue lifetime of graphite/epoxy prepregs, using single-hole compression specimens, and both matrix dominated and fibre dominated lay-ups. Variations constituted truncating, clipping of tension loads, and addition of overloads. The variations were compared to the F15 spectrum, which was truncated to 55% Test Limit Stress (which is the maximum stress occurring in the spectrum, in this case this was taken to be 85% of the ultimate compressive stress for the fibre dominated laminates, and 67% for the matrix dominated laminate). The most important finding in this article was, that addition of overloads reduced the fatigue life more than an order of magnitude. Addition of low loads (one of the variations was an untruncated spectrum) also reduced fatigue life, by 48% for the fibre dominated laminate, and 40 percent for the matrix dominated laminate.

Nyman, Ansell and Blom[231] [2000] have considered different truncations and elimination levels for different load spectra and constant amplitude block spectra. They used early design spectra of the Saab Gripen representing sections of the aft fin and the wing, and a (compression dominated) version of the FALSTAFF spectrum, named 'Short Inverted Falstaff'. Their most important finding was, that cycles up to 50 % of the maximum range could be eliminated from the spectra, saving considerable testing time, while still giving realistic estimates of the fatigue lifetime. This is corroborated by results in the literature that they found. They asserted, that life prediction methodology is also affected by this, since only a limited amount of load states have to be included in the prediction. They observed a significant influence of elimination of high loads on remaining life for fully reversed stress (R=-1) block loadings. They used a similar single-hole specimen as did Badaliance et al.[24] [1982]. See also Nymann[230] [1996], where an Anti-Buckling Guide (ABG) was used in the experiments.

Schön and Blom[285] [2002] validated a model that predicts delamination growth in spectrum fatigue and suggested, that for the case of load spectra related to fins of the JAS 39 aircraft, elimination of 50% of the spectum was validated. This means, that all loads up to 50% of the maximum spectrum load could be eliminated from the spectrum, yielding very similar damage. They found similar potential elimination levels in related work (Schön and Nyman[286], 2002).

Summarising, the previous paragraphs described many standardised load spectra to illustrate their use. The wind turbine reference spectra discussed in the next paragraphs are similar in the sense, that they have been developed for a particular application, are formulated as fixed, standardised, load sequences, but have been considered for modifications.

3.1.2 Description of WISPER standard load spectrum and variations

The WISPER variable amplitude loading sequence was devised in the eighties of the 20th century as a standard loading sequence for testing of wind turbine blade materials and components. It is not meant for design or certification, but for comparison purposes only (ten Have[116-119], 1988-92). The existing wind turbine reference spectra are shown in Figure 20.
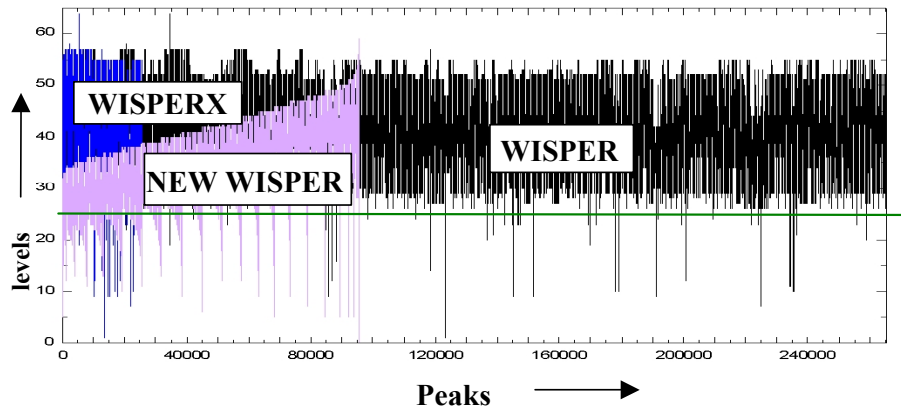
Figure 20: Wind turbine reference spectra, horizontal line indicates zero load

The predefined and fixed WISPER load sequence consists of a series of integers ranging from 1 to 64 indicating load reversal points. In total, there are 265,423 points, i.e. 132,711 cycles. The levels range from –24 to 39 (zero load is indicated by integer 25). Hence there are 64 levels and the maximum stress range of a cycle is 63 levels. In practice, the WISPER levels are multiplied by a certain factor in order to obtain the desired maximum load level. It should be noted, that the maximum peak in the WISPER spectrum is relatively large compared to the other peaks in the spectrum. In tests and (strength-based) analysis, this peak is where most of the failures are likely to occur.

In order to reduce testing time, the WISPER load sequence was decimated by removing all cycles with an amplitude of 8 levels or smaller. This resulted in the WISPERX load sequence (where the Roman numeral X refers to WISPERX having roughly 10 times as little cycles as WISPER, viz. 12,831 cycles). This is indicated in Figure 21. This figure shows the location of WISPER and WISPERX rainflow counted cycles in a mean-amplitude diagram (similar to the way the right-hand side of a CLD is plotted). The size of the circles indicates the number of cycles N_i for each cycle type (the logarithm of N_i was taken, for single cycles, the size of the circles was set to one).

For constant frequency tests, this means that testing time for a WISPERX sequence is 10 times shorter than for WISPER. In the case of constant loading

rate tests (which will be used in the OPTIMAT programme, see 4.2.7), testing time is about 7 times shorter.
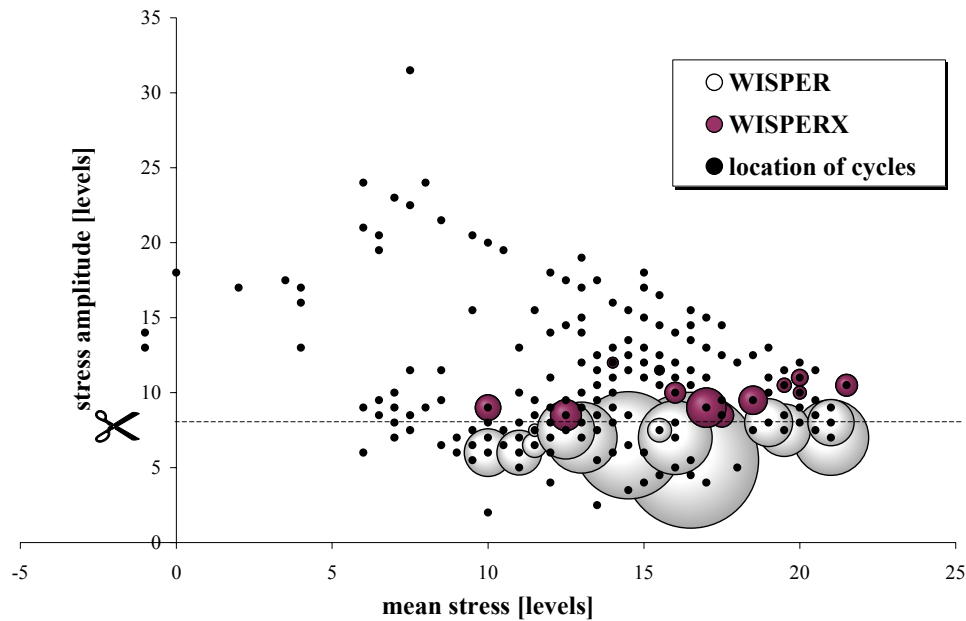
Figure 21: Omission of cycles to obtain WISPERX from WISPER

Using a range-pair-range algorithm to count the number and types of cycles in the WISPER(X) sequences, some more statistics on the load sequences can be obtained (see for counting methods 3.2). These are tabulated in Table 2. This table also includes the location of the maximum peak and minimum valleys for the spectra. These locations are the most probable locations where failure occurs according to the strength degradation method.

Table 2: Summary of wind turbine reference spectra

Spectrum	Integers					Levels				
	minimum	maximum	zero stress	no. of cycles	average R-value	cumulative levels	average segment length	average level	maximum at segment	minimum at segment
WISPER	1	64	25	132711	0.394	3612010	14	41	34482	123303
WISPERX	1	64	25	12831	0.248	487864	19	41	5298	13482
NEW WISPER	5	59	22	47735	0.213	1397142	15	34	95459	1

For a variable amplitude loading sequence such as WISPER(X), the R-value can be defined in two ways. It can be based on the ratio of the extreme trough and the extreme peak, or it can be defined as the average of all R-values of the individual cycles. As the Wisper sequence is divided in levels according to the above, the first definition is easily seen to amount to -0.615 for both WISPER and WISPERX. According to the second definition, the average R-values for WISPER and WISPERX are 0.4 and 0.25, respectively. For the Miner summation, the R-value is taken per (Rainflow counted) cycle.

It is clear from Table 2, that both loading sequences' parameters cover similar ranges of values. This would support the assertion that the damage incurred by them will be similar, too. When the WISPERX load sequence was derived from the WISPER sequence, it was assumed that the damage incurred would not change with respect to its ancestor.
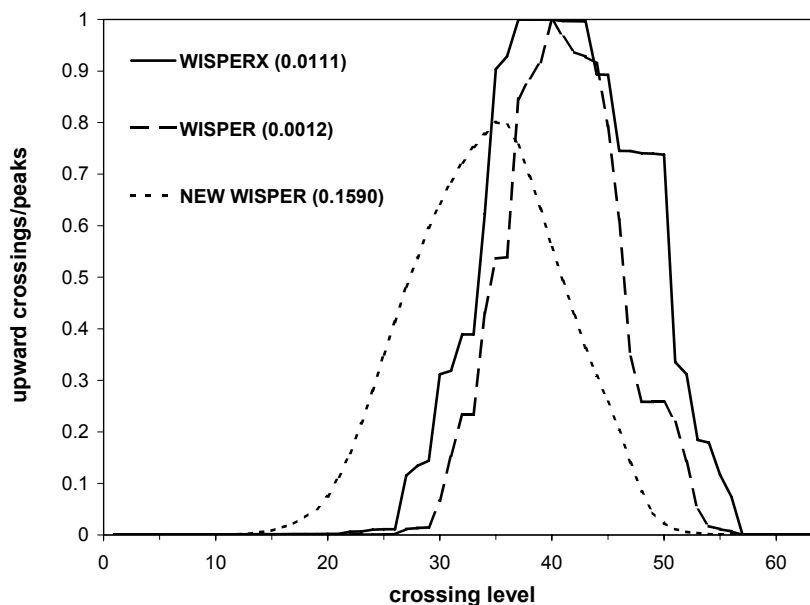
Figure 22: Irregularity factors for wind turbine reference spectra

In the framework of the OPTIMAT programme, variable amplitude testing was planned for evaluation of the life prediction methods developed in this project. Some of the project participants considered the WISPER(X) spectrum as out-of-date, since the measurements that were used as an input in the spectrum synthesis were taken from much smaller turbines than are currently common. Also, most of the turbines' power regulation has changed from stall to pitch, or active pitch control. Therefore, it was their ambition to devise a spectrum that would be more up-to-date, and a 'new' WISPER spectrum was synthesised. Apart from the last 'randomisation' step, the original synthesis procedure as followed by ten Have was used. The process and the results are described in

some detail in Söker et al.[303] [2004], and Bulder et al.[44] [2005]. The NEW WISPER spectrum was also used in the OPTIMAT programme for spectrum prediction validation. Unfortunately, the uncompleted randomisation makes this spectrum less consistent with the previously developed WISPER and WISPERX spectra than initially intended.

Figure 22 shows a representation of the level crossing count of the spectra. On the vertical axis, the ratio of upward level crossing and the number of peaks (i.e. total number of points excluding valleys) is given as a function of the crossing level. The 'irregularity factor' is the value of this parameter for zero-stress crossing level. As the irregularity factor approaches 1, the spectrum is more narrow band. For an irregularity factor of 0, the spectrum is 'wide band'. The irregularity factors are given for each spectrum, for zero stress level, in the figure (bracketed values).

Judging from the irregularity factors, the NEW WISPER spectrum is the most narrow band. However, this is valid for the zero crossing level. If the 'irregularity factors' at other crossing levels are included in the consideration, the WISPER(X) spectra are most narrow band, as the maximum values of this parameter are higher than for NEW WISPER, albeit at different crossing levels. The irregularity parameter is unity for WISPER and WISPERX in the range of levels 37-43 and at level 38, respectively. For NEW WISPER, the maximum irregularity parameter is ca. 0.8 at level 35.

Since WISPER(X) are predominantly tensile load sequences, incorporating only occasional excursions into the compressive regime (to which composites can be sensitive), an obvious modification would be to invert the sign of all peaks and valleys, creating 'Reversed' versions of WISPER(X), or 'RWISPER(X)'. These spectra were used in the OPTIMAT project (Chapter 4).

From an experimental point of view, the potential number of tests is proportional to the number of available load spectra. Having multiple 'standard' load spectra does not exactly mitigate the testing load for a particular material. Moreover, it is not necessary to have multiple standards for ranking materials. On the other hand, including e.g. Reversed WISPER(X) in a testing program does allow for an ascertainment of the effects of various conditions and therefore gives a valuable contribution to the spectral loading investigation. In the case where materials need to be ranked for design, but a time constraint exists, it would be recommended to first establish what the most representative spectrum would be (predominantly tensile or compressive), and choose this spectrum for testing.

3.2 Counting methods

All types of fatigue analysis require a description of the cycle content of a load sequence. Three main methods to obtain cyclic content are described here. The

measurement of load spectra is not treated.

3.2.1   *Level crossing*

In some cases, only peaks that are above a certain load or strain level (e.g. above the fatigue limit) may be of interest for a life prediction. In that case, level crossing methods can be employed. For instance, the number of crossings of the fatigue limit (in steels), or the number of exceedances of the cracking limit may be quantified. In addition, the ratio of level (up)-crossings and peaks is a descriptor of the 'regularity' of a load spectrum, the 'irregularity factor'. The level crossing method is not used in this work. For completeness, the irregularity factor is given for different crossing levels in the WISPER spectra in section 3.1. The level crossing counting results are expressed in number of peaks rather than number of cycles. See Figure 23.
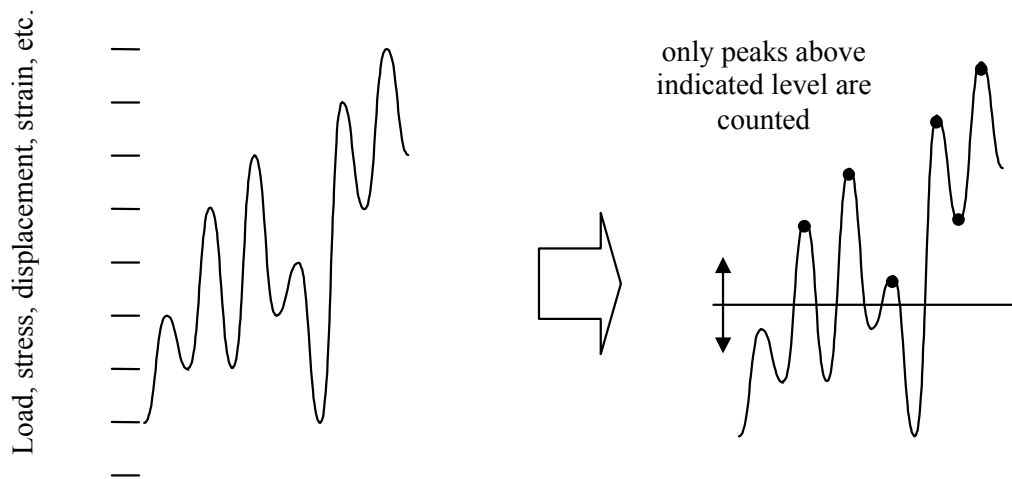
Figure 23: Level crossing counting method

3.2.2   *Range-mean*

In range-mean counting, the load spectrum is divided in segments. One segment is bounded by a peak and its adjacent valley. The segments are characterised one by one in terms of mean and range, and binned accordingly. Other characteristics may be used, so the method might as well be termed min-max counting', R-value-amplitude counting, etc. In the following, the term 'range-mean' definition is retained. The counting results are expressed in half cycles (see Figure 24).

In residual strength degradation models, where strength degradation evaluation should be based on a peak-by-peak cycle extraction and matched with the peak/valley under consideration, common Rainflow counting algorithms are not appropriate, because the Rainflow algorithm does not count each cycle at the exact time it occurs. In these cases, a cycle-by-cycle range-mean counting

method can be used. It is equivalent to range-mean counting, except for the fact, that the order of the cycles is taken into account. Dover[77] [1979] commented, that for cycle-by-cycle analysis, this method is more appropriate than the Rainflow method.
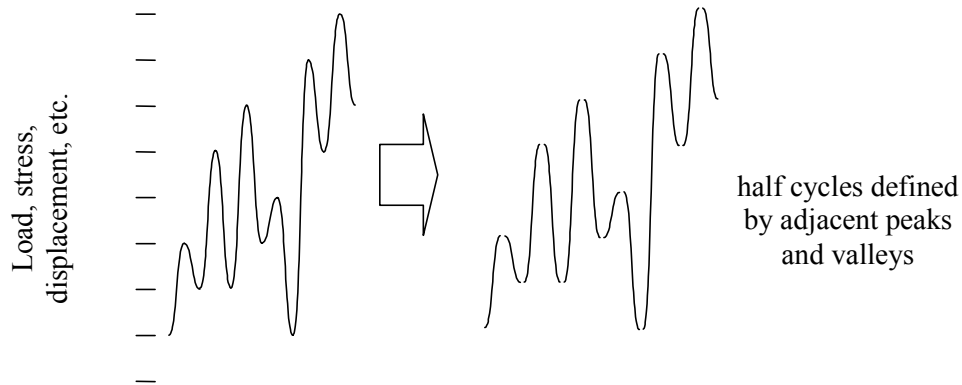
Figure 24: Range-mean counting method

3.2.3   Range counting

Range counting is identical to range-mean counting, where the mean (or R-value) information is discarded (sometimes, an average mean is retained).

3.2.4   Rainflow counting

An important drawback exists in range-mean or range counting algorithms. This is illustrated by Figure 25. Here, two schematic load spectra are shown. The left spectrum consists of large cycles, with a relatively small load-ripple superimposed. The right figure is a constant amplitude signal with interspersed larger peaks and valleys. Although both load spectra are artificial, they are realistic. The left figure represents a long-term load cycle combined with minor loads. This might occur in a dam, loaded by fluctuations in water level (large cycle) and waves (small cycles). The right figure might be a car axle, where the car is loaded and unloaded at the start and end of the journey, and occasionally hits a bump or pothole in the road.

The range-mean counting results from the range-mean method are obtained by creating half cycles from the signal, using the peaks and valleys as half cycle boundaries. The problem with these results is, that in neither case, the large tidal load (left figure) is counted, nor is the loading-unloading cycle combined with the loads from the potholes and bumps (right figure). Making life predictions for this type of load spectra, using range-mean counted cycle content, might result in non-conservative estimates, since these large, potentially damaging, cycles are, at best, partly included, but often separated into smaller, less damaging, parts.
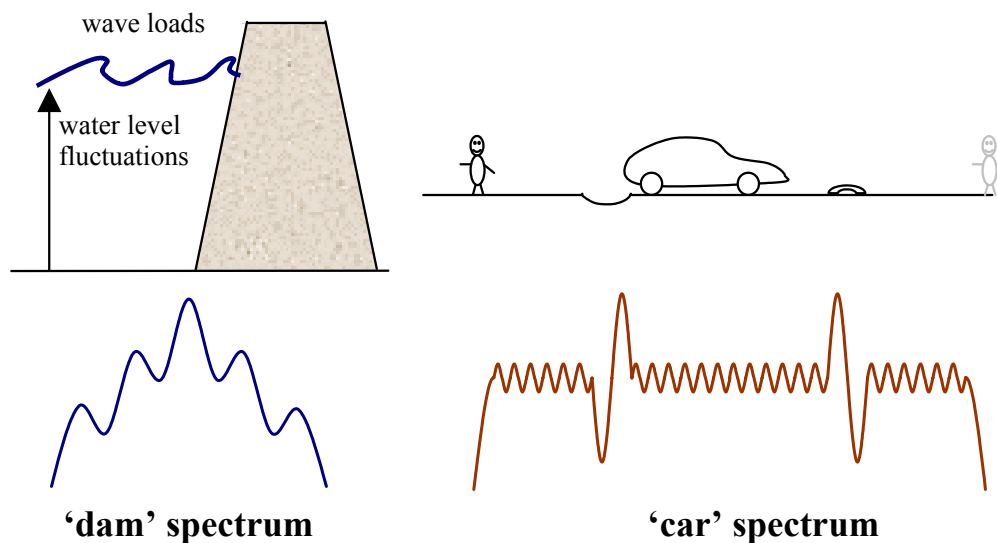
Figure 25: Dam spectrum and car spectrum types

One counting algorithm exists, which can account for these cycles. This is the Rainflow counting method. It is treated more elaborately here than the other algorithms. In section 3.2.5, it is demonstrated for the 'dam spectrum', why Rainflow counting is to be favoured over range-mean counting.

Multiple Rainflow-counting algorithms exist, which can be linked through the concept of 'cyclic counting'.

History

In the 1950s and 1960s, methods for quantification of the fatigue cycles in spectrum loading were limited to range counting or range-mean counting. Methods like these can yield unreasonable counting results, as they do not take into account the stress-strain history to which the material is subjected. For hysteretic materials, such as metals in plastic deformation, the stress- and strain cannot be directly related at a certain moment in a given load history, but they depend on the previous development of stresses and strains. As a result, the possible damage induced by a certain stress-or strain cycle depends on its location within the load history. A stress-strain-history resulting from a certain load history is visualised as a stress-strain hysteresis plot and shows hysteresis loops which represent stress-strain cycles (Figure 26). These hysteresis loops are believed to be related to the fatigue damage induced in the material. A method was needed that was capable of extracting hysteresis loops from a load history, rather than basic range-mean type information.

Prof. Tatsuo Endo of the Kyushu Institute of Technology in Japan formulated a method of counting stress-strain hysteresis loops instead of stress- or strain ranges. The fundamentals of this method, baptised the 'effective range count
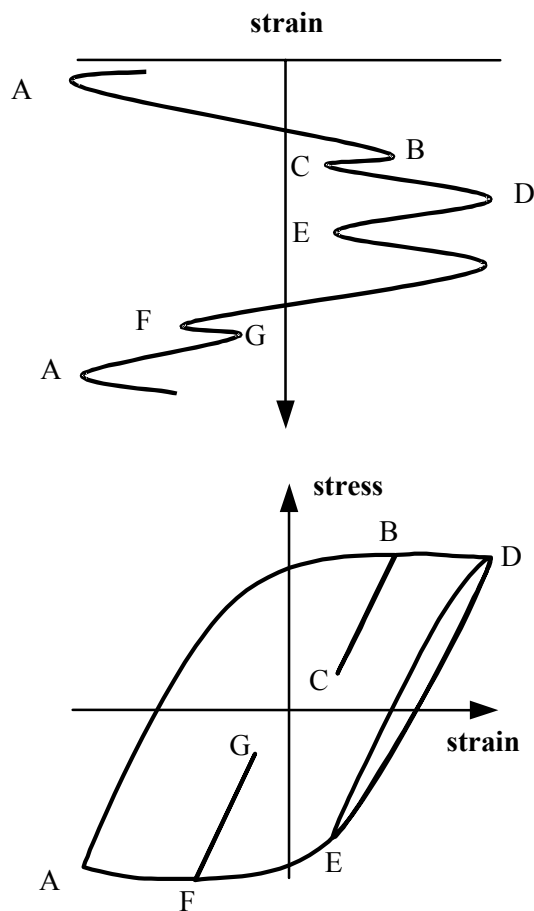
Figure 26: Stress-strain hysteresis capturing by Rainflow counting, drawing after fig.3 from Socie et al. [300]

method', were elaborated in three successive papers, (Endo, Mitsunaga, and Nakagawa[86, 87], 1967, Matsuishi and Endo[194], 1968). Detailed examples were
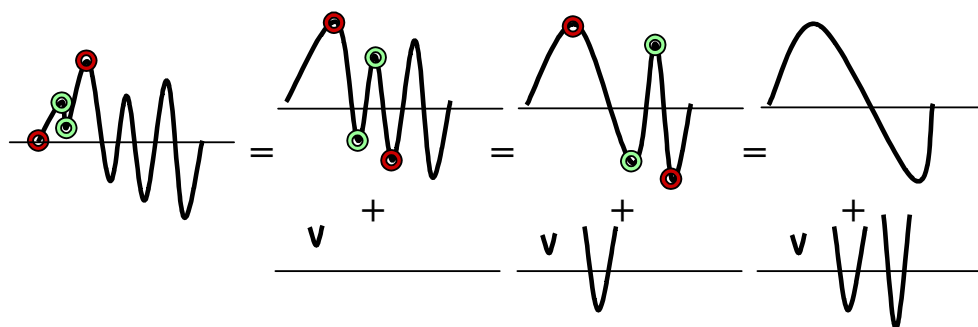
Figure 27: Extraction of range pairs

first described in English in the Master's Thesis by Masanori Matsuishi (Matsuishi[195], 1968), who also provided an alternate formulation of the method which he called the Rainflow method (Socie[299] in Murakami[207], 1992).

Simultaneously in the Netherlands, de Jonge[141] [1969] of the National Aerospace Institute of the Netherlands (NLR) independently devised an algorithm for a hysteresis loop counting method which he later claimed to yield the exact same result as the Rainflow method. An extensive description and discussion of the method can be found in de Jonge[142], [1983].

The algorithm is divided into two phases. In phase I, range pairs are extracted from the signal following a simple logic. The general algorithm is shown in Figure 27. Not all stress or strain ranges are extracted from the original signal. In phase II, the 'residual', consisting of the uncounted peaks and valleys (which are left once phase I has reached the final peak or valley), is treated by considering it as a sequence of ranges, which are extracted accordingly. The residual typically looks like the signal shown in Figure 28, consisting of a diverging part, followed by a converging part.

De Jonge named his algorithm the 'range-pair-range' method. He pointed out, that 'lower order' counting results, such as peak-count results or level-cross results can be derived from the Rainflow count results in a from-to or 'Markov'-matrix (see 'Post-processing').

Soon, the Rainflow counting method and equivalent algorithms found widespread use as a basis for fatigue load data analysis. Dowling[78] [1972] discussed several commonly used counting methods and concluded that only the Rainflow method and the earlier range-pair method were appropriate for a consistent and accurate fatigue load analysis. He also noted that the methods would yield equivalent results in most practical situations, and would give identical results if a sequence would be rearranged, starting at the maximum peak or minimum valley, prior to analysis. This last feature of the Rainflow (equivalent) algorithm(s) is also recognised in ASTM's Standard Practices for
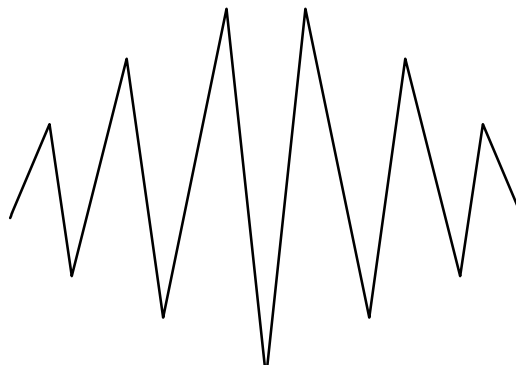
Figure 28: Typical shape of residual

Cycle Counting[5], 1985/1997).

Wetzel[337] [1971] simplified the description of stress-strain behavior of Martin et al.[192] [1971] and implemented a numerical integration technique which he claimed to be superior to the Rainflow method by virtue of being simpler and easier to program on a computer.

A slightly alternate Rainflow counting algorithm was devised by Downing et al.[79] [1976]. The history of peaks and valleys must be rearranged to start with the maximum peak or minimum valley prior to executing the algorithm. In a later (frequently cited) paper, Downing and Socie[80] [1982] present two algorithms, the first the original algorithm from Downing[79] [1976], the second a modification that they name a 'one-pass' algorithm, which can be used without rearranging the peak- and valley-sequence. Both algorithms yield identical results.

As a result, there are two different algorithms that co-exist as 'Rainflow counting'. These are the counting algorithm by Matsuishi and Endo[194] [1968]/de Jonge[141] [1969] (these yield identical results, allowing for half cycles), and the algorithms by Downing and Socie[80] [1982] (their 'algorithm I' and 'algorithm II' yield identical results, which are always expressed in full cycles). The differences between the algorithms are caused by the treatment of half-cycles. Both algorithms yield identical results if 'cyclic counting' is used (see below).

The Matsuishi&Endo/de Jonge algorithm was adopted e.g. by Braam et al.[38] [1998], for PRODETO, a computer tool for evaluation of structural reliability of wind turbine blades developed in an EC-funded project. This document later became part of the IEC-standard concerning measurement of mechanical loads[128]. The relevant ASTM standard describes both methods[5] [1985]. The European Recommended Practices (Madsen et al.[178], 1990) recommend the algorithm by Matsuishi&Endo/de Jonge. Sutherland[309] describes the implementation of Socie&Downing's algorithm in the wind turbine fatigue life evaluation code LIFE2.

Cyclic counting

In some cases, the peak-valley sequence should be rearranged to start and end with the maximum peak or minimum valley. This is referred to as *'cyclic counting'*. For instance, rearrangement in this manner is a prerequisite for 'algorithm I' proposed by Downing and Socie[80] [1982], as was pointed out earlier.

The need for cyclic counting of a repeated sequence was indicated in a paper by van Delft et al.[68, 69] [1996, 1997]. They asserted that 'cyclic counting' is necessary to correctly account for the large cycles in a load sequence. They also were the first to use this term. It is pointed out, that this is an academic exercise, since in reality, the location of the highest peak or lowest valley is unknown a priori. The difference in the counting results is most pronounced for short sequences containing large variations. The largest cycle is counted as a full

cycle in cyclic counting, whereas otherwise it can be counted as a half cycle, which is less conservative.

Rainflow counting of repeated sequences

In the case of stress histories built out of repeating blocks, the Rainflow counting for the entire sequence can be derived from a Rainflow count of the repeating blocks. Amzallag et al.[10] [1994] describe a method to obtain Rainflow counting results for stress histories which are composed of many short sequences. Glinka and Kam[106] [1987] suggested feeding long sequences into the algorithm in parts, for the purposes of speeding up the computations or avoiding computer memory limitations. The results of the method of Amzallag et al. can be approximated by multiplying the 'cyclically counted' Rainflow results for one block by the number of blocks. Generally, it is most straightforward to use the Rainflow counting results for the complete history. Especially in cases where a short sequence contains large variations in extremes, it is less accurate to express the counting result in multiples of short sequence cyclic counted results in the way described in the previous paragraph.

Endo[88] [1981], de Jonge[142] [1983], Socie[299] [1977], Socie and Shifflet[300] [1979], and Downing and Socie[80] [1982] have all described the Rainflow counting algorithm in computer-ready terms for practical application in field data acquisition and processing.

The Rainflow counting method only needs the extremes in a time series of a signal. Therefore, the extremes need to be extracted from the original signal, resulting in a sequence of peaks and valleys.

For practical and/or normalization reasons, the peaks and valleys are usually allocated to a finite number of integer levels. The recommended practices (ASTM[5], 1985) state 50 levels as a minimum (cf. WISPER and WISPERX have 64 levels). For a correct implementation of the Rainflow algorithm, this is not necessary.

Krause et al.[164] [2003] note the relative importance of both the Rainflow counting method and the constant life diagram in the life prediction, see section 5.2.1.

Limitations

There are two major limitations of the Rainflow method

- Loss of cycle order
- Use in cycle-by-cycle analysis

The order in which the cycles appear in the signal is, to a large extent, lost. Strictly speaking, some order information is retained in a from-to-matrix representation of the result (each half cycle is allocated to a matrix where cell

coordinates represent the start and end point of the cycles), but no practical use is made of this information.

The loss of cycle-order information was pointed out by de Jonge with regard to long load histories. The Rainflow counting method pairs the highest peak and the lowest valley into the largest (half) cycle. For time-wise very long peak-valley sequences, where the highest peak and lowest valley occur very far apart, it may not be physically correct to combine them into one cycle. De Jonge[142] [1983] therefore suggested to split the sequence into smaller parts in such cases. The question remains how much time/how many cycles can be between the initiation and closure of a hysteresis loop in composites.

The Rainflow method is not very suitable for cycle-by-cycle analysis, as will be pointed out on page 88.

Anthes[18] [1997] has proposed a modification of the Rainflow method, which allows for conservation of the load-order information and using it in a cycle-by-cycle analysis.

3.2.5   *Rainflow equivalent range-mean transformation*

Range-mean versus Rainflow
In this work, the range-mean and Rainflow counting method are used most. Range-mean counting is the most straightforward to implement in any cycle-by-cycle analysis method but potentially does not count large, damaging, cycles. Rainflow counting, on the other hand, allows for counting large, potentially damaging, cycles, but is not suitable for cycle-by-cycle analysis. The difference between the counting results can be quite significant for the life prediction. This section quantifies the potential difference between the range-mean and rainflow method using a worst-case scenario for the load spectrum.

The worst-case load spectrum is the 'dam spectrum' shown in Figure 25. It is
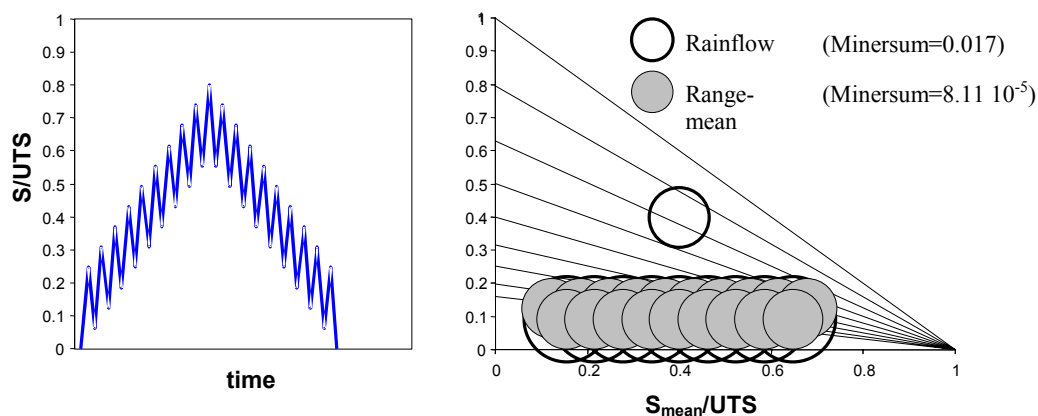
Figure 29: Comparison of Rainflow and Range-mean for dam spectrum

worst-case, because the difference between rainflow and range-mean calculated damage can be excessively large for this type of spectrum. This is due to the fact, that range-mean counting 'misses' the large load cycle.

Figure 29 shows a generic dam spectrum, with separate ranges indicated. Next to it, the number of Rainflow and range-mean counted cycles is plotted in the CLD. The number of cycles is indicated by bubble size. As an example, the linear Goodman formulation is plotted in the figure. Clearly, the Rainflow method counts the single large cycle, which is not counted by the range-mean spectrum. On the other hand, the range-mean spectrum counts the larger upward half-cycles. The damage by the Rainflow-counted and range-mean counted cycles is calculated using the linear Goodman diagram, and the Miner sums (see 3.3) are compared.

Another diagram shows the ratio of Miner sums from Rainflow counted and range-mean counted cycles (Figure 30). Depending on the number of small cycles in the large cycle, and on the ratio of upward to downward small cycle segments, the difference between Rainflow counted damage and range-mean counted damage can be quite excessive. In practice, if the large load cycles consists of a sufficient amount of smaller cycles, with similar upward- and downward segment length, the results of Rainflow counting and Range-mean counting are quite similar, resulting in a Miner's sum ratio close to 1. However, for larger differences between the upward and downward segments, the difference demonstrated is in the order of $>10^{10}$.
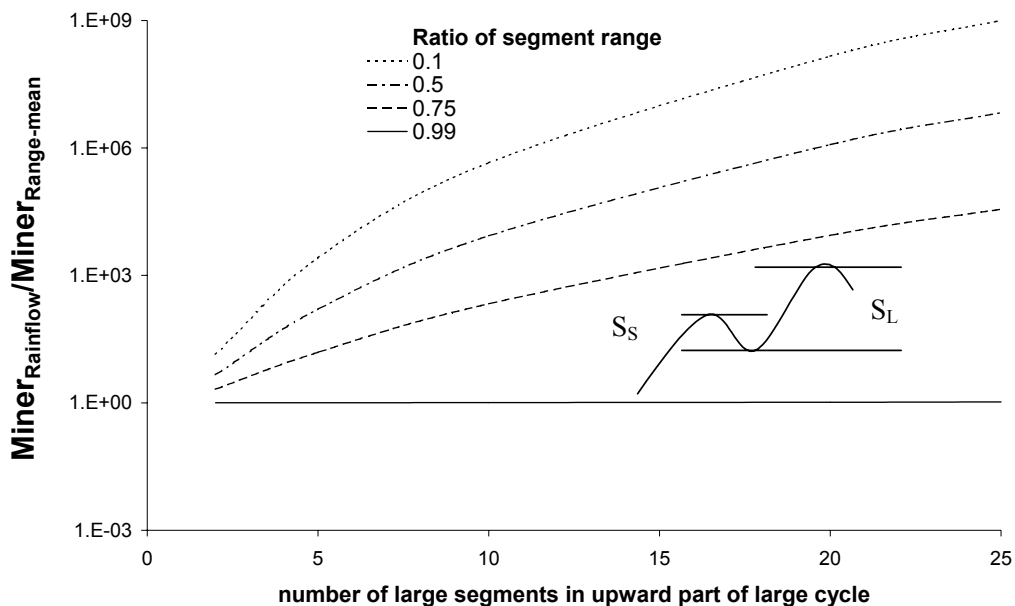
Figure 30: Ratio of segment range (S_S/S_L) Rainflow vs Range-mean

In section 5.2.1, it will be demonstrated, that for wind turbine reference spectra, the difference is much smaller. These spectra are much more forgiving with respect to the choice of counting method. Nevertheless, the above emphasises, that the choice of counting method should be related closely to the spectrum type.

For the 'dam type' spectrum, it is obvious, that Rainflow counting should be employed to correctly account for the large cycle's damage. In the other load spectrum discussed previously, the 'car axle' spectrum, this is less obvious. In this case, the large peak will be related to the minimum valley and counted as one single large cycle. However, in practice, it is debatable whether these load peaks are connected to each other in terms of damage accumulation. Even more so, the loading-unloading peak and valley can be argued to be related to each other, whereas the peaks and valleys from 'road bumps' should be a separate set of cycles. The Rainflow counting method does not see a distinction between the loading-unloading cycles and the driving-time cycles, and might relate them in terms of damage. So, while correctly counting large cycles, Rainflow counting is not capable of discriminating between cycle relationships.

Development of a Rainflow-equivalent range-mean count

For the cycle-by-cycle analysis of strength or stiffness, using recursive models such as the strength degradation model discussed below, it would be preferred to count Rainflow cycles instead of ranges, so as not to miss the large load cycles of e.g. the dam spectrum, or to correctly time singular large load cycles as in the car spectrum.

A potential solution would be to perform Rainflow counting, and count half cycles at the time they are stored in the residual. This allows for an acceptable sequencing of load cycle influence, and would be suitable for a car spectrum-type load sequence.

In the case of a dam-type spectrum, this would lead to the following problem, see Figure 31. At E, the Rainflow count yields BC (2x), AD, and DE; at F this is BC (2x), DE (2x) and AF. Thus, two changes occur simultaneously in the Rainflow matrix, leading to the question which change should be incorporated first.

In addition, for e.g. a strength degradation model, the problem arises, that the instantaneous strength is based on a set of fatigue cycles, which would be, at E: AD, BC(2x), DE. At F' (slightly above D), this would be: AF, BC (2x), DE (~2x). The first loading cycle has significantly changed (from AD to AF), and the strength degradation up to F' must be recalculated not only incorporating the extra segment EF' (which is, for illustration, similar to DE), but also starting with AF instead of AD. Thus, after extraction of a Rainflow cycle, the entire spectrum must be recalculated from the start.
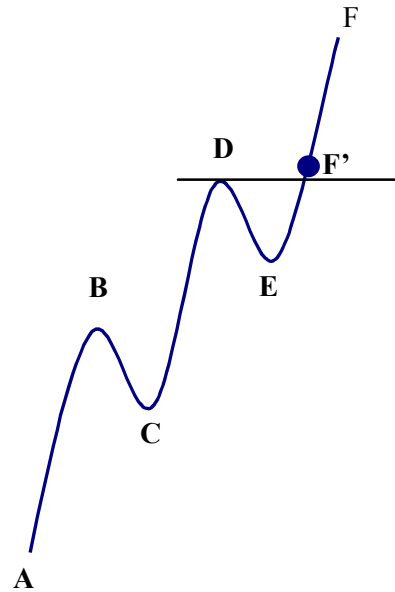
Figure 31: Section of dam spectrum

This is unattractive, since it is not only computationally intensive, but also unnecessary. A simpler method is proposed here, which avoids separating large residual Rainflow cycles in small range-mean cycles, and also avoids the need for re-performing the cycle-by-cycle analysis each time a Rainflow cycle is extracted.

transitional segments
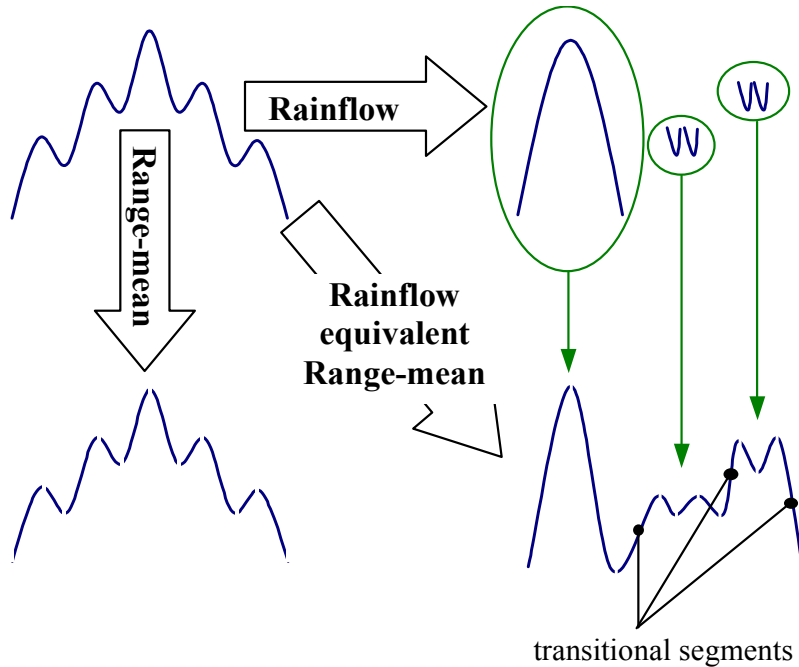
Figure 32: Rainflow-equivalent Range-mean transformation
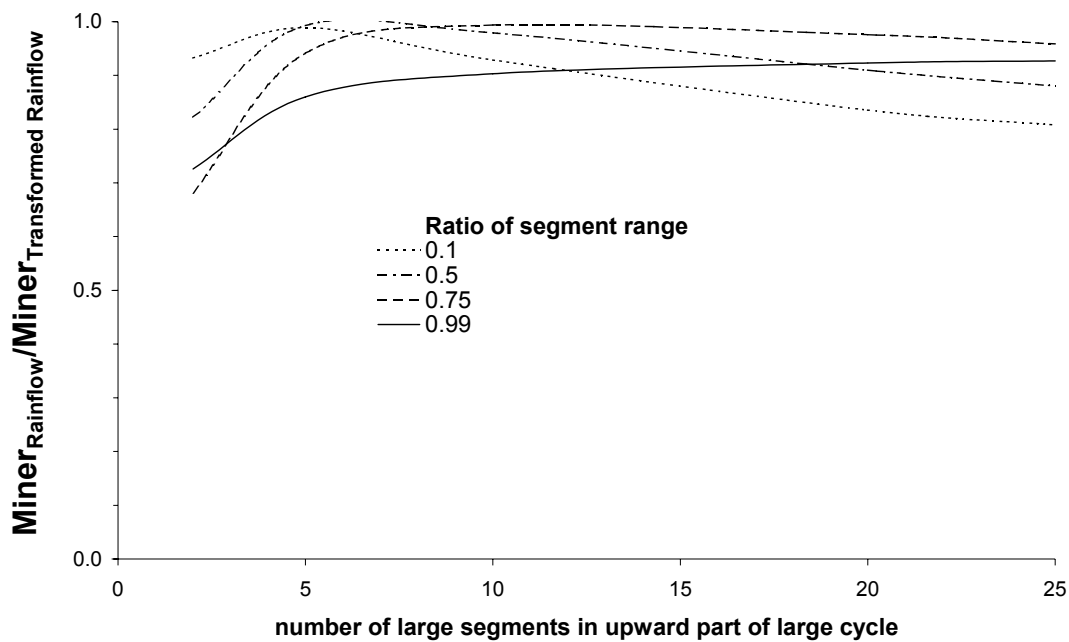
Figure 33: Ratio of Segment ratio (S_S/S_L) for Rainflow vs Rainflow-Equivalent Range-mean

The proposed method consists of two steps. First, the load sequence is Rainflow counted. The counting results can be stored in a list describing for each cycle type the range, minimum, and number of half cycles. Then, by taking the range, min, and number of segments from each bin, constructing load cycles sequentially, a transformed spectrum is created (Figure 32).

Thus, the new load sequence consists of ordered Rainflow counted cycles, and of 'transitional' cycles, connecting cycle blocks from different bins to each other. When this load sequence is processed using a range-mean count, the count result will be very similar to the Rainflow count results of the original sequence. Thus, this method is termed the Rainflow Equivalent Range-Mean count. This does not necessarily mean, that the damage arising from e.g. a Miner's sum calculation is equivalent for both spectra, since this depends on the CLD as well.

The timing problem of singular large cycles is not solved by this method. Ordering the Rainflow bins for constructing a new sequence may be important for the outcome of the cycle-by-cycle analysis. The bins may be ordered according to ascending range, or descending minimum, or by number of cycles per bin. When in doubt, the calculations can be performed with different ordering strategies.

Especially for repeated sequences, with a significant amount of subsequent sequences, it is not expected, that the analysis results will be very sensitive to the order of the cycles in the transformed bin.

Figure 33 is similar to Figure 30, but now shows the Rainflow equivalency of the range-mean-counted transformed spectrum. Miner's sums (using the Linear Goodman Diagram) for both spectra are close to each other, typically within 20% for the dam spectrum characteristics shown. This is much better than the range-mean counted original spectrum (cf. Figure 30).

3.3 Miner's sum

Given its significance in this work, and in fatigue in general, a brief historical account of Miner's rule is in order here. The linear damage accumulation rule which is commonly known as 'Miner's sum' does not describe accumulation of physical damage, nor was it first conceived by Miner. Arvid Palmgren[243] [1924] formulated a similar method more than 20 years before Miner[203] [1945], who based his work on Langer[169] [1937]. The term 'Palmgren-Miner' sum is therefore more appropriate. In this thesis, 'Miner's sum', or 'Miner-approach', is used.
Nowadays, design guidelines for wind turbine rotor blades prescribe the use of Miner's summation to predict lifetime of structures subjected to spectrum loading.

$$D = \sum_i \frac{n_i}{N_i} \qquad (32)$$

where N_i is the number of cycles to failure, n_i is the number of cycles present in the fatigue loading signal, and i is the cycle type. The parameter D is the 'damage' parameter. It is assumed to be equal to 1 at failure. In practice, Miner's sum can deviate from unity.
The limitations of the Miner's sum are:

- 'Damage' is not a physical parameter and does not necessarily relate to parameters such as strength or stiffness. The description of damage is, in a way, binary: the structure is either 'failed' or 'intact'. The definition of failure is arbitrary, and, both in literature and in practice, is seen to range between crack initiation and complete separation of structural components
- Damage contribution by any cycle is irrespective of the damage state prior to the load cycle, in other words, the potential effect of load sequence is not taken into account

The (in)accuracy of predictions using Miner's sum is not only affected by the limitations of the Miner's summation itself, but also by the formulations chosen for the constant amplitude fatigue behaviour. By an appropriate choice of the S-N formulation or the Constant Life Diagram formulation, for both of which exists considerable freedom (Chapter 2), the life prediction can be tailored to experimental data, as was demonstrated e.g. by Nijssen et al.[232] [2001].

Owing to its simplicity, Miner's rule is widely applied in engineering practice. However, potentially due to the abovementioned limitations, Miner's rule has been reported to generate inaccurate and non-conservative results for life prediction in spectrum loading situations. Van Delft[68, 69] et al. [1996, 1997] observed predictions up to a factor 100 longer life than experiment, although other relevant investigations by Schütz and Gerharz[288] [1977], and Schön and Nyman[286] [2002] suggest, that Miner's rule overpredicts fatigue life only by a factor of 2-3.

3.3.1 Factored Miner's sum

Modification of Miner's sum has also been a popular way of improving life prediction while retaining the amount of input information. One of the simplest modifications of Miner's sum is multiplying it by a factor K, usually smaller than 1:

$$D = \sum_i \frac{n_i}{N_i} \leq K \qquad (33)$$

For spectrum loading, a K of 0.1 was considered 'safe for most cases' by Echtermeyer et al.[83] [1996]. Later, based on experimental work on simple spectra and (modifications of) WISPERX, this recommendation was supported by Wahl[328] [2001]. Essentially, modifying Miner's rule in this way is identical to shifting the S-N curves towards lower lifetimes. K should be determined empirically.

3.3.2 Non-linear Miner's sum

In principle, the number of modifications to 'Miner' can be increased indeterminately. Several forms of multiple-parameter-Miner's sums have been found in the literature, which are mentioned here. The model parameters in these formulations typically take the quality of fitting parameters, rather than that they are parameters quantifying the physical background of material degradation.
One method of rewriting Palmgren-Miner's rule was proposed by Owen and Howe[240] [1972]:

$$D = \sum_i \left[A \cdot \frac{n_i}{N_i} + B \cdot \left(\frac{n_i}{N_i} \right)^C \right] \tag{34}$$

Originally, equation 34 was intended by Owen and Howe to describe damage in terms of normalised resin cracking. Bond[37] [1999] used this expression, and an iterative regression procedure to find the best values of *A*, *B*, and *C*. In equation 34, for different cycle types the parameters are assumed constant, but they may very well depend on e.g. R-value. Although this procedure can result in an accurate match with experimental results for a certain combination of material and test conditions, there are some deficiencies.

The prediction result is not very sensitive to the values of some of the constants. This means that for different situations, the values of the constants may be very different, as was indeed seen in the iteratively determined values in Bond's work. Moreover, when the abovementioned curve fit procedure is used, physical meaning to the parameters is diminished.

Philippidis and Vassilopoulos[257, 258] [2000] compared linear Miner and the nonlinear expression above in predicting failure under WISPERX and the EPET 573 spectrum, using values for A and B of 1.5 and −1.5. They noted that, although the parameters are fitting parameters rather than parameters describing physical material behaviour, the merit in this expression was its relative simplicity combined with a very reasonable life prediction. They also used a multi-axial failure criterion to predict the number of cycles to failure for specific loading conditions.

3.4 Strength degradation model

A potential candidate for accurate and reliable life prediction is a strength-based method, where strength degradation due to fatigue damage is tracked, and life is predicted based on exceedance of current strength by the load. It allows for quantifying the effect of load sequence, and it is based on physical damage. This type of model is described in the following paragraphs.

3.4.1 *Overview of strength degradation models*

Various work has been carried out on residual strength investigations from the 1970s. Early investigations are predominantly driven by a damage tolerance philosophy. Typically, coupons were notched or residual strength was measured after impact damage and subsequent fatigue. Predominantly, only tensile strength was considered, and mainly tensile strength after tensile fatigue was investigated only. Compressive strength after purely tensile fatigue, or tensile strength after purely compressive fatigue, are not prevalent in the literature, to say the least.

Broutman and Sahu[41] [1972] were the first to suggest linear strength degradation modelling for use in a life prediction methodology, and they demonstrated that this model is capable of correctly predicting their two-block experiments. Hahn and Kim[111, 112] [1975, 1976] introduced the notion that stronger specimens are likely to have longer fatigue lives. This would later be called the strength-life-equal-rank-assumption by Chou and Croman[49] [1978]. Hahn and Kim[111, 112], and Wang, Chou, Alper[50, 332] [1978–81] checked this assumption using proof tests to filter out weaker specimens and show that the remaining specimens indeed had longer lives. Ryder and Walker[273] [1976] provided extensive residual strength data, which were used for modelling by Yang et al.[354, 358] [1978-83]. Schaff and Davidson[278] [1997] revived the strength degradation approach to life prediction, and Wahl[328] [2001] has performed extensive spectrum loading research to validate strength-based life prediction for wind turbine composites.

The above authors limit themselves mainly to a phenomenological approach. Conversely, Reifsnider and co-workers[266-269] [1980-2000], and Subramanian et al.[308] [1995] have explored in some detail the microscopic processes that translate into macroscopic property degradation. Song and Otani[305, 306, 242] [1997-98] have explored microscopic damage as a result of fatigue, and included relationships of various damage types (fibre, transverse, and delamination crack density in cross-ply carbon fibre laminates) with residual strength.

van Paepegem et al.[244-248] [2001-02] interpreted residual strength as a measure of decrease of the effective cross-sectional area, coupled strength to damage in terms of stiffness degradation, and numerically implemented their method.

Extensive reviews of strength degradation modelling are provided in Degrieck and van Paepegem[70] [2001] and Philippidis and Passipoularidis[256] [2003].

All residual strength models have in common, that they describe strength as a monotonously degrading function of life fraction. Single parameter models can be tailored, such that the models are capable of describing linear degradation, 'sudden death' type behaviour, and 'early degradation'. Multiple parameter models have the advantage of describing a combination of rapid early degradation, and a moderate degradation ('plateau') at central life fractions.

Yao and Himmel[360] [2000] describe residual strength degradation using trigonometric functions:

$$S_r = S_0 - (S_0 - S_{max}) \left(\frac{\sin \beta \dfrac{n}{N} \cos(\beta - \alpha)}{\sin \beta \cos\left(\beta \dfrac{n}{N} - \alpha\right)} \right) \tag{35}$$

They recommended values for α and β of π/3 and 2π/3, respectively. The advantage of this formulation, is, that an S-type strength degradation curve can be described, albeit at the penalty of an additional model parameter. From the experimental data, it seems that such a multiple-parameter description is in some cases more appropriate than a single-parameter description.
Whitworth[345] [2000] uses a modified version of the model used by Hwang and Han[124, 125] [1986]:

$$S_r{}^\gamma = S_0{}^\gamma - (S_0{}^\gamma - S_{max}{}^\gamma)\left(\frac{n}{N}\right) \tag{36}$$

Wahl[328, 329] [2001, 2002] has adopted:

$$S_r = S_0 - (S_0 - S_{max})\left(\frac{n}{N}\right)^C \tag{37}$$

More precisely formulated:

$$S_{r_i} = S_0 - (S_0 - S_{max\,i})\left(\frac{n + n_{eq}}{N}\right)_i^{C_i} \tag{38}$$

where,

i	=	Current cycle type
S_{ri}	=	Residual Strength after n_i cycles at S_{maxi}
S_0	=	Initial Strength
S_{max}	=	Maximum load applied in fatigue
n_i	=	Number of cycles with S_{max}
n_{eq}	=	Number of cycles at S_{max} which would have led to strength $S_{r,i-1}$
N	=	Number of cycles at S_{max} which would lead to failure

The parameter C describes the nature of strength degradation: linear degradation, early degradation, or 'sudden death'. See also Figure 34.

The term n_{eq} was named 'equivalent number of cycles' by Wahl[328] [2001]. Schaff and Davidson[278] [1997] used 'effective number of cycles' for the same parameter. In formula:

$$N_{i-1}\left[\frac{S_{r_{i-1}} - S_0}{-(S_0 - S_{max\,i-1})}\right]^{\frac{1}{C_{i-1}}} = n_{eq\,i-1} \tag{39}$$

Calculation of the equivalent number of cycles typically occurs at a change of cycle type and is crucial to the strength degradation method. When, at a given point in the load sequence, the instantaneous strength at cycle *i-1* is known (S_{i-1}), the equivalent number of cycles at *i* is defined as that amount of cycles, which would have degraded strength down to S_{i-1}. The equivalent number of cycles is used as a starting point for the calculation of strength degradation due to cycle *i*.
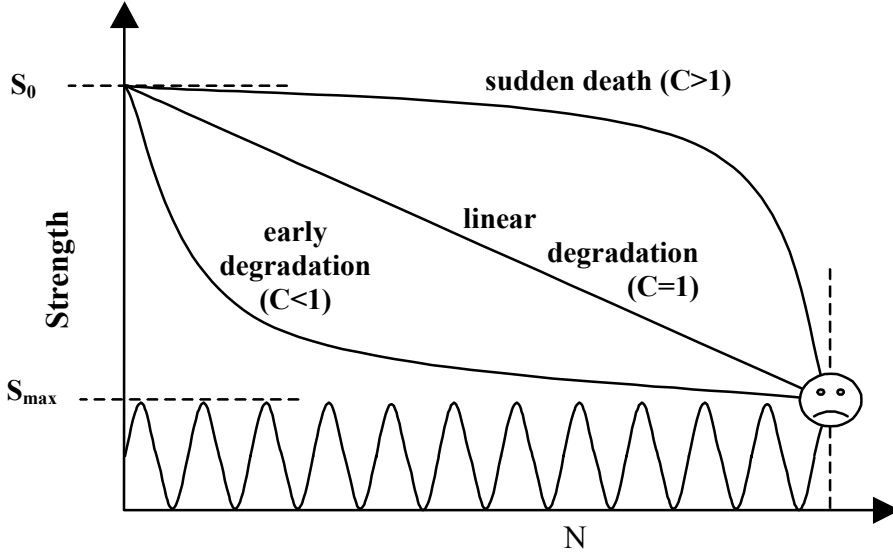
Figure 34: Classification of strength degradation (one-parameter model)

3.4.2 *Modification for mixed sign strength degradation*

The strength degradation model tracks the residual strength, based on the input load cycles. The formulation of the model as eq. 38 presumes, that the residual strength will, at failure (i.e. *n/N=1*), be equal to the maximum load. In the literature, it has been used to describe tensile strength after R=0.1 fatigue, e.g. Wahl[328] [2001].

How does the model behave if the tensile strength needs to be quantified after compressive fatigue, or vice versa? This could be important in realistic loading situations, where tensile and compressive loads are mixed, and the residual strength needs to be described both in tension and compression.

For further use in this work, the model is rewritten as:

$$S_{r,t} = S_{0,t} - (S_{0,t} - max[S_{max},0]_i)\left(\frac{n}{N}\right)_i^{c_i} \qquad (40)$$

$$S_{r,c} = S_{0,c} - (S_{0,c} - abs\{min[S_{min}, 0]_i\}) \left(\frac{n}{N} \right)_i^{C_i} \qquad (41)$$

The difference with the previous formulation (eq. 38) is, that for mixed-sign residual strength, residual strength is assumed to ultimately go to zero, as indicated by the *max/min* terms.

In a residual strength-based life prediction, both the tensile and compressive strength are tracked simultaneously. They must be, for *a priori* it is not known whether the structure will fail during a compressive or during a tensile peak. In the implementation of the model, both equations are therefore used, albeit sometimes with different values for the strength degradation parameters.

It is assumed, that tensile and compressive strength degrade independently of each other. This is an important assumption, which was made because there are no previous references covering this topic. However, it is possible, that tensile and compression strength degradation are somehow interrelated.

3.4.3   *Implementation in a computer programme*

The strength degradation methodology is best implemented in a computer programme, only the simplest cases can be treated analytically (section 3.5). A flow diagram of the computer program is shown in Figure 35.

The subdivision of the algorithm in 'pre-processing' and strength degradation evaluation is specifically tailored for pre-defined sequences. First, the sequence and number of cycles to failure is quantified. It would be possible to do this in a subroutine during the strength evaluation loop, but this can be considerably more time-consuming.

In treatment of actual load signals, cycle type occurrence can not be quantified on beforehand. However, it should be considered standard practice to start the prediction process with a cataloguing procedure, so that cycle characteristics for all potentially occurring cycles can be stored beforehand and quickly retrieved during the strength evaluation loop, without the need for much repetitive computation.

When the formulation of equation 38 is considered numerically, it is seen that it results in subtracting a very small number (with the *n*-term) from a relatively large number (Ultimate Stress *US*). Implementation in a computer programme tracking the residual strength, might lead to rounding errors inherent to the data type used for the strength. For example, with an average life to failure *N* in the order of 10^9, and a *C* of ~10, a number in the order of 10^{-90} is obtained. While this is still much larger than the smallest number representable by a double precision floating point 8 byte number (which ranges down to 10^{-308}), when subtracted from the ultimate strength (order of magnitude 100), the limited number of decimals causes the subtraction to go unnoticed by the computer programme. As a result, no numerical strength degradation occurs.
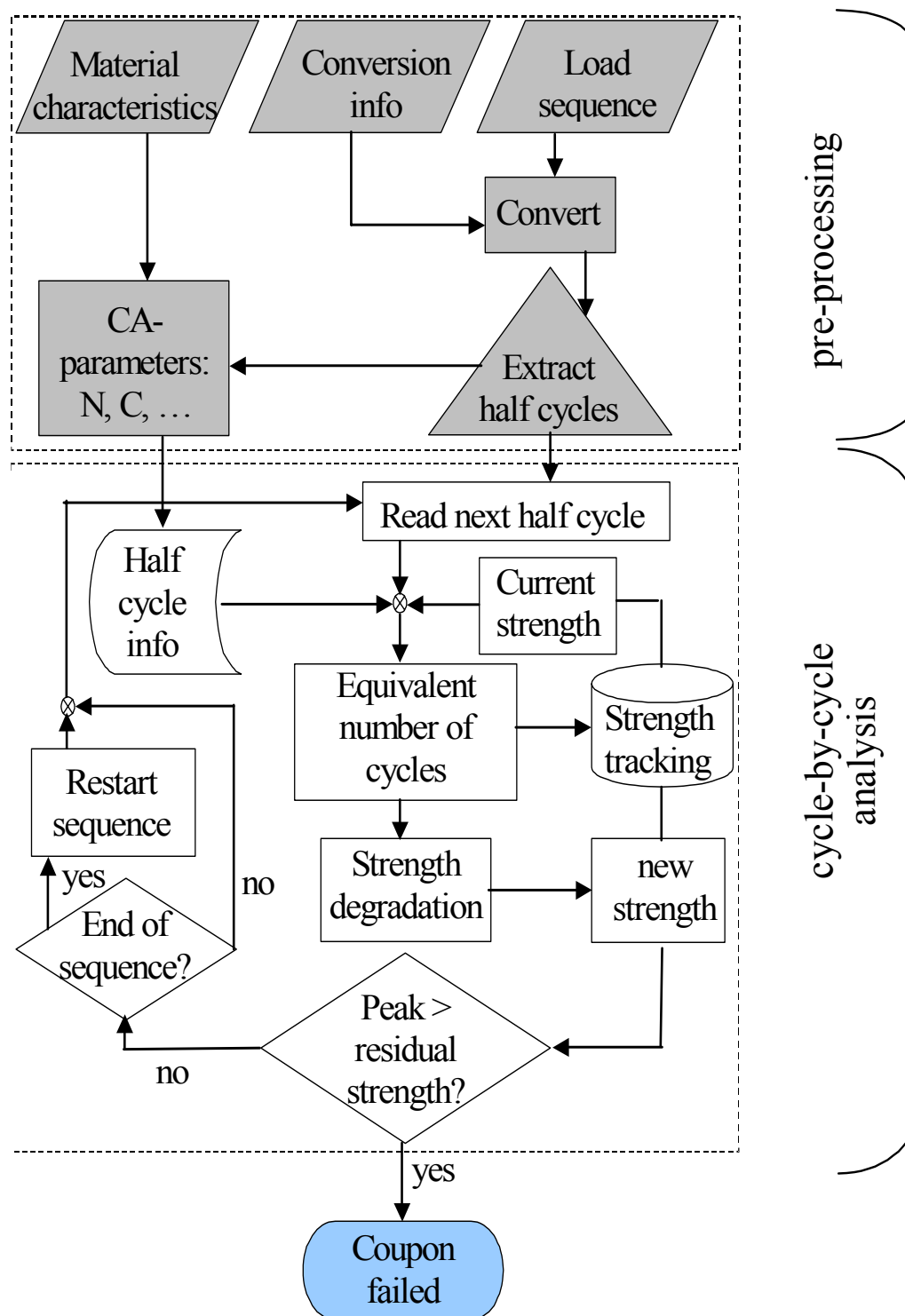
Figure 35: Flow diagram of strength-based life prediction

Tracking the cumulative strength degradation, instead of the current strength, helps avoiding rounding issues for relevant strength degradation parameters. This is done using the following formula set:

$$\frac{n_{eq}}{N} = \left[\frac{US - S_{r-1}}{US - S_{max}} \right]^{\frac{1}{C}} \tag{42}$$

$$US - S_r = (US - S_{max}) \left(\frac{n_{eq} + 0.5}{N} \right)^C \tag{43}$$

In this formulation, $US\text{-}S_r$ represents the cumulative strength degradation. Each half cycle (or segment) is considered separately, therefore, the term *0.5* is included in equation 43. This adaptation is particularly useful in the practical situation, where *C>0.2* (see Chapter 4).

3.4.4 *Extracting the strength degradation model parameters*

Description of the method
A few assumptions are made to extract strength degradation parameter *C* of equation 38 from strength degradation plots:

- The strength degradation parameter C is equal for all specimens in the strength degradation plot
- Strength degradation lines for different specimens do not intersect
- All specimens in the strength degradation plot come from the same population
- Coupon static strength and fatigue life are related

These assumptions are discussed on page 102. Rewrite equation 38 for individual test coupons:

$$S_i = S_{0,i} - (S_{0,i} - S_{max}) \left(\frac{n_i}{N_i} \right)^C \tag{44}$$

where the subscript *i* indicates, that individual specimen fatigue life and strength are described here. Next, an initial value of *C* is assumed. A value of 1 is usually an appropriate initial guess. Using this value of the degradation parameter, from the residual strength dataset (S_i, n_i), two new sets of data are created, viz. $S_{0,\ i}$, and N_i. This is enabled by the Strength-Life-Equal-Rank-Assumption (SLERA), which stipulates, that a specimen with a relatively high static strength will have a relatively long fatigue life, and a specimen with a

relatively low static strength will have a relatively short fatigue life. See Figure 36 and Figure 37.

$$S_{r,i}=S_{0,i}-(S_{0,i}-S_{max})(n_i/N_i)^C$$
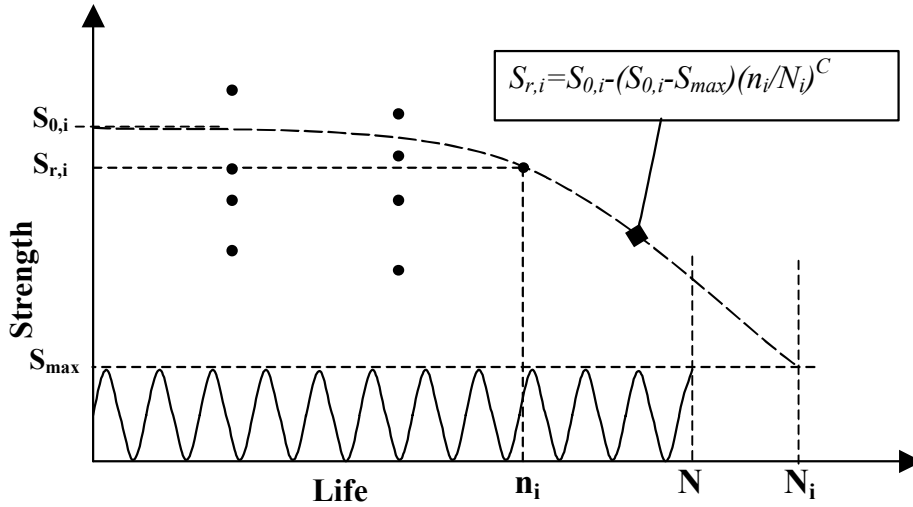
Figure 36: Procedure for finding Residual Strength Degradation Parameter

There are several ways to implement the SLERA, i.e. several manners in which static and fatigue strengths can be paired. The first is pairing static and fatigue data with equal, or similar, ranks to find, via regression analysis, a relationship between static and fatigue strength for use in the strength degradation model definition. This is most straightforward if the size of the static and fatigue datasets is equal or similar.
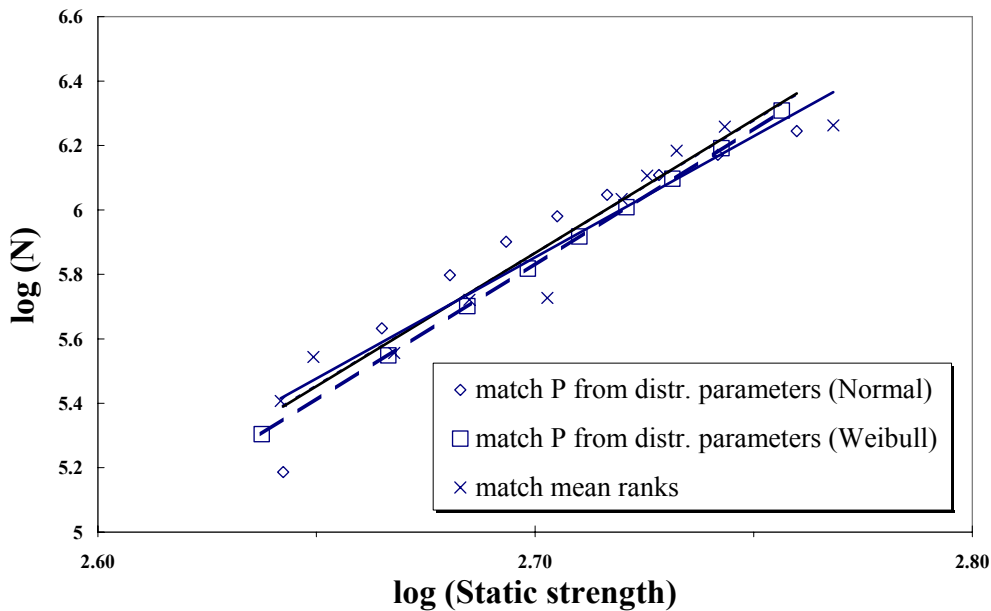
Figure 37: Example of relation between initial strength and fatigue life (SLERA)

Another method, which is applicable to virtually any combination of static and fatigue datasets, is to fit a distribution through the static and fatigue data, and use the distribution parameters to pair strengths and fatigue lives with equal probability of failure. A relationship between these (calculated) data pairs is, again, found through regression (Figure 37).

Typically, linear regression in the $(log(N), S)$, or $(log(N), log(S))$-space yields appropriate fits, see for example Figure 37. Acceptable results were even found with linear regression in the (N, S) space, e.g. Nijssen et al.[218] [2005]. Generally, goodness-of-fit-parameters R^2 of ~0.95 were attained. A suitable fit is generally obtained when both the static and fatigue datasets are described using the Weibull distribution with shape parameter α and scale parameter β: equate failure probabilities, and rewrite to obtain the relationship between strength and life:

$$P(N) = e^{-\left(\frac{N}{\beta_N}\right)^{\alpha_N}} = P(S) = e^{-\left(\frac{N}{\beta_S}\right)^{\alpha_S}} \tag{45}$$

$$N(P) = \beta_N \left(\frac{S(P)}{\beta_S}\right)^{\frac{\alpha_S}{\alpha_N}}, \text{ or, equivalently} \tag{46}$$

$$log[N(P)] = \frac{\alpha_S}{\alpha_N} log\, S(P) + \left[log\, \beta_N - \frac{\alpha_S}{\alpha_N} log\, \beta_S \right] \tag{47}$$

The same can be done for the Normal distribution, but the regression parameters have to be determined numerically.

Thus, a set of virtual fatigue data and a set of virtual static data are created from the residual strength data, using a guessed value of C. The validity of this strength degradation parameter used to create these virtual datasets can be evaluated by comparing the virtual constant amplitude fatigue and static datasets to the actual datasets.

For instance, mean static strengths or fatigue lives can be compared, or a combination of both. Furthermore, it is possible to make a comparison of other statistics of the dataset. This can be expressed in a cost function of general form:

$$J = \left\{ \frac{D}{\alpha_S} |\alpha_S - a_S(C)| + \frac{E}{\beta_S} |\beta_S - b_S(C)| \right\} + \left\{ \frac{F}{\alpha_N} |\alpha_N - a_N(C)| + \frac{G}{\beta_N} |\beta_N - b_N(C)| \right\}$$

$$\tag{48}$$

where D-G are weight factors indicating the relative importance of the criteria, S and N refer to the static and fatigue datasets, respectively, Greek symbols refer
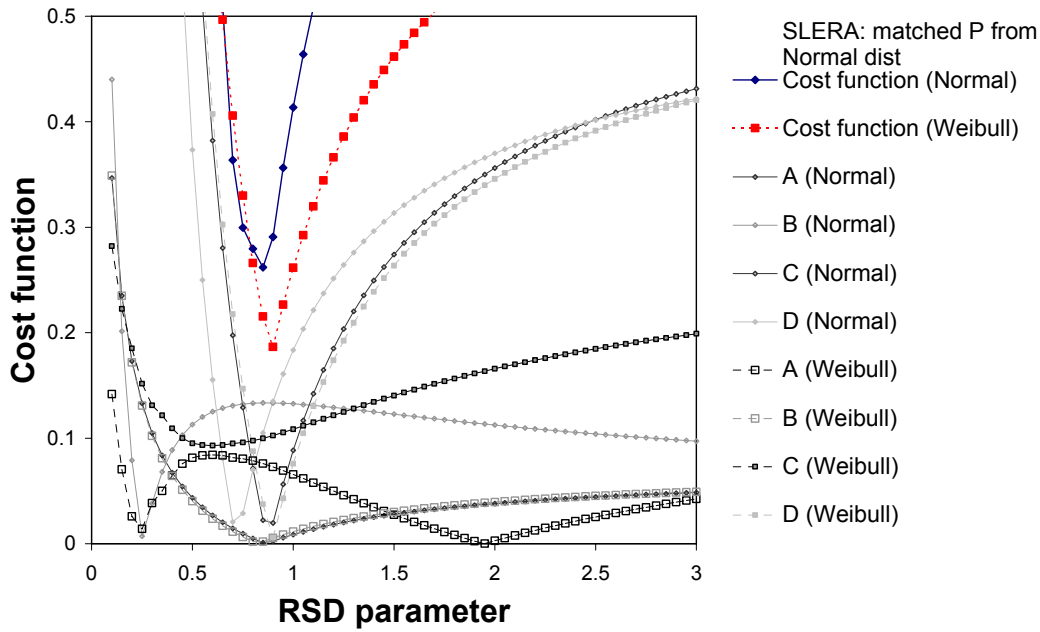
Figure 38: Weighted cost function breakdown

to the distribution parameters of the actual static and fatigue datasets (e.g. either Weibull shape and scale or Normal mean and standard deviation), and Roman letters refer to the distribution parameters of the virtual datasets.

The parameter C is modified to find the minimum value of J in eq. 48. Visual inspection of the resulting strength degradation function, and of the cost function is recommended. A plot of the cost function vs C helps to compare the influence of the various contributions. This may lead to modifying the weight parameters. E.g., if the importance of scatter in the virtual datasets is disregarded (i.e. setting D and F to 0), other solutions may emerge, yielding better fit of the dataset means, but larger spread in the virtual datasets. An example of the cost function and cost function break-down for the Normal and Weibull parameters is illustrated in Figure 38.

It is believed, that the scatter in the data does not justify determination of the strength degradation parameter with an accuracy exceeding 2 significant digits.

Discussion of the assumptions
The most controversial assumption that was made above is the strength-life-equal-rank assumption (SLERA). The SLERA stipulates, that for specimens from the same population, the ranks of strengths and lives are identical. In the frame of the residual strength degradation, this implies, that strength degradation lines connect static and fatigue data at equal percentiles of their respective probability distributions.

Fundamentally, it is not possible to verify the assumption, since one can only destroy a given coupon/structure once: both a static and a fatigue test until failure can not be done on the same specimen. In addition, as Curtis and Davies[57] have observed [2000], the SLERA neglects the possibility of failure mode changes as a function of stress level, and, similarly, is less likely to be valid if static failure mode is different from fatigue failure mode, Chou et al.[53] [1980]. Chou et al. also posed, that in sudden death models, where strength degrades without warning at the end of fatigue life, the SLERA is imposed, whereas in stronger degradation, the SLERA is implied. They advocate the use of models which have both deterministic, micromechanical, and statistical fundaments.

Whitney[343] [1983] discusses an example where the non-validity of the SLERA may be implied. He performed static, fatigue, and residual strength tests and employed a statistical strength-degradation model to predict the associated strength and life distributions. This prediction was successful, except for the distribution of residual strengths, and he attributed this to a difference in failure mode. In static strength, he observed localised delamination, in contrast with the fatigue failures, where extensive distributed delamination was visible. A similar observation on localised vs distributed damage was mentioned by Daniel[59] [1999], who also questioned (in fact: caricaturised) the significance of accelerated testing.

Hahn and Kim[111] [1975] and Awerbuch and Hahn[20] [1977], and later Wang, Chou, and Alper[52, 332] [1979, 1981], and Chou, Wang and Croman[53] [1980] have employed the concept of proof-testing to evaluate the SLERA. Awerbuch and Hahn concluded that it was very likely that there is a unique relationship between static strength and fatigue life. They hypothesise that, since the fatigue limit of steel is empirically related to the static strength (which could be interpreted as a formulation of the SLERA), the static and fatigue failure modes should be similar. From practice in composites testing, this seems inappropriate. Ryder and Walker[273] [1976] noted, that the static strength of composite specimens depends significantly on the test method. They related the differences in static strength to differences in failure mode. For example, if end-loading is used in a compressive test, the result is partially determined by the resistance of the end-loaded fibres to buckling, and not by e.g. the shear properties of the matrix. In a set-up with no end-loading, the compressive property is more significantly determined by the matrix shear resistance. Thus, in the relation between strength and life, the test method and failure mode should be taken into account. The same applies to the relation between the static strength, and the residual strength after fatigue.

Hwang and Han[126] [1987] noted a valuable merit of the SLERA, namely that 'non-statistical' cumulative damage theories, including the Miner's sum, can be modified for the prediction of multi-stress fatigue distribution, using the strength-life-equal-rank assumption.

The other assumptions that were made include the assumption, that the C-parameter is equal for all coupons in the strength degradation plot. This implies, that C depends on maximum load and R-value. The assumption, that strength degradation lines do not intersect can be seen as a combination of the SLERA and of the equal-C-parameter assumption.

Constraints to extracted parameters
The strength degradation parameter is subject to some constraints. An inconsistency might occur, when the strength degradation parameters are such, that lower maximum loads might cause more rapid (initial) strength degradation than higher maximum loads. In other words, the strength degradation lines of different load levels may not intersect. S_0, rewriting the strength degradation model (eq.38), for two load levels $S_1 > S_2$, with strength degradation parameters $C_{1,2}$:

$$S_1 = S_0 - (S_0 - S_1)\left(\frac{n}{N_1}\right)^{C_1} < S_2 = S_0 - (S_0 - S_2)\left(\frac{n}{N_2}\right)^{C_2} \quad (49)$$

$$C_1 < C_2 \frac{\left\{ log\left[\frac{(S_0 - S_2)}{(S_0 - S_1)}\right] + log\left(\frac{n}{N_2}\right) \right\}}{log\left(\frac{n}{N_1}\right)} \quad (50)$$

then, using: $x = n/N_1$,

$$C_1 < C_2 \frac{\left\{ log\left[\frac{(S_0 - S_2)}{(S_0 - S_1)}\right] + log(x) + log\left(\frac{N_1}{N_2}\right) \right\}}{log(x)} \quad (51)$$

$$C_1 < C_2 \left\{ 1 + \frac{log[K]}{log(x)} + \frac{log\left(\frac{N_1}{N_2}\right)}{log(x)} \right\} \quad (52)$$

This should be valid for all *n*. Since strength degradation is a monotonously decreasing function of life fraction, the limiting case is *x=0* (or, in practice, *x=1/N₁*. For *x<<1*, the term between accolades approaches unity.

Hence, strength degradation parameters at higher loads should be smaller than those at lower loads, in order not to violate the premise, that strength degradation at lower load should not exceed that at high load. Taking *n=1* as a limiting case, rather than *n=0*, the minimum strength degradation parameter can be derived at S_1 from that at S_2, and the value depends on the S-N parameters.

Role of premature failures

Premature failures occur naturally as a consequence of fatigue life scatter. The number of premature failures depends on the life fraction, which in turn is a function of average fatigue life.

In the two projects (MSU and OPTIMAT), the definition of average fatigue life and the according life fraction definitions were attained in different manners. At MSU, average fatigue life was determined first from constant amplitude fatigue tests. The advantage is, that the resulting life fractions at which residual strength tests were done, consequently are close to the actual life fractions. A disadvantage is, that most of the constant amplitude fatigue tests need to be done in advance, which makes randomisation of test order impossible.

In the OPTIMAT test programme, it was chosen to employ the concept of nominal life. The advantage is, that different test programmes (static, fatigue, residual strength, and block tests), that are interconnected, can be executed in parallel at different laboratories, thus avoiding delays, and promoting test order randomisation. A prerequisite is, that a benchmarked S-N curve must be predefined, from which the nominal load level-lifetime-pairs can be extracted.

The result of the discrepancy in approaches is, that the nominal life fraction, and the actual life fraction of the population, are likely to be closest when the average fatigue life is determined first (as in the MSU programme). In the OPTIMAT programme, nominal life fraction and actual life fraction depend on the accuracy of the predefined mean S-N curve.

In both cases, the number of premature failures in the residual strength test programme theoretically can aid in improving the accuracy of the mean life determination.

A prerequisite for successfully implementing such a procedure, is a record for each residual strength test of the intended life fraction. If this is available, premature failures can be allocated to an intended life fraction, and this is necessary for a correct evaluation of the number of premature failures. Such a record was available in both the OPTIMAT and the MSU programmes.

Use of stiffness degradation

In general, a relationship between the characteristics of coupon stiffness and fatigue life is expected, see e.g. section 2.3.1. Theoretically, this knowledge could be of use for the extraction of the strength degradation parameter. In particular, comparison of initial stiffness to the stiffness prior to or during residual strength testing, may yield information on the actual life consumption of the coupon. For example, imagine three coupons tested for residual strength at a certain nominal life fraction. If an expression for stiffness degradation versus life is known, and this expression is a monotonic function, the actual life fraction of the coupon can be estimated from the (relative) stiffness decrease. This can be used instead of the SLERA to reduce equation 44 to a formulation with a single unknown.

A committee chaired by Waddoups[327] [1991] noted, that stiffness degradation usually displayed a monotonous degradation, whereas strength could degrade or improve, depending on the material and structural characteristics. Ryder and Walker[273] [1976] complemented their measurements with measurement of the initial modulus. Tang et al.[321] [2004] observed, that for unidirectional materials, the stiffness is a poor measure for the residual strength, since the stiffness degradation is only minor. They proposed to use torsional stiffness as a quantification of damage, but their test set-up is relatively unconventional, and they did not evaluate the practical applicability of torsional stiffness measurements on a laminate as part of a (blade) structure.

In practice, the stiffness degradation of the MSU coupons was not tracked. For the OPTIMAT coupons, no apparent correlation between stiffness degradation and residual strength was found by Nijssen and van Wingerde[225] [2006] for the standard coupons. Mild correlations were reported by Philippidis and Assimakopoulou[259, 260] et al. [2005].

3.4.5 Interpolation of the strength parameters

Similar to interpolation of the constant amplitude fatigue behaviour between R-values, the strength degradation parameters should be interpolated for conditions that are not covered by experiments. Considerable effort is needed to determine strength degradation parameters from residual strength tests at, typically, three R-values (-1, 0.1, and 10). For other R-values - presupposing that strength degradation parameters are R-value dependent-, the strength degradation behaviour must be determined from these data, to avoid an excessive number of additional experiments. A master-diagram approach as suggested by Schaff and Davidson[278, 279] [1997] is appropriate, however, it will be demonstrated in Chapter 5, that it is likely that interpolation of strength degradation parameters has limited effects on prediction accuracy.

3.4.6 Advantages and drawbacks of strength degradation models

The two major benefits, of strength-based life prediction are:

- A physical parameter is tracked
- sequence effects are accounted for

A residual strength degradation model has the advantage of physical interpretation of some of the effects of fatigue loading. One of the important implications of including effective strength degradation-based lifetime prediction methods is, that the residual strength of a blade could be tracked based on bending moment measurements, and assessment of the blade's structural reserves could be made during the economical lifetime.

The residual strength model takes into account the order of the load cycles in the sequence by tracking the macroscopic strength. Thus, cycles that produce significant strength degradation influence the strength degradation in later cycles. In these later cycles, the strength tracking starts at a higher equivalent number of cycles. For $C>1$, this means, that the rate of strength degradation in a particular cyclic loading block is higher, if the previous block resulted in a lower strength. The reverse holds for $C<1$, strength degradation rate in the constant amplitude block is lower as strength degrades more in the previous block. Sequence effects will be elaborated on in more detail in section 3.6.

The drawbacks of strength-based life prediction are:

- only a single physical parameter is tracked
- large experimental effort to determine model parameter(s)
- computationally intensive

The advantage, that a physical parameter is tracked instead of a dimensionless quantity in Miner's sum, is limited in the sense that only one parameter is tracked. It is likely, that for instance stiffness can also be useful in the description fatigue degradation. In order to describe strength degradation in constant amplitude fatigue, a large number of destructive tests are required. Furthermore, the strength degradation analysis of a load spectrum is a cycle-by-cycle process requiring more calculations than Miner's approximation.

3.4.7   Strength degradation data from literature

Strength degradation plot
Residual strength data are plotted in a so-called 'strength degradation plot', of which an explanatory example is shown in Figure 39. Such a plot contains the static, fatigue, and residual strength results for a particular combination of R-value and load level. In principle, the strength degradation plot is similar to an S-N diagram. The ordinate represents the load, whereas the abscissa represents life. Either axis may be normalised in various manners. In this case, static strength was normalised by UTS, and fatigue life was normalised by average fatigue life of constant amplitude tests done at the depicted load level.
The abscissa is plotted in a linear manner, rather than using a logarithmic scale. This is useful, since this allows for recognition of 'linear' degradation trends. In a log-plot, most degradation trends would appear 'sudden death'. Moreover, the normalisation facilitates comparison with residual strength trends at other load levels or R-values.
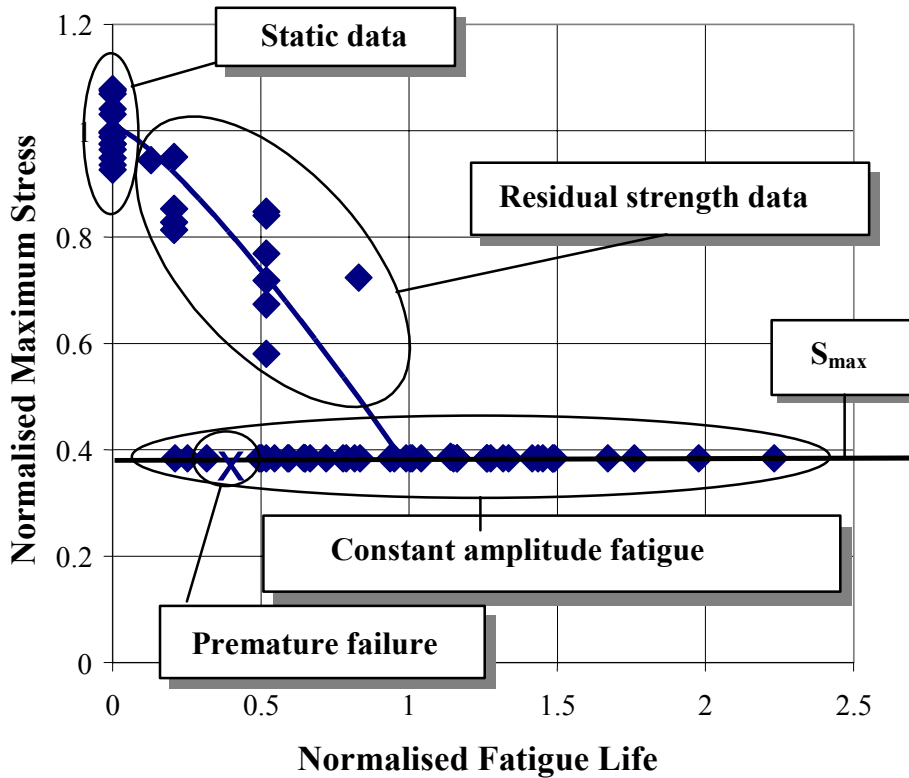
Figure 39: Strength degradation plot

Various reference parameters may be used for the normalisation. For instance, if fatigue failure was compressive, strength was normalised with UCS instead of UTS. Also, to find average fatigue life on the load level used for residual strength testing, S-N data from other load levels may be used, resulting in a slightly different normalisation. Note, that normalising using the average fatigue life results in a plot, where normalised fatigue life n/N_{avg} can exceed unity.

Data from literature

In composite fatigue literature, strength and stiffness degradation models are quite abundant, as opposed to actual strength degradation data. An overview is presented of the most relevant data for comparison with the present results.

Ryder and Walker[273] [1976] have produced extensive residual strength degradation data on graphite/epoxy materials, and they have investigated various R-values as well as mixed-sign residual strength. A selection of results by Ryder and Walker is presented in Figure 40. Only a single life fraction was investigated, which does not facilitate finding the strength degradation trend, although linear degradation seems appropriate. Some of the data of Ryder and Walker were extensively analysed by Yang and Jones[355], e.g. [1978].
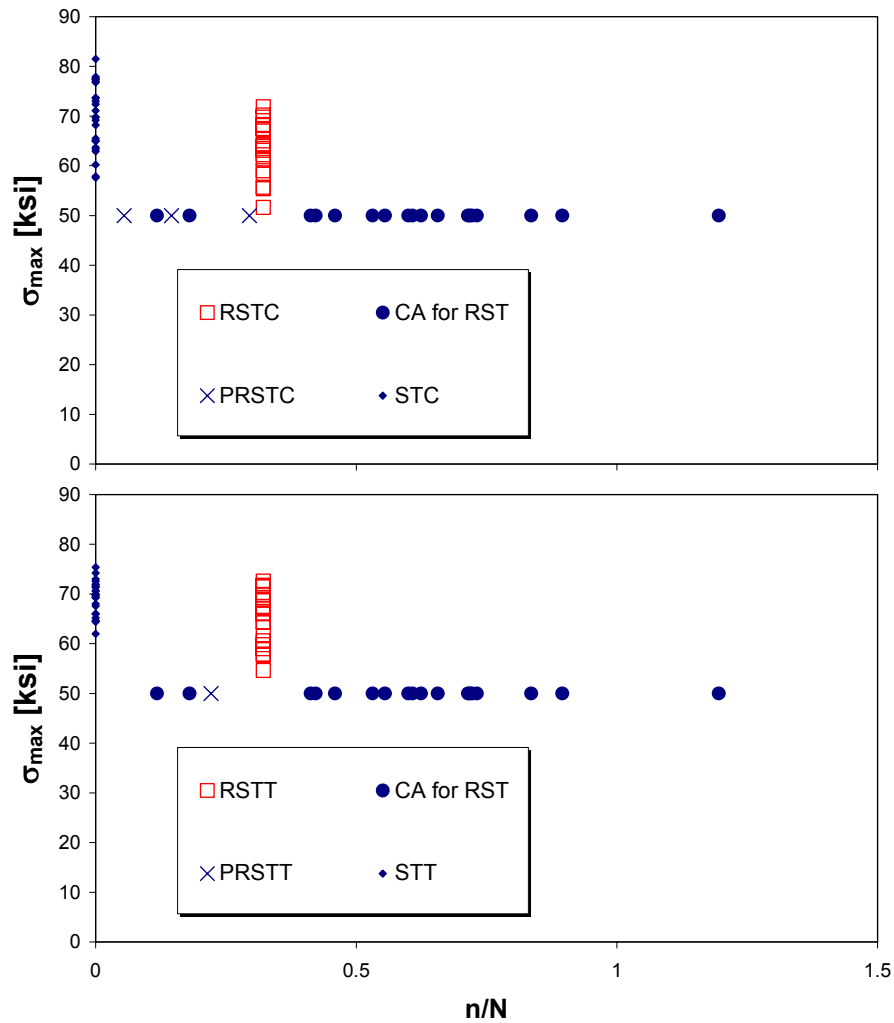
Figure 40: Residual compressive (top) and tensile strength data from Ryder and Walker

Yang and Jones have also presented strength degradation in shear fatigue, on ±45° graphite/epoxy specimens. There seems to be some initial strength degradation in early life, but then the strength remains constant up to a high fraction of life, see Figure 41. Strength degradation is consistent with stiffness degradation. Fatigue stress was approximately 50% of the ultimate shear strength (14.25 ksi). Whitworth[345] [2000] presents residual strength data for [±35°]$_s$ graphite/epoxy laminates after R=0.1 fatigue, and notes a non-linear strength degradation that is best described by γ=4 in eq. 36.

Joneja[139] [1986] presented strength and modulus degradation data for unidirectional glass-fibre epoxy after 25%, 50%, and 75% of the fatigue life. Essentially the strength and stiffness remained within the scatter bands of the
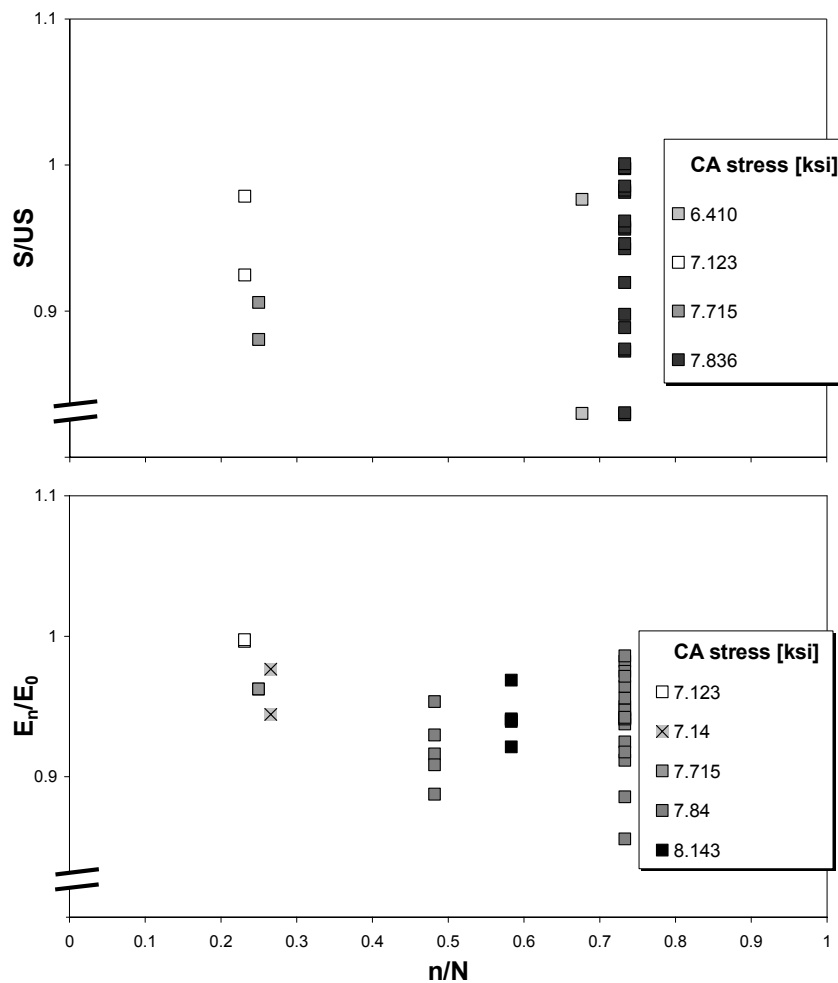
Figure 41: Strength and modulus from Yang and Jones

(legend indicates fatigue stress in ksi)

static strengths up to the highest fatigue fraction. Data obtained at 40%, 60%, and 80% of ultimate tensile strength are reproduced in Figure 42.

Andersons and Korsgaard[14-16] [1997, 1999] published strength degradation data for tensile fatigue of wind turbine rotor blade glass-fibre/epoxy composites. Their data are reproduced in Figure 43. Within a small fraction of life (ca. 5%), the strength degraded noticeably. Data were collected at several stress levels, but no stress level dependency was evident. Information on premature failures, unfortunately, was not retrievable.

Wahl[328] [2001] has reproduced some tensile residual strength data for R=0.1 from Samborsky[276] [1999], and generated data for R=0.5 (Figure 44[328], 2001). From adjusting the model parameter to favourably compare strength-based life estimates to (modified) WISPERX data, he deemed a strength degradation

parameter *C* of 0.265 as describing strength degradation best. This parameter was later successfully used by Sutherland[314] [2004] for strength-based life estimates.
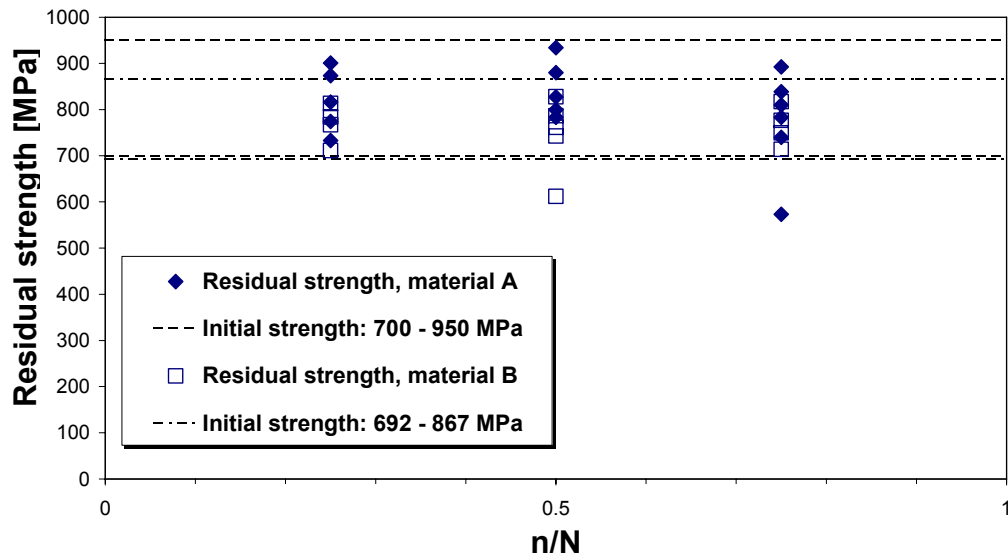
Figure 42: Residual strength data by Joneja [1986], horizontal lines indicate scatter boundaries of static data
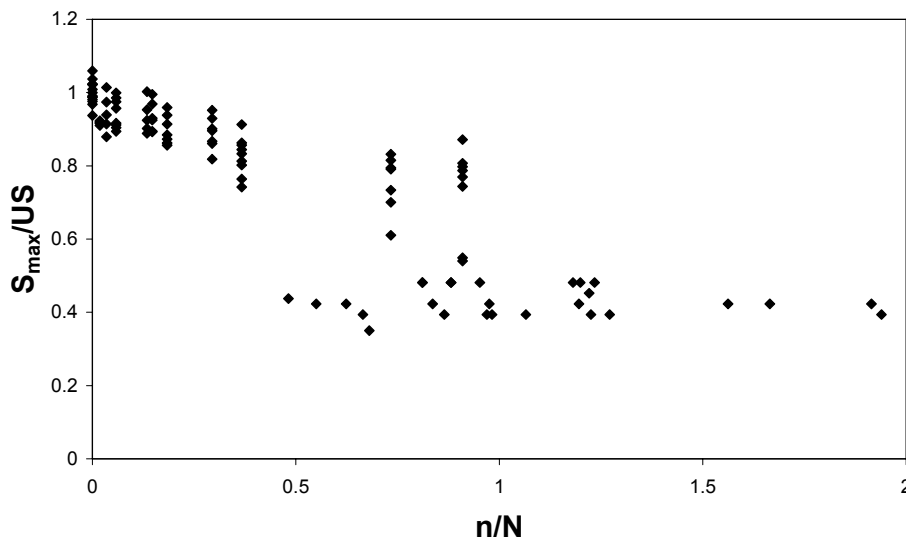
Figure 43: Tensile residual strength data at R=0.1 for different load levels, Andersons and Korsgaard [1997]

111
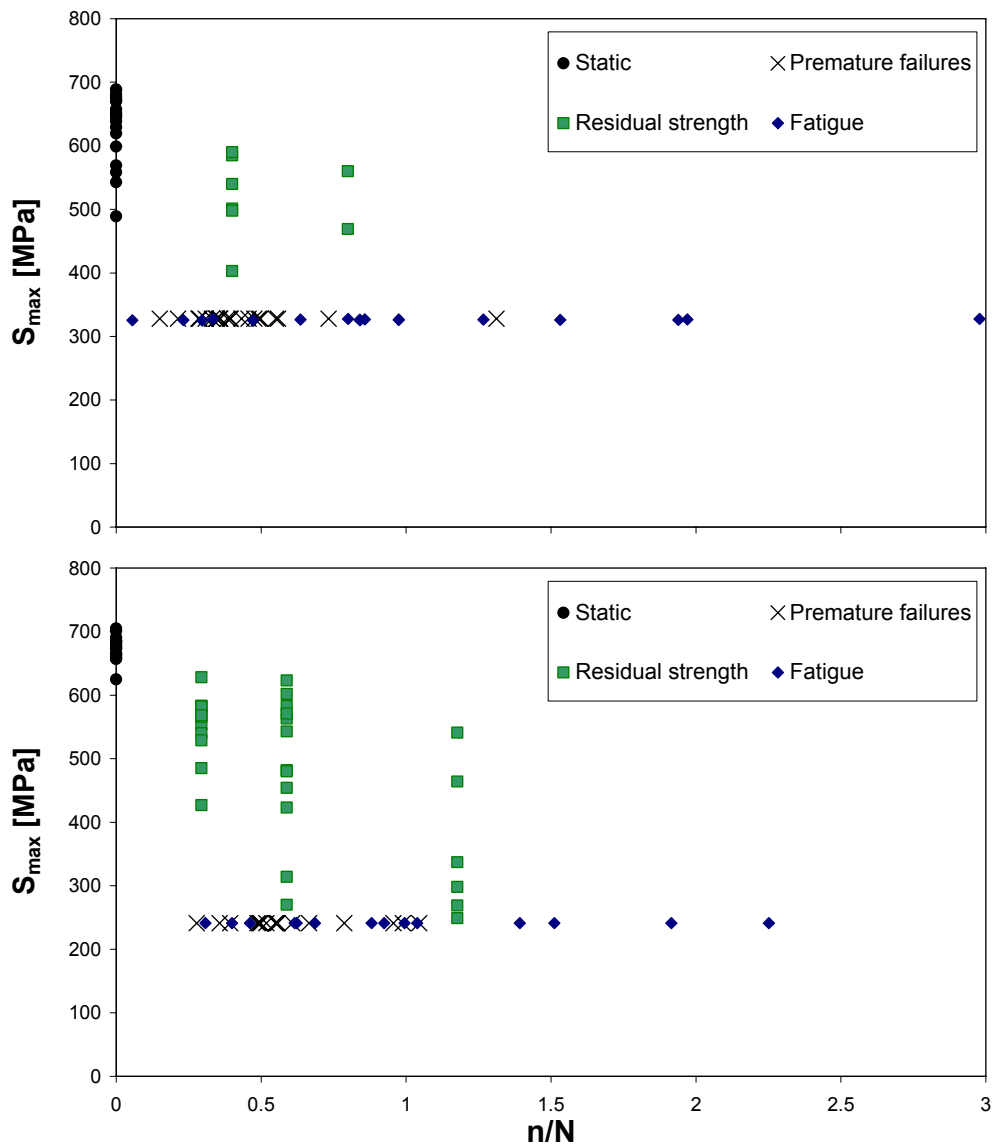
Figure 44: Tensile residual strength data after R=0.1 (top), and R=0.5, reproduced and normalised from Samborsky and Wahl

3.5 Spectrum strength-based life prediction examples

The strength degradation model is demonstrated in practical use. For complicated reference spectra, the computer implementation will be demonstrated, but simple load spectra can be treated analytically, and some formulas are provided for two-block and repeated block strength-based life prediction.

The life prediction using Miner's sum is not treated in detail. The main issue, that needs to be mentioned, is the potential difference in counting method between Miner's sum and the strength degradation model. This was addressed in 3.2.5, and will be subject of section 5.2.1.

By limiting the variation of range and amplitude in a load sequence, the need for interpolation of e.g. S-N curves is limited, and potential sequence effects can be more easily distilled from the results compared to complicated loading spectra. Simple spectrum tests are not realistic loading spectra, but they are of a more academic nature. Two block, and repeated block tests are examples of simple spectra. A two-block spectrum consists of two blocks of constant amplitude cycles. Failure typically occurs in the second block. A repeated block spectrum is similar, but the blocks are typically shorter and the two-block sequence is repeated until failure. Here, the strength-based life prediction for two-block spectra and repeated block spectra are discussed.

3.5.1 Two-block spectrum

For a two-block test, the algorithm works as follows: In the first block, strength degrades according to the trend described by a given degradation parameter C, which is derived for the particular loading condition by residual strength experiments. Upon starting the second block, strength follows the degradation curve for the loading conditions of this second block, starting at the strength at the end of the first block. Therefore, instead of starting at $n=0$, the second block starts at an equivalent life fraction, determined by the instantaneous strength. In formula:

$$S_{next} = S_0 - (S_0 - S_{max,next})\left(\frac{n}{N} + \frac{n_{eq}}{N} \right)^C \tag{53}$$

$$\frac{n_{eq}}{N_{next}} = \left[\frac{n_{current}}{N_{current}} \frac{S_0 - S_{max,current}}{\left(S_0 - S_{max,next} \right)} \right]^{\frac{1}{C}} \tag{54}$$

The general algorithm is illustrated in Figure 45. Each block shows three different types of strength degradation: sudden death (top), linear strength degradation, and early degradation.
From this figure, two important general aspects of the significance of strength degradation in life prediction models are obvious. First, the 'sudden death' type strength degradation gives Miner's sums that are closest to unity.
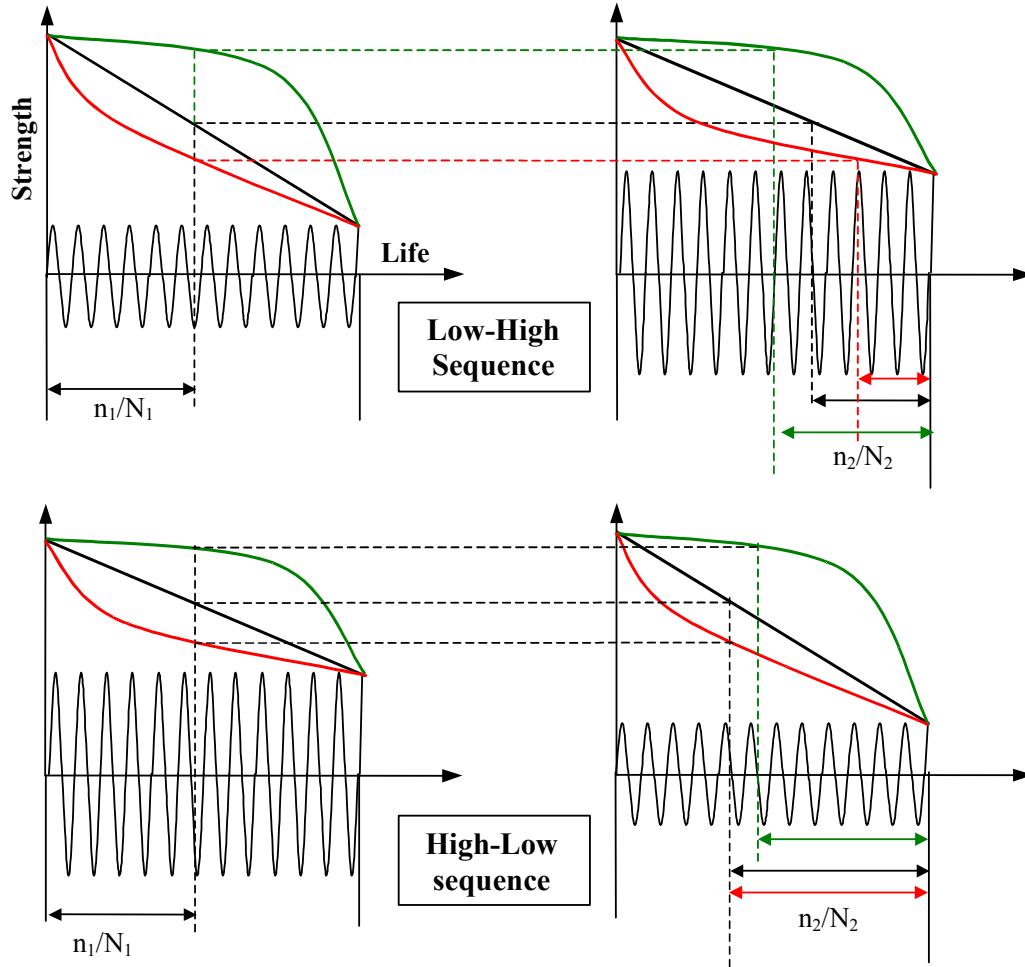
Figure 45: Strength-based life prediction for two-block loading sequences: Low-High (LH) and High-Low (HL)

This is also true for repeated block tests, as will be detailed in section 3.5.3. In other words, if strength degradation is of the sudden-death type, which is characterised by no significant strength degradation up to a large fraction of life, and precipitous strength degradation near the end of fatigue life, the residual strength model yields comparable predictions to the Miner's sum. Intuitively, it would be expected that linear strength degradation resembles the linear damage accumulation of Miner's sum best, but from theory this is clearly not the case.

In addition, the range of Miner's sums that can be predicted by the residual strength degradation model is limited. For the two block tests, the predicted Miner's sum is by definition in the range:

$$\frac{n_1}{N_1} < D < \frac{n_1}{N_1} + 1 \tag{55}$$

This is because the life in the second block is not likely to be extended beyond average constant amplitude fatigue life by the occurrence of the first block. For a two-block test, consisting of block A and B, Miner's sum at failure can be derived from eqs. 53 and 54:

$$D = \frac{n_A}{N_A} + \frac{n_B}{N_B} = \frac{n_A}{N_A} + 1 - \frac{n_{eq}}{N_B} = \frac{n_A}{N_A} \left(1 - \left[\frac{S_0 - S_A}{(S_0 - S_B)} \right]^{\frac{1}{C}} \right) + 1 \qquad (56)$$

In this expression, S_A and S_B the maximum stresses in blocks A and B, respectively. For large values of C, as well as for maximum block stresses approaching each other, Miner's sum approaches unity.

Moreover, for any value of the parameter C, two-block tests that start with a high load block (High/Low tests) will fail at a predicted Miner's sum that is greater than 1, whereas the opposite Low/High sequence results in a predicted Miner's sum, that is smaller than unity. Refer to section 4.4.3 for an overview of typical two-block test results from literature, and to 4.2.6 and 4.3.6 for block test results obtained in the current research.

The strength degradation model does not necessarily result in Miner's sums exceeding unity for *HL* and smaller than unity for *LH* tests. If the value of the strength degradation parameter in the first block is different from the value in the second block, for instance because the R-value is different, opposite results might be obtained. Thus, the strength degradation model is sufficiently flexible to accommodate various damage accumulations.

3.5.2   *Block test data from literature*

Van Paepegem[247] [2002] noted in his review of two-block literature, that similar block tests sometimes lead to contradictory conclusions.

Found et al.[95] [2003] probably provide the most recent and comprehensive literature review of two-block tests on carbon fibre and added to the data with some two-stage loading experiments. They limited their summary of the literature to tensile fatigue.

Historically, Broutman and Sahu[41] [1972] are abundantly referenced for their two-block fatigue tests and modeling, although the data in the literature are limited. Three decades after their experiments, their data are still quoted to validate new fatigue models (e.g. by Schaff and Davidson[278, 279] [1997]).

Boller[33, 34] [1964] produced extensive two-block data on glass-fibre/epoxy, to explore the effect of pre-cycling on the fatigue performance of these laminates. He used three different resin types, and two lay-ups for two of the resins ([0°, 90°] and [±5°]). See Figure 46.
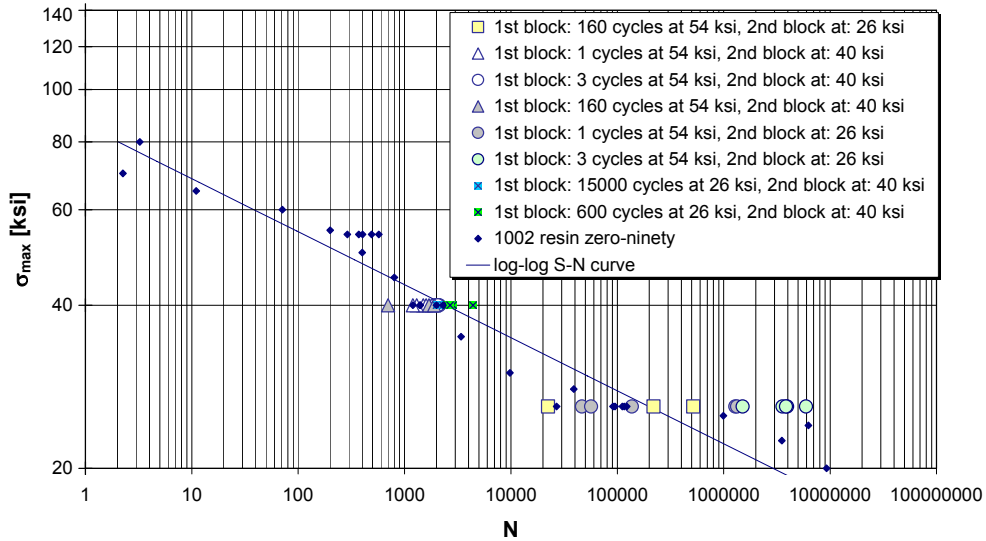
Figure 46: Two-block data from Boller

There seems to be a limited negative effect of pre-cycling on fatigue life in the second block, which is more pronounced for the [0°, 90°] than for the [±5°] lay-up. Boller was consistent in ensuring that some constant amplitude data became
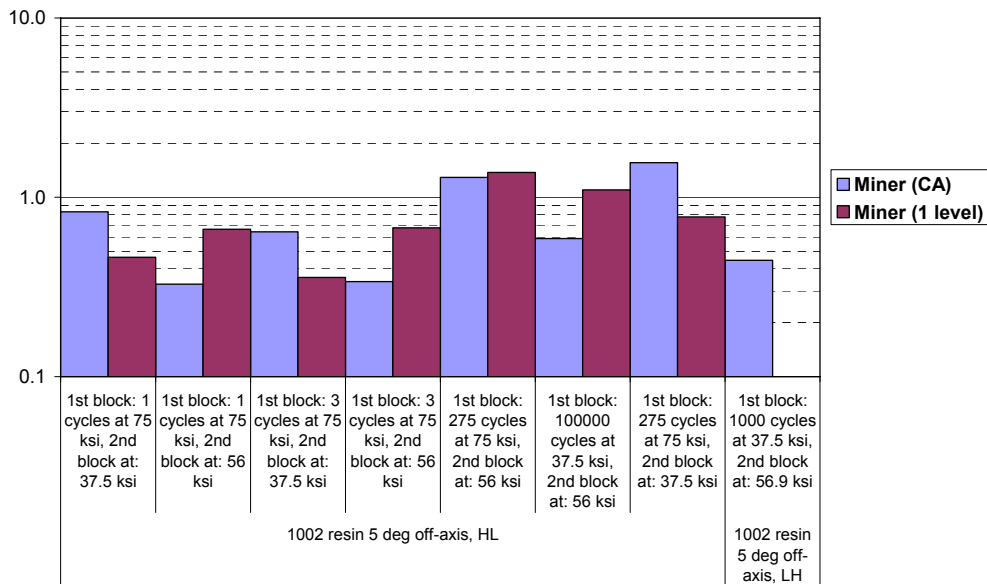
Figure 47: Two-block data from Boller (selection)

available at the same distinct stress levels as the two-block tests were carried out. This enables the plotting of average Miner's sum determined either by mean stress level life, or by a calculated mean life, derived from a log-log interpolation of the S-N data. In most cases, the two Miner sums are similar. It must be pointed out, that the log-log S-N curve is probably not the best description of the S-N curve for these data, since at lower stresses, there is a hint of an endurance limit in the raw data (cf. section 2.3.2). Miner's sum was plotted on a logarithmical scale, so as to visualise the contribution of the pre-cycles, Figure 47.

In a later publication, Boller[35] [1966] investigated the effect of a change in amplitude to a greater extent, using the same test set-up and materials as in his 1964 programme.

As Boller indicated, it appears from the data that these materials do not obey the 'usual' damage laws and that pre-cycling may improve fatigue life. However, significant improvement or deterioration of the fatigue life was only indicated in a minority of the tests, and he recommended that additional replications be made in similar future programs for better statistical analysis.
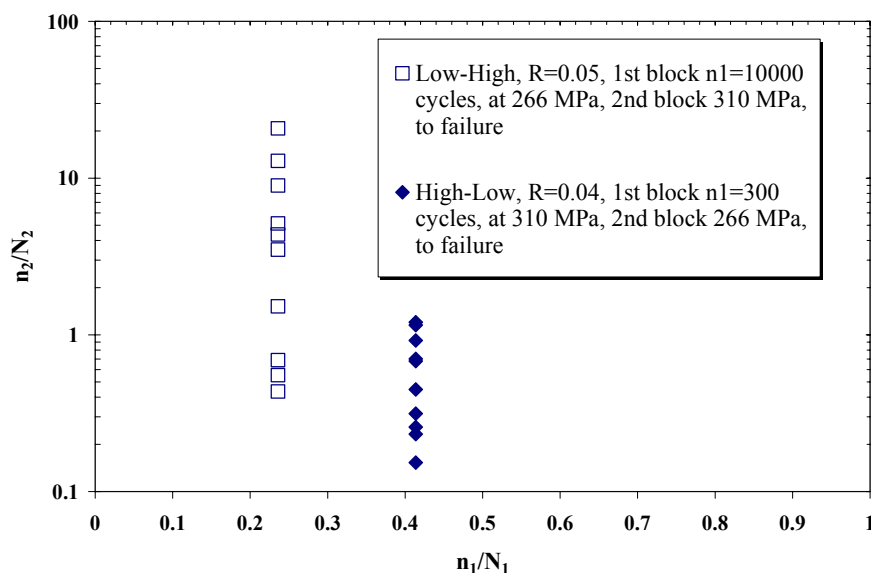
Figure 48: Two-block tests by Hwang and Han [1987]

Hwang and Han[124-126] [1986, 1987] present two-block fatigue data on glass-fibre reinforced epoxy rods. They observed, that the remaining life after the first block was longer than predicted for the low-high-test, and shorter than the predictions for the high-low test. Their data are plotted in Figure 48. For the prediction, they used a modified Miner's rule which allowed for statistical treatment of the fatigue data using a Weibull distribution, and the 'percent-failure-rule' by Chou and Alper[52] [1979].
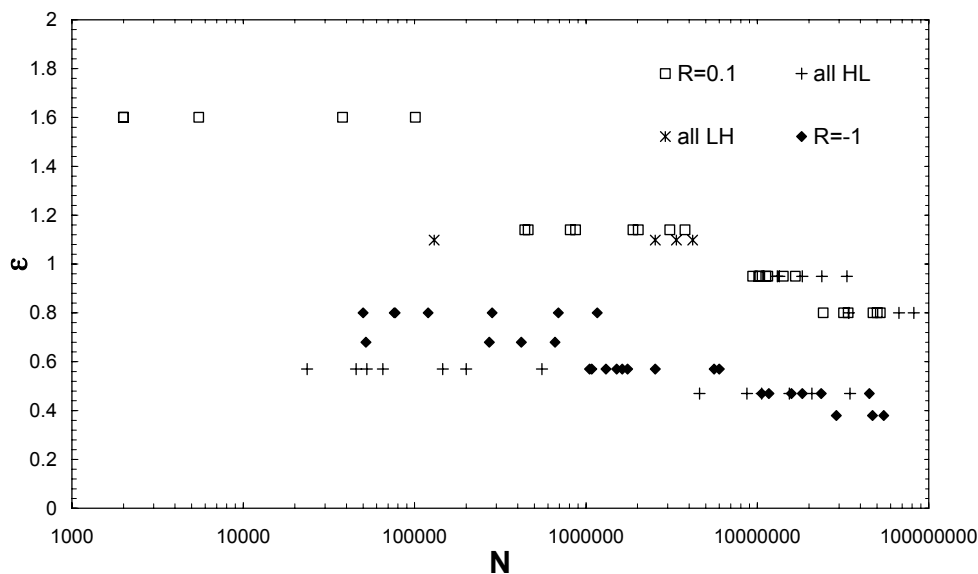
Figure 49: Block test results by Bach [1991]

Bach[22] [1991] has reported on the effect of pre-cycling with a load factor of 1.3 – 2 for dogboned glass-fibre/polyester specimens at R-values of 0.1 and –1. His data are reproduced in Figure 49 (although the data are available from the FACT database, some differences were noted in the data between the report and the database and it was decided to reproduce the data from the report instead). Pre-cycling causes distinctly smaller fatigue lives for R=-1. The effect of pre-cycling diminishes for low strain fatigue at R=-1. At R=0.1 longer lives are seen for pre-cycled specimens. Bach noted that the longer lives in the R=0.1 tests could be attributed to proof-testing effect, although it is expected that this should be reflected in the number of premature failures. No premature failure data were found, and the life fraction of the pre-cycling section of the load blocks did not exceed 10%. Also, he suggested, that microbuckling might restrict some of the second block lives. Overall, Bach concluded that there was no clear effect of pre-cycling, but that the evidence provided by his experiments, nor that in literature, was by any means conclusive.

Otani and Song[242] [1997] found, for R=0 two-stage fatigue on satin woven glass-fibre composites, that High-Low tests yielded Miner's sums larger than unity, whereas Low-High tests showed an opposite trend. Stress amplitude, normalised by tensile strength, ranged between 0.4-0.9. They related fatigue failure in their specimens to the transverse crack density, which was found to linearly increase with number of cycles. From their observations, they derived the following expression for two-stage fatigue loading, which described both their GFRP and SiC-Al coupon data reasonably:

$$\left(\frac{S_1}{S_2}\right)^2\left(\frac{n_1}{N_1}\right)+\left(\frac{n_2}{N_2}\right)=1 \qquad\qquad (57)$$

Recently, Andersons et al.[16] [1999] reported on the effect of cyclic overloading. They submitted glass/epoxy dogbone specimens to a low stress level, followed by a limited amount of high stress cycles. Then they either tested for residual strength or for residual life by resuming the low stress cycles to failure. From their results, they concluded, that the effect on residual strength by this overload was negligible, whereas a 75% decrease in residual life was observed due to the overloading.

Bartley-Cho et al.[26] [1998] have also performed constant amplitude and block testing under tensile and zero mean stress fatigue on carbon/epoxy specimens. Based on a comparison in terms of crack density, they noted that the low-high sequence was more deleterious, and that this effect was more pronounced for tension-compression relative to tension-tension blocks.
Wahl[328] [2001] has focussed primarily on doing simple spectrum load tests, to validate the residual strength degradation model described earlier. Most of his spectrum tests were 'repeated' block tests, and (modified) WISPERX tests. He has done no two-block tests.

Limited data is available on (sub)structures in step loading. Clark et al.[54] [1999] described in detail the failure process and modelling of sandwich core, using a degradation model based on the fatigue modulus concept by Hwang and Han[124, 125] [1986]. Without attempting to be conclusive, they indicated that a slightly more detrimental effect of a high-low sequence compared to the low-high sequence might be observed from their data, with respect to strength degradation.

Kawai and Hachinohe[150] [2002] present 'step-up' and 'step-down' two level fatigue data for a metal-fibre hybrid (GLARE 2), with different fibre orientations, subjected to R=0.1 fatigue. They observed a strong effect of load sequence. In high-low tests, the fatigue life in the second block was significantly enhanced for laminates with the fibres oriented in load direction. For large off-axis angles (30°), the high-low sequence resulted in worse fatigue life, with Miner's sums smaller than unity. This behaviour was not strongly influenced by the length of the first loading block. In the low-high sequence, the off-axis influence tends to disappear, and for most of the off-axis angles, the total Miner's sum is smaller than unity. For large off-axis angles, Miner is larger than unity.

It may be postulated from the results by Kawai and Hachinohe[150], that the High-Low and Low-High behaviour of the glass-fibre is reflected in the behaviour of

the on-axis GLARE laminates, where the contribution to the fatigue behaviour of the metal component of the material may be disregarded. Thus, from a uni-directional glass-fibre point of view, they conclude, that HL-fatigue at R=0.1 results in Miner's sums exceeding unity, whereas for LH-sequences they are smaller than unity.

3.5.3 Repeated block tests

Similar to eq. 56, life for repeated block tests can also be described analytically. It is assumed, that the repeated block tests is built from blocks of length n_A/N_A and n_B/N_B. See Figure 50.
Residual strength at the end of the first block A_1 is:

$$X_{A_1} = X_0 - (X_0 - S_A)\left(\frac{n_A}{N_A}\right)^{C_A} \tag{58}$$

Residual strength at the end of block B_1 is:

$$X_B = X_0 - (X_0 - S_B)\left(\frac{n_B}{N_B} + \frac{n_{eqB}}{N_B}\right)^{C_B} \tag{59}$$

where the equivalent life fraction is:

$$\frac{n_{eqB}}{N_B} = \left[\frac{(X_0 - S_A)}{(X_0 - S_B)}\right]^{\frac{1}{C_B}}\left(\frac{n_A}{N_A}\right)^{\frac{C_A}{C_B}} \tag{60}$$

Theoretically, the derivation can be continued for blocks A_2, B_2, ...A_i, B_i, in which case the expressions for residual strength expand rapidly. However, a few simplifications can be made by assuming, that the life fractions per block are equal, and that each block has an equal strength degradation parameter C:
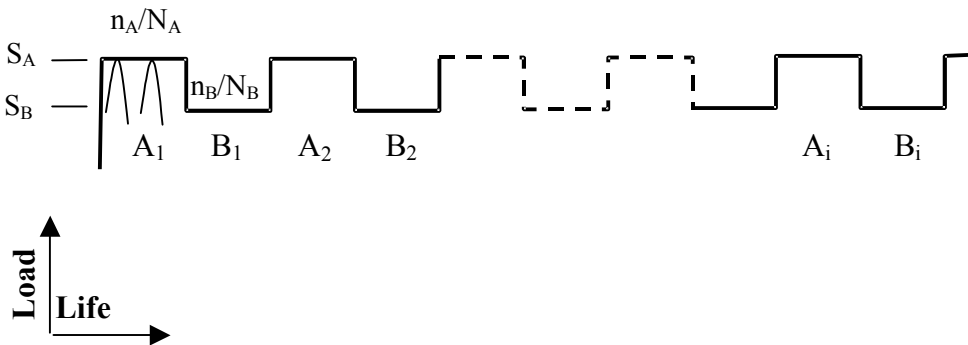
Figure 50: Schematic of repeated block tests

$$C_B = C_A, \frac{n_A}{N_A} = \frac{n_B}{N_B} \tag{61}$$

The block test is schematically shown in Figure 51 with additional parameters which will be needed below.

Repeating the above exercise with these simplifications yields the following expressions for residual strength at the end of each block (see Nijssen et al.[225] [2006] for a complete derivation):

$$X_{A_i} = X_0 - (X_0 - S_A) \left(f \left((i-1) \frac{1}{K}^{\frac{1}{C}} + i \right) \right)^C \tag{62}$$

$$X_{B_i} = X_0 - (X_0 - S_B) \left\{ fi \left[1 + K^{\frac{1}{C}} \right] \right\}^C \tag{63}$$

In these expressions, f is the life fraction per block, C is the strength degradation parameter, and K is a constant which quantifies the difference between S_A and S_B:

$$K = \frac{X_0 - S_A}{X_0 - S_B} \tag{64}$$

In Figure 51, three different failure modes are indicated. It is assumed, that the load in block *A* is higher than that in block *B*. The structure can fail, because the strength in block *B* has sunken beneath the load of block *A* (mode A), because the strength in block *A* has sunken beneath the load in block *A* (mode B), or because the strength in block *B* has sunken beneath the load in block *B* (mode
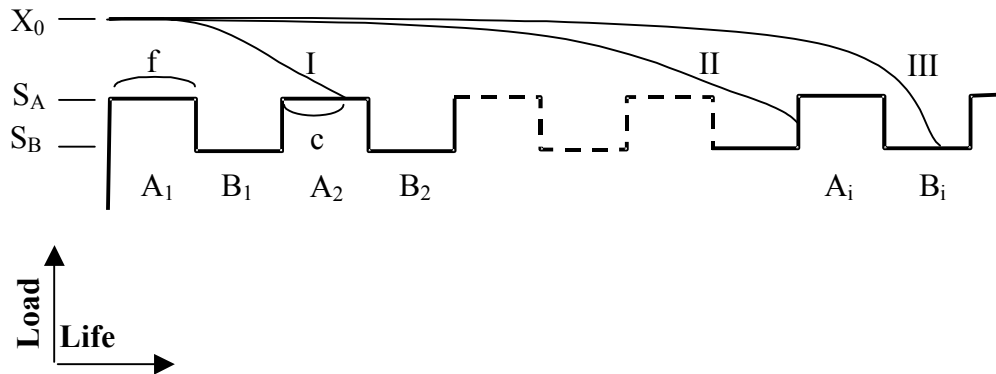
Figure 51: Schematic of repeated block tests, with different failure mode

C). Substituting the appropriate conditions, it is found from eq. 62 and 63, that the blocks in which failure occurs for these modes are:

$$i \geq \frac{K^{\frac{1}{C}}}{f} \frac{1}{1 + K^{\frac{1}{C}}} \quad \text{(Mode A)} \tag{65}$$

$$i > \frac{\frac{1}{f} K^{\frac{1}{C}} + 1}{K^{\frac{1}{C}} + 1} \quad \text{(Mode B)} \tag{66}$$

$$i > \frac{1}{f\left[1 + K^{\frac{1}{C}}\right]} \quad \text{(Mode C)} \tag{67}$$

According to Figure 51, Miner's sum for the three modes is given by:

$$D = 2if = 2 \frac{K^{\frac{1}{C}}}{1 + K^{\frac{1}{C}}} \quad \text{(Mode A)} \tag{68}$$

$$D = f[2(i-1) + c] \sim 2 \frac{K^{\frac{1}{C}}}{K^{\frac{1}{C}} + 1} \quad \text{(Mode B)} \tag{69}$$

$$D = 2 \frac{1}{\left[1 + K^{\frac{1}{C}}\right]} - f(1-c) \sim 2 \frac{1}{\left[1 + K^{\frac{1}{C}}\right]} \quad \text{(Mode C)} \tag{70}$$

In these expressions, c is a fraction of f ($c<1$). For sufficiently small life fractions per block, f can be neglected. Note that $K<1$, since $S_A<S_B$. As a result, all Miner's sums approach unity for strength degradation parameters $C\gg1$.
Failure occurs for whichever Miner's sum is smallest. This is for Mode A or B. Moreover, the Mode A and B expressions lead to Miner's sums smaller than 1 for all strength degradation parameters.
Summarising, the repeated block tests may be seen as a repetition of Low-High tests rather than a repetition of High-Low tests. This is evident from the above derivations, where it was found that Miner's sum for repeated block tests is smaller than unity under the condition that the strength degradation parameter does not change from one block to another.

Qualitatively, this can be explained by regarding the low load blocks as interspersed with high loads. If the distance between high loads is sufficiently small, the structure will fail when encountering a high load. This excludes all following low loads from happening, thus lowering the total life fraction in the low load block, consequently lowering Miner's sum.

Wahl[328] [2001] observed, that non-linear residual strength predictions with degradation parameter of 0.265 were not always accurate. Wahl noted under-conservative predictions for large high-amplitude cycle fractions, and over-conservative predictions for smaller fractions of high-amplitude cycles. Note, that the strength degradation parameter of 0.265 is conservative with respect to the degradation parameters observed in Chapter 4. Residual strength-based predictions may still be non-conservative for larger degradation parameters. Thus, it seems an additional phenomenon may exist apart from strength degradation, which could account for the difference between prediction and results. Wahl suggested, that future work be aimed at refining the strength degradation model with a second parameter of as yet unknown nature.

Filis et al.[93] [2004] have introduced a cyclic mix factor, which accounts for early failure of composite structures under repeated block type loading. It is not clear what the physical background behind a cyclic mix factor would be, and they did not apply a residual strength model for the predictions. From Wahl's results, something along the lines of such a cyclic mix factor might be required to augment the strength degradation prediction. This factor would be a function of the irregularity of the load spectrum investigated.

3.6 Sequence effects

An important question in spectrum loading a structure, is whether it is sensitive to load sequence effects. Various authors have used this term without specifying the exact deposition. In this work, sequence effects are defined as:

The effects on life or strength of the order in which all, or part of the varying cycles in a load spectrum occur relative to each other

Essentially, the existence of a sequence effect depends on the magnitude of the load cycles, and on the damage mechanisms in the material. Generally, a sequence effect can only exist if the damage accumulation due to a given cycle type is affected by the damage induced previously by another load cycle, and this implies the existence of different, interacting, damage states or damage mechanisms.

It should be noted, that by this definition of sequence effects, it should be explicitly mentioned whether the sequence effect is expressed in terms of

strength or life. These two types of sequence effects are not necessarily mutually exclusive, as the following derivation will illustrate.

Consider a two-block test, with maximum loads S_1 and S_2. This is an example that was already discussed in chapter 3.5.1, to demonstrate life prediction using a strength degradation model. There, it was shown, that a sequence effect in terms of life can be predicted by a strength degradation model, where High-Low sequence results in higher Miner's sums than a low-high sequence.

Does this sequence effect in life also reflect in a sequence effect in strength? In other words, after expending an equal amount of life (Miner sum) in the second block, does the remaining strength depend on the order of the loading blocks? For the one-parameter strength degradation, the answer is negative.

Strength degradation after a constant amplitude life fraction f is described by:

$$S_{R1} = S_0 - (S_0 - S_1)(f_1)^{C_1}, \text{ for the first block, and} \tag{71}$$

$$S_{R2} = S_0 - (S_0 - S_2)(f_2)^{C_2} \text{ for the second block} \tag{72}$$

The strength at any point in the second block is given through calculating the equivalent number of cycles, and adding the number of cycles in the second block.

$$\left[\frac{-(S_{R1} - S_0)}{(S_0 - S_2)}\right]^{1/C_2} = (f_{eq2}) \tag{73}$$

$$\left[\frac{(S_0 - S_1)(f_1)^{C_1}}{(S_0 - S_2)}\right]^{1/C_2} = (f_{eq2}) \tag{74}$$

$$S_{R2} = S_0 - (S_0 - S_2)(f_2 + f_{eq2})^{C_2}, \text{ or} \tag{75}$$

$$S_{R2} = S_0 - (S_0 - S_2)\left(f_2 + \left[\frac{(S_0 - S_1)(f_1)^{C_1}}{(S_0 - S_2)}\right]^{1/C_2}\right)^{C_2} \tag{76}$$

Assume, that the strength degradation parameter is independent of load level, so that $C_1 = C_2 = C$.

$$S_{R2} = S_0 - (S_0 - S_2)\left(f_2 + \left[\frac{(S_0 - S_1)(f_1)^{C}}{(S_0 - S_2)}\right]^{1/C}\right)^{C} \tag{77}$$

$$S_{R2} = S_0 - (S_0 - S_2)\left(f_2 + \left[\frac{(S_0 - S_1)}{(S_0 - S_2)} \right]^{\frac{1}{C}} (f_1) \right)^C \tag{78}$$

$$\left(\frac{S_{R2} - S_0}{-(S_0 - S_2)} \right)^{\frac{1}{C}} = f_2 + \left[\left(\frac{(S_0 - S_1)}{(S_0 - S_2)} \right)^{\frac{1}{C}} (f_1) \right] \tag{79}$$

This can be rewritten into:

$$S_{R2} - S_0 = -\left\{ (S_0 - S_2)^{\frac{1}{C}} f_2 + (S_0 - S_1)^{\frac{1}{C}} (f_1) \right\}^C \tag{80}$$

Note, from this expression, that strength degradation is independent of load sequence. On the other hand, in terms of life, there is a load sequence effect, as the total amount of strength reduction must differ due to the difference in maximum load.

For a sequence effect to exist in terms of strength, the value of the strength degradation parameter should vary, and the variation should depend on the previously induced damage. For instance, if a certain load type would have sudden death strength degradation in constant amplitude loading, a sequence effect in strength would be introduced, when strength degradation would be linear if the cycle type would be preceded by another cycle type, which would change the strength characteristic to linear degradation.

Summary of this chapter

After the discussion of constant amplitude fatigue in Chapter 2, Chapter 3 gives background on variable amplitude load spectra, notably the WISPER spectra, which are used in this dissertation for experiments and prediction. It describes how the CA formulations can be used for spectrum fatigue life prediction using Miner's summation and strength degradation methods. To this end, counting methods, which are used to separate the variable load sequence in constant amplitude constituents, are described. Notably the Rainflow counting method and range-mean counting are discussed.

- *Rainflow counting is considered the most appropriate counting method, but it is not suitable for cycle-by-cycle prediction methods such as the strength degradation method. Range-mean counting can be used in any prediction method, but it does not necessarily count the largest cycle in the spectrum. A Rainflow-equivalent range-mean transformation of the spectrum is proposed to work around this problem.*
- *A cycle-by-cycle strength degradation model is discussed as an alternative for Miner's sum. The advantages are, that a physical parameter is tracked, and that sequence effects affecting life can be accounted for. An adaptation is made for mixed-sign strength degradation (tensile strength after compressive fatigue and vice versa). Furthermore, a method for extracting strength degradation parameter from data is outlined. Strength degradation data from literature are scarce. Some data are reproduced for later comparison with the data obtained in the experiments of Chapter 4.*
- *For simple two-block and two-block repeated load spectra, analytical approximations of strength-based life predictions are given.*
- *A definition of sequence effects, and the difference between sequence effects in life and in strength are given.*

Chapter 3 provides the computational tools for the analyses in Chapter 5. In the next chapter, the test programmes carried out are described, as well as the test results.

Chapter 4

Experiments and Results

Numerous experiments were carried out to obtain the material life and strength characteristics, and to allow for validation of the life prediction methodology. This chapter describes the materials, experimental set-up, test methods, and results.

4.1 General test set-up

Data were collected from two separate, independent testing campaigns. The first was part of the OPTIMAT blades project, the second set of results was obtained in the composites laboratory of Montana State University. The test methods and results from these projects will be presented separately, since the test conditions, coupons and programme constraints were quite different. The general approach that was followed in both projects, however, is very similar, and therefore this chapter starts with a description of the common denominators of both test programmes.

Both test programmes were aimed at evaluating the material behaviour in spectrum fatigue, and at describing strength degradation after constant amplitude fatigue. Baseline tests were carried out to establish material strength and constant amplitude fatigue behaviour. Simple spectrum tests were done in both programmes, as well as residual strength tests.

4.1.1   Definition of failure

Failure is defined by inability of the specimen to bear the applied load. In practice, this amounts to severe damage to the coupon or separation of the coupon between the machine grips.

4.1.2 Static tests and constant amplitude fatigue

The objective of static tests and constant amplitude fatigue tests is to provide a basic material characterisation. This serves as a framework for evaluating strength degradation and for estimates of strength and life.

A schematic of static and fatigue tests is shown in Figure 52. In the fatigue tests, the coupons were subjected to cyclic loads of predefined mean and amplitude, until failure. The machine was in load control mode, and the load settings were kept constant during the entire test (see chapter 2.3.1). The load waveform was sinusoidal. Accuracy of the load control typically was within 1%. In the static tests, the specimens were loaded monotonically in either tension or compression until failure. The experiments were conducted in displacement control mode, and the displacement rate was predefined.

In some laboratories, slow cycles were used prior to the test, as will be described in 4.1.4.
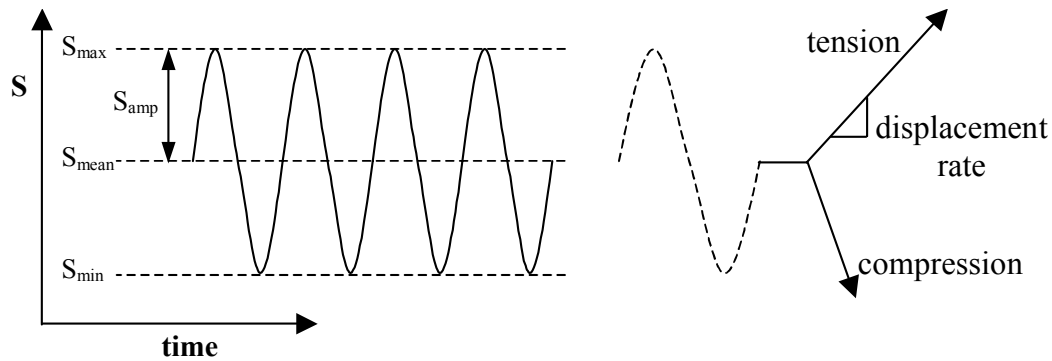
Figure 52: Schematic of constant amplitude fatigue and static tests

Measurements

Load at failure was recorded, as well as number of cycles to failure (set to 1 for static tests). Mounting procedure, data acquisition, and loading rates were different between, and within, the OPTIMAT and MSU programmes. Most of the (fatigue) tests included (continuous) measurement of load, displacement, and strains.

4.1.3 Spectrum tests

Various spectrum tests were carried out in the program:

- Two-block tests
- Repeated block tests
- Spectrum tests (OPTIMAT only)

A block test is defined here as a simple load spectrum test, consisting of two constant amplitude cyclic loading blocks. A schematic is shown in Figure 53. Each cyclic load block is specified at load levels and frequencies which comply with the constant amplitude tests done for the determination of the S-N curves. Different block lengths and block characteristics were used in the OPTIMAT and MSU programmes.
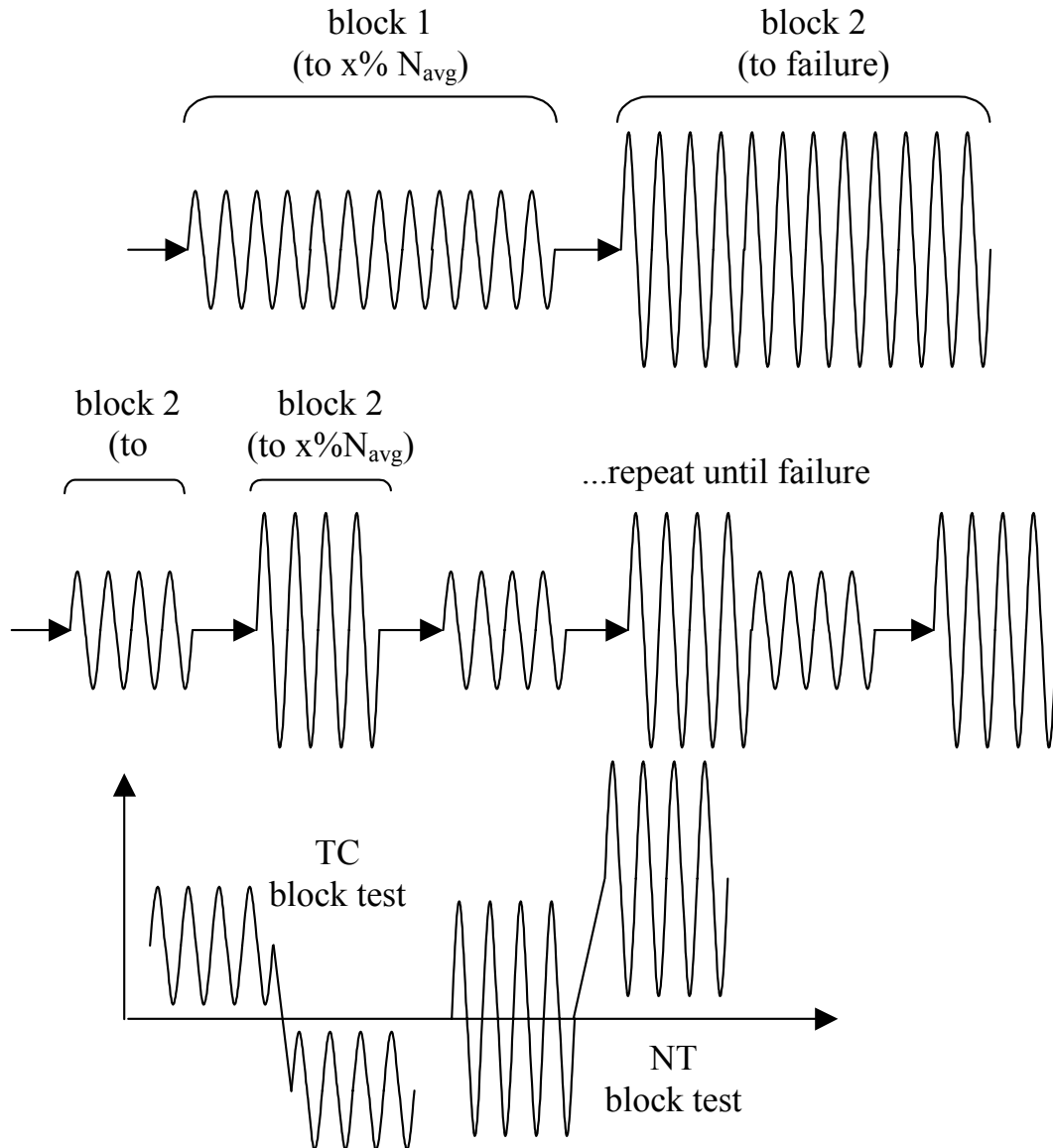
Figure 53: Schematic of two-block test (LH), repeated block test, and examples of TC and NT block tests; strain (or stress or load) on vertical axis

Classically, two-block tests using a high load and a low load are used to evaluate sequence effects. These are referred to as *HL* and *LH* tests. In the

current work, this designation is not sufficient to describe all block test variations investigated. Block tests have been performed also at two R-values in one block test. In these cases combinations of *C* (compression), *N* (neutral), and *T* (tension) were used to designate R=10, -1, and 0.1 blocks. Mixed R-value block tests are therefore designated as, for example, *CN*, *TC*, or *NT*.

Repeated block tests are a sequence of alternating constant amplitude cyclic load blocks, each with a predetermined fraction of nominal life, the sequence being repeated until failure. Multiple block tests, with more than two different blocks, such as e.g. the three-block and six-block repeated block tests done by Wahl[328] [2001], were not planned.

Load spectrum tests using WISPER-type load sequences were exclusively done in the OPTIMAT programme.

4.1.4   Residual strength tests

The residual strength test essentially consists of a constant amplitude fatigue section, followed by a static test to failure. See Figure 54. The constant amplitude section is specified at load levels and frequencies which comply with the constant amplitude tests done for the determination of the S-N curves. The final static test quantifies the influence of prior fatigue on residual, post-fatigue, strength. The static test is done after a pre-defined fraction of the nominal fatigue life.
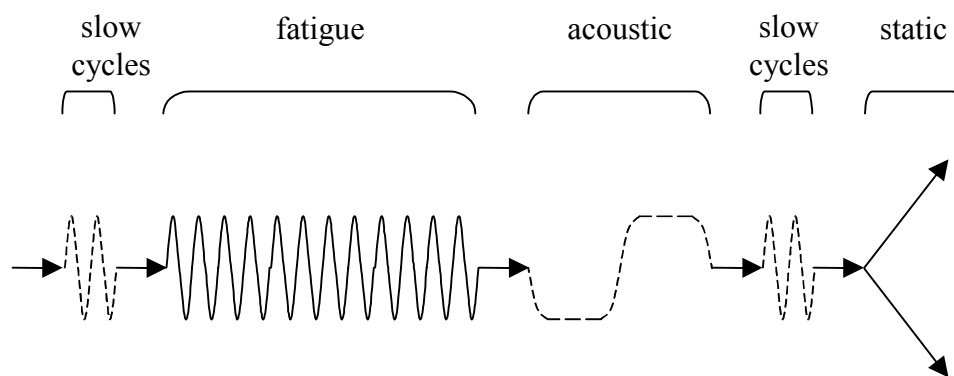
Figure 54: Schematic of residual strength test procedure

In the OPTIMAT programme, the constant amplitude fatigue, static, and residual strength test also comprises a (series of) slow cycle(s) prior to fatigue and the static test, sometimes including acoustic emission or acousto-ultrasonic measurements. This is indicated in Figure 54 with dotted lines, since these techniques were not used at all participating laboratories. The slow cycle(s) enable measurement of both the tensile and compressive modulus and/or initial maximum strain. The final acoustic emission measurement, and slow cycle(s) serve to provide additional information on the influence of prior fatigue on

remaining strength and stiffness of the coupon. Acoustic emission was only measured by UP and RAL, see e.g. Blanch et al.[30, 31] [2002, 2003], Dutton[81] [2006], and Assimakopoulou et al.[19] [2004].

4.1.5 Post-experimental

The test results were recorded using various measurement software. At WMC, in-house software was used (Smissaert and van Beek[298], 2001). The most important characteristics and quantities were recorded in either the OptiDAT[221] [2006] or the DOE/MSU[189] databases [2006]. Photographs were taken of the failed specimens, so as to enable post-mortem evaluation of the failure location and mode. The specimens, measurement files, processed measurement files, and pictures were archived for future reference.

4.2 OPTIMAT

4.2.1 Brief project overview

The OPTIMAT project is a relatively large rotor blade materials fatigue research project, which is partly funded by the European Union. A considerable part of the research in this thesis was carried out in the framework of this project.

In the project, 18 partners from 8 European Union countries, including 2 certification bodies, blade manufacturers and 8 research laboratories, joined their efforts to investigate various aspects of rotor blade fatigue. The ultimate goal was to improve design guidelines. The project was finalised in May 2006.

More details on the project's organisation and main research topics are found in e.g. Nijssen et al.[217] [2003], and van Wingerde et al.[349] [2006]. All test results are summarised in the OptiDAT[221] database [2006]; all project technical reports are available from the Web site.

4.2.2 Fatigue database: OptiDAT

All of the OPTIMAT results discussed here are taken from the OptiDAT[221] database. The OptiDAT database is a materials fatigue database, started during the OPTIMAT project. All data collected during this project are included in the database.

A brief description is given here. To ensure compatibility and basic data retrieval, the database is set-up in spreadsheet format (MS Excel). It contains several 'worksheets', most of which give background information on specimen
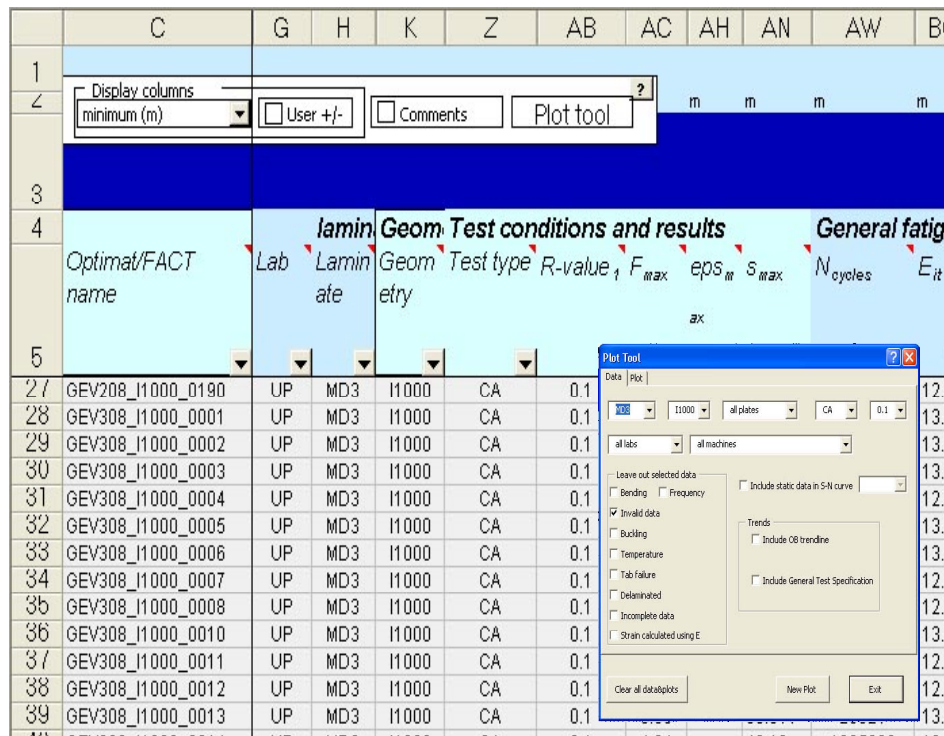
Figure 55: Screenshot of the OptiDAT database

geometry, materials, test methods, and equipment. During the project, a delivery/manufacturing log was included, to track shipments of specimens; a change log, and several sheets with information on the Detailed Plans of Action (DPAs) were dedicated to tracking progress. This allowed for a comparison of the planned tests, with the completed and reported tests. This information was available per test type, specimen type, laboratory, and task group. Any change of plans, or data submission, was automatically included. Thus, besides functioning as a medium to distribute the project results, the database also contained useful information on the current status of the work at any time during the project. In the final version of the database, this information was taken out.

The actual experimental data are in a single worksheet. See Figure 55 for a screenshot. The database contains some 3000 test results from the OPTIMAT project, varying from the static, fatigue, residual strength, and spectrum tests discussed in this work, to the results of tests on off-axis, extreme condition, thermal expansion, bi-axial/complex stress state, and thick laminate coupons (mostly glass/epoxy with ca. 53% fibre volume fraction). A multitude of parameters is directly recorded, including coupon characteristics, test characteristics, and main results. Each specimen occupies a row in the database (record), for each parameter a column is reserved. For reasons of data limitations and ease of access, it was not feasible to include all the information

recorded during a test in the single database sheet. Therefore, some of the meta-information is included in separate sheet, and a reference to the relevant test report is given, if available. Thus, information on stress-strain diagrams in static tests, or the modulus or temperature development during a test, can be accessed via reports. Each specimen in this project has a unique identification code, which also contains information on the specimen type and material. In addition, each database row was allocated a unique sequential number, for quick reference and redundancy in identification.

It should be mentioned, that, during the project, the database was continuously updated with input from the different participating laboratories. Consistency of the datasets was facilitated by a 'data submission sheet', which aided the participants in delivering data in a prescribed format, and to indicate necessary modifications to the database. The basic set-up of the database is sufficiently flexible to allow for extra parameters to be included, or redundant or unnecessary parameters to be excluded.

There are two other comparable databases, describing fatigue behaviour of wind turbine rotor blade composites. One is the MSU database (see section 4.3.2). The other one is the FACT database (de Smet and Bach[71], 1994), which largely consists of data found from the literature (before 1994), brought together during the Joule[154] project, which was funded by the European Union. In a sense, it can be regarded as the predecessor of OptiDAT, since it emerges from a European joint research effort, and since the format of the database worksheet was the basis for the OptiDAT datasheet. Nevertheless, to allow for the accommodation of the more diverse results from OPTIMAT, significant restructuring was necessary.

For a detailed image of the database, the reader is referred to the reference documents[220, 224], or to the database[221] itself.

4.2.3 *Material, coupons and test set-up*

In the OPTIMAT project, glass-fibre-reinforced epoxy specimens were tested in various lay-ups and specimen geometries, see e.g. OptiDAT[221]. The geometries and lay-ups that are most relevant to this research are the 'standard OPTIMAT specimens', depicted in Figure 56.

There are two standard OPTIMAT specimens, one for each 'standard OPTIMAT lay-up'. In the project, two lay-ups were used in most coupons. The first lay-up is unidirectional and coded 'UD2', the second is multi-directional ('MD2'), see Figure 56. These were manufactured in large batches, from the same constituent fibres and resin, by the same manufacturer using identical processing techniques for each batch (vacuum assisted resin transfer moulding,

4 hr post-cured at 80°C). The UD2 material consists of a 1250 g/m^2 E-glass reinforcement (PPG 2002 roving) in a [0°]$_4$ lay-up. This material is representative for the laminates used in the outer parts of the main spar. The MD2 material consists of the same unidirectional roving in combination with a 810 g/m^2 biaxial reinforcement (PPG 2002 roving), in a [[±45°, 0°]$_4$;±45°] lay-up. This material is representative for e.g. the spar web or blade root. The resin, Prime 20 from SP Systems, is mixed with slow hardener. The fibre volume fraction for both laminates is approximately 54 %. See also Jacobsen[135] [2002]. The design of the standard OPTIMAT specimens follows from extensive preliminary testing[147, 162, 163, 196, 254, 255], where the performance in terms of fatigue strength and static strength of various dogbone-shaped and parallel-sided (rectangular) geometries and lay-ups was investigated.
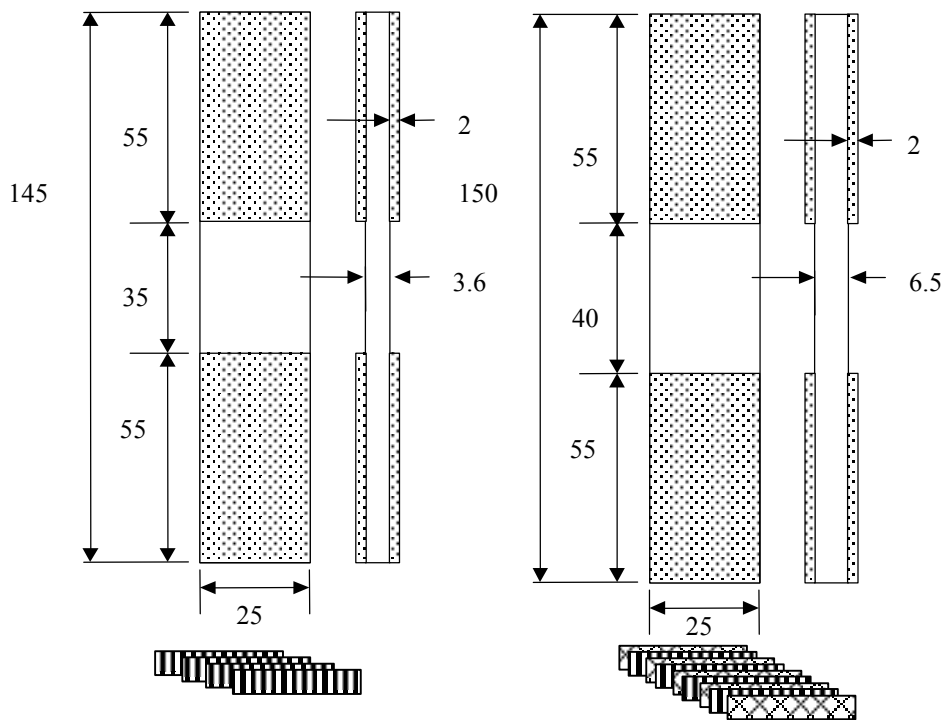
Figure 56: Standard OPTIMAT coupons for UD2 and MD2 (right), dimensions in mm

The OPTIMAT specimen geometry is a compromise between general applicability and consistency of failure mode. The standard OPTIMAT specimens are used under ambient, and various extreme conditions, in static, fatigue, residual strength, and spectrum tests. The laminate configuration of any unidirectional specimen does not allow for failure outside the gripping area. Dogbone-shaped (or 'waisted') specimens have a tendency to essentially become parallel-sided specimens in fatigue and fail in the gripping area. In order to use the same specimens for static and fatigue testing, and to enable comparison of the UD2 laminates to the MD2 laminates, the rectangular
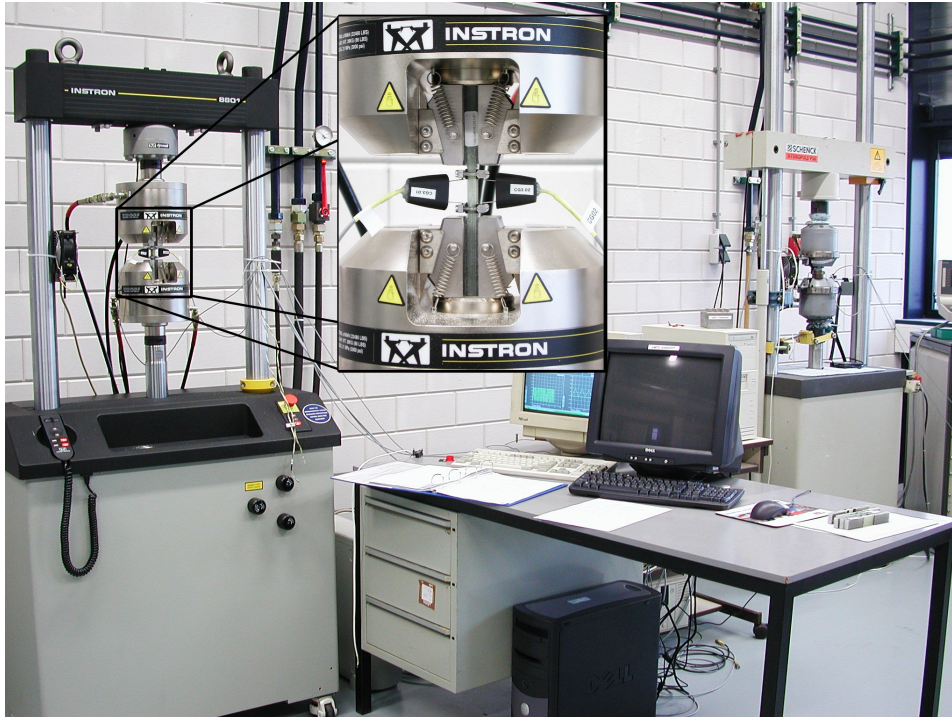
Figure 57: Representative OPTIMAT test-set up at WMC

geometry was preferred. As a result, all standard specimens tend to fail in the gripping area.

Testing standards prescribe, that results are valid only when failure occurs outside the gripping area. However, the majority of the OPTIMAT testing programme is not focussed on obtaining the best possible results in terms of material performance. Material performance is subordinate to the investigation of the effects of e.g. extreme conditions, or spectrum effects. Also, emphasis in the project definition was on the investigation of interaction effects. For example, an 'interaction test' could involve fatigue tests in extreme conditions under spectrum loading. It was expected, that specimen size and geometry effects might obscure the effects that are actually under consideration. Therefore, for the OPTIMAT coupons, the occurrence of grip failures was favoured over having to explain difference in performance between a dog-bone coupon and a rectangular coupon in different circumstances.

Parallel to the experiments on standard OPTIMAT geometries, the 'best achievable' material performance has also been obtained in the project through static and fatigue tests on (ISO/ASTM) standardised specimen shapes and test set-ups.

Comparison of ISO tensile and compression coupons showed, that the OPTIMAT coupons result in similar tensile strengths, and that the compression

strength for the OPTIMAT coupons is roughly 20% lower[224] than the compression strength for optimised geometries and testing equipment, following the ASTM combined-loading procedure. This procedure encompasses a delicately balanced load introduction using both shear and end-loading (instead of exclusive shear loading).

With respect to fatigue loading, tests were done on the standard laminates with a dogbone geometry. Originally, these were meant for comparison with dogbones under extreme conditions, but they can also be used to compare with the performance of the OPTIMAT standard coupons. In the case of MD2 laminate, the low-cycle fatigue life of the coupons was improved, but this improvement diminished at higher cycles. For the UD2 laminate, no significant improvement was seen[224]. Only tensile fatigue could be compared. A thorough investigation into the effect of coupon geometry was not carried out for the laminates investigated.

A representative test set-up for tests carried out at WMC in the framework of the OPTIMAT programme is displayed in Figure 57. This set-up is representative for the equipment that was used in the project. The figure shows the test station including a servo-hydraulic test machine, and a computer for data acquisition. The inset shows a gripped OPTIMAT coupon, equipped with custom clip-gauges. On the left side of the machine, a fan is mounted to generate a constant airflow around the coupon.

4.2.4   Static and fatigue tests

OptiDAT contains some 250 static tests on standard coupons. These can be found by looking for 'STT' and 'STC' in the column 'Test type', filtering for 'd, RT' (dry, Room Temperature) in the database, excluding tests done at high strain rates or using a LUR loading pattern (loading-unloading-reloading).

Table 3: Summary of static data from OptiDAT

(STC = STatic Compression, STT=STatic Tension, for geometries, see Figure 52; UD3 is similar to UD2, but with extra layer)

Test type	laminate	Geometry	mean	stdev	n
STC	*MD2*	*R0400*	-461	34	47
	UD2	*R0300*	-509	52	81
	UD3	*R0300*	-577	33	5
STT	*MD2*	*R0400*	530	19	48
	UD2	*R0300*	800	37	79

The displacement rate in the OPTIMAT standard specimens was different for tension and compression. The displacement rates stipulated by the ISO-guidelines, are similar in tension and compression, albeit at distinctly different gauge lengths. In the OPTIMAT programme, the ISO-rates were converted to rates/gauge-length. The standard OPTIMAT specimen is shorter than the ISO tensile specimen, hence the OPTIMAT displacement rate was specified below the ISO rate. For compression tests, ISO and OPTIMAT specimens had roughly comparable gauge lengths, hence the displacement rate was similar to the ISO-specification. As a result, tensile tests were conducted at a displacement rate of 0.25 mm/min, compressive tests at 1 mm/min. In practice, standard static displacement rates for both tests vary between 0.25 and 1 mm/min. For effect of strain rate on static strength, refer to 2.3.5.

Load, displacement, and strain were recorded. Strain measurements occurred through adhesively bonded strain gauges or clip gauges (the strain gauges typically failed after ca. 1000 cycles; clip gauges permitted continuous strain evaluation throughout the coupon's lifetime). In compression, the specimen is prone to buckling or S-bending, which leads to diverging strain readings for specimens equipped with dual strain gauges in a back-to-back configuration. In the case of pure bending, calculation of bending can facilitate validation of the experiment. The experiment was considered invalid in OPTIMAT, if bending strain exceeds 10% at 0.8 of maximum load (this is a modification with respect to the relevant ISO-guideline[133], which prescribes this limit until failure). Strain gauges and clip gauges are prone to giving unreliable measurements near failure, as the specimen, or the strain gauge adhesive layer, may be (partially) damaged already.
Static strengths for the standard OPTIMAT specimens are given in Table 3. This table shows the cross-section stress (mean and standard deviations) from static tests in tension and compression, coded STT and STC, respectively.

The value of the distribution parameters listed in Table 3 show, that in general, the spread in static strengths, in terms of σ/μ, is limited to some 5%. Compressive tests tend to result in a higher spread, which is attributed to differences in bending/buckling of the coupons.
Example probability plots were shown in section 2.3.6. These plots contain strength parameters in terms of Normal and Weibull distribution parameters. The K-S distances in these plots also reveal, that there is no preferred distribution type to fit the data. In practice, two-parameter Weibull or Normal statistics can be used, whichever is most suitable for further analysis. These data were reported in OptiDAT and also in Nijssen[224] [2006].

Fatigue tests in OptiDAT were coded 'CA' (Constant Amplitude). Fatigue tests were preceded by a slow cycle (ca. 0.02 Hz) for modulus measurement, and, for some test frames to test the machine settings or calibrate the load control. Figure
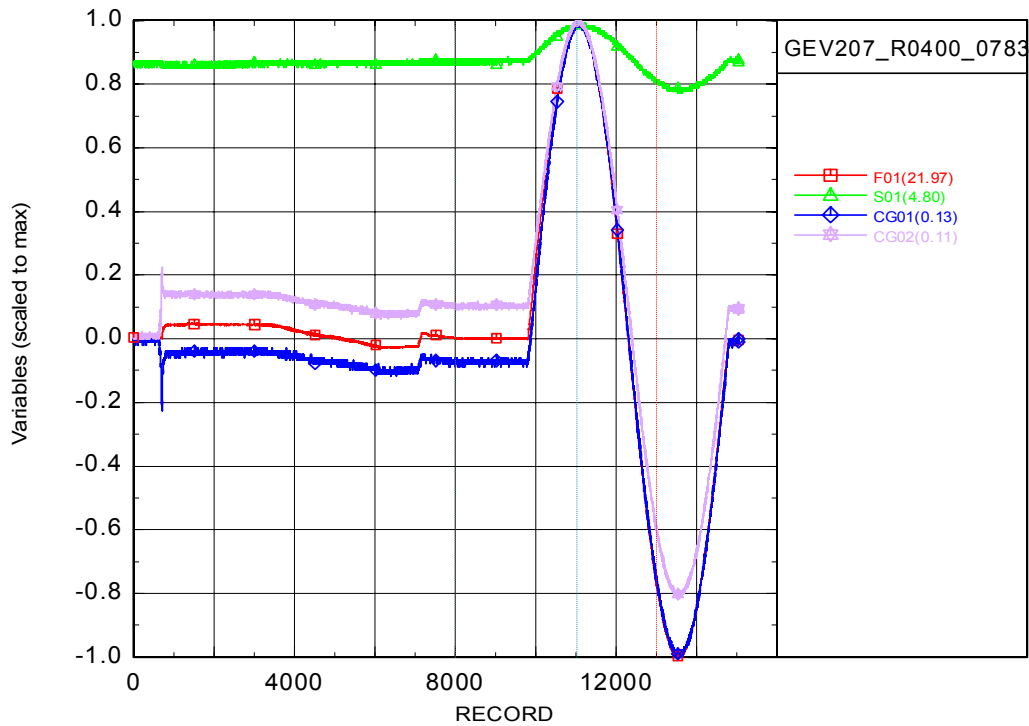
Figure 58: Sample measurement file (slow cycle buffer file)

58 shows results from a representative measurement file for the slow cycle. The file was expanded from binary format using in-house software and plotted using a dedicated graphical programming module from the FOCUS package[347].

This plot shows force (F01), displacement (S01), and strain sensor measurements (CG01, 02) from the complete slow-cycle measurement. The values are normalised with the maximum occurring sensor reading.

In the first recorded seconds, the coupon is mounted only in the lower grips. The strain sensor readings are set to zero before closing the upper grip. All signals are zero, except for the displacement, which is an absolute displacement in the actuator coordinate system. The strain sensor measurements instantaneously diverge from a zero reading at grip closing. This diverging of strain sensors represents the bending induced by closing of the second grip.

Note, that setting the strain readings to zero should ideally be done before gripping the coupon at all (gripping causes non-zero strains in the coupon). For practicality, the procedure described here was used.

The servo-hydraulic actuator control mode is changed from displacement control to load control after closing the grips, and load is set to zero (around record 8000). Then the slow cycle is started. The strain and load measurements taken in the slow cycle are processed according to ISO[132] to obtain the elastic modulus. This standard prescribes to calculate the modulus from strains between 0.05% and 0.25%.
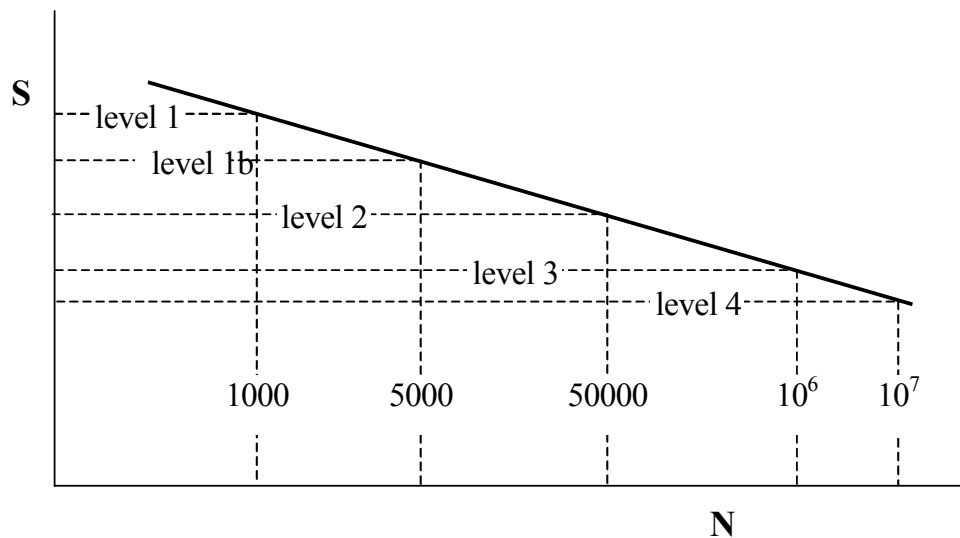
Figure 59: Standard OPTIMAT load levels

Strain measurements were also used to calculate bending, following ISO[133].

Originally, the slow cycle was done at the same R-value and magnitude as the fatigue cycles. Later, for fatigue tests that did not include both tensile and compressive loads, a slow cycle was done at R=-1, to obtain both tensile and compressive modulus of the coupon. The load was then limited to 10 kN. It was assumed, that this low load did not significantly damage the coupon.

Standard test load levels were defined for the fatigue tests. This was done to obtain as much information on a single load level fatigue data population, which helped analysis of block tests and residual strength tests. Thus, potential errors induced by interpolation of 'non-stratified' (i.e. not concentrated at distinct loading levels) S-N data could be minimised. These standard load levels were used in all constant amplitude tests, block testing, and residual strength testing. The exact load levels were initially determined from the basic S-N curve characterization, so that the load levels led to a mean lifetime of 10^3, 5×10^4 and 10^6 cycles. These stress levels are referred to as level 1, 2 and 3, respectively, see Figure 59: Standard OPTIMAT load levels.
In a later phase of the project, the highest load level was lowered to a nominal life of 5000 cycles. This level is designated as '1b'. In addition, some additional extra-long life residual strength were done, on the nominal level for 10 million cycles. This was called level 4.

In the standard OB specimens, it was found, that fatigue life was in some cases very sensitive to loading frequency. This was attributed to an unacceptable temperature rise in the specimens (Krause[161], 2002). As a result, standard

loading frequencies were established using a strain range criterion. These frequencies were connected to the standard load level, Material, and R-value and are specified in Krause[165] [2004]. These frequencies ensured the measured temperature not to exceed the (arbitrarily set) limit of 35°C.

Testing temperatures were measured on the surface of the specimen on the side

Table 4: Parameters of $F_{max}/width = A\, N^{1/B}$,

according to test specification (regular font), linear regression (italics)

		MD R0400		UD R0300	
		A	B	A	B
R-value	*-1*	3.7939	-9.4933	3.73	-8.04
		3.4619	*-9.633*	*3.1309*	*9.036*
	0.1	5.2419	-9.9585	4.35	-9.743
		5.0359	*-9.9585*	*4.4767*	*-9.135*
	10	2.8356	-28.82		
		3.0293	*-25.35*		

near the lower tab. Temperatures were recorded in the database. Surface temperature was limited by the use of a fan.

Variable amplitude block tests and residual strength tests use these 'standard' constant amplitude blocks, because this creates the possibility to:

- Minimise the need for interpolation of the S-N data.
- Parallel execution of tests

For example, strength degradation plots can be normalised using the average life of coupons tested in CA on that level, instead of calculating the nominal average life from an S-N curve.

Second, using standard levels allows for the parallel execution of tests. There is no need for one part of the test program to wait for the completion of another one. For example, the residual strength tests can be done at nominal life fractions, without the need for a full constant amplitude dataset at that level. Thus, in this case, the S-N programme and the residual strength programme can be carried out at the same time at different machines or laboratories.

An anti-buckling guide was hardly ever used in the OPTIMAT programme, except for some R=10 fatigue tests on UD coupons.

For the standard OPTIMAT geometries, S-N curves have been collected at various R-values. In Figure 60, an example S-N curve is plotted on log-log
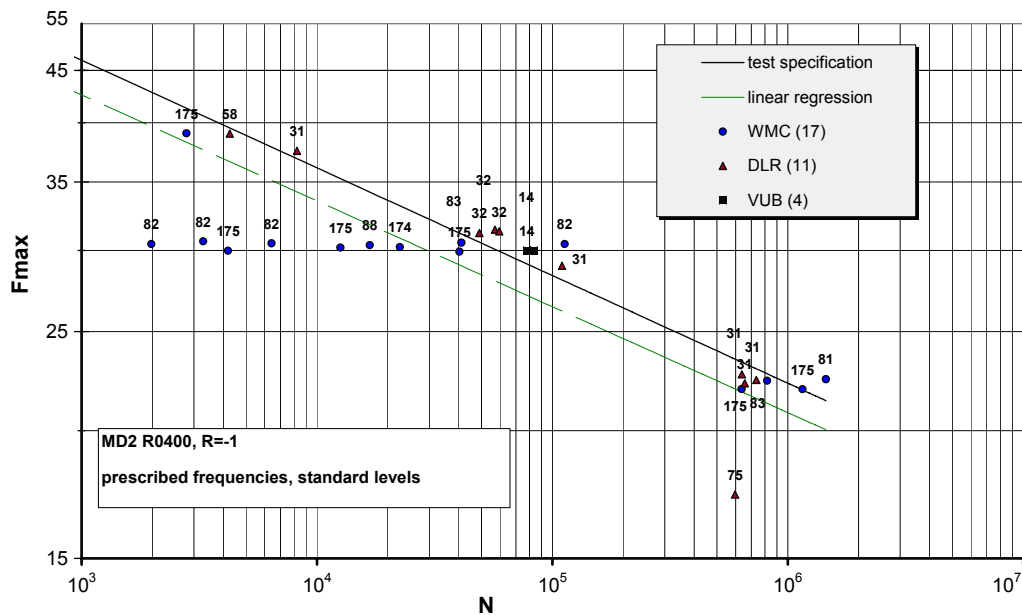
Figure 60: Example S-N curve, from OptiDAT[224]

Numbers next to data are plate numbers

basis. These data are also in the data summary of OptiDAT (Nijssen[224], 2006), which shows the plate numbers next to the datapoints. In Table 4, the power law coefficients of the S-N curves are given for the MD and UD material, in a different format from Eq. 3.

The fatigue behaviour is further summarised in the Constant Life Diagrams (CLDs), which are plotted in Figure 61, see Nijssen[227] [2006]. The constant life diagrams were constructed by plotting the S_{mean}, S_{amp} coordinates for each R-value and decade in lifetime. On the tensile side, the constant life lines for $N=1$ and $N=10$ yielded maximum stresses, which exceed the value for UTS. This is because the fatigue data were obtained at lower stresses and then extrapolated to higher stresses. The fact that this may lead to unrealistic low cycle stresses has been discussed already in section 2.3.4. They are excluded from Figure 61. The constant life lines were obtained by connecting all points with equal N with straight lines. For the region between the R-values closest to $R=1$ ($R=0.5$ and $R=10$ for MD2; $R=0.1$ and $R=1$ for UD2) and $R=1$, straight lines were drawn from the respective R-values to UTS for the tensile side of the diagram (right), and UCS for the compressive side (left).

The range of data, which was used to determine the S-N parameters with which the CLD was constructed, is indicated with radial lines. These lines represent the part of the CLD where actual data are available; the rest of the CLD is interpolated or extrapolated from data. The plot is limited to the mean life CLD.
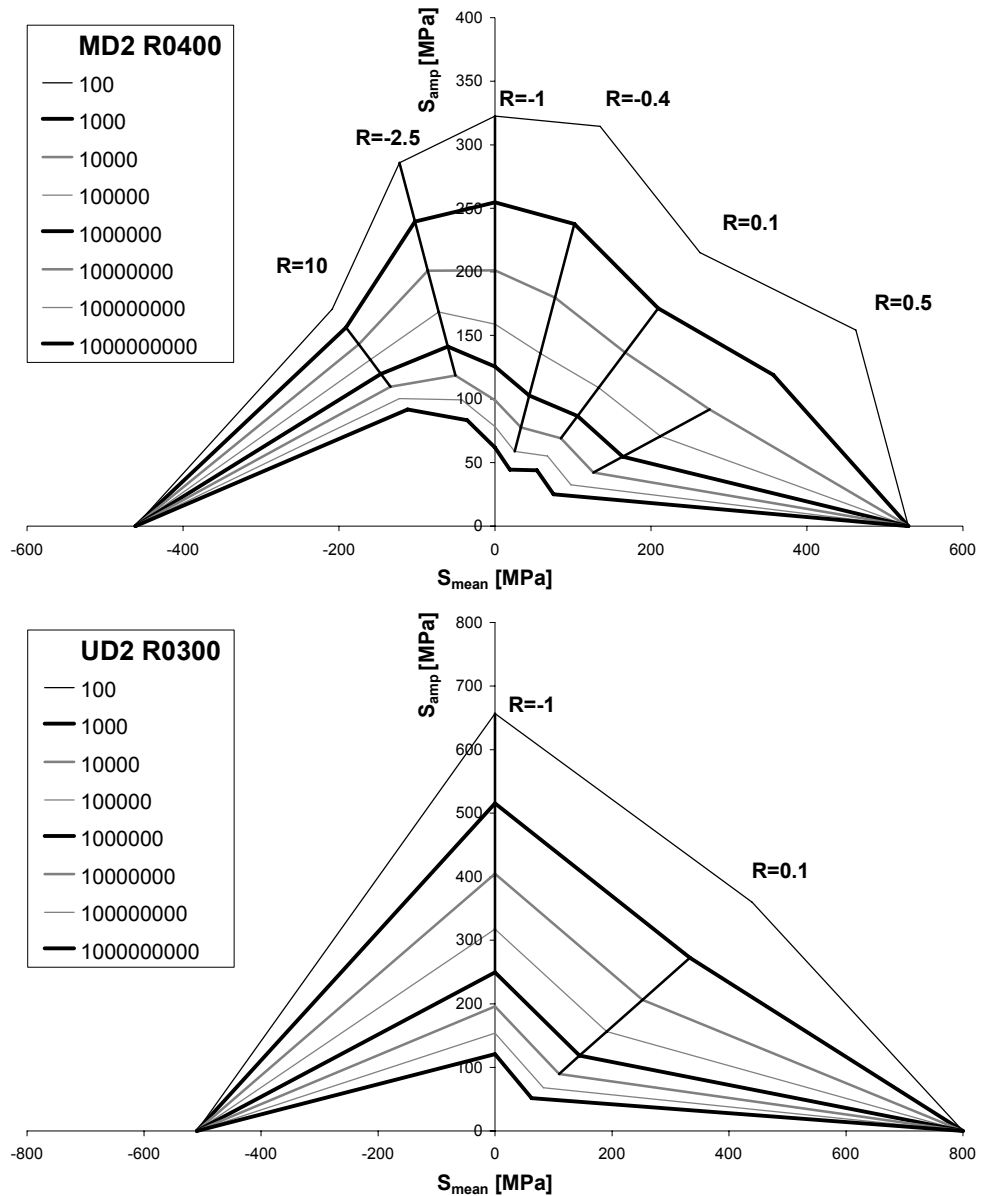
Figure 61: CLDs for standard MD2 and UD2 coupons

4.2.5 *Residual strength*

An extensive strength degradation investigation was done, totalling some 600 residual strength experiments in various loading conditions, of which some 150 failed prematurely. In OptiDAT, the data can be found by looking for entries (P)RST/C## in the test type column.
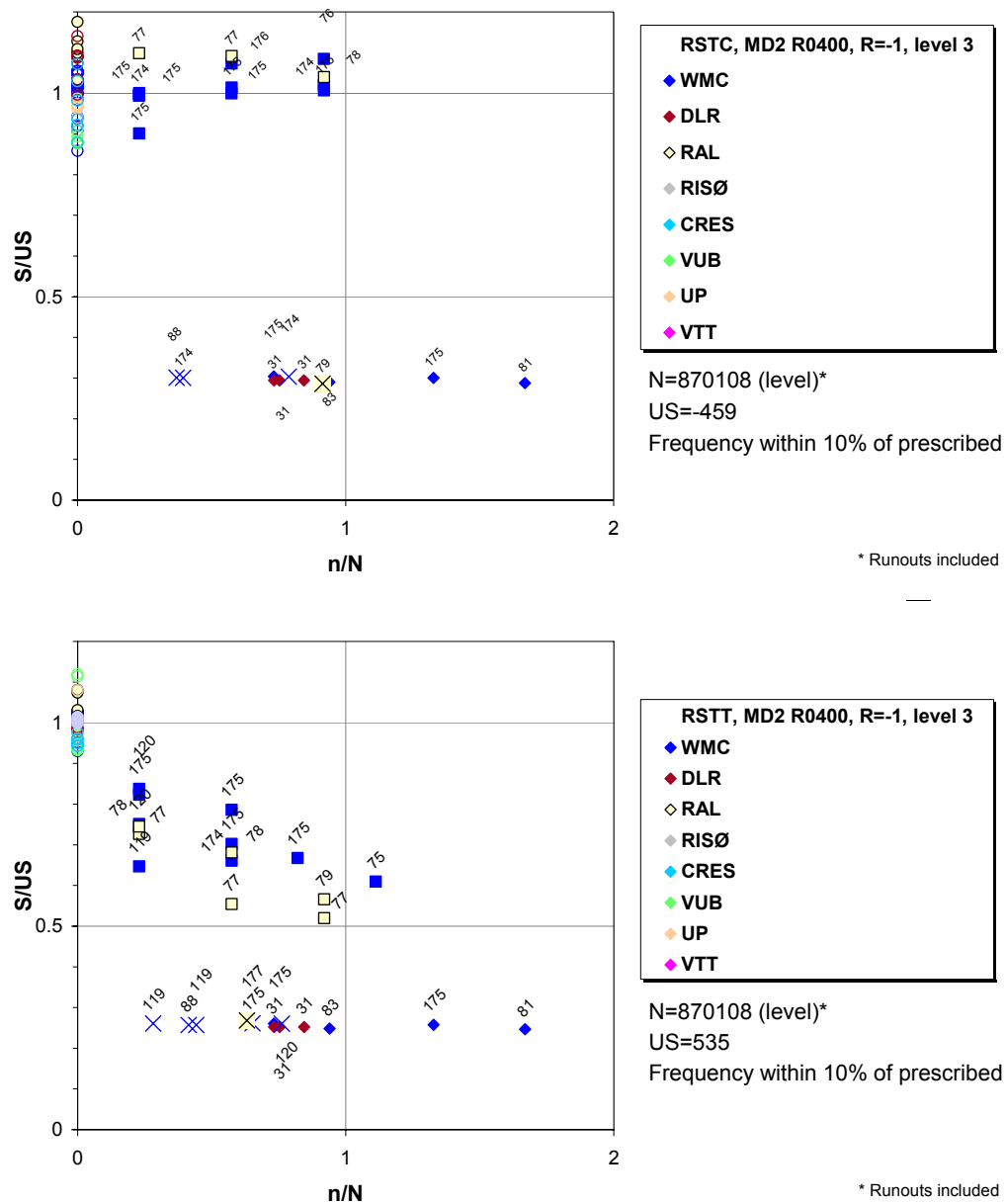
Figure 62: Example residual strength plots, reproduced from[225]

Numbers next to data are plate numbers

Two example plots of strength degradation of the material are given in Figure 62. The figure shows normalised tensile and compressive strength degradation at R=-1. Both plots are for standard MD2 coupons, and for level 3 (nominal life 10^6 cycles). The plot shows static, fatigue, and residual strength data; the test laboratories are colour coded, plates are indicated by numbers next to the datapoints. Tensile strength degradation is evident in early life. On the contrary,

compressive residual strength after fatigue is within the scatter bands of the static data.
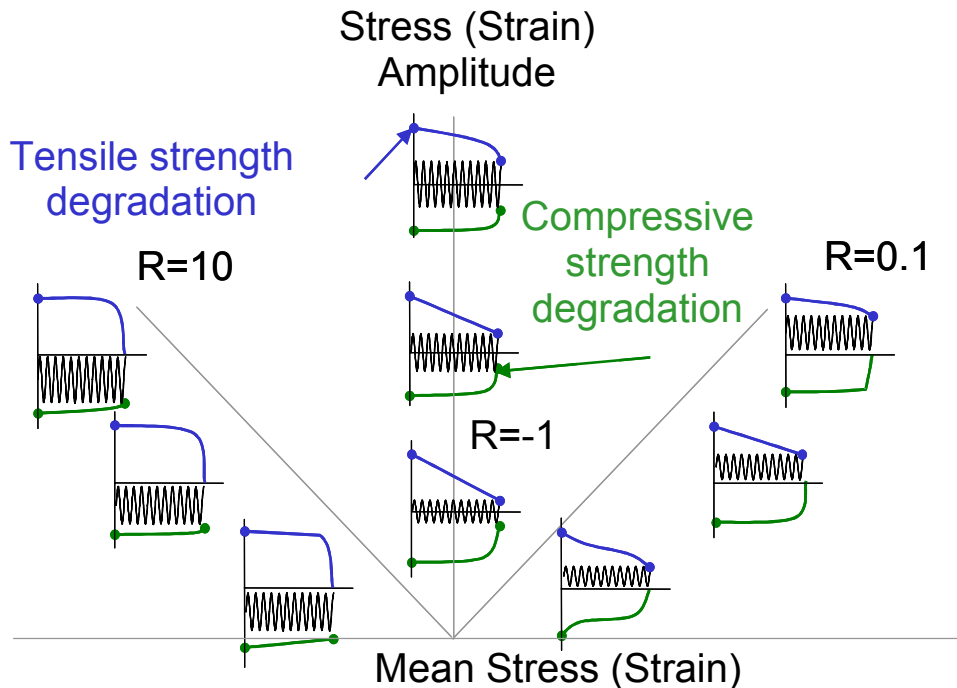
Figure 63: Schematic summary of strength degradation trends from various OPTIMAT laminates and geometries, in CLD format

The figures illustrate some of the variability issues mentioned in section 4.2.9. For instance, static, fatigue, and residual strength data were obtained from different laboratories and plates. This may explain some of the scatter in the results. For analysis of the results, such variability poses interesting challenges, since e.g. the residual strength after fatigue needs to be related to fatigue lives and initial strength from different datasets.

Most of the residual strength data from the OPTIMAT project are given in Nijssen[225] [2006]. The strength degradation parameters for each combination of R-value and standard load level were extracted from these plots following the algorithm suggested in section 3.4.4., see for the results section 4.4.

As will be demonstrated in Chapter 5, the value of these parameters is, for the load sequences investigated, not very influential in terms of prediction results, compared to other factors. The residual strength data can be summarised roughly by determining if the strength degradation behaviour is of the types 'early degradation', 'linear degradation', or 'sudden death'.

The strength degradation trends, summarised from various OPTIMAT laminates and geometries are summarised in Figure 63. These are based on the residual strength plots of Nijssen[225] [2006]. Schematically, the fatigue load is shown

(sinusoidal waveform), together with a line for tensile strength (starting at UTS, and ending at the maximum tensile load, or at zero) and compressive strength (starting at UCS, and ending at the maximum compressive load, or at zero).

This schematic shows, that for all load cases where some tensile component was present, tensile strength degraded in a linear manner. In most cases, compressive strength exhibited a clear 'sudden death' behaviour. Early degradation is not seen in any of the plots, although some data seemed to suggest, that a large part of the strength degradation occurred in early life, followed by a plateau in strength, and then another phase with considerable degradation toward the end of fatigue life. This is represented in the plots as an S-shaped curve. Such a curve would require two parameters to the strength degradation formulation.
In general, there is limited dependency of strength degradation pattern on load level. For some of the higher load levels, a slightly different strength degradation pattern seemed to be discernible in the data than for the lower load levels. For example, for R=-1, the low load levels showed linear strength degradation, whereas at higher load levels, the rate of strength degradation gradually increased.

For the UD and MD materials, the strength degradation trends are very similar. Surprisingly, this summary seems to be valid for various laminates. For instance, both the OPTIMAT UD2 and MD2 materials (standard coupon geometries R0300 and R0400, respectively) show linear degradation for R=0.1 fatigue. That strength degradation is similar for UD2 and MD2 is not extremely surprising, since both have most of the fibres in load direction. However, the MD3 laminate in I1000 geometry, which has only ±45° layers and is considerably longer than the standard OB geometry, also shows linear degradation of tensile strength. Transverse OB coupons show sudden-death behaviour with respect to compressive residual strength, which is again very similar to the standard UD and MD coupons, although the laminate is oriented at 90°.

The strength degradation patterns found in the OPTIMAT project are similar to the patterns found in the MSU programme, see section 4.4.

4.2.6   Block tests

Block test results are found in the database OptiDAT under test types starting with 'BT' for two-block tests, or 'RBT' for repeated block tests. Premature failures are indicated by 'P'. Various different block tests were done, combining blocks of different amplitude as well as different R-values. These are indicated in the database by a letter code. A schematic of the block tests in the OPTIMAT project, including the code per test type, is shown in Figure 64. For example, a

block tests which contains a block of R=0.1 at level 1b, and a block of R=0.1 at level 2 is coded 'E'.

The results of the block tests are reported in Nijssen[226] [2006], and will also be discussed below.

In OPTIMAT, the two-block tests all started with a block of 50% of the nominal fatigue life. Standard OB load levels and frequencies were used. The repeated block tests were programmed as repeating sequences, with block lengths of 1% of nominal fatigue life, i.e. a Miner-based life estimate predicts failure after 50 sequences.

Ultimately, one would like to compare the Miner's sums at failure to the predicted Miner's sums, to validate the life prediction methodologies. To this end, the OPTIMAT results are presented in tabular form in terms of Miner's sum at failure.
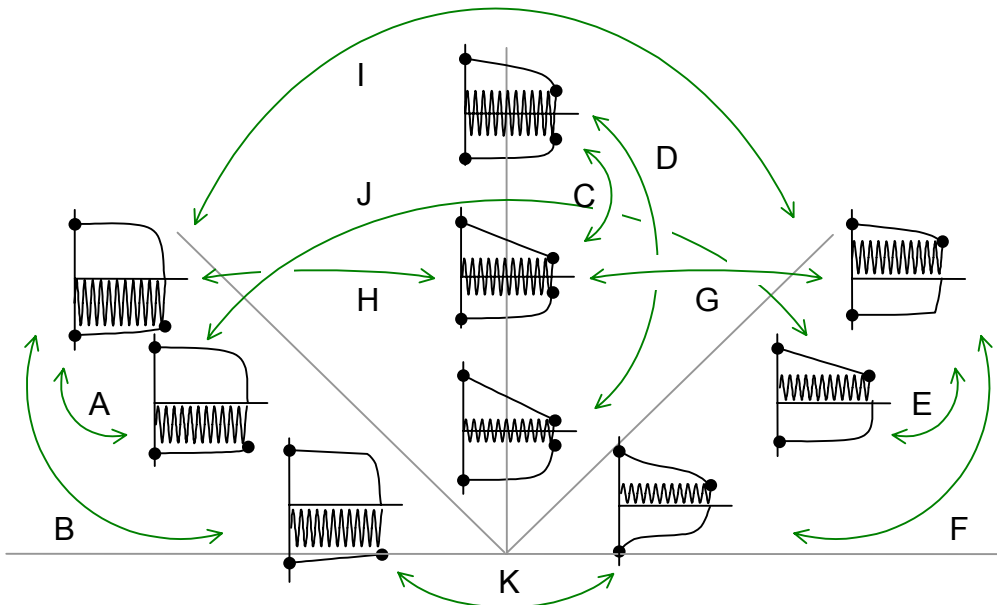
Figure 64: Letter codes for block tests

Some discrepancy in average fatigue life was observed, when based on nominal cycles to failure, cycles to failure per level, or cycle to failure based on a log-log S-N curve from regression analysis. All these can be used to calculate Miner's sum. This is indicated by the 4 columns under 'Miner's sum'. The first column reflects Miner's sum at failure when using the S-N curve from the general test specification (Krause and Philippidis[165], [2005]. The column 'single level average' uses the fatigue life calculated using only CA data taken at the same standard load level. This number is different if all CA data in the S-N dataset (i.e. all load levels) are used for the calculation of Miner's sum (3rd column). Finally, the single level average of the log life was included in the 4th column.

As was done for the residual strength tests, the preferred normalisation life is the average fatigue life of all coupons tested at the relevant load level and R-value, i.e. single level average.
The results are summarised separately for constant R-value block tests, mixed R-value block tests, and repeated block tests, in Table 5, Table 6, and Table 7, respectively. In these tables, small samples (n<=3) are indicated in italics.
In addition, the strength-based predictions are indicated.

In Table 5 and Table 6, the number in brackets indicates the ratio M_{AB}/M_{BA} of Miner's sum for a particular test type to the Miner's sum of its 'opponent'. The opponent is the block test, which consists of the same type of blocks, but in reverse order. For instance, the opponent of BTC1b2 is BTC21b. These bracketed numbers help in interpreting the data. For instance, in Table 5, test of type BTE shows a Miner's sum of 1.69 for the HL case, and 1.16 for the LH case (in the column for single level average). If the number in brackets exceeds unity, the cell is highlighted.

Since the repeated block tests do not have opponents, they are compared to the Miner's sums of the corresponding two-block tests. The ratio $M_{BlockTest}/M_{RepeatedBlockTest}$ is indicated in brackets. Sometimes, two numbers are given, for the ratio of *HL/RBT* and *LH/RBT*.

Generally, High-Low sequences yield higher Miner's sums than Low-High sequences. This is clearly the case for the constant R-value two-block tests with R=-1 and 0.1. However, for the R=10 block tests, the opposite seems true. It must be stated, that the R=10 block test evaluation is hampered considerably by the small slope of the S-N curve, combined with significant scatter. The statistical basis for conclusions on the R=10 block tests is marginal.

For mixed R-value block tests, preceding a loading block with an R=-1 constant amplitude load seems to degrade performance in the second block. This is evident from the results, where $M_{CN}>M_{NC}$, and $M_{TN}>M_{NT}$. It seems, that preceding a compressive block by a purely tensile load helps to increase fatigue life in the second, tensile block, i.e. $M_{CT}>M_{TC}$.

There is no clear correlation of the resulting Miner's sum and the difference between load levels from block to block.

The Miner's sum from the repeated block tests was compared to that of the corresponding block test. In all cases without R=10 blocks, the repeated block tests failed earlier than the corresponding two-block test.

Table 5: Single R-value two-block test results summary

Test type I	Test type II	R 1	R 2	level 1	level 2	Miner's sum (M_{AB}/M_{BA}) test specification	single level average	all CA	single level average log N	rsd prediction (M_{AB}/M_{BA})	n
HL	BTA1b2	10	10	1b	2	18.62 (0.58)	12.68 (5.45)	9.76 (0.78)	21.41 (3.08)	1.08 (1.19)C	5
	BTB1b3	*10*	*10*	*1b*	*3*	*1.07 (0.09)*	*0.40 (0.38)*	*0.86 (0.17)*	*0.47 (0.18)*	*1.14 (1.43)C*	*3*
	BTC1b2	-1	-1	1b	2	1.39 (1.70)	2.59 (1.70)	4.50 (1.67)	4.27 (1.73)	1.08 (1.19)T	6
	BTD1b3	*-1*	*-1*	*1b*	*3*	*1.21 (0.85)*	*1.72 (0.76)*	*3.52 (0.68)*	*1.76 (0.77)*	*1.13 (1.36)T*	*3*
	BTE1b2	0.1	0.1	1b	2	1.09 (1.43)	1.69 (1.45)	1.79 (1.42)	2.19 (1.39)	1.14 (1.41)T	6
	BTF1b3	*0.1*	*0.1*	*1b*	*3*	*1.69 (1.66)*	*1.83 (1.43)*	*2.17 (1.55)*	*2.00 (1.45)*	*1.22 (1.97)T*	*2*
LH	BTA21b	10	10	2	1b	32.07 (1.72)	2.33 (0.18)	12.51 (1.28)	6.95 (0.32)	0.91 (0.84)C	5
	BTB31b	10	10	3	1b	12.19 (11.36)	1.05 (2.65)	5.12 (5.96)	2.68 (5.67)	0.80 (0.70)C	4
	BTC21	*-1*	*-1*	*2*	*1*	*0.77*	*1.65*	*2.38*	*2.6*	*0.81 T*	*3*
	BTC21b	*-1*	*-1*	*2*	*1b*	*0.82 (0.59)*	*1.52 (0.59)*	*2.70 (0.60)*	*2.47 (0.58)*	*0.91 (0.84)T*	*3*
	BTD31b	*-1*	*-1*	*3*	*1b*	*1.43 (1.18)*	*2.24 (1.31)*	*5.15 (1.46)*	*2.27 (1.29)*	*0.83 (0.73)T*	*2*
	BTE21b	0.1	0.1	2	1b	0.76 (0.70)	1.16 (0.69)	1.26 (0.70)	1.57 (0.72)	0.81 (0.71)T	5
	BTF31b	0.1	0.1	3	1b	1.02 (0.60)	1.28 (0.70)	1.40 (0.64)	1.38 (0.69)	0.62 (0.51)T	4
PHL	*PBTB1b3*	*10*	*10*	*1b*	*3*	*0.48*	*0.03*	*0.18*	*0.1*		*1*
	PBTC12	*-1*	*-1*	*1*	*2*	*0.40 (6.11)*	*1.03 (8.29)*	*1.69 (10.57)*	*1.03 (4.17)*		*2*
	PBTC1b2	-1	-1	1b	2	0.22 (0.53)	0.40 (0.50)	1.03 (0.99)	0.40 (0.25)		5
	PBTC21b	*-1*	*-1*	*2*	*1b*	*0.42 (1.89)*	*0.81 (2.01)*	*1.04 (1.01)*	*1.60 (4.01)*		*1*
	PBTF1b3	*0.1*	*0.1*	*1b*	*3*	*0.45 (2.76)*	*0.74 (5.34)*	*0.71 (3.73)*	*0.79 (4.99)*		*1*
PLH	*PBTA21b*	*10*	*10*	*2*	*1b*	*0.19*	*0.13*	*0.1*	*0.22*		*2*
	PBTC21	*-1*	*-1*	*2*	*1*	*0.06 (0.16)*	*0.12 (0.12)*	*0.16 (0.09)*	*0.25 (0.24)*		*1*
	PBTD31b	*-1*	*-1*	*3*	*1b*	*0.34*	*0.39*	*0.57*	*0.41*		*1*
	PBTF31b	*0.1*	*0.1*	*3*	*1b*	*0.16 (0.36)*	*0.14 (0.19)*	*0.19 (0.27)*	*0.16 (0.20)*		*1*

For Block test letter codes, see Figure 64

Table 6: Mixed R-value two-block test results summary

Test type I	Test type II	R		level		Miner's sum (M_AB/M_BA)				rsd prediction (M_AB/M_BA)	n
		1	2	1	2	test specification	single level average	all CA	single level average log N		
CN	BTH1b2	10	-1	1b	2	2.07 (1.08)	3.04 (2.91)	4.08 (2.29)	6.09 (2.78)	1.50 (1.00)T	5
										0.63 (0.42)C	
CT	BTI1b1b	10	0.1	1b	1b	1.47 (2.10)	1.62 (1.95)	1.71 (1.99)	1.77 (1.96)	1.50 (1.00)T	4
	BTJ22	10	0.1	2	2	1.10 (0.17)	1.24 (0.25)	1.29 (0.32)	1.94 (0.24)	1.50 (1.00)T	4
	BTK33	*10*	*0.1*	*3*	*3*	*1.30 (0.33)*	*1.00 (0.38)*	*1.51 (0.33)*	*1.09 (0.40)*	*1.50 (1.00)T*	*1*
NC	BTH21b	-1	10	2	1b	1.92 (0.92)	1.04 (0.34)	1.79 (0.44)	2.19 (0.36)	1.50 (2.38)C	4
NT	BTG21b	-1	0.1	2	1b	0.63 (0.46)	1.16 (0.47)	1.44 (0.49)	2.12 (0.51)	0.58 (0.47)T	5
TC	*BTI1b1b*	*0.1*	*10*	*1b*	*1b*	*0.70 (0.48)*	*0.83 (0.51)*	*0.86 (0.50)*	*0.90 (0.51)*	*1.50 (1.00)C*	*2*
	BTJ22	*0.1*	*10*	*2*	*2*	*6.52 (5.91)*	*4.94 (3.99)*	*4.03 (3.12)*	*8.20 (4.22)*	*1.50 (1.00)C*	*2*
	BTK33	*0.1*	*10*	*3*	*3*	*3.93 (3.02)*	*2.61 (2.61)*	*4.56 (3.02)*	*2.71 (2.48)*	*1.50 (1.00)C*	*1*
TN	BTG1b2	0.1	-1	1b	2	1.37 (2.18)	2.48 (2.13)	2.93 (2.04)	4.18 (1.97)	1.23 (2.12)T	6
										0.97 (1.67)C	
PTC	*PBTK33*	*0.1*	*10*	*3*	*3*	*0.45*	*0.38*	*0.52*	*0.43*		*1*
PNT	*PBTG21b*	*-1*	*0.1*	*2*	*1b*	*0.12*	*0.23*	*0.29*	*0.45*		*1*

Table 7: Repeated block test results summary

Test type I	Test type II	R 1	R 2	level 1	level 2	Miner's sum (M_{BT}/M_{RBT}) test specification	single level average	all CA	single level average log N	rsd prediction (M_{BT}/M_{RBT})	n
CN	*RBTH1b2*	*10*	*-1*	*1b*	*2*	*2.44 (1.18)*	*2.40 (0.79)*	*3.49 (0.85)*	*4.88 (0.80)*	*0.42 (3.57)C*	*2*
CT	RBTI1b1b	10	0.1	1b	1b	1.12 (0.76)	0.95 (0.59)	1.09 (0.64)	1.08 (0.61)	0.41 (3.66)C	5
	RBTJ22	10	0.1	2	2	0.63 (0.57)	0.68 (0.55)	0.70 (0.54)	1.08 (0.55)	0.41 (3.66)C	5
	RBTK33	*10*	*0.1*	*3*	*3*	*0.33 (0.26)*	*0.25 (0.25)*	*0.39 (0.26)*	*0.27 (0.24)*	*0.41 (3.66)C*	*1*
HL	RBTA1b2	10	10	1b	1b	32.53 (1.75)	7.16 (0.56)	13.75 (1.41)	14.41 (0.67)	0.91 (1.00-1.19)C	5
	RBTB1b3	*10*	*10*	*1b*	*3*	*2.24 (2.09)*	*0.64 (1.62)*	*1.55 (1.80)*	*0.84 (1.78)*	*0.83 (0.96-1.37)C*	*3*
	RBTC1b2	-1	-1	1b	2	1.08 (0.77)	1.99 (0.77)	3.81 (0.85)	3.01 (0.70)	0.91 (1.00-1.19)T	6
	RBTD1b3	-1	-1	1b	3	0.42 (0.35)	0.62 (0.36)	1.34 (0.38)	0.63 (0.36)	0.85 (0.71-0.96)T	7
	RBTE1b2	0.1	0.1	1b	2	0.44 (0.41)	0.69 (0.41)	0.72 (0.41)	0.88 (0.40)	0.85 (0.95-1.34)T	5
	RBTF1b3	0.1	0.1	1b	3	0.20 (0.12)	0.25 (0.14)	0.28 (0.13)	0.27 (0.14)	0.73 (0.85-1.67)T	5
NC	*RBTH21b*	*-1*	*10*	*2*	*1b*	*1.66 (0.86)*	*1.58 (1.52)*	*2.31 (1.29)*	*3.21 (1.47)*	*0.42 (3.57)C*	*3*
NT	RBTG21b	-1	0.1	2	1b	0.31 (0.49)	0.55 (0.47)	0.62 (0.43)	0.86 (0.40)	0.70 (0.83-1.76)T	5

Block test predictions

The column with the residual strength prediction contains three elements. First, the Miner's sum predicted using a residual strength model is shown. For the RSD model, strength degradation parameters of 1 and 10 were used, depending on the R-value and whether strength degradation in tension or compression was considered.

Second, the number between brackets is similar to the bracketed numbers in the other columns and indicates the ratio of predicted Miner's sum for a load sequence and its reverse. For the repeated block tests, the bracketed number is the ratio of Miner's sum predicted for a block test, compared to Miner's sum from a repeated block tests. For example, for the BTE single R-value block tests, RSD-predicted Miner's sums are 1.14 and 0.81, respectively. The ratio between a HL and LH test, however, is very similar to the single level average value (1.45 vs 1.41). This might be caused by limited number of samples on one or two levels, which gives a mean life for that level which is different from the populations mean level. In this case, the experimental single level average might be lower than the actual single level average, resulting in normalisation of fatigue life with a number that is too small. Thus, the Miner's sums from the block tests can be too high.

Third, a letter 'T' or 'C' indicates if failure was assumed to occur in tension or in compression. This is of interest, since tensile strength degradation governs tensile failure and compressive strength degradation governs compressive failure. Thus, for R=0.1 in the second block, failure is tensile, and for R=10, failure is compressive. For R-1, failure was assumed to occur in tension. No apparent improvement of the predictions for R=-1 was seen when using compression strength as failure driver. For the repeated block tests, two predictions were made, and the prediction with the smallest Miner's sum was reported in this column.

The predictions are compared to the experimental results, calculating Miner's sums using the average fatigue life of single stress level. The performance of the prediction is poor for the R=10 tests. For tests containing R=0.1 blocks, however, the strength degradation predictions seems more satisfactory, considering the scatter in the results.

Summarising, the predictions follow the general trends that were observed in the data for R=-1 and R=0.1 two-block tests. The trend $M_{TN} > M_{NT}$, that was observed in the tests, is predicted by the RSD model.

For tests containing R=10, however, the predictions behave poorly. For the *CN* tests, the predictions do not show the same behaviour as the tests, not even when the compression strength is used to determine failure in the R=-1 block.

The repeated block test predictions all give Miner's sums below unity; when compared to the non-repetitive block tests, they give lower Miner's sums.

4.2.7 (NEW) WISPER(X) tests

Spectrum tests were done on standard OPTIMAT MD2 and UD2 specimens (geometries R0300 and R0400), for details see Figure 65, and Nijssen[227] [2006]. For a description of the load spectra, see section 3.1. The spectral tests were evenly distributed between the laboratories of DLR and WMC. UP also performed spectrum testing.
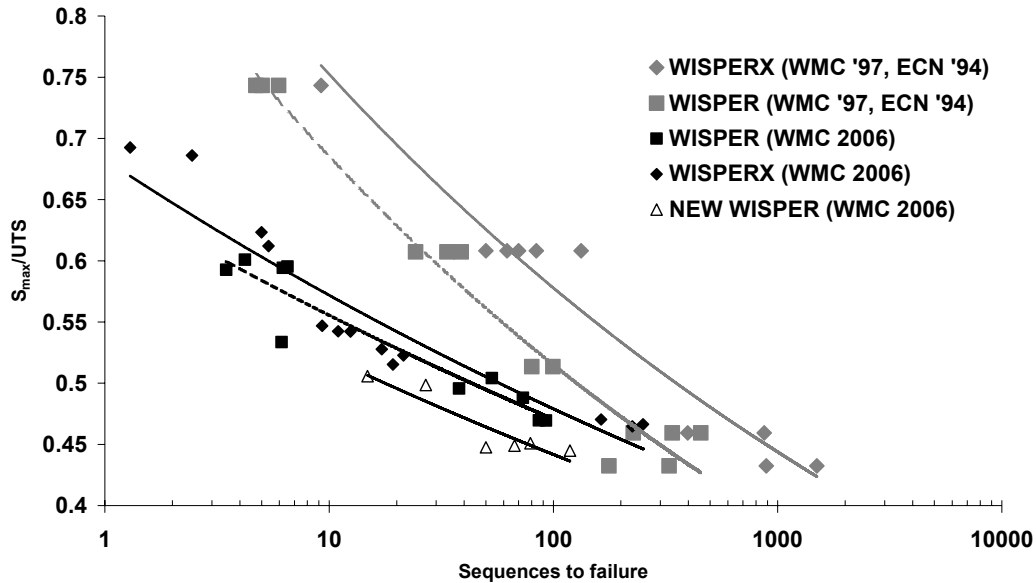
Figure 65: WISPER(X) data from OPTIMAT and previous projects

Different spectrum loading software was used by the different partners. Essentially, spectrum loading software is designed to interpolate a sequence of peaks and valleys from an input file with a sine or triangular waveshape (a sine wave was used in OPTIMAT), and load the specimen accordingly. The spectrum input files are scaled by varying the load level of the maximum peak. The loading rate is scaled accordingly. The loads and loading rates were predetermined using the Miner-based routine taken from Brøndsted[39, 40] [1997, 2005] (section 2.2.4), and prescribed in Krause and Philippidis[166] [2005]. Loading rate was constant for a single spectrum, and was scaled with the maximum load, giving higher rates at lower stresses. The loading rate for the spectral tests (ca. 400 kN/s) was smaller than for the constant amplitude tests, and heating of the specimen was not likely to cause problems. This is confirmed by temperature measurements on the side-surface of the specimen near the tab. Force range, displacement range, and strains were measured (the latter using a standard OB clip-gauge in a back-to-back configuration) prior to the test and

during the test. In addition, deviations from the command value were tracked and recorded in a separate log file.

The results are plotted in Figure 65. This plot shows maximum spectrum stress, normalised with ultimate tensile stress, versus sequences to failure. Data are shown for WISPER, WISPERX, and NEW WISPER. There are two datasets, one for tests done previously, in 1994 and 1997, by ECN and WMC; and the other set is from OPTIMAT. All maximum stresses are normalised with static strength obtained at low loading rates (0.25 mm/min for the OPTIMAT 2006 coupons, 0.56 kN/s for the 1994, 1997 results).

Based on the previous results, van Delft et al.[69] [1997] argued, that the small cycles in WISPER do incur some damage in the material, as the WISPERX spectrum results in slightly longer fatigue lives. In the 2006 data, the difference between WISPER and WISPERX is not so pronounced, whereas NEW WISPER is slightly more damaging per sequence than the other two load spectra.

The normalised spectral S-N curves in Figure 65 are quite different for high loads. The 2006 data have much shorter fatigue lives at high loads than the data collected previously. The curves seem to converge at 1000 sequences, roughly. The cause for the better performance of the earlier coupons is not clear. It could be attributed to the difference in machines, laminate, and geometry (the 1994-7 data were from glass-fibre reinforced polyester, 7 layers of 500 g/m^2 unidirectional, 8 layers 480 g/m^2 ±45°, hand lay-up, dog-bone coupons, UTS=428, UCS=291 MPa, Fibre volume fraction 30% (50% by weight). Coupons were bolted in mechanical clamps).

4.2.8 Failure mode

Failure mode was not recorded in the OptiDAT database. For some tests, photographs of the failed coupons have been published in OPTIMAT reports.

In static tests, failure was characterised by damage throughout the gauge section. In some tensile tests, axial cracks formed near ultimate failure. In compression tests, delamination and buckling of the delaminated layers occurred.

Failure mode in the residual static tests usually resembled static failure, although inspection of the tabbed section frequently indicated, that fatigue damage had localised there and formed a starting point for failure. This depended on the R-value and load level.

In fatigue, failure was in general more localised than in the static case. Grip failure is the dominant failure mode. For the WMC tests, Table 8 shows the number of failures for specified failure modes of a selection of specimens for

two machines in the WMC laboratory. Only valid fatigue tests are tabulated. Overall, most failures occurred at the bottom side of the specimen. This is, for the WMC equipment, the location of the moving grip. The bottom grip operates at a slightly higher temperature than the top grip, since it is connected directly to the hydraulic actuator. The predisposition for failure at the lower grip may be connected to the suspected temperature sensitivity of the laminate. The relative amount of lower grip failures was higher for the Schenck machine. Overall fatigue performance at this machine was not obviously better than the Instron.

Table 8: Fatigue failure location
occurrences for selected data

	Test machine	
failure location	**Instron**	**Schenck**
bottom	11	81
bottom between tabs	40	57
top	9	47
top between tabs	31	26
middle	1	12

For R~-1 fatigue, it was not recorded if failure occurred in compression or in the tensile part of the load cycle. This could be of interest for residual strength lifetime prediction at these R-values. The actual failure mode can be masked by machine displacement limit settings. For example, if the upward displacement limit is less stringent than the downward setting, it is possible, that the coupon fails in the compressive section of the load cycle, but the machine actually stops in the tensile cycle (or vice versa). It is therefore recommended, that the data acquisition be programmed to retain the measurements the last few load cycles before failure.

4.2.9 Variability Issues

Most of the coupons were manufactured by a single supplier (except for some of the repair test coupons, which are not discussed in this book). These batches were manufactured and delivered over the course of the project to the 8 laboratories participating in the project. In some cases, a material batch was split up to supply multiple laboratories, in other cases a batch of material would be delivered to a single laboratory only. For each shipment, record was kept of coupon geometry, plate number, number of coupons, date of shipment, and more. In addition, plate properties such as fibre volume fraction and glass-transition temperature were measured at the supplier. These data are in the OptiDAT database.

This method of coupon distribution is a potential source of batch-to-batch variations. It was not in the spirit of the cooperative OPTIMAT project to test all coupons on a single testing frame, nor was it feasible. Also, it was impossible to manufacture and randomise a single batch of specimens containing over 4000 different coupons of different lay-ups and thicknesses. Instead, the coupons were manufactured over a 4-year period, and sent out in subsequent batches to different laboratories, and tested in different machines. The unavoidable result is, that the project has to deal with scatter introduced by potential plate-to-plate, lab-to-lab, and machine-to-machine variations.

Plate-to-plate variations are caused mainly by the variability in manufacturing, and are expressed in terms of variations in:

- fibre volume fraction
- fibre wetting
- cure conditions
- glass-transition temperature
- thickness
- fibre alignment
- fibre bundle strength

The plates in OPTIMAT were extensively characterised by the main manufacturer, LM Glasfiber AG, and by the test laboratories. This information is available from OptiDAT.

Machine-to-machine variations are, for example:

- test frame stiffness
- geometry of grips
- (distribution of) gripping pressure
- grip alignment
- measures to prevent torsion

These quantities are difficult to quantify, and their effect is difficult to measure if data from the same plates are not available for similar tests on different machines. In addition, they are hard to decouple from lab-to-lab variations, which exist in terms of:

- ambient conditions
- (small) procedural differences

An added source of complication is, that some of the sources of variation only have consequences for particular test results. Static compression strength and fatigue life may be very sensitive to machine variations (alignment, gripping characteristics), whereas static tensile strength is more sensitive to plate

variations. Examples of machine-to-machine variations, or plate-to-plate variations caused by e.g. differences in fibre volume fractions may be found in Nijssen[224] [2006].

4.3 Montana State University (MSU)

4.3.1 Fatigue research at MSU

The composites group at MSU, whose research is mostly funded by Sandia National Laboratories, boasts two decades of intensive research dedicated to wind turbine composites. A summary of a major part of the research in this group was published by Samborsky[276] [1999]. Their recent achievements include:

- Giga-cycle strand fatigue tests (Samborsky[276], 1999)
- Extensive description of a CLD for a wind turbine blade representative composite (e.g. Sutherland and Mandell[315], 2005)
- Spectrum fatigue load effects (Wahl[328], 2001; Nijssen[227], 2006)
- Substructure testing (Mandell, Samborsky et al.[184], 1998)
- Influence of laminate details (Mandell, Samborsky, and Sutherland[185], 1999)

4.3.2 Project database: DOE/MSU

The DOE/MSU database is maintained by Montana State University under auspices of the US Department of Energy (DOE/MSU) and Sandia National Laboratories. It is updated once a year, and is available at the Sandia Web site[189], where numerous reports on the MSU research are also found. The database contains mainly fatigue data of small coupons under diverse conditions. Some other 10000 test results on 150 different materials are contained in the database, which focusses on polyester-glass-fibre laminates, but also includes vinyl-ester and epoxy matrix materials. Also, some carbon fibre data are in the database. Most of the pioneering work mentioned above is included in this database.

4.3.3 Material, coupons and test set-up

A single material was used in this program, which is a multi-directional glass-fibre/polyester material, representative for the material used in a wind turbine blade. This material is designated *DD16* in the DOE/MSU fatigue database, which contains detailed information on this particular composite. Some 10000 test results extensively characterise the material in terms of static strength, constant amplitude fatigue behavior and influence of design details. It has also been used in the study by Wahl[328] [2001] on spectrum fatigue, so it was an excellent candidate material for the present investigation.

Plate preparation

The material was manufactured in plates in a vacuum assisted resin transfer molding (VARTM)-process, using the DD16 laminate, which has a [90°/0°/±45°/0°]s lay-up. The polyester resin was Corezyn 63-AX-031, mixed with 1% of MEKP (catalyst). The procedure followed is identical to the one described in detail in Samborsky's thesis[276] [1999]. Prior to cutting the plates into specimens, using a diamond saw, the plates were numbered and labeled with information on material and amount of catalyst. Subsequently, they were photographed, and marked with a plate-specific hatching. In some cases, resin-poor areas were identified by visual inspection and marked. Also, each specimen was given a unique number, so that the location on the plate of each tested specimen would be known at all times. An alphanumeric number was given, consisting of a letter indicating the position along the longitudinal axis of the plate, and a number indicating the position along the transverse axis of the plate. This procedure was not followed for the specimens of plate 3, these specimens were delivered in random order. This number can be identical for specimens from different plates. In addition, a sequential number was allocated to each coupon. This number consisted of four digits, of which the first is the plate number. This numbering system allows rapid identification of the parent plate and approximate location on the plate.

An example of a marked plate is shown in Figure 66. Although the marked side was on the bottom of the mould, this is called the front of the plate. On all plates, text direction of the alphanumeric coupon codes was parallel to the long side of the rectangular plate. In the top-right corner, details on the resin, the amount of catalyst, manufacturing date, and plate number are marked.
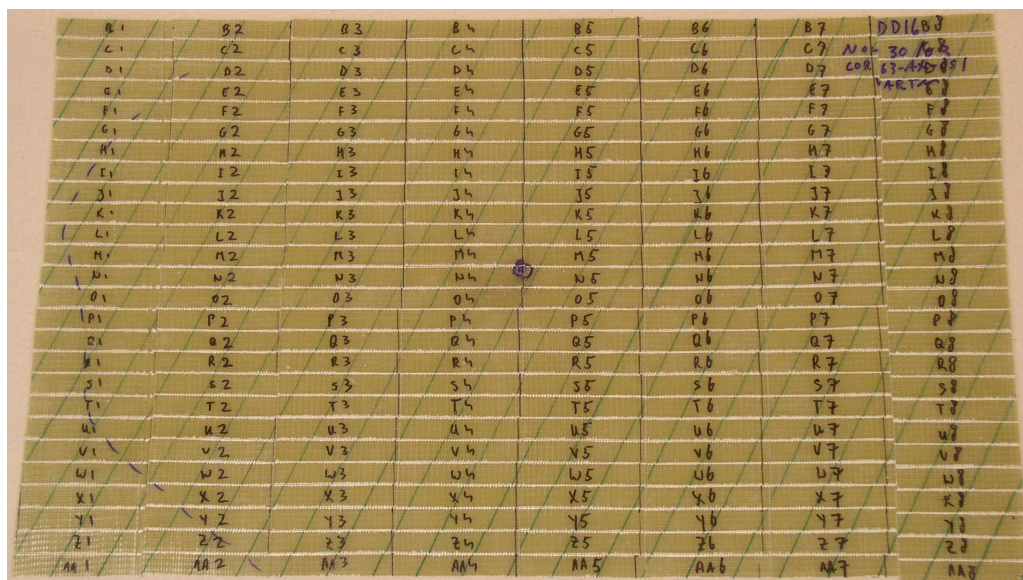
Figure 66: MSU specimen source plate with identification markings
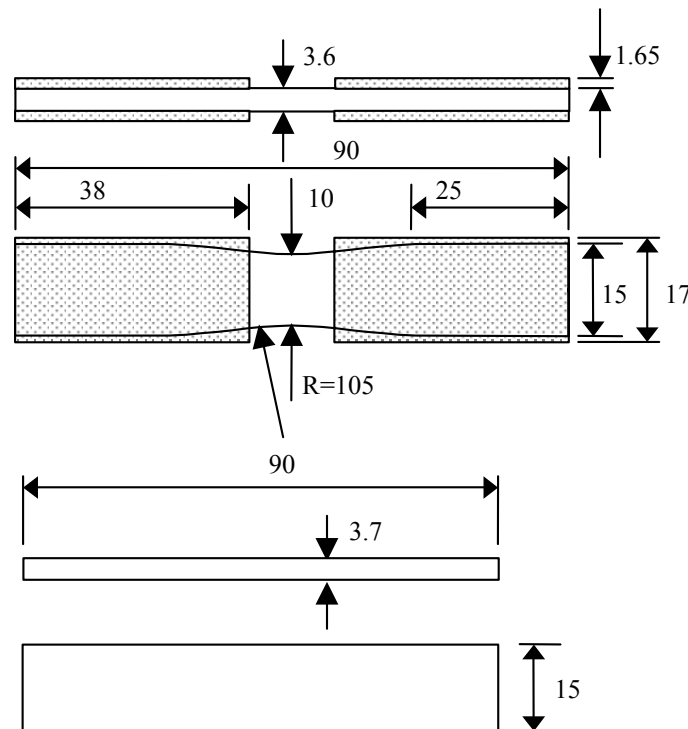
Figure 67: MSU specimens, dimensions in mm

Specimen preparation

For the R=-1 and R=0.1 tests, the specimens cut from plate 3, 4, and 5, were machined into a dog-bone shape using a pin-router set-up as described in e.g. Wahl[239] [2001]. The milling process did cause some damage in the outer 90° layers, but these layers were considered not to contribute significantly to the coupon static strength. In both the dog-bone and rectangular geometries, the 90°-layers on the specimen surfaces were believed to aid the load introduction by the grips. In stress calculations, the outer layers were included. Not much knowledge is available on the effect of machining on the mechanical properties of composites; Ghidossi et al.[103, 104] [2003] made recommendations on the tool and process parameters for Iosipescu, ring, and off-axis specimens of unidirectional material, based on experience with the effect on static properties. After the milling process, the specimens were lightly sanded and washed. Prior to adhesively bonding the tabs, the location of the tabs was sanded using 3M 80 grit sandpaper. The tabs were applied by hand using Hysol EA 9309 2NA QT two-component adhesive, and post-cured in the oven at 70° C for 3 hours. While curing, clamping pressure was applied to the tab-specimen assembly.

The shape and nominal dimensions of the dog-boned specimens used are shown in Figure 67. The specimens were slightly longer and wider than the reversing test coupons of Neil Wahl[328] [2001], but the dimensions of the gauge section were nominally equal. The actual specimen dimensions varied slightly, due to

tolerances during plate manufacturing, specimen milling and application of the tabs. The average thickness and width were 3.6 and 10.0 mm, respectively. The average gauge length was 12.9 mm. The specimens were tabbed by hand, which resulted in some specimen-to-specimen variation of the free gauge lengths. Any influence was most likely to be found on the compressive strength of the specimens. Therefore, careful measurements were taken of the distance between tabs on each corner of the gauge section (to quantify gauge length), specimen thickness, minimum width, and misalignment of the specimens in the test machine.

After tabbing the specimens, the specimens were numbered using a fine-tipped marking pen. For plate 3, this number was sequential, for plates 4 to 8, this number referred to the location on the plate. Thickness, minimum width and gage section length were measured using a digital vernier caliper with a 1/100th of a millimeter read-out. Repeated measurement of the same dimensions indicated, that the measurements were repeatable within 1/20th of a millimeter. This repeatability reflects the presence of irregularities in the specimen's surface.

Specimens from plate 6, 7, and 8 were not machined into a dogbone shape, since the fatigue behaviour at R=10 was not satisfactory (scatter exceeded two decades). Coupons from these plates are rectangular and untabbed. Nominal dimensions are given in Figure 67. The dimensions are similar to the specimen dimensions of Wahl's compression specimens[239], except that the length is smaller (82.5 mm instead of 90 mm). This length provided a better fit in the currently used hydraulic wedge grip equipment.

The development of the dogbone geometry is described in Mandell and Samborsky[189] [2006]. During this development, essentially the same phenomena were observed as in the OPTIMAT preliminary programme, such as splitting of the laminate in fatigue, reducing an original dogbone to a rectangular coupon. However, because of the lower 0° dominance, the dogbone geometry was preferred.

Material characterisation
The material used in the tests was extensively characterised in terms of:

- Fibre volume fraction
- Fibre angles
- Modulus measurements
- Optical/SEM observations
- Tow strength

The DD16 material is made from the D155 fabric, which has approximately 10 tows per 20 mm fabric width. There is some variation in the tow distance, which
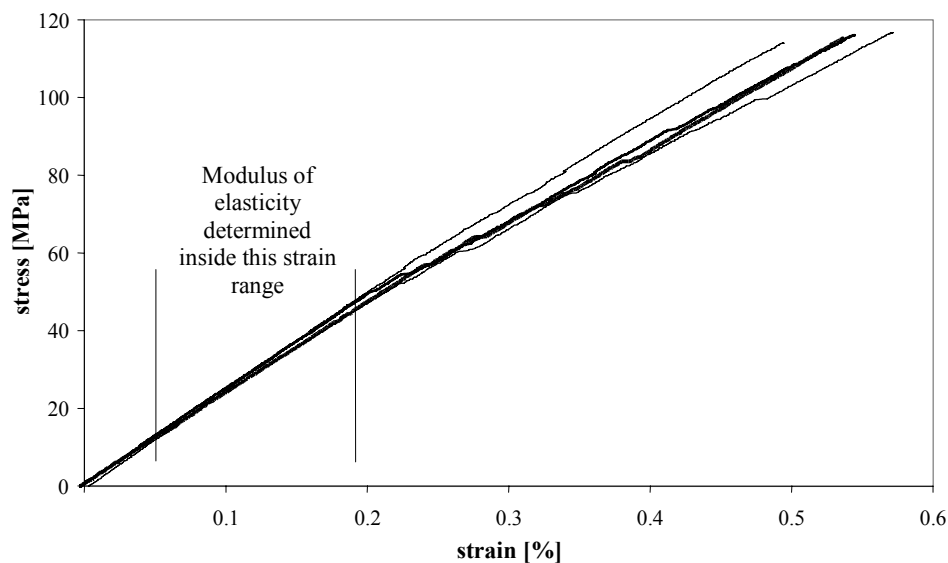
Figure 68: Modulus measurements on selected MSU coupons

is reflected in a variation of the number of tows in a specimen. Thus, the number of load-carrying fibres is not equal per specimen, adding uncertainty to the determination of tow stress during a test. This is worse for the dogbone-shaped specimens, since they have a smaller minimum cross-sectional area, and therefore a larger relative variation in the number of (partial) tows in the specimen. This should be kept in mind when comparing stress-life data between dogbone shaped specimens and straight-sided specimens.

In addition, it should be noted, that edge tows are prone to buckling, and may be (partially) discontinuous. This is especially true in case of bad fibre alignment and with dogbone shaped specimens.

Table 9: Modulus results for selected specimens

Plate	specimen ID	modulus [GPa]	stdev [MPa]
6	*D3 (6055)*	24.04	292
	P8 (6197)	24.64	342
7	*V4 (7100)*	25.10	385
	M3 (7065)	24.04	395
averages		24.46	354

Fibre volume fraction was measured for a selection of specimens. The specimen mass was determined using a scale with an accuracy of 0.01g. The matrix material was digested in an oven at 650° Celsius. A minimum time of 15

minutes was necessary to remove both the matrix material and the intermediate products of the incineration (soot). The remaining fibre material was transferred to the scale. Using the density of glass (2.55 g/cm^3), the fibre volume could be determined. The volume of the initial specimen was also measured and could be used to double-check the fibre volume calculation. To facilitate specimen dry volume measurements, the dogbone-shaped specimens were trimmed to obtain a rectangular specimen.

Given the uncertainties in the volume and mass measurements, the fibre volume fraction could be determined with a 1% accuracy to 42%. This is slightly higher than the nominal fibre volume fraction of 36% of the DD16 material, e.g. Mandell[183] [1997]. As was described e.g. by Samborsky[277] [2002], departure from the governing ASTM guidelines in the sense that larger amounts of material were digested, leads to improved accuracy of the fibre volume fraction-determination for this laminate (although localised variations can not be measured).

It was only feasible to measure strains for a limited number of specimens, and obtain some quantification of the laminate's modulus. Specimens were equipped with an Instron extensometer, and loaded in tension. Table 9 and Figure 68 summarise the modulus measurement results. The moduli are, on average, slightly higher than the nominal modulus for the DD16 material (18 GPa, Mandell[183] [1997]. This higher modulus is consistent with the higher value for the fibre volume fraction.

Table 10: Fibre angle measurements

2nd number indicates double measurement

Specimen ID (plate 6)	1st +45s	1st -45	2nd +45s	2nd -45s	Remarks
AA1	38°	-39.5°	37°	-41°, -41°	0° slightly off-axis
N8	32°, 48°	-36°, -37°	34°, 41°	-40°, -41°	
K5	41.5°, 41.5°	-37.5°, -37.5°	-42.5°	-41.5°, -41.5°	

It was desired to quantify how the manufacturing process might have led to deviations from nominal fibre angles. These deviations occur in the manufacturing process, when preparing the laminae from the fabric rolls, during lamina positioning in the mold, during resin inflow, and possibly during curing of the material.

There are no prescriptions for determining fibre angles in a laminate. The specimens that had been used in the fibre volume determination were manually disected and the fibre angles were measured per layer. This gave a qualitative
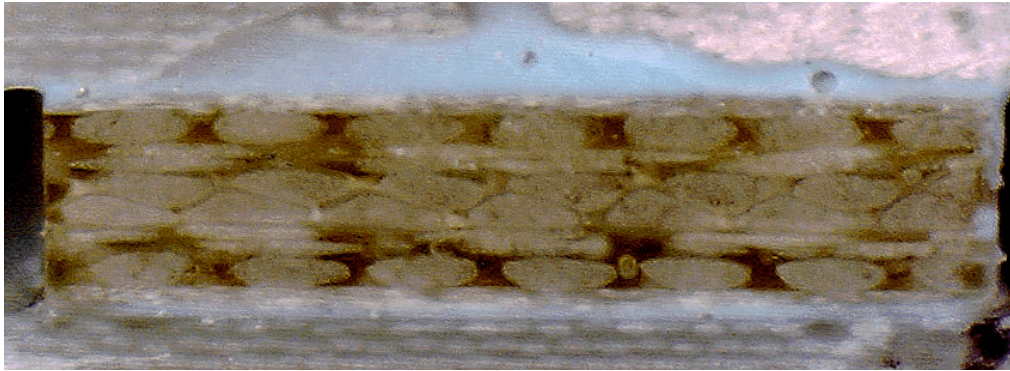
Figure 69: Top edge of specimen 4209 (Optical Microscope)

estimate of the accuracy in laminate fibre angle with respect to the nominal values. The results are shown in Table 10.

Samborsky has extensively reported on similar fibre angle deviations (cf. Samborsky[276] [1999], pp.147 onwards). The current fibre angles are within the limits of these previous measurements on similar material made in the same mould and manner. Samborsky has also reported on static and fatigue behaviour of off-axis balanced plies, to quantify effects of fibre misalignment.

In addition, Samborsky described the variation of tow strength, based on the static tests he has performed on tows taken from plain fabric rolls. Typical data obtained per roll show a variation of ca. 20% between the weakest and strongest tow coupons. The overall variation for all fabric rolls was approximately 50%.

Finally, the material can be characterised through microscopical observations. Figure 69 shows an image top of the specimen, which has been polished and treated with hydrofluoridic acid to expose the fibre ends. The 0° tows are clearly distinguishable from the more elliptical ±45° layers. Observations from the Scanning Electron Microscope (SEM) reveal in more detail the structure of the laminate. Refer to section 4.3.7 for a description of the untested material structure, in comparison with the microstructure of a coupon after having been subjected to different types of loading.

Machines and testing procedure

For these tests, two servo-hydraulic machines were available. An Instron 8501 ±100 kN machine was used for all static- and residual strength tests and some of the constant amplitude- and block tests. An Instron 8872 table-top machine with ±20 kN maximum load capacity was used for constant- amplitude and block tests. Both machines were controlled by an Instron 8800 controller. The waveforms for the static, constant amplitude, and block tests were programmed and executed using Instron software[130]. The general set-up is shown in Figure 70. In principle, it is similar to the WMC set-up shown previously.

In programming the fatigue waveform, the first part was usually a load controlled ramp to zero load. This was followed by a load controlled ramp to the
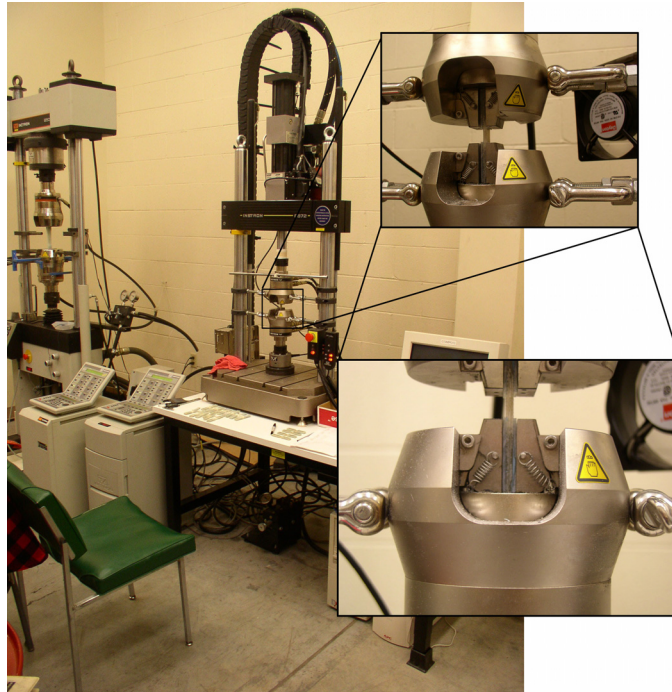
Figure 70: Test set-up at Montana State University (MSU)

mean load, from which a sine-shaped waveform was initiated, starting in the first quadrant and at the appropriate amplitude.

For a static waveform, a load controlled ramp to zero load was performed first, followed by a displacement controlled ramp. In some cases, the PC-control was
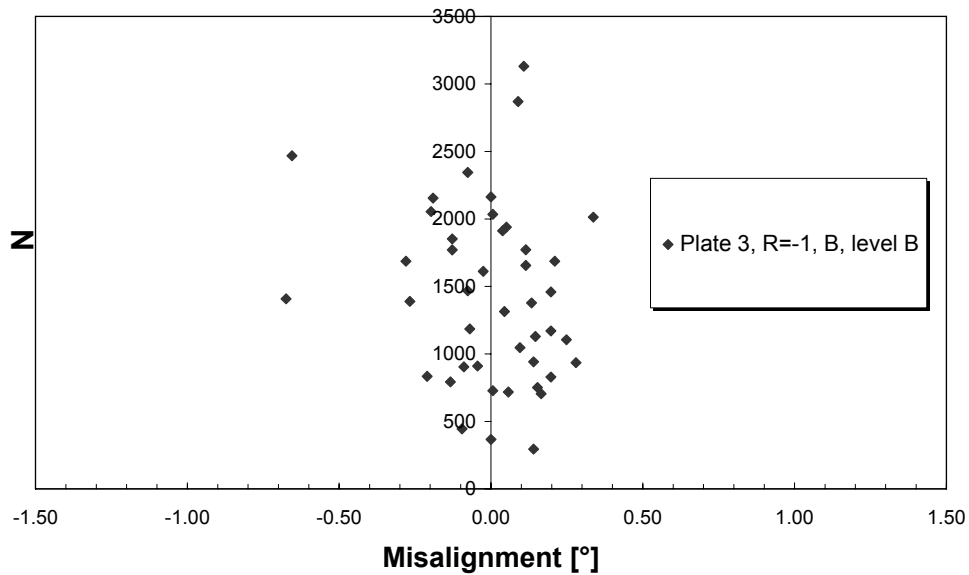
Figure 71: Sample misalignment data

bypassed and the static test was performed using the 8800 controller only.

Specimen alignment was ensured by an alignment tool, and was measured and recorded. Analysis of the alignment data revealed, that this alignment procedure resulted in a misalignment of at most 1.35°, and that no correlation exists between specimen performance and misalignment in either fatigue or static tests. Such correlation is not expected, given the alignment of the fibres in the specimen. A sample of misalignment data is given in Figure 71.

4.3.4 Static and fatigue tests

Refer to section 4.1.2 for the general test set-up. Displacement rates were in the same order of magnitude as the fatigue tests (12.5 mm/s). Maximum and minimum load were recorded. Stress was calculated by dividing load by the cross-sectional area.

Table 11: Static data from MSU programme

Plate	3		4		5	7
machine	Instron 8872	Instron 8501	Instron 8872	Instron 8501	Instron 8872	Instron 8501
STT		718		740		696
stdev		35		29		12
STC	-419	-433	-415		-382	-385
stdev	28	25	24		20	16
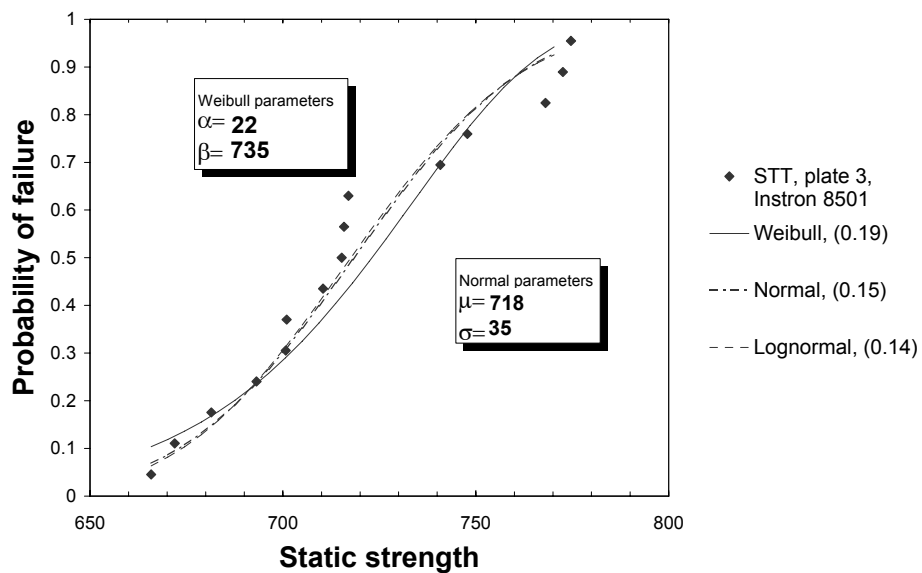
Figure 72: Sample probability plot for static data from the MSU programme
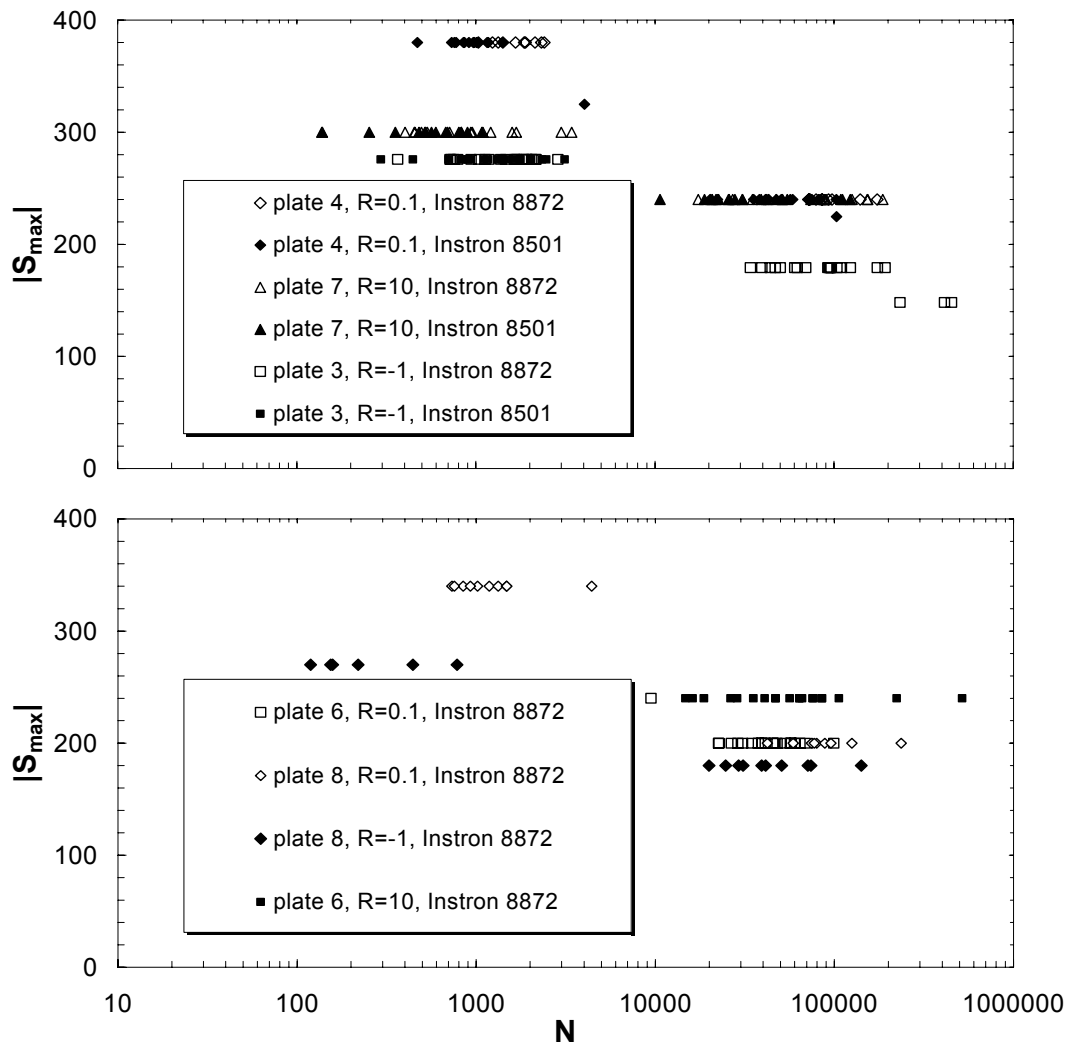
Figure 73: S-N data from MSU programme

The results of the static tests are shown in Table 11. No tensile tests were performed on the Instron 8872 test frame, since the required load was likely to exceed the capacity of the frame. For plate 3 specimens, compression tests were done on both test frames; the average values are within 5%, the standard deviations are within 10%. Compressive strength is slightly lower for plate 5 and 7 specimens than for plate 3 and 4 specimens, but all are within acceptable limits.

A sample probability plot is given in Figure 72. These plots show the raw data, fit with three types of distribution functions, viz. the Lognormal, Normal, and 2-parameter Weibull plots. Also, the distribution parameters are plotted for the Normal and Weibull distributions (for the Normal distribution, these parameters

are identical to those in Table 11). The goodness of fit is again expressed in terms of the Kolmogorov-Smirnoff distance parameter, as was done for the OPTIMAT tests.

Figure 73 shows all relevant constant amplitude data collected in the MSU programme.

The results of the fatigue tests are summarised in Table 12 and Table 13. The table is arbitrarily divided in two parts. Table 12 lists fatigue lives for plates that were used in residuals strength testing, Table 13 for other plates.

Table 12: Fatigue data for plate 6 and 8

Plate	6				8					
R	0.1				0.1				-1	
machine	8872	8872	8501	8501	8872	8872	8501	8501	8872	8872
level	A	B	A	B	A	B	A	B	A	B
N_{avg}	46127	9480	78314	24531	95227	1416	n/a	n/a	52246	1166
N_{min}	22551	9480	50331	10533	42189	732	n/a	n/a	19953	133
N_{max}	99155	9480	127923	37300	235683	4414	n/a	n/a	141124	2729
N_{stdev}	18481	n/a	34053	10573	53953	1089	n/a	n/a	36227	840
count	20	1	4	6	10	10	n/a	n/a	10	10
S_{max}	200	240	200	240	200	340	n/a	n/a	180	240

Typically, two load levels were tested in constant amplitude fatigue; level A and B. The load levels were estimated from the DOE/MSU database, to target nominal lives of ca. 100,000 cycles or 1,000 cycles, respectively. Frequency of level A tests was 3 Hz, frequency of level B tests was 1 Hz. Occasional temperature probing using an external infrared sensor did not indicate, that the specimen surface heated during fatigue at these loading rates.

Table 13: Fatigue data for plate 3, 4, and 7

(plates used in residual strength testing)

Plate	3				4				7			
R	-1				0.1				10			
machine	8872	8872	8501	8501	8872	8872	8501	8501	8872	8872	8501	8501
level	A	B	A	B	A	B	A	B	A	B	A	B
N_{avg}	87667	1451	n/a	1402	97347	1731	55543	938	77004	1139	46088	617
N_{min}	34184	366	n/a	295	72056	1031	20324	471	17432	138	7063	139
N_{max}	193117	2870	n/a	3131	174306	2407	103006	1414	186916	3427	123295	1080
N_{stdev}	45250	629	n/a	698	33663	473	22829	220	53804	952	35725	253
count	17	21	n/a	22	10	10	17	15	16	15	18	15
S_{max}	179	276	n/a	276	240	380	240	380	-240	-300	-240	-300
N_{8872}/N_{8501}	A	B			A	B			A	B		
	n/a	1.035			1.753	1.845			1.671	1.848		

To avoid distortion of normalised residual strength plots due to machine-to-machine variations (see section 4.3.5), for each level datasets were collected at both machines.

As is apparent from the numbers at the bottom of Table 13, the Instron 8872 results are located at slightly higher average lives than results for the 8501, at R=0.1 and R=10. Such machine-to-machine variations are virtually unavoidable, since the machines have different, only partially quantifiable gripping conditions and, possibly, slightly different alignment. Load control of the machine is in the order of 1% accuracy; given the slope of a typical S-N curve for glass/epoxy of 8-10, a 5% difference in load would be necessary to yield difference of 50% in life.

Standard deviation on life (as a measure of scatter) is approximately $0.5 \cdot N_{avg}$ for R=-1, smaller than $0.5 \cdot N_{avg}$ for R=0.1, and larger than $0.5 \cdot N_{avg}$ for R=10.

4.3.5   Residual strength

Residual strength degradation was measured by statically testing coupons, which had been subjected to fatigue, as outlined in section 4.1.4. Loading rates and control modes were identical to the fatigue and static tests. Because of machine maximum load, all residual strength tests were carried out on the Instron 8501, except for the residual compressive strength R=-1 tests of plate 3 (5 specimens were residual strength tested on the 8501, of which one coupon did not fail prematurely).
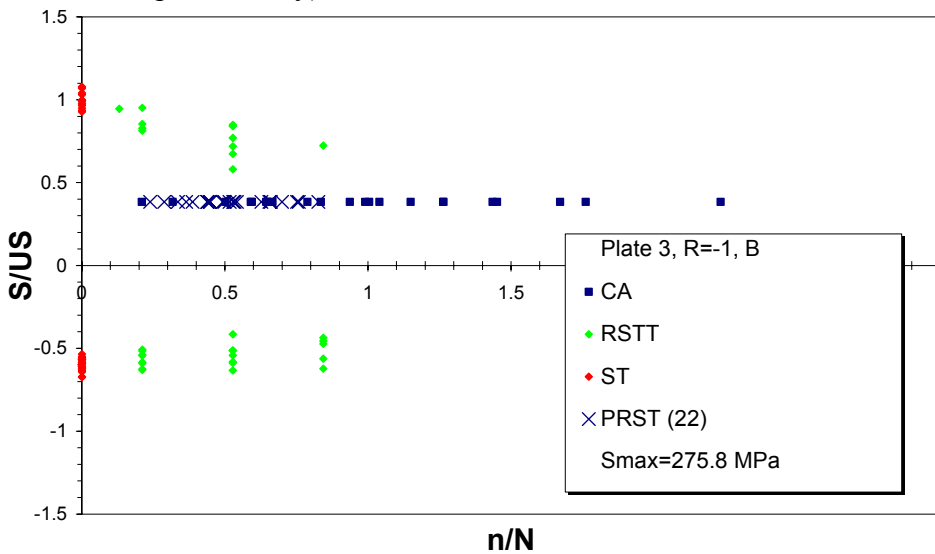
Figure 74: Example of strength degradation plot (MSU)

The strength degradation data plot contains static strength, constant amplitude fatigue life, premature failures, and residual strength data, as was outlined in

Figure 39. An example of tensile and compressive strength degradation data at R=-1, is shown in Figure 74. The constant amplitude tests are plotted on the tension side; this does not mean that they all failed in tension, however, this is following common practice of how R=-1 S-N data are usually plotted.

All maximum stresses were normalised by the static strengths of specimens from the same plate. All fatigue lives were normalised by the average fatigue life at the frame where most of the strength degradation data were obtained.

In practice, all plots are normalised by average fatigue life at the Instron 8501; only the R=-1 compressive residual strength is normalised by the Instron 8872 mean fatigue life (refer to Table 13 for the appropriate mean fatigue lives).

An important aspect of the MSU dataset, is the avoidance of plate-to-plate and machine-to-machine variations. Where time and equipment allowed it, all data in the strength degradation plots were collected from specimens from the same plate, and on the same machine. This procedure was not possible in the OPTIMAT project, resulting in suspected plate-to-plate/lab-to-lab variations, see section 4.2.9.
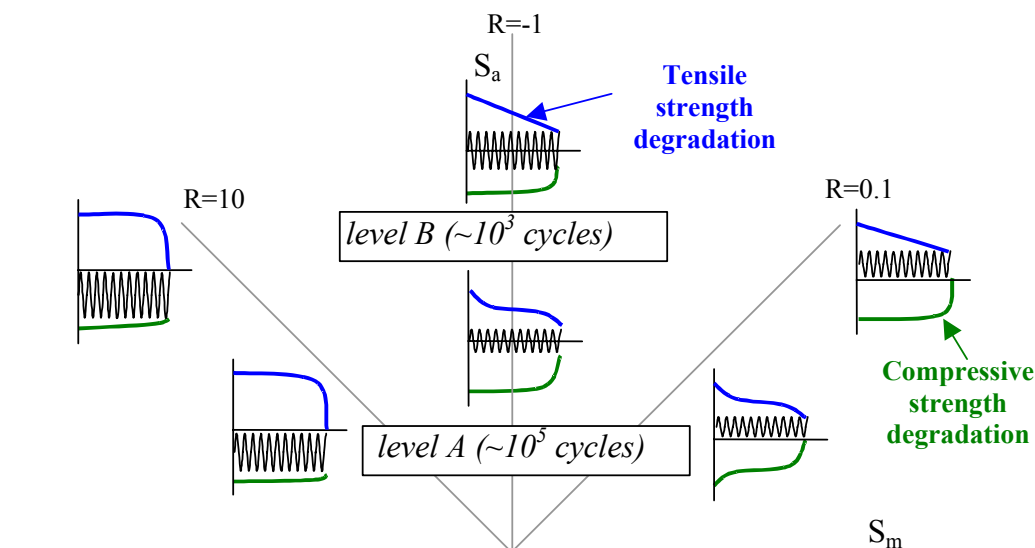
Figure 75: Summary of MSU residual strength trends in CLD format

The strength degradation trends found in the MSU programme are summarised in Figure 75, in a format similar to Figure 63.

4.3.6 Block tests

The block-tests are subdivided in two-block tests and repeated block tests, see 4.1.3 for the general set-up. All block tests were done at loading rates and load

levels identical to constant amplitude fatigue tests, see Table 13. Block tests are summarised in terms of Miner's sum. The contribution to Miner's sum of each block was calculated using the average constant amplitude fatigue life at identical conditions.

Two-block tests

The two-block tests are again subdivided in two categories, viz. single-R-value and mixed R-value tests. The single R-value block tests were carried out at the same plate and R-value for which the residual strength tests were done.

Different from the OPTIMAT programme, more than 1 life fractions were used for the first block length. The life fraction of the first block was identical to one of three life fractions at which the residual strength experiments were done. Thus, regardless of the strength degradation parameter fit, the residual strength at the end of the first block can be directly estimated from the residual strength results at that particular combination of plate, R-value and life fraction. This can eliminate some of the uncertainty in subsequent strength-based life prediction. These block tests are the most appropriate dataset to validate the strength degradation model for simple load spectra.
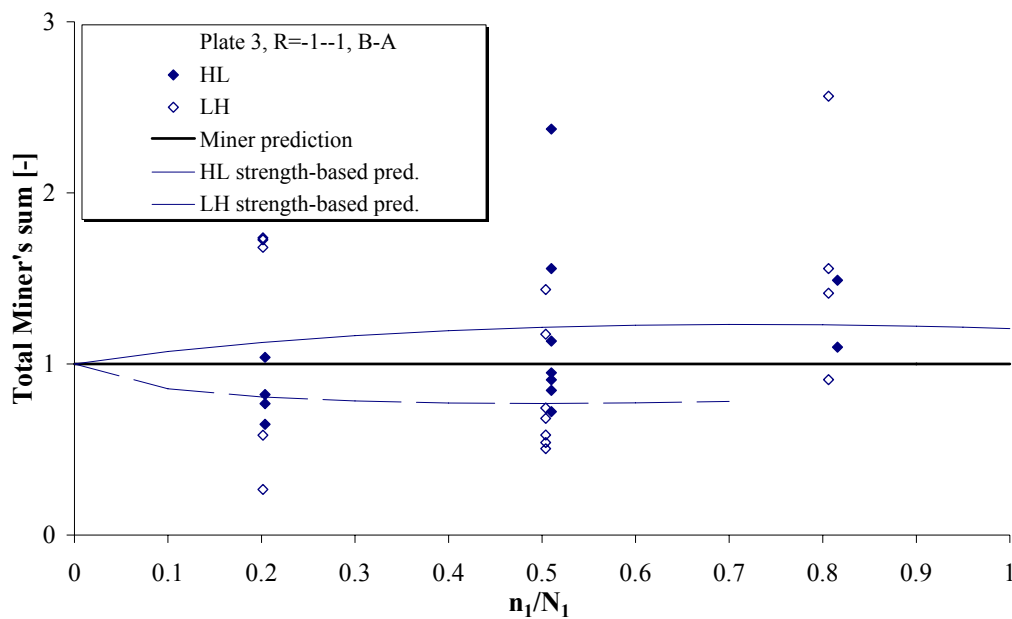
Figure 76: Two-block test results for R=-1

The mixed R-value block tests were typically done on plates for which no residual strength tests were performed. However, it was expected that these experiments allowed for the validation of simple spectra containing two R-values.
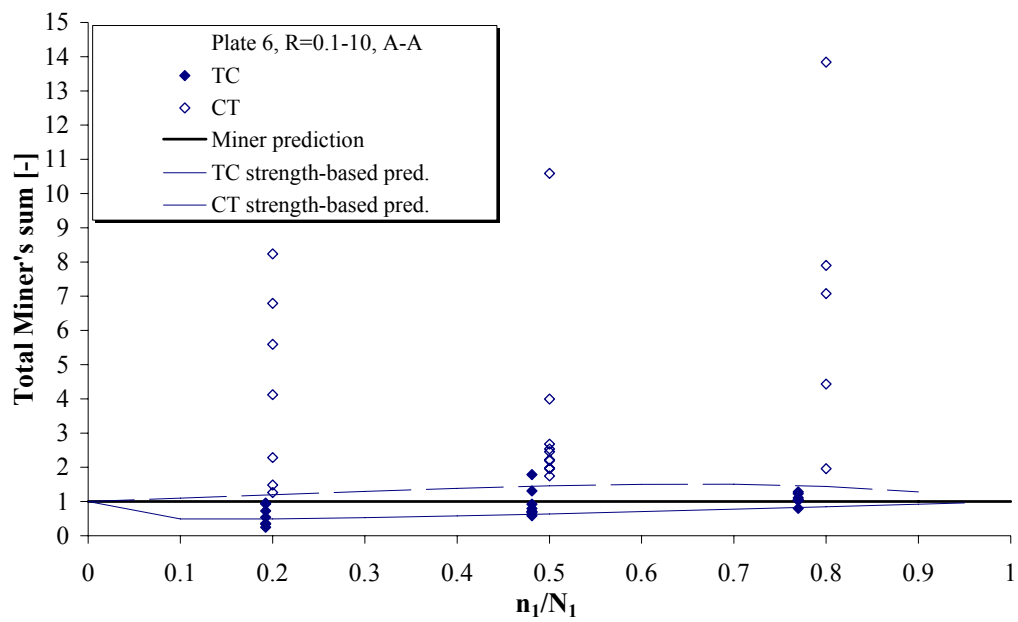
Figure 77: Two block test results for mixed R-value
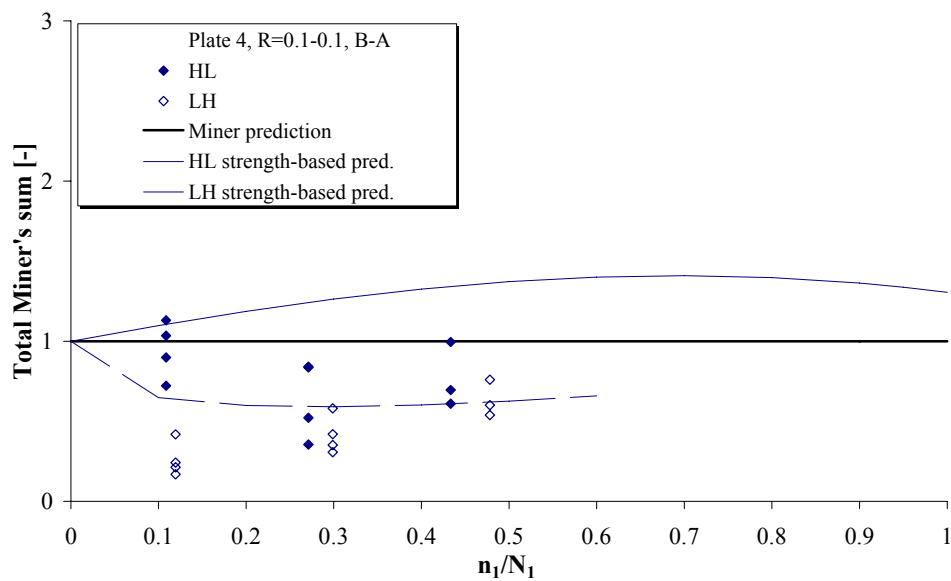
Figure 78: Two-block test results for R=0.1

All two-block tests were done on the Instron 8872. Therefore, the block test results have been normalised using the constant amplitude fatigue lives measured at this frame. An example of the results is shown for the constant R-value block tests in Figure 76, along with the line that represents a Miner's sum of unity. A similar graph is presented for the mixed R-value block tests in Figure 77.

For the R=-1 two-block tests, Miner's sum is around unity for both the LH and HL tests. For higher life fractions in the first block, there is a tendency for the Miner's sum at failure to increase for both HL and LH. This could be partly attributed to the filtering effect caused by not plotting the premature failures. The actual average Miner's sum would be lower if the premature failures were plotted.

For the R=0.1 two-block tests, the constant amplitude tests were done on the 8501 prior to the block test programme. The life fraction in the first block was based on these measurements. The two-block programme, however, was executed on the 8872 test frame, and the life fractions are shown, normalised by the 8872 lives. Since average fatigue life was about 2 times longer than on the 8501, the normalised data do not exceed the 50% life fraction, Figure 78. In both cases, Miner's sum was lower than unity, the HL (High-Low) tests being higher than the LH (Low-High) tests (refer to section 4.1.3 for an explanation of block test abbreviations).

In compression-compression (R=10) two-block tests, High-Low tests were only done for the 20% life fraction. Some data were collected at higher life fractions for the LH tests. The results do not suggest, that Miner's sum at failure is different from unity.

Miner's sum in the High-Low tests is not significantly higher than that in Low-High tests, although a tentative sequence effect can be discerned for most life fractions, notably for R=0.1.

As far as the mixed-R-value block tests are concerned, the results for alternating R=-1 and R=0.1 are close to unity. Some filtering of weak specimens seems to occur for higher block 1 life fractions. An unexpected result is obtained for mixed R-value tests involving R=0.1 and R=10. It seems from the results, that R=0.1 fatigue life is significantly improved when preceded by R=10 fatigue.

Repeated block tests
Repeated block tests were done for R=-1 and R=10 on the same plates as were used for the residual strength and two-block tests (plate 3 and 7). R=0.1 repeated block tests were not done, for lack of specimens from plate 4. Some mixed-R-value repeated block test results are available for plate 6, for which similar two-block tests were performed.

The results of the repeated block tests are shown in Figure 79 and Figure 80. Block length was typically 20% of N_{avg}, but shorter block lengths (2% of N_{avg}) were also programmed. For sufficiently small block lengths, the influence of which block is the starting block is negligible.

Only a limited number of the repeated block test results approach or exceed Miner's sum of unity. For the repeated block tests with smallest block lengths, the contributions to Miner's sum of the respective blocks approach each other.
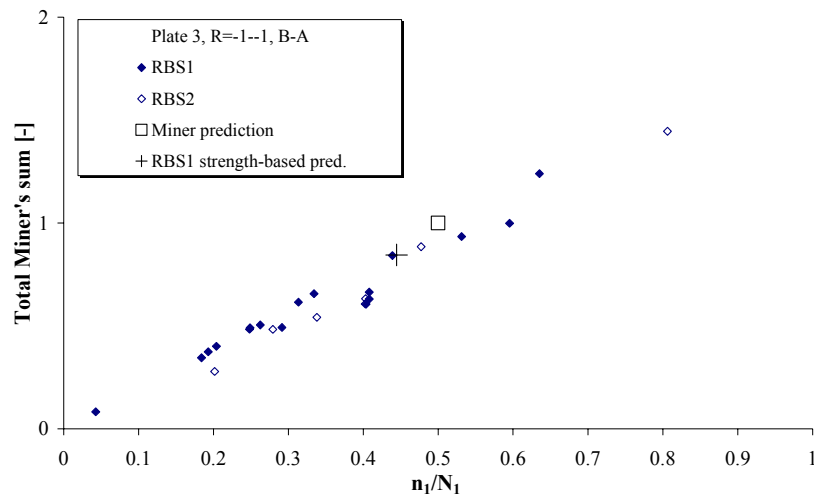
Figure 79: Repeated block test results for R=-1
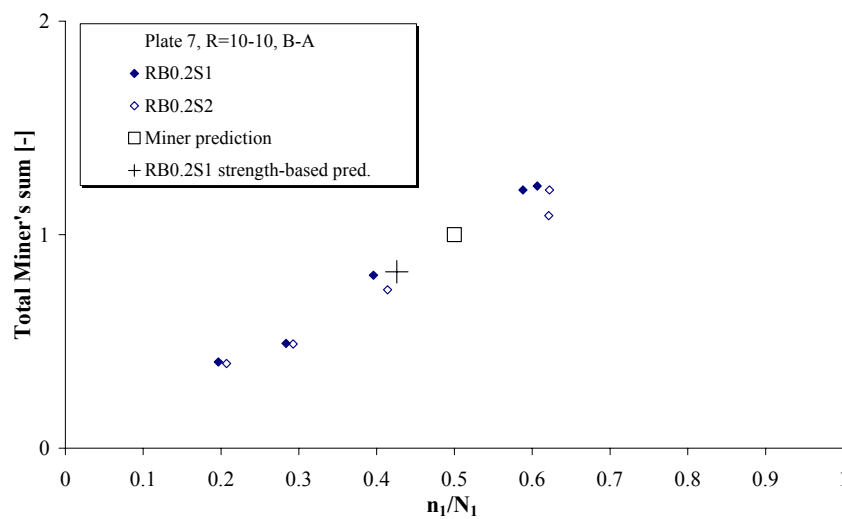
Figure 80: Repeated block test results for R=10

Block test predictions

For the MSU predictions, the parameters from the heuristic model were used for the strength-based predictions. These are given in (Table 15).

In general, the scatter in the data is much larger than the deviation of the strength-based prediction from Miner's prediction. This hampers validation of the strength-based prediction. Nevertheless, the trends in strength-based

prediction follow the data favourably. In the case of R=-1 and R=0.1-10 mixed R-value, the relative location of the average Miner's sum and that of the predicted Miner's sum agree: if Miner's sum was predicted to be larger for *HL* tests than for *LH* tests, the data also show this. For the R=0.1 two-block tests, average Miner's sum for the *HL* tests is predicted to exceed unity, however, the coupons almost all failed at Miner's sum<1. Nevertheless, the *HL* data gave Miner's sums larger than the *LH* data.

A special case is the mixed R-value *TC/CT* tests (with R=0.1 and 10). Although a strength-based prediction agrees favourably with the data trends and even agrees quantitatively with the *TC* block tests, exceptionally high Miner's sums were found in the *CT* tests. These tests seem to indicate, that fatigue life in tension is actually extended when previous R=0.1 fatigue has taken place. The mechanism that could have caused this is not clear.

For the repeated block test predictions, only a single point is plotted, as the predicted Miner's sum at failure is only a function of block characteristics, not of number of blocks. Most of the data trends compare favourably with the predictions, giving lower average Miner's sums than unity. However, the scatter is too large to make a quantitative comparison.

4.3.7 *Microscopic observations after loading*

Selected specimens were subjected to purely tensile R=0.1 and compressive R=10 loading, for life fractions ranging between 1 cycle to 50% of average fatigue life. These specimens were prepared for Scanning Electron Microscopy (SEM) by cutting them approximately along the cross-section of interest, and encasing them in translucent resin. Subsequently, the specimens were polished until the cross-section of interest was visible at the surface.

In the axial cross section of a virgin specimen it is seen, more clearly than was already observed in the optical microscope, the internal structure of the material, which is mainly defined by the interweaved tows.

The SEM images show the stitching material perpendicular to the tows, see e.g. Figure 81. The stitching bundles and the fibre tows have been compressed and rearranged by the pressure applied during the manufacturing process. Their cross-section is roughly elliptic but generally irregular, and the fibre density also varies within the tow.

A close-up of the virgin fibre material shows, that the edges of the fibres have in many cases been damaged by the polishing. This results in a fibre-cross-section that is not circular, but shows irregular edges. The large depth-of-field of the SEM does enable clear identification of the circular fibre cross section deeper into the material. No cracks are visible in the available photographs of the virgin specimen.
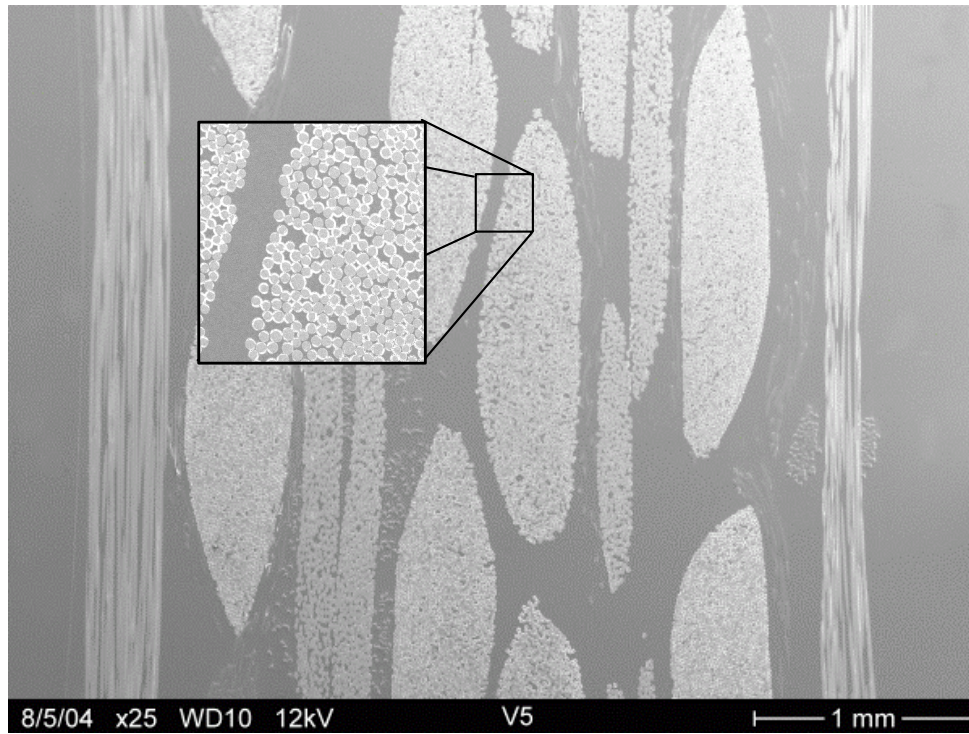
Figure 81: Virgin specimen, cross section seen from top

At higher tensile loads, matrix cracks are seen as soon as after a single cycle, notably in the ±45° degree layers and in the outer 90° layers, Figure 82.
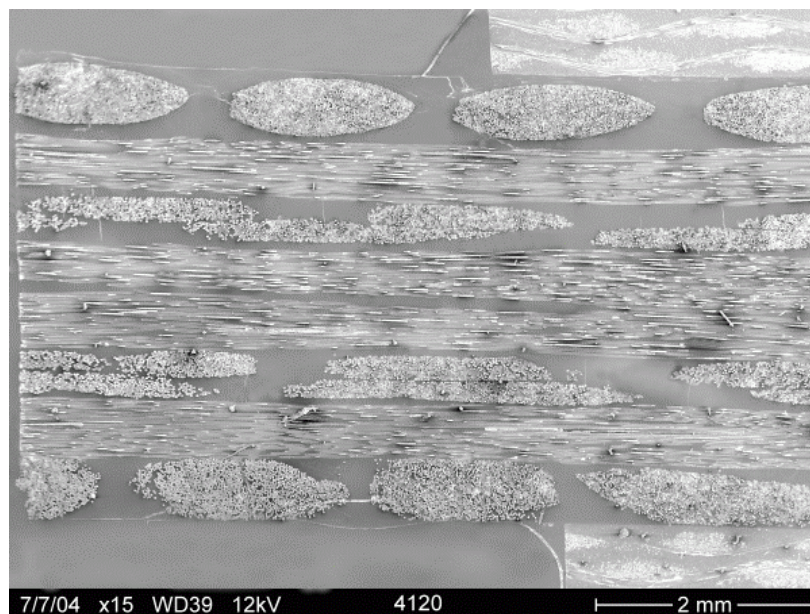
Figure 82: Specimen 4120, 1 cycle at 380 MPa

Also, no damage is found in specimens that have been in the test machine for a single cycle. Refer to Figure 83. The damage in the right figure are fibre pull-outs from polishing.
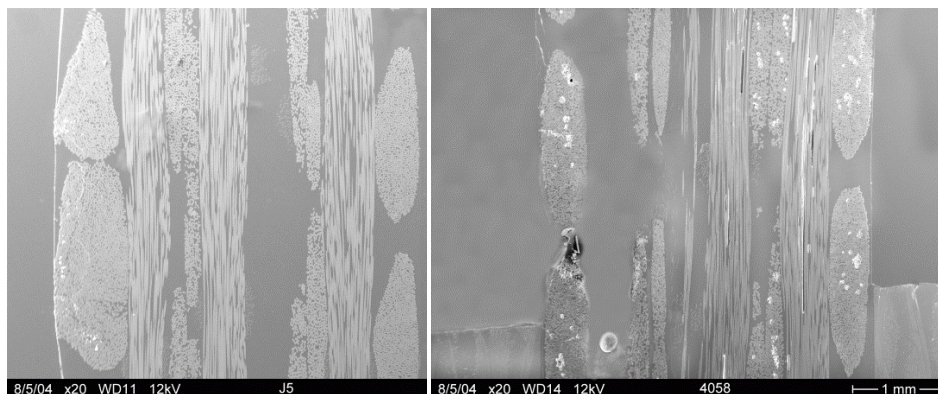
Figure 83: Coupon 7114 (left, single compression cycle level B) and 4058 (right, single tension cycle, level A)

After applying more cycles, some cracks start to enter tows. Especially at stress concentrators such as the near the tabs, at fabric stitches, and around porosity, matrix cracking results in tow splitting, see Figure 84. Comparing the axial cross-section of coupon 4097 and 4013 to the transverse cross-section taken from the same specimens suggests, that the majority of the matrix cracks occur perpendicular to the principal loading direction. Axial cracking is instigated by e.g. stitching material.

Compression fatigue does not seem to cause any transverse matrix cracking, as can be seen from several images that were taken of specimens loaded in R=10 at different stress levels and life fractions. Damage from prolonged compressive cycling is most apparent in the 45° layers, and results in delaminations (Figure 85).

Note, that the cracking patterns in this wind turbine laminate are only remotely reminiscent of the more regular patterns observed by numerous authors (Reifsnider[267] [1983], Gamstedt[96], [1997]) in cross-ply laminates. In the current laminate, with its almost random internal structure, quantification of crack densities or crack distances is likely to prove inaccurate and not quite useful. Samborsky[277] [2002] has reported detailed information on a similar lay-up, including visualisations of matrix and through-tow cracking, albeit taken at static strains rather than after fatigue loading.
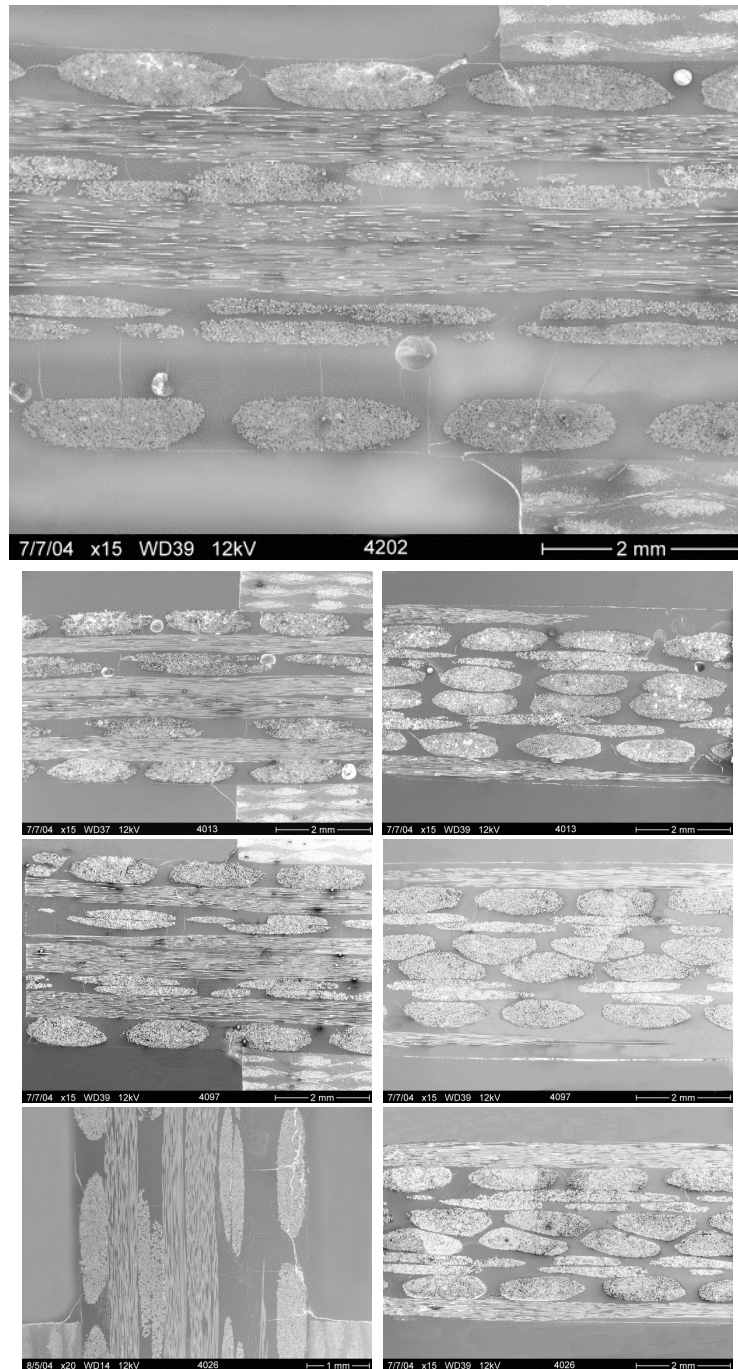
Figure 84: Extensive cracking in ±45° tows for coupon loaded up to 50% of nominal life at level A or B

The observations are summarised in Table 14.
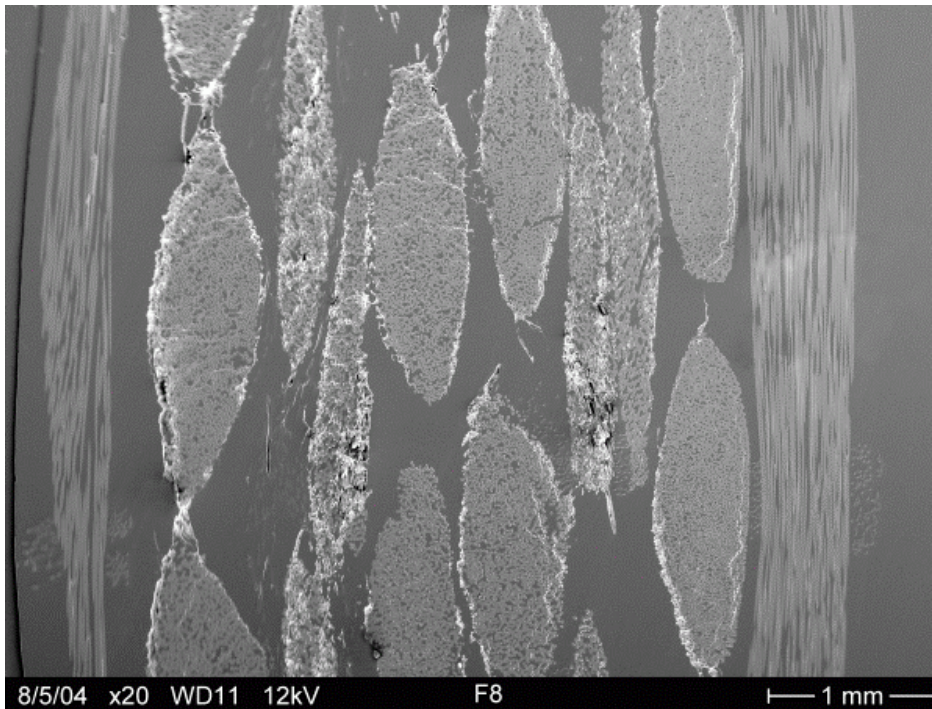
Figure 85: Extensive cracking in ±45° tows for coupon loaded to 50% of nominal life at high stress level, R=10

Table 14: SEM observations on MSU coupons

R-	#	code	level	s_{max}	n	n/N_{avg}	SEM observations
-	7126	V5				-	virgin coupon, no damage
10	7033	G2	A	-240	10906	0.24	lots of damage in ±45°, 90° cracks
	7119	O5	A	-240	19607	0.25	delaminations in ±45°, delam. in 90°
	7038	L2	B	-300	223	0.20	some 90° damage
	7188	F8	B	-300	558	0.49	lots of cracks, delaminations in all plies (mostly ±45°)
	7164	H7	B	-300	1	0	90° damage
	7114	J5	B	-300	1	0	pull-out damage
0.1	4058	AC2	A	240	2	0	no damage
	4076	R3	A	240	10016	0.18	cracks in ±45°, cracks in 90°
	4097	J4	A	240	31502	0.57	cracks in ±45°, cracks in 90°
	4013	M1	B	380	469	0.50	cracks in ±45°
	4120	D5	B	380	1	0.00	cracks in ±45°
	4202	AB7	B	380	188	0.20	cracks in ±45°, cracks in 90°

Summarising, the microscopic observations were useful in characterising the laminate. In addition, the observations showed, that:

- A single load cycle caused cracking parallel to the 45° layers, at level B, R=0.1

- A single load cycle did not cause cracking at level A, R=0.1
- A single load cycle did not cause cracking at level B, R=10
- R=0.1, level A and B fatigue caused cracking in the 45° and 90° layers, up to 50% of nominal life
- R=10, level A and B fatigue did not cause matrix cracking, but delamination damage at both levels, up to 50% of nominal life

From these microscopic observations on the specimens, it seems, that (finite element-) modelling of microscopic damage modes can only have limited success for the typical laminate quality under investigation. Microscopic damage modelling would involve describing tows as straight, cylindrical regular fibre bundles, embedded in undamaged resin. In practice, the tows suffer from macroscopic waviness, as they must follow the contours of neighbouring tows, and as the resin moulding process also introduces some fibre displacement. In addition, intra-tow waviness can be expected, as tows are spread out by the pressure applied by the surrounding material, and this pressure is not equal along the fibre direction. Inside the tows, the distribution of the fibres is not regular.

4.4 Comparison of the results from OPTIMAT and MSU

4.4.1 *Strength degradation parameters from heuristic method*

The heuristic method outlined in section 3.4.4 was used to extract strength degradation parameters from both the MSU and the OPTIMAT datasets.

As was mentioned in that section, several methods can be used to pair ranks of the static and fatigue datasets (match rank, match probabilities from fitted Normal or two-parameter Weibull distributions). Each pairing method corresponds to a different expression for the SLERA, giving a different result for the cost function.

In addition, the experimental and virtual static and fatigue datasets can be expressed in terms of Weibull or Normal distributions. This means, that there are two versions of the cost function. This is excluding other versions of the cost function, which perhaps use only the datasets' shape or scale factors (i.e. setting the weight factors for some parameters to 0). In this case, the analysis was performed with all weight factors set to 1. Note that all contributions to the cost function are normalised by the parameter of the experimental dataset. This means, that a deviation between the experimental and virtual datasets' means is equally important as a deviation in the spread of the two datasets, and that goodness-of-fit of the static datasets is equally important as goodness-of-fit of the fatigue datasets.

Table 15: Strength degradation parameters

	Laminate	R	N_{target}	C	cost	ranking	distribution type	Phil. & Pas.[261]
Tension	MD2	-1	10^6	1.3	0.01	W	W	1.9519
	MD2	0.1	10^6	1.25	0.44	N	N	2.6465
	MD2	-1	10^3	2.5	0.73	N	W	1.9519
	MD2	10	10^6	55.5	0.80	R	W	
	MD2	0.1	10^3	0.85	0.87	N	N	2.6465
	MD2	-1	10^5	7	0.98	W	W	1.9519
	DD16	0.1	10^5	0.9	0.03	W	N	
	DD16	-1	10^5	0.85	0.16	W	N	
	DD16	0.1	10^3	2.2	0.70	W	N	
	DD16	-1	10^3	1.25**	0.81	R	N	
	DD16	10	10^5	4.15	0.76	W	N	
	UD2	-1	10^3	3	0.37	N	W	3.189
	UD2	0.1	10^3	9.9*	0.25	W	W	2.774
	UD2	-1	10^6	1.9	0.74	N	N	3.189
	UD2	0.1	10^6	0.85	0.90	R	N	2.774
Compression	MD2	-1	10^5	133	0.64	N	N	
	MD2	-1	10^6	3.6	0.47	R	N	
	MD2	0.1	10^3	6	0.62	N	W	
	MD2	0.1	10^5	10.2	0.10	N	W	
	MD2	0.1	10^6	2.2	0.08	N	N	
	MD2	10	10^5	400	0.81	W	N	
	MD2	10	10^6	210	0.11	W	W	
	DD16	-1	10^5	3.2	0.23	W	N	
	DD16	-1	10^3	3.5	0.10	N	N	
	DD16	0.1	10^5	7.6	0.50	W	W	
	DD16	0.1	10^3	2.95	0.44	N	N	
	DD16	10	10^5	2.3	0.93	R	N	
	DD16	10	10^3	1.1	0.94	W	N	
	UD2	-1	10^3	120	0.96	W	N	~50
	UD2	0.1	10^5	10	0.95	N	W	~50
	UD2	0.1	10^6	120	0.51	R	W	~50

* censored, left out coupon 428 (CA misaligned)

** Normal result preferred after visual inspection of RSD plot (Figure 86)

Table 15 displays the results from the heuristic method for tensile and compressive residual strength. The table shows both the degradation parameters and the associated value of the cost function. In total, each dataset has a total of 6 values for the C-parameter, and 6 corresponding values of the cost function per material, R-value, and load level (3 ranking methods, 2 distribution types). Of these 6 parameters, only the parameters corresponding to the lowest cost function are tabulated. The ranking method and distribution type relevant to this cost value are also tabulated.
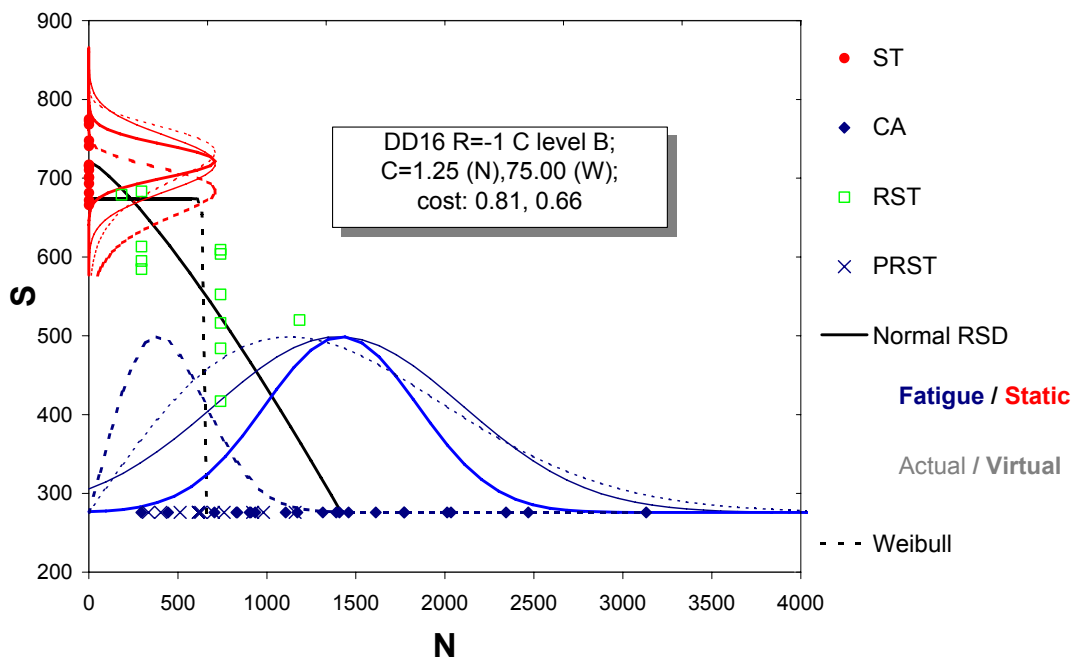
Figure 86: Example RSD plot with derived degradation trends

A further selection was made based on the values of the cost function. This value was limited by an (arbitrary) value of 1. Solutions with higher cost function values were excluded. Thus, the included, 'valid', solutions are characterised by at most an average discrepancy between the experimental and virtual distributions of 25%.

Philippidis and Passipoularidis[261] [2006] have performed similar analysis for different models, describing the strength degradation parameters for the UD2 material. For the single-parameter strength degradation model, they give a single value for the model parameter for all load levels rather than a separate value per load level. The values they found for this model are also shown in the table.

Some issues were encountered during the processing of the results, which can be explained by the nature of the dataset or the formulation of the cost function.

First, the cost function typically is not very sensitive to C-parameter for a large range of *C*-parameters (typically >>1).

Furthermore, it was found that it sometimes has multiple local minima. Typically, a local minimum was found for *C*<10, and another local minimum for *C* >> 10. The cost function was, in that case, smaller in many cases, but as was mentioned, the value of the cost function was hardly sensitive to *C*. This was frequently the case for the Weibull distributions.

Furthermore, it was found, that if some censoring was performed on the data, the *C*-parameter could change significantly compared to the uncensored dataset. An example is tensile residual strength at level 1, R=0.1 for UD2 material. The

original dataset gives a *C* of 46 at a cost parameter of 0.25. After discarding a very low CA result from the data (coupon GEV206_R0300_0428, which was misaligned and had a much shorter fatigue life than the other CA coupons), the parameter went down to 9.9 at the same total cost.

Furthermore, the importance of visually inspecting the plot is illustrated by Figure 86. This shows the *C*-parameter derived by trying to match Normal and Weibull distributions of virtual and experimental datasets. The plot shows static, fatigue, and (prematurely failed) residual strength data. The thick continuous lines represent the Normal distributions of the static and fatigue datasets; the thin lines are the virtual distributions. In this case, the algorithm found a very high *C*-parameter when trying to match the Weibull distributions, whereas visual inspection shows, that the approximately linear trend following from the Normal distribution matching is much more appropriate (this latter value was tabulated in Table 15). Closer inspection of the raw data shows, that, in this case, the influence of the Weibull shape parameters led to an overestimation of *C*.

This practical determination of strength parameters was not further complicated by the theoretically required constraints as discussed in 3.4.4. Thus, in some cases the strength degradation parameters at higher loads are larger than at lower loads.

Tensile strength degradation can be described by low degradation parameters, for R=-1 and R=0.1. Compression strength degradation after R=-1 and 0.1 is characterised by higher values of *C*, as is tensile strength after compression fatigue, and compression strength after tensile fatigue.

The scatter in the data, and the variability in the results from the heuristic method, does not justify determination of the strength degradation parameter with an accuracy exceeding 1 significant digit.

4.4.2 Strength degradation trends

Simplification of numerical trends
In the previous section, the numerical values for the strength degradation trends were calculated from the dataset, with varying results. In the following paragraphs, strength degradation is formulated in terms of general trends, to simplify further analysis.

Figure 87 summarises the strength degradation trends. The figure shows a schematic of the tensile and compressive strength degradation after fatigue. It is a qualitative summary of data from the OPTIMAT MD and UD materials, and the MSU data, for all available R-values. It is based upon a simplification of Table 15:

- Strength degradation trends are independent of load level

- Compressive strength is not significantly affected by fatigue
- Tensile strength is not significantly affected if fatigue is strictly compressive
- Strength degradation is either close to linear, or 'sudden death'. Early failure-type degradation was not observed.

The observation, that strength degradation trends are not dependent on load level is useful, in the sense that it warrants validity of extrapolation to realistically low load levels. In the course of the OPTIMAT project, strength degradation investigations were extended from the initially planned load level 3 to the load level 4, associated with a nominal life of 10^7 cycles. Still, the strength degradation trend was similar to that observed at higher loads.

Compressive strength did not degrade significantly due to purely tensile fatigue at R=0.1, nor was a decrease observed in R=-1 fatigue. For compression-compression fatigue, no decrease in residual strength beyond the scatter boundaries of static strength was observed either. However, in this case, the maximum fatigue load was close to the initial strength, due to the small slope of the S-N curve. Therefore, description of the strength degradation as linear may be justified in these cases, as was indicated by the values for DD16 after R=10 in Table 15. Tensile strength does not degrade, i.e. follows a 'sudden death' trend, if fatigue is governed by compressive loads. These observations could be generalised to the notion, that 'mixed sign residual strength', i.e. tensile strength after strictly compressive fatigue, and vice versa, is not affected by fatigue damage.
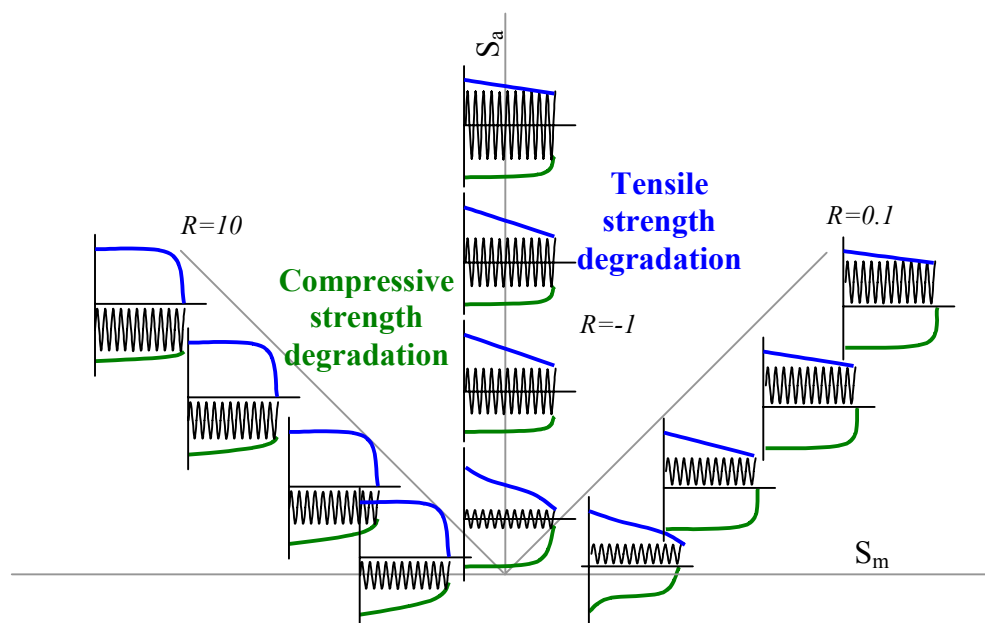
Figure 87: Summary of residual strength trends

The similarity of all residual strength data, allowing for plotting in a single schematic, for different lay-ups, resin systems, and geometries, has wide implications for the general applicability.

Early failure has been successfully used as a parameter for strength degradation behaviour in tensile fatigue. However, from a qualitative analysis of residual strength data, it is seen that this is not an appropriate descriptor of physical material degradation. As will be discussed in section 5.3, this has important consequences for the usefulness of using strength-based life predictions.

4.4.3 Two-block tests

From the OPTIMAT programme, Miner's sums for High-Low sequences were approximately 50% higher than for the corresponding Low-High sequences. In the MSU programme, the sequence effect was smaller. In this programme, load sequence effects were investigated at different life fractions of the first block, but first-block length does not seem to have a systematic effect on fatigue life in the second block.

For mixed R-value block tests, the OPTIMAT results indicate the relative severity of preceding a block with an R=-1 loading block. Also, pure tensile loading blocks seem to adversely influence life in a subsequent pure compressive loading block. From the MSU programme, a similar, though inflated, result was obtained; an R=10 block had a fatigue life that exceeded expectation, when preceded by an R=0.1 block.

From the OPTIMAT programme, where block tests were done at different combinations of load levels, since, per R-value, three load levels were available for block testing, there is no clear correlation of the resulting Miner's sum and the difference between load levels from block to block.

Many of the test parameters in the OPTIMAT and MSU programmes were distinctly different. Although they were based on the same principles of self-consistency, the test matrices were only partly similar. Materials, geometries, and test machines were inherently different. In both cases, statistical basis for a thorough quantification of the Miner's sums at failure is questionable, but in general, two-block test results from the different programmes do not imply severe contradictions. This is encouraging in terms of generality of the results, since the test and coupon conditions were distinctly different.

Summarising, minor sequence effects in terms of life were observed, indicating that High-Low sequences result in Miner's sums exceeding those from Low-High tests. In mixed R-value tests, the presence of an R=-1 block prior to a second block, has detrimental effects on fatigue life of the second block. Repeated sequences of alternating blocks, each block being a fraction of

nominal lifetime, results in reduction of fatigue life compared with both the corresponding two-block tests and a Miner-based prediction.

The material investigated is therefore sensitive to load sequence in terms of life, although the sensitivity is not very pronounced and is of negligible consequence in realistic loading.

Sequence effects in terms of strength were not experimentally validated.

Qualitatively, the experimental results are in accordance with the general trend in strength degradation. It was seen, that for loading types which showed sudden death behaviour in strength degradation, Miner's sums are close to unity. Sudden death behaviour occurs in compressive strength after fatigue. For the two-block results at R=-1, Miner's sums were close to unity, strength degradation showed a sudden death pattern (section 4.3.5), and failure mode in these tests was predominantly compressive. The R=10 two-block tests also suggested unity as resulting Miner's sum. For tensile strength after tensile fatigue (roughly linear strength degradation), the absolute value of Miner's sums was below unity for High-Low and Low-High tests, High-Low tests yielding higher Miner's sums than Low-High tests.

For the mixed-R-value tests, Miner's sum for tests starting with R=10 were a factor of 10 higher than for tests with an R=0.1 first block. This can not be explained by the experimental strength degradation, nor by any theoretical combination of strength degradation parameters in the two blocks. Rather, it seems from these results, that average fatigue life is improved in tensile fatigue, by preceding the tensile block with compressive cycles.

Verification of the residual strength model as a life predictor using spectral loads is hampered by the discrepancy between the possible range of lives estimated using a strength degradation model, and the inherent scatter in coupon experiments. For two-block experiments, the strength degradation-based life estimates in the OPTIMAT project have a maximum range between Miner's sums of 0.5 and 1.5. For the block tests done at MSU, this was 0.2 to 1.8. In practice, constant amplitude fatigue scatter is in the order of a decade. Consequently, a large sample is necessary to favourably compare data to predictions. In most datasets, however, the sample size was insufficient. For two-block simple load spectra, therefore, validity of the strength degradation method could not be proven through comparison of predictions with experimental results, although the general data trends favour the validity of strength-based life predictions. Both in High-Low/Low-High two-block tests, and in repeated block tests, the residual strength model life prediction correlates favourably with the relatively low experimentally determined Miner's sums.

In addition, the sensitivity of the life prediction to the strength degradation parameter is low, especially in the region of $1<C<\infty$. The sensitivity also

depends on the ratio of the maximum peak and the mean peak level; if a single peak stands out relative to the spectrum, the influence of strength degradation parameter is more pronounced than when all peaks in the spectrum are closer to each other.

4.4.4   Repeated block tests

In both programmes, the Miner's sums at failure were below those of the corresponding two-block tests. In most of the cases, Miner's sums were distinctly below unity. Again, despite significant differences in test set-up, test programme design and coupon characteristics, but with comparable self-consistency of the tests, the conclusions from both testing programmes are, that repeated block tests are more damaging than load spectra with longer, non-repeating constant amplitude blocks.

In the OPTIMAT programme, where repeated block tests were done for different combinations of load levels, the Miner's sum in the repeated block tests was lower for larger discrepancy of the loads in the two blocks. Although in the MSU programme for this work, only two levels were available, prohibiting a comparison of block tests at various combinations of load levels, this is in agreement with a similar observation made by Wahl[328] [2001] for repeated block tests on the DD16 material.

Summary of this chapter

This chapter describes the experimental set-up and results. Two similar datasets are available. One was obtained in the framework of the OPTIMAT programme, the other during a research visit at Montana State University (MSU). Both datasets contain:

- *Static tests*
- *Constant amplitude fatigue tests*
- *Residual strength tests*
- *Two-block and two-block repeated simple spectrum tests*

In addition, the OPTIMAT test programme contains tests using WISPER, WISPERX, NEW WISPER, and Reversed WISPERX.

The experiments were designed to have a high level of inter-consistency. This means, that the load levels and rates at which static and fatigue data were obtained correspond to the load levels and rates of the simple spectrum tests and the residual strength tests. This is to minimise the need for interpolation in the predictions.

The residual strength datasets described here are probably among the most extensive strength degradation datasets available, describing both tensile and compressive residual strength for a wide range of life fractions, various R-values, and lay-ups.

The test preparations, set-up, procedures, and (pre-and post testing) material characterisation also cover detailed issues such as e.g. coupon misalignment, and microscopic observations on virgin and failed coupons. Especially the OPTIMAT programme was subject to some variability issues.

The similar datasets from both programmes call for a comparison of OPTIMAT to MSU data. Residual strength degradation parameters, calculated using the methods described in Chapter 3; suggest that strength degradation trends could be generalised using the results from both testing programmes.

Chapter 5

Analysis

This chapter compares the life and strength predictions using the experimentally determined model parameters with the experimental load spectrum lives and strengths. Various life prediction models are used and compared. In addition, a sensitivity analysis is carried out for the complex spectrum predictions. This analysis demonstrates how and why variations in counting method, S-N curve parameters, CLD interpolation, and damage rule, affect the life predictions for different representative load spectra.

5.1 Comparison of prediction methods for complex spectra

In the previous chapters, the use of Miner based, and strength-based life estimation methods was discussed. In the following paragraphs, life prediction methods are compared to the experimental data for the WISPER, WISPERX, and NEW WISPER spectra. In addition, the influence of variations in the prediction method is quantified.

Various prediction methods are compared. These are:

- Linear Goodman + Miner
- Shifted Goodman + Miner
- CLD with 3 'basic' R-values R=0.1,-1, 10 + Miner
- CLD with 6 R-values (full CLD) + Miner
- Single R-value CLD (R=0.1) + Miner
- Equivalent stress level method
- Full CLD + non-linear strength degradation model

The elements of the prediction methods have been explained in Chapter 2 and Chapter 3. Essentially, two major variations are introduced: variation in the definition of constant life diagram, and variation in the damage accumulation rule. In all cases, the power law formulation was used to describe one or more S-N curves.

All methods except the strength degradation model use Miner's linear damage accumulation rule to estimate fatigue life (no additional factors as discussed in section 3.3), each time using different forms of the constant life diagram.

Goodman diagrams
The linear and shifted Goodman Diagrams are the simplest forms of CLDs, from which the expected life for each cycle type can be obtained analytically.
In the case of the 3 R-value and multiple R-value CLD, the interpolation method by Philippidis and Vassilopoulos was used, see 2.2.3.
The single-R-value CLD is a derivative of the multiple R-value CLD, where, of all available R-values, a single one is chosen to construct a CLD with. By choice of the R-value in the region where the spectrum's dominant fatigue cycle types are, an accurate prediction may arise with a minimum of constant amplitude fatigue tests required. Choosing R=-1 for the construction of this CLD would result in the Linear Goodman Diagram, although differences may occur, see 2.3.8.

Equivalent stress method
The equivalent stress method amounts to doing a Miner-type analysis with a CLD constructed from parallel lines, see section 2.2.4. A reference R-value is needed as a basis for the CLD. Given the predominantly tensile nature of the (NEW) WISPER(X) spectra, and the availability of data at R=0.1 and R=0.5, these R-values were used as reference R-values.

Strength degradation model
The strength degradation model was implemented in a computer programme, which evaluates the strength loss due to each subsequent segment in the loading sequence. The lay-out of the algorithm was illustrated schematically in Figure 35, and explained in 3.4.3.

The strength degradation parameters were based on the qualitative notion, that mixed sign strength degradation is negligible, and that tensile strength degradation is close to linear for fatigue loads containing a tensile component. This is a simplification compared to the master-diagram approach (cf. Schaff and Davidson[278, 279], 1997). A value of 10 is used for the strength degradation parameter if negligible strength degradation is seen, a value of 1 is used for linear degradation (see equation 38).
The full CLD was used for the strength degradation predictions, which is the Multiple R-value CLD with 6 R-values used for MD2 material.

The various prediction results are compared to the WISPER, WISPERX, and NEW WISPER experimental data in Figure 88.

In these figures, in all cases the same S-N parameters were used for S-N curves at the same R-values. Different CLD formulations were used.

In terms of counting method, Rainflow-equivalent range-mean counting results were used. This was done to warrant a straightforward comparison between Miner's approach and the strength degradation method. However, range-mean counting leads to less conservative fatigue lives than Rainflow counting, as is discussed in section 5.2.

A few main observations arise from the figures:

- First, the linear and shifted linear Goodman diagrams yield highly non-conservative fatigue life predictions. The predictions are in the order of 1 to 2 decades longer than the experimental data
- The 3 R-value CLD gives non-conservative predictions (but more conservative than the Linear Goodman Diagrams)
- The multiple-R-value CLD gives reasonable predictions in all cases, albeit slightly non-conservative, especially in the case of WISPERX and NEW WISPER
- The single-R-value prediction using a tensile R-value (R=0.1), gives highly conservative predictions
- The equivalent load method, with reference R-values R=0.1 or R=0.5 yields predictions, which are in the vicinity of the multiple R-value prediction
- The residual strength-based predictions are close to the multiple-R-value predictions, on the conservative side.

The strength-based life predictions are made here for the full CLD only. Basically, if another CLD was chosen as a basis for the strength-based method, the prediction would be close to the Miner-based prediction for that CLD.

Furthermore, the Linear Goodman Diagram predictions yield slightly non-linear prediction curves (in a log-log plot); which can be explained through the anomaly in section 2.3.8. The strength degradation curves are fairly linear, although in the first few sequences the failure peak shifts, resulting in non-linear behaviour in that region.

A grey, dashed line is shown indicating the arbitrary stress level of 213 MPa. This line will be referred to in section 5.2.
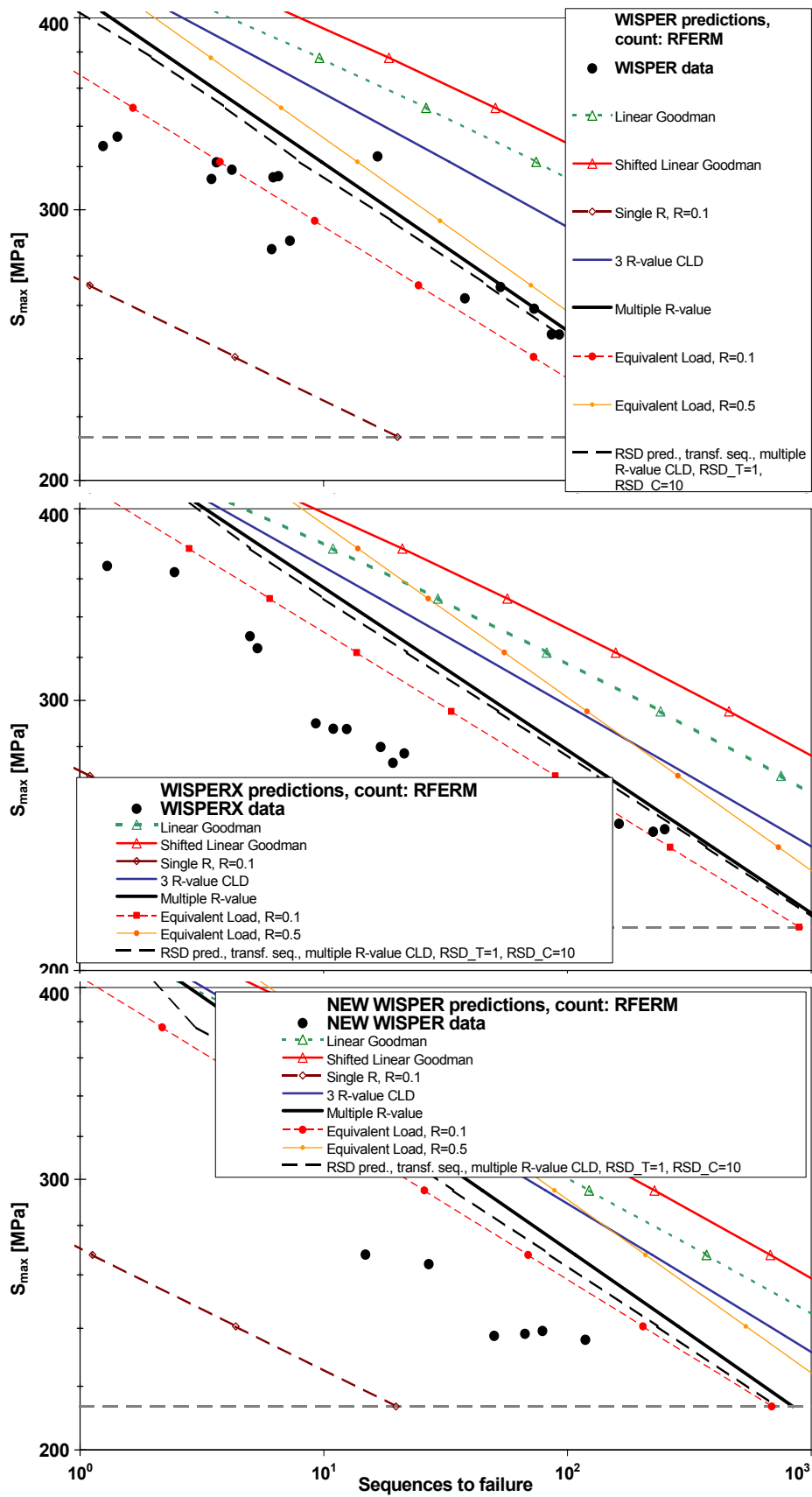
Figure 88: Life predictions using Rainflow-equivalent Range-mean counted spectra and various CLDs

From the first four observations, it can be concluded, that either a multiple R-value CLD should be used, preferably the full CLD, or an R-value, which is representative for the spectrum under investigation.
The general trends in prediction versus data are very similar for all load spectra.

Building on the qualitative analysis above, a quantitative analysis is made next of the influence on predictions of changes in the counting method, S-N model parameters, CLD-formulation and strength degradation parameters.

5.2 Sensitivity analysis

From the above plots, the sensitivity of the predictions to the choice of CLD formulation can be derived. How does this compare to the influence of other parameters of the prediction? To answer this question, predictions are compared quantitatively.
The predictions are tabulated for a selection of the models in Table 17. They are shown for a single maximum stress of ca. 0.4 of UTS (~213 MPa, dotted grey line in the figures). This value was chosen arbitrarily to represent long-term fatigue. As the prediction lines are not necessarily parallel, the values in the table will change for other load levels. However, in combination with the figures, they should give a good indication of the models' sensitivity to choice of constituent formulations.

In each row, predictions at 0.4 UTS are shown for different CLDs. Each column represents a combination of counting method and damage rule. The table is duplicated with a normalised table, Table 18. As a basis for the normalisation, Rainflow counted Miner prediction using a Linear Goodman Diagram is used (grey cell). Thus, the table allows for a quantification of the influence of changing the counting methods, the constant life formulation, and damage rule. These influences and their interrelations are discussed separately below. In section 5.2.2, a similar discussion on sensitivity of prediction methods to variations in S-N curve parameters is given.

5.2.1 *Influence of counting method*

As was discussed in 3.2.4, Rainflow counting can be performed in a cyclic and in a non-cyclic manner. In addition, range-mean counting is appropriate for strength-based predictions and can also be used in Miner predictions. For a better comparison between Miner's sum predictions and strength predictions, either a range-mean counted spectrum or a Rainflow-equivalent range-mean counted spectrum should be used. The consequences for the prediction are shown for three different prediction methods in Table 17.
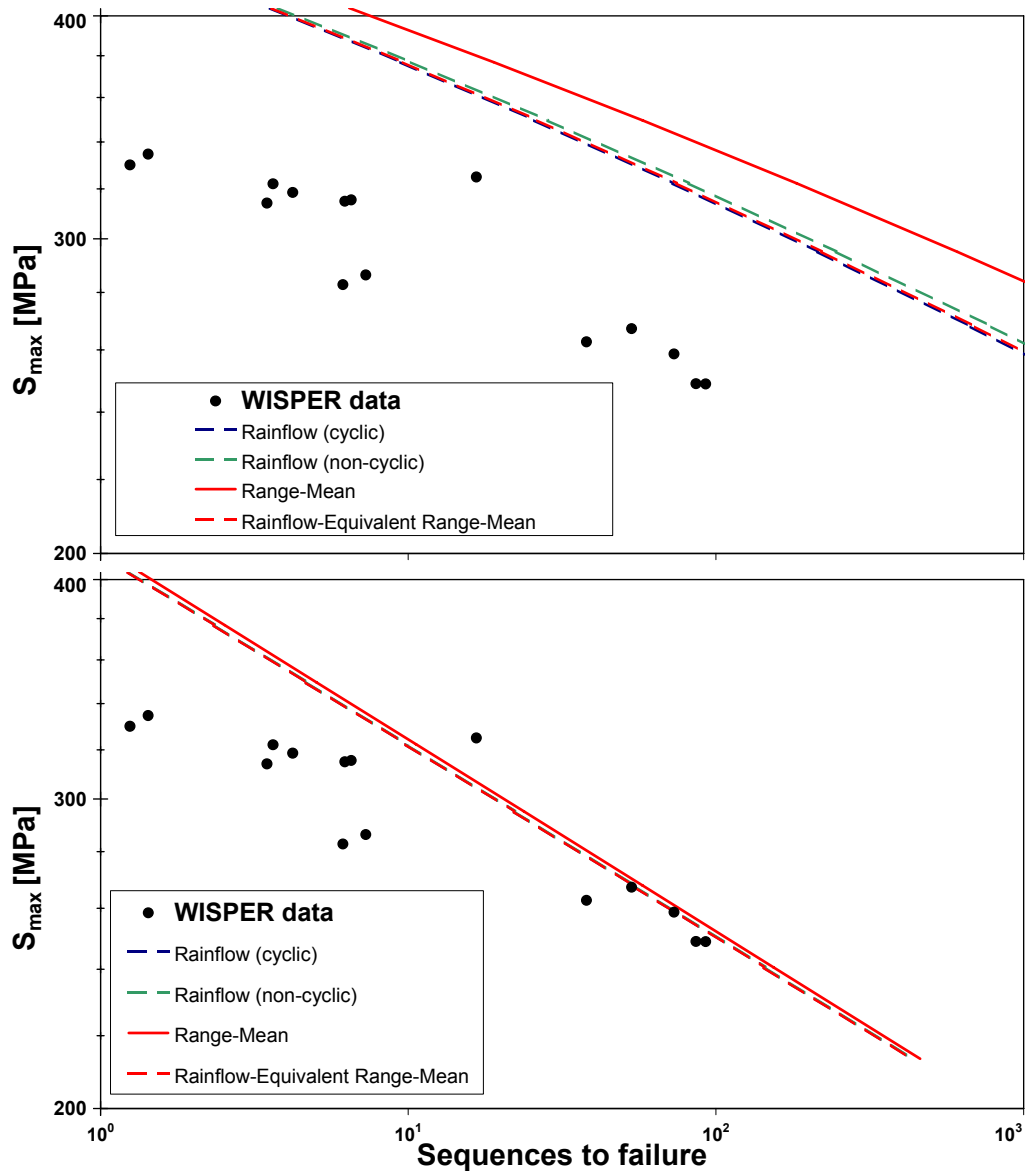
Figure 89: Influence of counting method on life prediction for WISPER data on MD2 R0400 coupons, using a LGD (top) and 6 R-value CLD

The results show, that predictions using a Linear or Shifted Goodman diagram show different sensitivity to the counting method than the full CLD. For predictions using the full CLD, changing the counting method from cyclic to non-cyclic Rainflow or to range-mean, affects the predictions less significantly than when linear Goodman diagrams are used. In the case of the linear Goodman diagrams, the life prediction can be a factor of 3~4 different for this load level, for the WISPER(X) spectra. In the case of the NEW WISPER

spectrum, the shift in counting method results in a more limited shift in life prediction. Thus, not taking into account the predictions for the single R-value (R=0.1), the fatigue life can differ a factor of 12, 5, or 1 for WISPER, WISPERX, and NEW WISPER, respectively. Note also, that the difference in prediction between Rainflow and Rainflow equivalent range-mean counted spectra is very limited.

The different results are a consequence of the manner in which damage is allocated to the various cycle types. In Figure 90, a plot is shown where the centre of each bubble represents mean and amplitude of a cycle type, and the size of the bubble represents the damage fraction that the cycle incurs in the spectrum. The plot basically has the lay-out of a CLD, but with the actual inflicted damage in it. This is shown both for the Linear Goodman Diagram and for the full CLD.
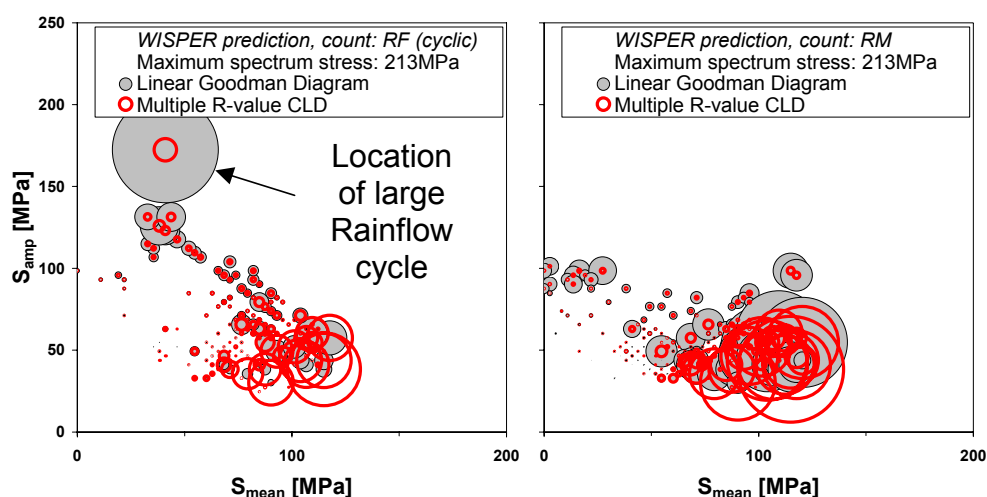
Figure 90: WISPER damage plots using different counting methods

Bubble size is proportional to relative damage

The single large amplitude Rainflow cycle from the WISPER spectrum, which arises from connecting the maximum peak to the minimum valley, is shown. The relative damage that follows from a Linear Goodman diagram clearly is smaller than that from the full CLD. This large Rainflow cycle is not counted in a range-mean count, as is evident from a similar 'damage plot' from a range-mean count. As the contribution to damage of the single large cycle was less significant for the full CLD, it can be expected, that the predictions from a full CLD are less sensitive to counting method than those from the Goodman diagram. Similar reasoning explains the insensitivity of the equivalent loading method to cycle counting method; the parallel-line CLD of the equivalent

loading method results in very limited relative contribution of the large loading cycle to the Miner damage.

From this example, it can be concluded, that the sensitivity to counting method depends on the formulation of the CLD, as well as on the spectrum. If the single large cycle would have been absent, or if it would have been counted in the same manner by both counting methods, the influence of counting method could be smaller. In the NEW WISPER spectrum, the maximum peak and minimum valley are at the end and the beginning, respectively, of the load sequence. This means, that they are counted in a similar manner by both the Rainflow algorithm and range-mean counting. Thus, for this spectrum, the influence of counting method can be expected to be smaller than for the WISPER spectrum, which is confirmed by the values in Table 17 and Table 18.

This seems a fortunate characteristic of the NEW WISPER spectrum but it is due to the fact that the final 'randomisation' step was not taken in the construction of this spectrum (cf. section 3.1).

The actual relative influence of the various loading cycles does not facilitate easy assessment of the influence of counting method. The counting results between cyclic and non-cyclic counting generally only differ in terms of a small number of cycle types (see Krause et al.[164] [2003]), so there the influence of counting method may be qualitatively assessed in a manner similar to the above. The fact, that the WISPER(X) spectra consist mainly of constant amplitude blocks, also implies, that the counting results will be similar and only differ for a few cycle types. This justifies observations as made above.

For more irregular spectra, the counting results may be binned in an altogether different manner, hampering analysis.

5.2.2   *Influence of S-N curve parameters*

The influence of the S-N formulation is demonstrated by varying the parameters of the S-N curve. A 1% variation gives fatigue lives, which are typically 10-20% different from the baseline predictions. A 5% change in the *a* and *b* parameters of equation 3 results in a discrepancy with the baseline results of roughly a factor of 2. For illustration purposes, the CLD associated with 5% inflated *a* and *b* parameters is compared to the original CLD in Figure 91, Table 16.

Table 16: Influence of S-N curve parameter variations

S-N curve parameter deviations	CLD	Miner			
		predictions		normalised w.r.t. original S-N curves	
		RF (cyclic)	RM	RF (cyclic)	RM
+5%	Linear Goodman	17455	98029	1.97	2.72
	Shifted Goodman	34501	174907	2.04	2.74
	Multiple R	1001	1086	2.32	2.36
	Equivalent load, R=0.1	557	557	2.27	2.27
-5%	Linear Goodman	4288	13062	0.48	0.36
	Shifted Goodman	7937	22851	0.47	0.36
	Multiple R	185	195	0.43	0.42
	Equivalent load, R=0.1	108	108	0.44	0.44
+1%	Linear Goodman	10188	44062	1.15	1.22
	Shifted Goodman	19611	78176	1.16	1.23
	Multiple R	511	547	1.18	1.19
	Equivalent load, R=0.1	289	289	1.18	1.18
-1%	Linear Goodman	7697	29443	0.87	0.82
	Shifted Goodman	14624	52031	0.86	0.82
	Multiple R	365	388	0.84	0.84
	Equivalent load, R=0.1	208	208	0.85	0.85
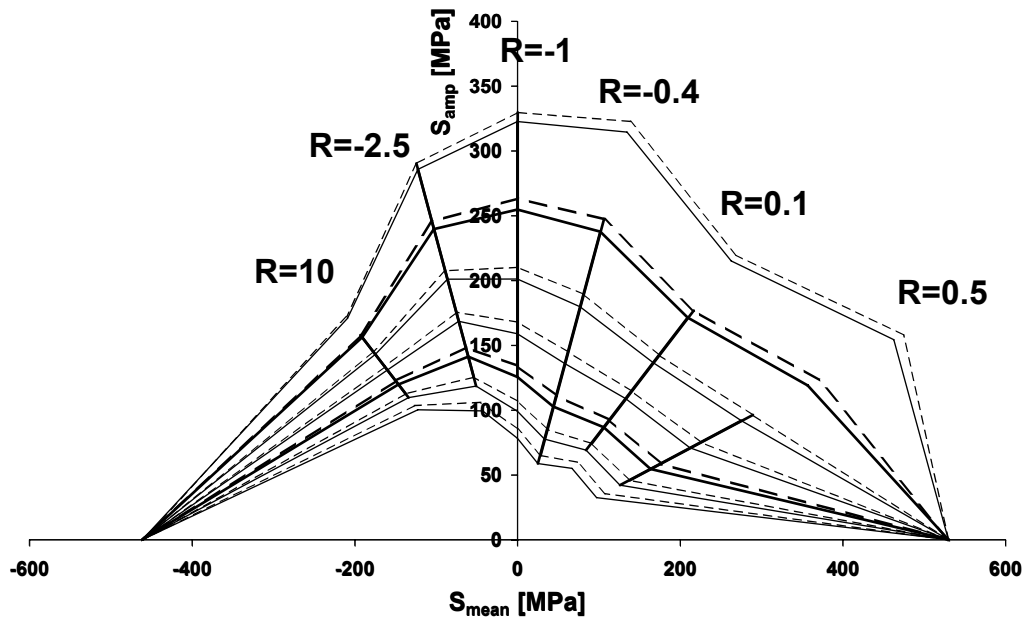
Figure 91: Effect of 5% upward variation in S-N curve parameters on 6-R-value CLD

(continuous=original, dotted=+5%)

5.2.3 Influence of constant life diagram

Table 17 shows, that the influence of the formulation of the CLD is by far the most significant. Also, its influence works in two ways.

First, changing from e.g. a multiple R-value CLD to an LGD, changes the prediction by a factor of ca. 50. Even larger differences can be achieved when using the Single R-value, R=0.1 CLD. Thus, the influence of CLD can be an order of magnitude larger than influence of counting method.

Second, the CLD influence is related to the influence of counting method and spectrum, as was demonstrated in the section on influence of counting method (5.2.1).

Implicit in the CLD is also the influence of the S-N formulation. Notably the extrapolation of fatigue life to longer lives is significant for the predictions, since many of the load cycle types that occur in the WISPER sequences have constant amplitude lifetimes that are far beyond the region where experimental constant amplitude data are available. This is illustrated by a comparison between the 3 R-value CLD and the 6 R-value CLD. The fatigue life predictions for the 6 R-value CLD are much more conservative than for the 3 R-value CLD. Since the load spectra are predominantly tensile, this can be largely attributed to the R-values –0.4 and 0.5. From a comparison of the CLDs (Figure 92), these R-values make the CLD more conservative in the long-life range. This part of

the CLD is based on extrapolation of the data beyond the range where testing was practically possible.
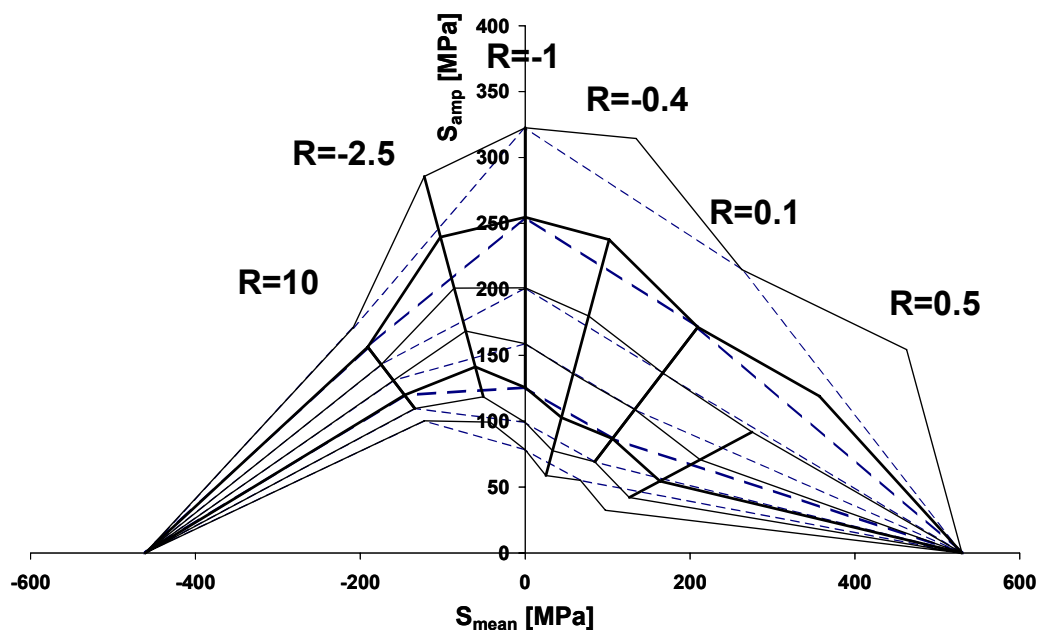
Figure 92: Comparison of 3 R-value (dotted) and 6 R-value CLDs

When compared to the data, the Multiple R-value CLD seems to give acceptable results, and in addition it is one of the CLDs which are least sensitive to differences in counting method.

5.2.4 *Influence of damage accumulation rule*

In terms of computational effort, the strength degradation model is most computationally intensive, since it is a cycle-by-cycle analysis. All Miner-based methods are computationally least intensive, since repetitive sequences like the (NEW) WISPER(X) spectra only need to be subjected to a damage quantification once, and then the contribution of each cycle type can be added.
In terms of experimental effort, Miner or strength-based methods are equal as far as determining S-N curve behaviour is concerned. Strength-based life estimates can be based on the same information as Miner-based life estimates. However, additional determination of the strength degradation behaviour of a material can be extremely resource-consuming.

The main conclusion from the residual strength degradation experiments, modeling, and predictions is, that the strength degradation model, given the experimentally determined range of strength degradation parameters, is not capable of significantly improving life prediction for spectrum loading relative

to a Miner's approach. A change in the choice of CLD, or a variation in the S-N parameters is equally or more influential on the life prediction.

Only for very small strength degradation parameters, the strength degradation model can predict failure significantly more conservatively than Miner's sum. These small values of the degradation parameter do not congrue with experiments.
The addition of a second modelling parameter, allowing for an S-shaped strength degradation curve, is not likely to have a large influence on the life prediction. For the prediction of (the statistical distribution of) residual strength after fatigue, a more accurate description of strength degradation seems justified in some cases.

In the previous chapter, it was pointed out, that the data scatter does not justify determination of the strength degradation parameter within narrow ranges. Also from the point of view of life prediction using the residual strength degradation model, the definition of the strength degradation parameter does not require a high accuracy. In the range of observed strength degradation parameters, i.e. between linear and sudden death, the life estimate using the strength degradation model varies by approximately 25%. Considering that this is within the scatter of the actual spectrum load predictions, determining the strength degradation factor with a high accuracy is not necessary.

The general conception is, that Miner's sum, being a linear damage accumulation model, must congrue with linear strength degradation. This is not correct. An important observation, that has been demonstrated both analytically and through implementation of the residual strength model, is, that *sudden death* strength degradation behaviour implies, that the life estimates approach those made with Miner's sum. Qualitatively, strength is not affected by fatigue, and mean fatigue life remains the same for each cycle type, thus, the order of load cycles is of no effect in the strength degradation life prediction. This renders the life estimate equal to that of Miner's sum. Linear strength degradation will give a more conservative life estimate than sudden death.

Table 17: Life prediction comparison

for 0.4 UTS, MD2 R0400 coupons

spectrum	damage rule / counting method	Miner					RSD					
		RF (cyclic)	RM	RF (non-cyclic)	RFERM		RM	RM	RM	RFERM	RFERM	RFERM
	CLD					T, C	10,10	1,10	1,1	10,10	1,10	1,1
WISPER	Linear Goodman	8864	36028	10692	9191							
	Shifted Goodman	16951	63801	19686	16993							
	R=0.1, 10, -1	3349	7180	3578	3333							
	Multiple R	432	461	435	430		446	383	330	418	390	291
	Equivalent load, R=0.1	246	246	246	246							
	Equivalent load, R=0.5	531	531	531								
	Single R, R=-1	11500	136595	14896	12152							
	Single R, R=0.1	16	1005	24	20							
WISPERX	Linear Goodman	9465	26940	11578	9757							
	Shifted Goodman	18090	45079	21239	17993							
	R=0.1, 10, -1	3735	5653	4022	3694							
	Multiple R	1238	1386	1262	1222		1341	1184	995	1214	1172	855
	Equivalent load, R=0.1	892	892	892	892							
	Equivalent load, R=0.5	2129	2129	2129								
	Single R, R=-1	11549	55470	14979	12073							
	Single R, R=0.1	16	148	24	20							
NEW WISPER	Linear Goodman	5463	6460	5186	4613							
	Shifted Goodman	9326	10825	8906	7977							
	R=0.1, 10, -1	2645	2890		2308							
	Multiple R	887	908	881	841		902	766	752	840	719	706
	Equivalent load, R=0.1	690	690	690	690							
	Equivalent load, R=0.5	1564	1564	1564								
	Single R, R=-1	6230	7631	5868	5139							
	Single R, R=0.1	21	26	15	20							

RM=Range-Mean; RF=Rainflow; RFERM; Rainflow Equivalent Range Mean; RSD=Residual Strength Degradation

Table 18: Normalised Life prediction comparison

for 0.4 UTS, MD2 R0400 coupons
(normalised per spectrum with values in grey cells)

spectrum	damage rule	Miner					RSD					
	counting method	RF (cyclic)	RM	RF (non-cyclic)	RFERM		RM	RM	RM	RFERM	RFERM	RFERM
	CLD					T, C	10,10	1,10	1,1	10,10	1,10	1,1
WISPER	Linear Goodman	1.000	4.064	1.206	1.037							
	Shifted Goodman	1.912	7.197	2.221	1.917							
	R=0.1, 10, -1	0.38	0.81	0.40	0.38							
	Multiple R	0.049	0.052	0.049	0.049		0.050	0.043	0.037	0.047	0.044	0.033
	Equivalent load, R=0.1	0.028	0.028	0.028	0.028							
	Equivalent load, R=0.5	0.060	0.060	0.060								
	Single R, R=-1	1.297	15.410	1.680	1.371							
	Single R, R=0.1	0.002	0.113	0.003	0.002							
WISPERX	Linear Goodman	1.000	2.846	1.223	1.031							
	Shifted Goodman	1.911	4.763	2.244	1.901							
	R=0.1, 10, -1	0.39	0.60	0.42	0.39							
	Multiple R	0.131	0.146	0.133	0.129		0.142	0.125	0.105	0.128	0.124	0.090
	Equivalent load, R=0.1	0.094	0.094	0.094	0.094							
	Equivalent load, R=0.5	0.225	0.225	0.225								
	Single R, R=-1	1.220	5.861	1.583	1.276							
	Single R, R=0.1	0.002	0.016	0.003	0.002							
NEW WISPER	Linear Goodman	1.000	1.183	0.949	0.844							
	Shifted Goodman	1.707	1.981	1.630	1.460							
	R=0.1, 10, -1	0.48	0.53	0.00	0.42							
	Multiple R	0.162	0.166	0.161	0.154		0.165	0.140	0.138	0.154	0.132	0.129
	Equivalent load, R=0.1	0.126	0.126	0.126	0.126							
	Equivalent load, R=0.5	0.286	0.286	0.286								
	Single R, R=-1	1.140	1.397	1.074	0.941							
	Single R, R=0.1	0.004	0.005	0.003	0.004							

RM=Range-Mean; RF=Rainflow; RFERM; Rainflow Equivalent Range Mean; RSD=Residual Strength Degradation

5.3 Strength prediction in spectrum loading

In Figure 93, the strength degradation is shown, as calculated using the strength degradation method. The plots are made for a single stress level, for WISPERX on MD2 R0400 material. The plots show the theoretical strength degradation using the same strength degradation parameter sets as used in the predictions, i.e.:

- Linear tensile strength degradation and sudden death compressive strength degradation (T=1, C=10)
- Sudden death degradation for tensile and compressive strength (T, C=10)
- Linear degradation for both tensile and compressive strength (T, C=1)

Failure was predicted at segments 5298 (tensile failure), and 13482 (compressive failure), respectively. These segments are either the maximum peak and minimum valleys, depending on whether failure was tensile or compressive, recall Table 2.

The main observation with regard to these plots is, that the macroscopic variable amplitude strength degradation pattern follows the constant amplitude input strength degradation pattern. With the exception of minor changes in slope of the strength degradation lines (e.g. due to slightly more rapid degradation at the occurrence of a relatively high load segment), variable amplitude strength degradation is linear if the CA strength degradation parameter is linear; it is sudden-death if the CA strength degradation parameter is sudden death. In fact, a curve fit of the strength degradation plots of Figure 93 yields degradation parameters which are very close to the input CA strength degradation parameters.

It should be pointed out, that for the much less random NEW WISPER spectrum, this behaviour of the prediction is less explicit (see Figure 20).

Also, residual strength tests after variable amplitude fatigue should be carried out in order to back-up these assertions experimentally.

In the OPTIMAT programme, a limited number of residual strength tests after modified NEW WISPER were carried out at UP, see Philippidis et al.[262] [2006], for the MD3 ±45° material. For this material, only R=0.1 CLD data are available, so the NEW WISPER spectrum was modified to pure R=0 cycles by discarding all valleys. Nevertheless, the data presented in Figure 94 indicate, that linear strength degradation in VA seems realistic. This would also be

suggested by the constant amplitude fatigue data and strength degradation, which is also linear.
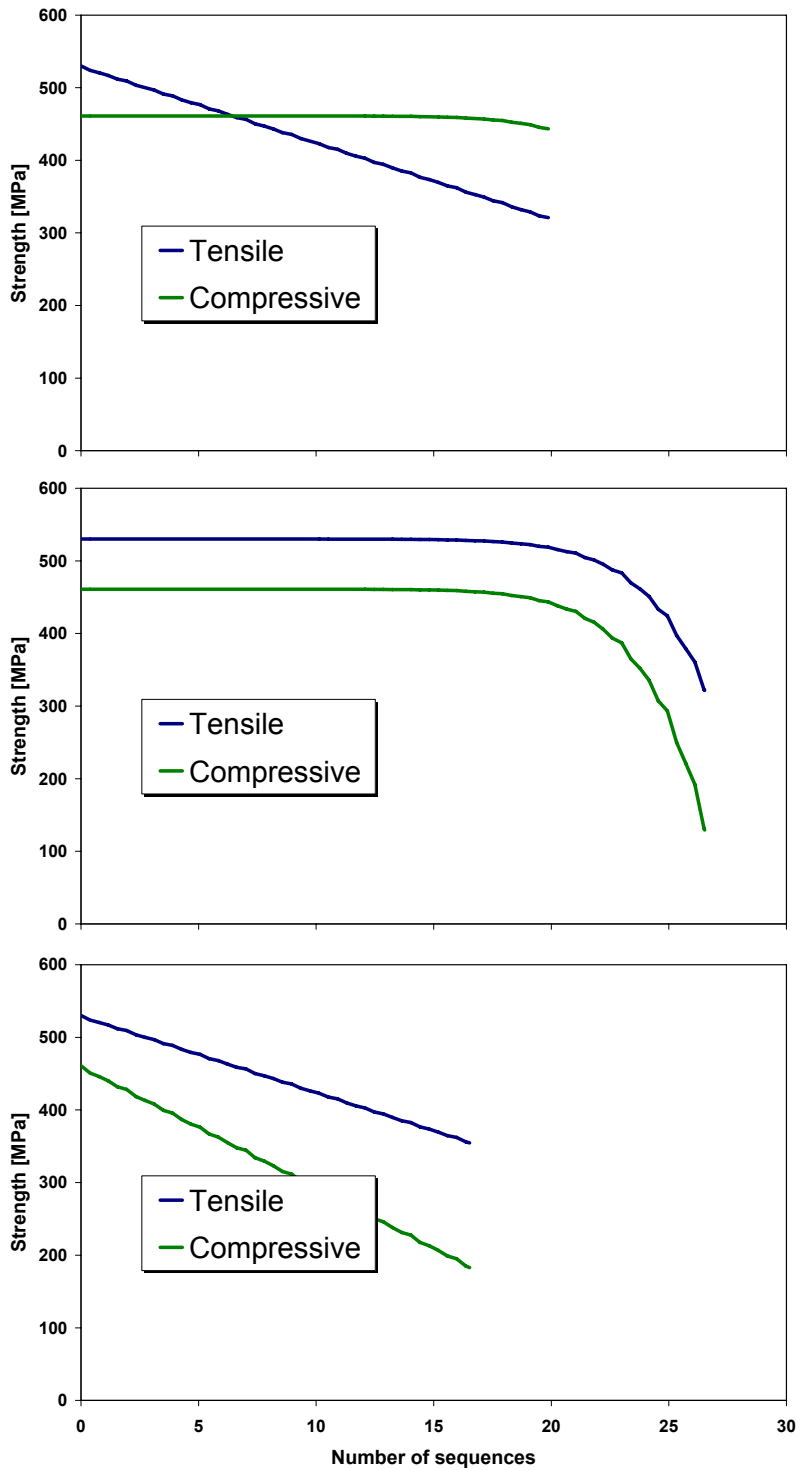
Figure 93: Calculated strength at Smax=+322 MPa
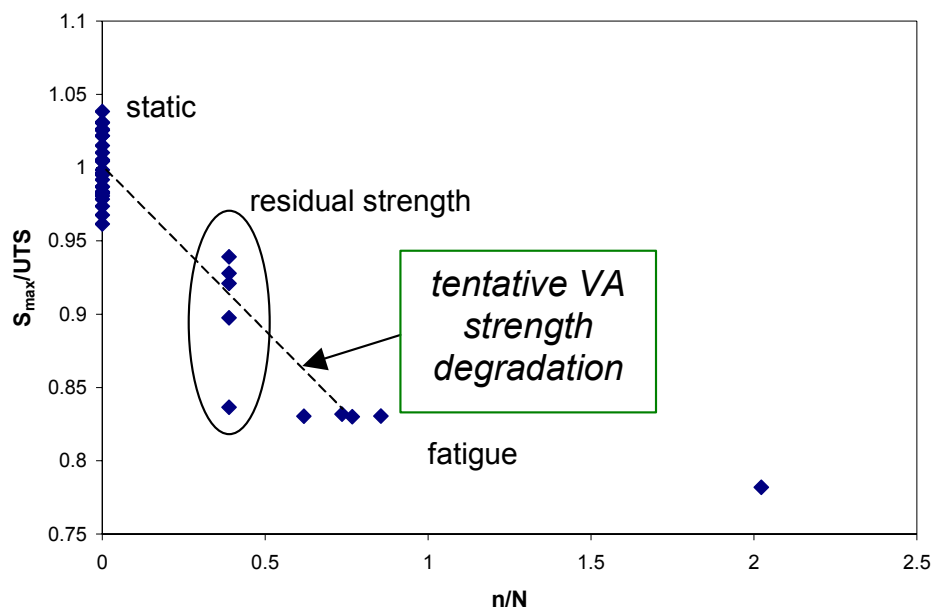
Figure 94: OPTIMAT residual strength data after NEW WISPER fatigue

MD3 I1000 (±45° laminate, ISO tension geometry)

5.4 Reversed loading spectra

Finally, life prediction under compression dominated fatigue loading is discussed. Figure 95 shows results for Reversed WISPERX fatigue loading (S_{max} is plotted as absolute values.) The reversed WISPERX spectrum is obtained by mirroring all peaks and valleys in level 25 (zero stress level). In the plot, the predictions using Goodman diagrams and a 3 R-value CLD are shown. In the 3 R-value CLD, R=-1, R=10 and 0.1 were used.

As might have been expected, the Linear Goodman Diagram yields a slightly more conservative prediction than for WISPERX; the constant life lines now converge at UCS instead of at the higher UTS. For the same reason, the Shifted Linear Goodman diagram is more conservative than the LGD, as opposed to the WISPERX case.

Adding R=10 to the CLD, the compression constant life lines become more convex than the LGD, which can be expected to result in less conservative life predictions. This is indeed seen in the case of the 3 R-value CLD.

The two main differences with the tension dominated spectra are, that:

- the predictions are now more conservative than the data
- the data are acquired at a higher S_{max}
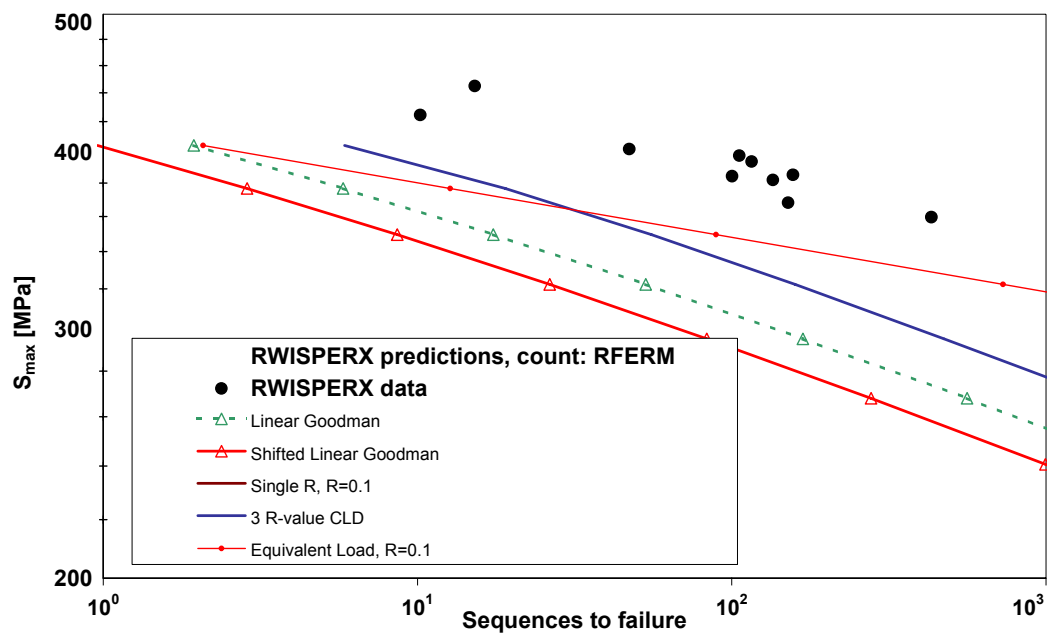
Figure 95: Reversed WISPERX results (absolute maximum plotted) compared to predictions

At the same S_{max}, much more cycles are required for failure for the compression spectrum than for the tensile case. Also in CA testing, the R=10 S-N curve was much flatter than the R=0.1 curve. Thus, to keep testing time within feasible limits, the maximum load on the coupon (in absolute sense) should be increased.

In this respect, the WISPER(X) spectra are particularly unsuitable for reversing, since the maximum load can come very close to UCS, whereas the remaining cycles remain relatively undamaging. The RWISPERX tests have a maximum S_{max} close to the average UCS, as is shown in Figure 95. Even then, the fatigue life is ~130,000 cycles (10 sequences). Some unsuccessful attempts were made in testing Reversed WISPER, but these tests were taken out of the test machine as run-outs.

The strength-based prediction is not included, but, as in the previous plots, it would be close to the Miner summations, especially since compressive strength degradation is governed by sudden death-type degradation curves.

Summary of this chapter

Chapter 5 uses the information collected in the previous chapters for analysis, and an appraisal of life prediction methods. It compares Miner and strength-based life predictions for different load spectra, and focusses on the sensitivity of the predictions as a function of different counting methods, S-N curves, CLDs, and damage accumulation rules.

The formulation of the constant life diagram is identified as the most important and most influential component of life prediction. It seems that the multiple R-value formulation of the CLD gives the most reliable results. Versions of the linear Goodman Diagram tend to give non-conservative results, the equivalent load method is not accurate (sometimes conservative, sometimes non-conservative). The influence of S-N curve parameter variations and counting method is secondary to the influence of CLD.

For the range of strength degradation parameters encountered in the residual strength tests, only a relatively small influence on prediction can be found. This is somewhat surprising, as the expectations with respect to the predictive capabilities of the strength-based life prediction are not fulfilled. This is in terms of life; in terms of strength prediction the strength degradation method is the only available candidate discussed in this thesis.

Chapter 6

Concluding Remarks

6.1 Significance of the research with respect to existing knowledge

This research has resulted in an extensive database describing constant and variable amplitude results suitable for spectrum investigation. The test programme was characterised by a high level of consistency: block loading and residual strength tests were performed at load levels and frequencies consistent with constant amplitude tests.

The test programme is complimentary to previous work in the sense that strength degradation was investigated in unprecedented detail, and associated variable amplitude tests on the same material facilitate model validation.

Various glass-fibre-reinforced materials were included in the research, as well as different coupon geometries. This facilitates generalisation of the results.

All parts of the lifetime prediction methodology were included in detail in the research. The influence of counting method, S-N curve definition, CLD formulation and damage accumulation method were compared and relative influences quantified. This was done for multiple load spectra.

6.2 Conclusions

Strength after fatigue:

- Fatigue has an effect on composite strength for cases where tensile load components are present. Given the accuracy with which strength degradation parameter could be determined from the

dataset, and the fact that early degradation was not observed, it is safe to say, that tensile strength degrades approximately linearly
- Compressive strength is mainly unaffected up to very near failure (sudden death, high strength degradation parameters)
- In fully compressive fatigue, tensile nor compressive strength were observed to degrade.

Block tests:

- There is a sequence effect in life for the block tests, where reversing the load sequence leads to a different Miner's sum at failure
- The sequence effects are not predicted by Miner's rule; data trends are predicted qualitatively using the strength-based method, although not quantitatively
- Almost all repeated block tests showed Miner's sums smaller than unity, as predicted by the strength-based method
- Sequence effects should be defined in terms of life or in terms of strength and are not mutually exclusive.

VA fatigue and predictions:

- The Miner summation with the full CLD gives the best agreement with data in the investigated cases
- Variation of 1% in the power law parameters of the S-N curves used for the Constant Life diagram leads to 20% variation in fatigue life estimate. A variation of 5% in model parameters leads to 100% variation in fatigue life estimate
- (Cyclic) Rainflow counting is more conservative than range-mean counting. For WISPER, WISPERX, and NEW WISPER, range-mean counting leads to maximum of ca. 100-200% longer fatigue life estimates. Cyclic Rainflow counting is believed to be the most correct cycle counting method
- The severity of the influence of counting method depends on the formulation of the constant life diagram. For the investigated spectra, the Multiple R-value CLD (using 6 R-values) is less sensitive to variations in counting method, exhibiting change in fatigue life estimate of ca. 5% instead of 100% for the Linear and Shifted Goodman Diagrams
- When using a strength degradation model for life prediction, variation of the separate tensile and compressive strength degradation in the region of linear to sudden death behaviour, leads to a variation in fatigue life prediction of ~30%

- The formulation of the constant life diagram has the most significant influence on the fatigue life estimate. A simplified Linear Goodman Diagram can predict fatigue lives that are an order of magnitude longer than a constant life diagram constructed from detailed fatigue data
- A sudden death strength degradation model gives the longest life estimates in a variable amplitude spectrum. The estimate is equal to the Miner prediction
- From theoretical predictions, strength degradation in a sufficiently random and regular load spectrum resembles strength degradation in a constant amplitude load spectrum
- Sequence effects in terms of strength are not expected, but could be explored.

The above conclusions were verified predominantly for tensile load cases and a multidirectional glass-fibre composite.

The simple load spectra did suggest the existence of sequence effects, hence these data show, that Miner summation is inappropriate for variable amplitude load sequences. However, from the WISPER tests and predictions, Miner is still found most appropriate, because the sensitivity of the prediction to the CLD is more significant than of damage accumulation rule, Miner is more easily implemented (less computationally intensive), and the strength degradation data do not suggest strength degradation described by parameters *C<1* (if the strength degradation would be 'early degradation', using a strength-based prediction would give more conservative lives than is justified by the current dataset).

Most of the cyclic loads in the spectra were very small, outside the range where experimental data were obtained. This, combined with the outcome, that the CLD is the most significant component of a life prediction, suggests, that long-life testing will prove to be valuable for improving fatigue life prediction.

6.3 Relevance of the conclusions for blade design

This work has confirmed the suspicion that commonly used variable amplitude life predictions can be highly inaccurate. Especially the formulation of the constant life diagram should be based on more detailed knowledge on material fatigue behaviour than is common practice.

The focus is on fatigue life prediction of rotor blade material coupons. As such, it can be argued, that it is of limited applicability for full structures or structural

details. The conclusions may not apply to development of specific failure modes such as delamination in multi-axially loaded (sub)structures.

Furthermore, improved knowledge on fatigue life prediction is of limited use in situations where fatigue is not the dominant design driver (although it is important to determine which is the design driver!). Rotor blade designs often turn out to be stiffness-driven; the amount of material allocated to the load carrying structure is not determined by the fatigue damage, but by the clearance requirement between tower and blade.

Determination of a representative test load for accelerated fatigue testing of (prototype) rotor blades is a procedure, which is affected by the accuracy of the life prediction models. Improved prediction methods lead to more accurate determination of the test load for a blade.

It should be mentioned, that all conclusions are based on mean life and mean strength data; detailed approaches for using the discussed formulations in probabilistic design are not discussed, although some attention is given to scatter and the formulation of tolerance bounds in constant amplitude fatigue.

6.4 Recommendations

The significance of the constant life diagram leads to two main recommendations. The first one is to focus on long-life tests. These will be very useful for enhancing existing constant life diagrams. In addition, formulations of the constant life diagram which aim to minimise experimental effort while maximising the accuracy should be explored. These include formulations which use non-linear regression to determine model parameters, not from single R-values, but from the entire dataset.

For life prediction, the strength-based method investigated here was not preferred. However, the potential of strength degradation models for strength prediction has not been explored in full detail. Variable amplitude fatigue or sequence effects on strength should be investigated in more detail, including:

- Residual strength testing in the (n^{th}) second block of (repeated) block tests
- Residual strength testing after spectrum fatigue

The aim of this investigation is to validate the expected similarity of the constant amplitude fatigue strength degradation, which would lead to a considerable simplification of strength prediction after fatigue.

The effect of coupon geometry could be quantified more for the type of laminate investigated. Notably the significance of the occurrence of grip failures should be explored in general. From available information, the effect of grip failure on static strength could be quantified. However, for fatigue the effect is not as well described. An aspect that can be expected to be influenced by grip failures is the use of stiffness measurements to describe remaining strength or life. Due to the measurements and the lay-up of the laminate, it was not possible in this work to reliably couple residual stiffness to residual strength. Part of the lack of correlation may have been caused by the fact that progressive damage and fatigue failure occurred in the grips, away from where the stiffness measurement was performed. Waisted coupons may, in this respect, be more useful.

Furthermore, substructures resembling the behaviour of (parts of) the full-size blade structure, should be subjected to spectrum loading. Sequence effects on life or strength may be expected there, even if 'bulk material' sequence effects are absent.

Issues such as (panel) buckling were not covered in this thesis, but are very relevant for rotor blade design on the compressive side especially. Similarly, adhesive bonds in rotor blades, e.g. the connection between spar and skin, were not treated here, but the fatigue behaviour of these structural details should certainly be investigated in the future.

More extensive characterisation of the microscopic damage induced by fatigue may lead to improved methods for predicting fatigue life or strength.

The work above also focussed on tension/reversed loading. In rotor blades, a large part of the blade structure is loaded in compression. This work has confirmed, that compression fatigue is characterised by very flat S-N curves, demonstrated that no significant strength degradation occurs, and that fatigue life predictions for compression dominated spectrum are conservative. On the other hand, some work needs to be done on test methodology in compression, in avoiding bending/buckling problems and obtaining S-N data with less scatter. Also, reversing WISPER(X) was, in terms of testing, not very practical. Summarising, compression is not expected to be problematic as a fatigue design driver, but CA/VA test methods should be further investigated.

Finally, on a general note, future research should emphasise the need for consistency of experiment design, minimising material and equipment variations, while at the same time giving an accurate quantification of these variations. It is recommended that all coupons are made in a single batch, preferably a single plate. All manufacturing conditions should be documented, including the location of coupons within the plate(s). The coupons should be distributed randomly to all participating parties and tested in random order.

Acknowledgements

References

A

[1]   Adali, S., 'Optimization of Fibre Reinforced Composite Laminates Subject to Fatigue Loading', 3rd Int. Conference on Composite Structures, 1985, pp. 43-55

[2]   Adam T., Dickson R.F., Jones C.J., Reiter H., Harris B., 'A power law fatigue damage model for fiber-reinforced plastic laminates', Proc Instn Mech Engrs, Vol. 200, 1986, NoC3, pp. 155-166

[3]   Adam, T., Gathercole, N., Reiter, H., et al., 'Life prediction for fatigue of T800/5245 carbon fibre composites: II-Variable amplitude loading', International Journal of Fatigue, Vol. 16, 1994, pp. 533-547

[4]   Akshantala, N.V., Talreja, R., 'A micromechanics based model for predicting fatigue life of composite laminates', Materials Science and Engineering, Vol. A285, 2000, pp. 303-313

[5]   American Society for Testing and Materials (ASTM), 'Standard Practices for Cycle Counting in Fatigue Analysis', E 1049 – 85, ASTM subcommittee E08.04, June 1985 (Reapproved 1997)

[6]   American Society for Testing and Materials (ASTM), 'Standard Practice for Statistical Analysis of Linear or Linearized Stress-Life (S-N) and Strain-Life (ε-N) Fatigue Data', ASTM E 739-91, 1991 (Reapproved 1998)

[7]   American Society for Testing and Materials (ASTM), 'Standard Test Method for Tension-Tension Fatigue of Polymer Matrix Composite Materials', ASTM 3479/D3479M-96, August 1996

[8]   American Society for Testing and Materials (ASTM), 'ASTM D3039: Standard Test Method for Tensile Properties of Polymer Matrix Composite Materials', 2000

[9]   Amijima, S., Tanimoto, T., Matsuoka, T., 'A study on the fatigue life estimation of FRP under Random Loading', Fourth International Conference on Composite Materials, ICCM-IV, Tokyo, Japan, 1982, pp. 701-708

[10]   Amzallag, C., Gerey, J.P., Robert, J.L.,Bahuaud, J., 'Standardization of the rainflow counting method for fatigue analysis', Fatigue, Vol. 16, June 1994, pp. 287-293

[11]   Andersen, S.I., Lilholt, H., 'Fatigue of glass/polyester composite materials for wingblades', proc. European Community Wind Energy Conference, 1988, pp. 342-346

[12]   Andersen, S.I., Lilholt, H., 'Fatigue of glass/polyester composite materials for wingblades', proc. Euroforum New Energies Congress, 1988, pp. 776-779

[13]   Andersen, S.I., Brøndsted, P., Lilholt, H., 'Fatigue of polymeric composites for wingblades and the establishment of stiffness-controlled fatigue diagrams', proc. European Union Wind Energy Conference, 1996, pp. 950-953

14   Andersons, J., Korsgaard, J., 'Residual strength of GRP at high cycle fatigue', proc. 11th International Conference on Composite Materials, 1997, pp. II-(135-144)

15   Andersons, J., Korsgaard, J., 'Residual strength of GFRP at high-cycle fatigue', Mechanics of Composite Materials, translated from Mekhanika Kompozitnykh Materialov ,Vol. 35, no. 5, 1999, pp. 395-402

16   Andersons, J., Grušeckis, I., Korsgaard, J., 'The effect of overloads on the residual strength and life of laminated GRP', Mechanics of Composite Materials, translated from Mekhanika Kompozitnykh Materialov, Vol. 35, no. 6, 1999, pp. 701-706

17   Ansell, M.P, Bond, I.P., Bonfield, P.W., 'Constant life diagrams for wood composites and polymer matrix composites', proc. 9th International Conference on Composite Materials, Vol. 5, 1993, pp. 692-699

18   Anthes, R.J., 'Modified rainflow counting keeping the load sequence', International Journal of Fatigue, Vol. 19, No. 7, 1997, pp. 529-535

19   Assimakopoulou, T.T., Antoniou, A.E., Passipoularidis, V., Philippidis, T.P., 'Experimental procedure of residual strength tests', OPTIMAT report: OB_TG5_O002, doc. no. 10205, June 2004

20   Awerbuch, J., Hahn, H.T., 'Fatigue and Proof-Testing of Unidirectional Graphite/Epoxy Composite', ASTM STP 636, 1977, pp. 248-266

B

21   Bach, P.W., Schaap, B.A.J., 'Vermoeiingsonderzoek aan windturbinematerialen en -bladverbindingen', Energy research Centre of the Netherlands report: ECN-C-90-012, Petten, the Netherlands, 1990 (in Dutch)

22   Bach, P.W., 'High cycle fatigue testing of glass fibre reinforced polyester and welded structural details', Energy research Centre of the Netherlands report: ECN-C-91-010, Petten, the Netherlands, 1991

23   Bach, P.W., 'Fatigue properties of glass- and glass/carbon-polyester composites for wind turbines', Energy research Centre of the Netherlands report: ECN-C-92-072, Petten, the Netherlands, 1992

24   Badaliance, R., Dill, H.D., Potter, J.M., 'Effects of Spectrum Variations on Fatigue Life of Composites', ASTM STP 787, 1982, pp. 274-286

25   Barnard, P.M., Butler, R.J., Curtis, P.T., 'Fatigue Scatter of UD Glass Epoxy, a Fact or Fiction?', proc. 3rd Conference on Composite Structures, 1985, pp. 69-82

26   Bartley-Cho, J., Seung Gyu, L., Thomas Hahn, H., et al., 'Damage accumulation in quasi-isotropic graphite/epoxy laminates under constant-amplitude fatigue and block loading', Composites Science and Technology, Vol. 58, 1998, pp. 1535-1547

27   Beheshty, M.H., Harris, B., Adam, T., 'An empirical fatigue-life model for high-performance fibre composites with and without impact damage', Composites: Part A, Vol. 30, 1999, pp. 971-987

28   Berger, C., Eulitz, K.-G., Heuler, P., et al., 'Betriebsfestigkeit in Germany - an overview', International Journal of Fatigue, Vol. 24, 2002, pp. 603-625

29   Berkovits, A., Fang, D., 'An analytical master curve for Goodman Diagram data', International Journal of Fatigue, Vol. 15, no. 3, 1993, pp. 173-180

30 Blanch, M.J., Kouroussis, D.A., Anastassopoulos, A.A., et al., 'Damage classification of acoustic emission using aegis pattern recognition software from ten small wind turbine blade tests', proc. Global Windpower, Paris, France, 2-5 April, 2002

31 Blanch, M.J., Dutton, A.G., Philippidis, T.P., Nijssen, R., 'Recommended procedure for conducting OPTIMAT Blades residual strength tests', OPTIMAT report: OB_TG5_R002_001, doc. no. 10108, August 2003

32 Boerstra, G.K., 'A descriptive model for the fatigue behaviour of fibre reinforced plastics', AE-Rotortechniek report no. D0003301, October 2005

33 Boller, K. H., 'Effect of tensile mean stresses on fatigue properties of plastic laminates reinforced with unwoven glass fibers', ML-TDR-64-86, 1964

34 Boller, K. H., 'Effect of pre-cyclic stresses on fatigue life of plastic laminates reinforced with unwoven fibers', ML-TDR-64-168, 1964

35 Boller, K. H., 'Effect of single-step change in stress on fatigue life of plastic laminates reinforced with unwoven "E" glass fibers', AFML-TR-66-220, 1966

36 Boller, K.H., 'Fatigue fundamentals for composite materials', ASTM STP 460, Composite Materials: Testing and Design, 1969, pp. 217-235

37 Bond, I.P., 'Fatigue life prediction for GRP subjected to variable amplitude loading', Composites Part A, Vol. 30, 1999, pp. 961-970

38 Braam, H., Ronold, K.O., Christensen, C.J., 'PRODETO - computer program. Theory and program structure', Energy research Centre of the Netherlands report: ECN-C-97-093, Petten, The Netherlands, May 1998

39 Brøndsted, P., Andersen, S.I., Lilholt, H., 'Fatigue damage accumulation and lifetime prediction of GFRP materials under block loading and stochastic loading', proc. 18th International Symposium on Materials Science: Polymeric Composites - Expanding the limits, eds: S.I. Andersen, P. Brøndsted, H. Lilholt et al., 1997, pp. 269-278

40 Brøndsted, P., Lilholt, H., Lystrup, A., 'Composite Materials for Wind Power Turbine Blades', Annu. Rev. Mater. Res., Vol. 35, 2005, pp. 505-538

41 Broutman, L.J., Sahu, S., 'A New Theory to Predict Cumulative Fatigue Damage in Fiberglass Reinforced Plastics', Composite Materials: Testing and Design (Second Conference), ASTM STP 497, American Society for Testing and Materials, 1972, pp. 170-188

42 Buggy, M., Dillon, G., 'Flexural fatigue of carbon fibre-reinforced PEEK laminates', Composites, Vol. 22, no. 3, 1991, pp. 191-198

43 Bulder, B.H., Bach, P.W., 'A literature survey on the effects of moisture on the mechanical properties of glass and carbon fibre plastic laminates', Energy research Centre of the Netherlands report: ECN-C-91-033, Petten, the Netherlands, 1991

44 Bulder, B., Peeringa, J. M., Lekou, D., et al., 'NEW WISPER - Creating a New Standard Load Sequence From Modern Wind Turbine Data', OPTIMAT BLADES report OB_TG1_R020, doc. no 10278, 2005

C

[45] Caprile, C., Sala, G., Buzzi, A., 'Environmental and Mechanical Fatigue of Wind Turbine Blades Made of Composites Materials', Journal of Reinforced Plastics and Composites, reprinted from proc. ICCME, 1995, no. 15, 1996, pp. 673-691

[46] Caprino, G., D'Amore, A., 'Flexural fatigue behaviour of random continuous-fibre-reinforced thermoplastic composites', Composites Science and Technology, Vol. 58, 1998, pp. 957-965

[47] Caprino, G., Giorlea, G., 'Fatigue lifetime of glass fabric/epoxy composites', Composites Part A, no. 30, 1999, pp. 299-304

[48] Cinquin, J., Chabert, B., Chauchard, J., et al., 'Characterization of a thermoplastic (polyamide 66) reinforced with unidirectional glass fibres. Matrix additives and fibre surface treatment influence on the mechanical and viscoelastic properties', Composites, Vol. 21, no. 2, 1990, pp. 141-147

[49] Chou, P. C., Croman, R., 'Residual Strength in Fatigue Based on the Strength-Life Equal Rank Assumption', Journal of Composite Materials, Vol. 12, 1978, pp. 177-194

[50] Chou, P. C., Wang, A.S.D., 'Statistical Analysis of Fatigue of Composite Materials', AFML-TR-78-96, July 1978

[51] Chou, P. C., Miller, H., 'Maximum likelihood estimation of a Two-segment Weibull distribution for fatigue life', as manuscript of paper presented at ASTM symposium on Statistical Analyses of Fatigue Data, Pittsburgh, PA in appendix A in AFWAL-TR-80-4049, 1979

[52] Chou, P. C., Alper, J., 'A cumulative damage rule for fatigue of composite materials', as appendix B in AFWAL-TR-80-4049 (presented in December 4, 1979 winter annual meeting of ASME, New York, with additional data), 1979

[53] Chou, P. C., Wang, A.S.D., Croman, R., et al., 'Statistical Analysis of strength and life of composite materials', AFWAL-TR-80-4049, 1980, pp. 65

[54] Clark, S.D., Shenoi, R.A., Allen, H.G., 'Modelling the fatigue behaviour of sandwich beams under monotonic, 2-step and block-loading regimes', Composites Science and Technology, Vol. 59, 1999, pp. 471-486

[55] Croman, R. B., 'Flex fatigue of AS-4 Graphite reinforced thermoplastics', proc. 6th International Conference on Composite Materials and 2nd European Conference on Composite Materials, 1987, pp. 4.76-4.88

[56] Curtis, D.C., Moore, D.R., Slater, B., et al., 'Fatigue testing of multi-angle laminates of CF/PEEK', Composites, Vol. 19, no. 6, 1988, pp. 446-452

[57] Curtis, P.T., Davies, A.J., 'Fatigue life prediction of polymer composite materials', proc. 9th European Conference on Composite Materials, Brighton, 2000

D

[58] Daniel, I.M., Lee, J.W., Yaniv, G., 'Damage Mechanisms and stiffness degradation in grahite/epoxy composites', proc. 6th International Conference on Composite Materials and 2nd European Conference on Composite Materials, 1987, pp. 4.129-4.138

59 Daniel, I.M., '1998 William M. Murray Lecture: Experimentation and Modeling of Composite Materials', Experimental Mechanics, Vol. 39, No. 1, 1999, pp. 1-19

60 van Delft, D.R.V., van Leeuwen, J.L., Noordhoek, C., et al., 'Fatigue Testing of a Full Scale Steel Rotor Blade of the WPS-30 Wind Turbine', Journal of Wind Engineering and Industrial Aerodynamics, Vol. 27, 1988

61 van Delft, D.R.V., Hagg, F., Joosse, P.A., 'The influence of fatigue design line criteria on the rotor blade design', proc. European Wind Energy Conference, September 1990, pp. 395-399

62 van Delft, D.R.V., Rink, H.D., Joosse, P.A., 'Fatigue behaviour of fibreglass wind turbine blade material in the very high cycle range', proc. 15th British Wind Energy Association Conference, K.F. Pitcher (Ed.), London, October 1993

63 van Delft, D.R.V., Drost, L., van Leeuwen, J.L., et al., 'Full scale test on the GRP rotor blade of the 500 kW NedWind-35 wind turbine', proc. European Community Wind Energy Conference, 1993, pp. 160-163

64 van Delft, D.R.V., Rink, H.D., Joosse, P.A., et al., 'Fatigue Behaviour of Fiberglass Wind Turbine Blade Material at the Very High Cycle Range', proc. EWEA Conference and Exhibition, 1994, pp. 379-384

65 van Delft, D.R.V., Rink, H.D., Joosse, P.A., et al., 'Fatigue Behaviour of Fiberglass Wind Turbine Blade Material at the Very High Cycle Range', proc. EWEA Conference and Exhibition, 1994, pp. 379-384

66 van Delft, D.R.V., van Leeuwen, J.L., 'Full Scale Testing of Wind Turbine Rotor Blades', proc. EWEA Conference and Exhibition, 1994, pp. 727-737

67 van Delft, D.R.V., 'IEC-TC88-WG8 (Testing of Rotor Blades)', proc. European Union Wind Energy Conference, 1996, pp. 1012-1015

68 van Delft, D.R.V., de Winkel, G.D., Joosse, P.A., 'Fatigue Behaviour of Fibreglass Wind Turbine Blade Material under Variable Amplitude Loading', proc. European Union Wind Energy Conference, 1996, pp. 914-918

69 van Delft, D.R.V., de Winkel, G.D., Joosse, P.A., 'Fatigue behaviour of fibreglass wind turbine blade material under variable amplitude loading', proc. AIAA/ASME Wind Energy Symposium, no. AIAA-97-0951, Reno, Nevada, January 1997, pp. 180-188

70 Degrieck, J., van Paepegem, W., 'Fatigue Damage Modelling of fibre-reinforced composite materials: a Review', Applied Mechanics Reviews, Vol. 54, no. 4, 2001, pp. 279-300

71 De Smet, B.J., Bach, P.W., 'DATABASE FACT', Energy research Centre of the Netherlands report: ECN-C-94-045, Petten, the Netherlands, 1994

72 Diao, X., Ye, L., Mai, Y.-W., 'A statistical model of residual strength and fatigue life of composite laminates', Composites Science and Technology, Vol. 54, 1995, pp. 329-336

73 DIN, 'Statistische Auswertung an Stichproben mit Beispielen aus der Elastomer- und Kunststoffprüfung', DIN 53-598, Teil 1., Beuth Verlag GmbH, Berlin, July 1983

74 DIN, 'Statistische Auswertung von Daten – Bestimmung eines statistischen Anteilsbereiches', DIN 55-303, Teil 5, Beuth Verlag GmbH, Berlin, February 1987

75 DNV, 'Implementation of OPTIMAT in Technical Standards', OPTIMAT report OB_TG6_R002, doc. no. 10317, 2006

[76] Donaldson, S.L., 'Fracture toughness testing of graphite/epoxy and graphite/PEEK composites', Composites, Vol. 16, no. 2, 1985, pp. 103-112

[77] Dover, W.D., 'Variable amplitude fatigue of welded structures', Fracture Mechanics, Current Status, Future Prospects, 1979, pp. 129-147

[78] Dowling, N.E., 'Fatigue Failure Predictions for Complicated Stress-Strain Histories', Journal of Materials, JMLSA, Vol. 7, No. 1, March 1972, pp. 71-87

[79] Downing, S., Galliart, D., Berenyi, T., 'A Neuber's Rule Fatigue Analysis Procedure for Use with a Mobile Computer', paper 760317 in proc. SAE Automotive Engineering Congress and Exposition, Detroit, MI, February 23-27, 1976.

[80] Downing, S.D., Socie, D.F., 'Simple rainflow counting algorithms', International Journal of Fatigue, Vol.4, no.1, January 1982, pp. 31-40

[81] Dutton, A.G., 'Feasibility of various condition assessment techniques for residual strength and life prediction', OB_TG5_R015, 2006

E

[82] Echtermeyer, A.T., 'Fatigue of Glass Reinforced Composites Described by One Standard Fatigue Lifetime Curve', proc. EWEA Conference and Exhibition, 1994, pp. 391-396

[83] Echtermeyer, A.T., Kensche, C., Bach, P., Poppen, M., Lilholt, H., Andersen, S.I., Brøndsted, P., 'Method to predict fatigue lifetimes of GRP wind turbine blades and comparison with experiments', proc. European Wind Energy Conference, May 20-24, 1996, Göteborg, Sweden, pp. 907-913

[84] El Kadi, H., Ellyin, F., 'Effect of stress ratio on the fatigue of unidirectional glass fibre/epoxy composite laminae', Composites, Vol. 25, no. 10, 1994, pp. 917-924

[85] Ellyin, F., Kujawski, D., 'Tensile and fatigue behaviour of glassfibre/epoxy laminates', Construction and Building Materials, Vol. 9, no. 6, 1995, pp. 425-430

[86] Endo, T., Mitsunaga, K., Nakagawa, H., 'Fatigue of Metals Subjected to Varying Stress – Prediction of Fatigue Lives', preliminary proceedings of the Chigoku-Shikoku District Meeting, Japan Society of Mechanical Engineers, November 1967, pp. 41-44

[87] Endo, T., Mitsunaga, K., Nakagawa, H., Ikeda, K., 'Fatigue of Metals Subjected to Varying Stress – Low Cycle, Middle Cycle Fatigue', preliminary proceedings of the Chugoku-Shikoku District Meeting, Japan Society of Mechanical Engineers, November 1967, pp. 45-48

[88] Endo, Tatsuo, Anzai, Hiroyuki, 'Refined Rainflow Algorithm: P/V Difference Method (in Japanese)', Journal of the Society of Materials Science, Japan, Vol. 30, no. 328, 1981, pp. 89-93

[89] Epaarachchi, J. A., Clausen, P. D., 'An empirical model for fatigue behavior prediction of glass fibre-reinforced plastic composites for various stress ratios and test frequencies', Composites Part A, Vol. 34, 2003, pp. 313-326

[90] European Commission, 'Energy for the future: Renewable sources of energy', COM(97)599, 1997

[91] Eyring, H., 'Viscosity, Plasticity, and Diffusion as examples of absolute reaction rates', The Journal of Chemical Physics, Vol. 4, 1936, pp. 283-291

F

[92]   Fatemi, A., Yang, L., 'Cumulative fatigue damage and life prediction theories: a survey of the state of the art for homogeneous materials', International Journal of Fatigue, Vol. 20, no. 1, 1998, pp. 9-34

[93]   Filis, P.A., Farrow, I.R., Bond, I.P., 'Classical fatigue analysis and load cycle mix-event damage accumulation in fibre reinforced laminates', International Journal of Fatigue, Vol. 26, 2004, pp. 565-573

[94]   Foley, G.E., Roylance, M.E., Houghton, W.W., 'Life prediction of glass/epoxy composites under fatigue loading', proc. International Conference on Advances in Life Prediction Methods, 1983, pp. 301-305

[95]   Found, M.S., Quaresimin, M., 'Two-stage fatigue loading of woven carbon fibre reinforced laminates', Fatigue and Fracture of Engineering Materials and Structures, Vol. 26, 2003, pp. 17-26

G

[96]   Gamstedt, E.K., 'Fatigue damage mechanisms in polymer matrix composites', PhD thesis, nr. LTU-DT-1997:36-SE, Luleå Tekniska Universitet, 1997

[97]   Gamstedt, E.K., Talreja, R., 'Fatigue damage mechanisms in unidirectional carbon-fibre-reinforced plastics', Journal of Materials Science, no. 34, 1999, pp. 2535-2546

[98]   Gamstedt, E.K., Andersen, S. I., 'Fatigue degradation and failure of Rotating Composite Structures - Materials Characterisation and Underlying Mechanisms', 2001

[99]   Gamstedt, E.K., Sjögren, B.A., 'An experimental investigation of the sequence effect in block amplitude loading of cross-ply composite laminates', International Journal of Fatigue, Vol. 24, 2002, pp. 437-446

[100] Ganczakowski, H.L., Smith, P.A., Beaumont, P.W.R., 'On the modulus of KFRP laminates in static and fatigue loading', proc. 6th International Conference on Composite Materials and 2nd European Conference on Composite Materials, 1987, pp. 3.166-3.175

[101] Germanischer Lloyd, 'Rules and Regulations, IV-Non-Marine Technology, Part I: Wind Energy, Hamburg, Germany, 1993, pp. 2-2

[102] Germanischer Lloyd, 'Rules and Regulations, IV-Non-Marine Technology, Part I: Wind Energy, Hamburg, Germany, 2003, pp. 5-19

[103] Ghidossi, P., El Mansori, M., Pierron, F., 'Edge machining effects on the failure of polymer matrix composite coupons', Composites Part A, Vol. 35, 989-999, 2004

[104] Ghidossi, P., 'Contribution à l'étude de l'effet des conditions d'usinage d'éprouvettes en composites a matrice polymère sur leur réponse mécanique', (in French), December 2003, pp. 166

[105] Gardner, P., Garrad, A., Jamieson, P., Snodin, H., Nicholls, G., Tindall, A., Morthorst, P.E., Jacobsen, H., Hohmeyer, O., Wetzig, F., Mora, D., et al., 'Wind Energy – The Facts, an analysis of wind energy in the EU-25', 2004

[106] Glinka, G., Kam, J.C.P., 'Rainflow counting algorithm for very long stress histories', International Journal of Fatigue, Vol. 9, no. 3, October 1987, pp. 223-228

107   Graham, I.J., Mohamadian, H.P., Wang, C.S., 'Fatigue Life Characteristics of E-Glass Fiber Reinforced Polyester and Polyvinylester Composites', proc. Windpower '89, 1989, pp. 105-113

108   Griffin, D. A., 'WindPACT Turbine Design Scaling Studies Technical Area 1 - Composite Blades for 80- to 120- Meter Rotor', 2000-2001

109   Griffin, D. A., Ashwill, Thomas D., 'Alternative Composite Materials for Megawatt-ScaleWind Turbine Blades: Design Considerations and Recommended Testing', proc. AIAA/ASME Wind Energy Symposium, 2003, pp. 1-11

110   Guemes, A., Glez-Vecino, J.A., Castrillo, M.A., 'Matrix selection for GRP Fatigue Loaded structures', proc. 3rd European Conference on Composite Matierals, 1989, pp. 457-462

H

111   Hahn, H.T., Kim, R.Y., 'Proof Testing of Composite Materials', Journal of Composite Materials, Vol. 9, 1975, p.297

112   Hahn, H.T., Kim, R.Y., 'Fatigue Behavior of Composite Laminate', Journal of Composite Materials, Vol. 10, 1976, pp. 156-180

113   Hahn, H. T., 'Fatigue behavior and life prediction of composite laminates, AFML-TR-78-43', 1978

114   Hamstad, M. A., 'A review: Acoustic Emission, a Tool for Composite-Materials Studies', Experimental Mechanics, Vol. 26, 1986, pp. 7-13

115   Harik, V.M., Klinger, J.R., Bogetti, T.A., 'Low-cycle fatigue of unidirectional composites: Bi-linear S-N curves', International Journal of Fatigue, Vol. 24, 2002, pp. 455-462

116   ten Have, A.A., 'Wisper: a standardized fatigue load sequence for HAWT-blades', proc. European Community Wind Energy Conference, June 1988

117   ten Have, A.A., 'WISPER: introducing variable-amplitude loading in wind turbine research', proc. Wind Energy Conversion 1988, 1988, pp. 407-412

118   ten Have, A A., 'European Approaches in Standard Spectrum Development', Development of Fatigue Loading Spectra, ASTM STP 1006, J.M. Potter and R.T. Watanabe, Eds., American Society for Testing and Materials, Philadelphia, 1989, pp. 17-35

119   ten Have, A.A., 'WISPER and WISPERX - a summary paper describing their background, derivation and statistics', National Aerospace Laboratory of the Netherlands report: NLR TP 92410 L, 1992

120   van Hemelrijck, D., Smits, A., 'Biaxial testing of fibre reinforced composites', OPTIMAT report: OB_TG2 R006_VUB, rev. 0, January 2003

121   Henaff-Gardin, C., Lafarie-Frenot, M.C., 'Fatigue Behaviour of thermoset and thermoplastic cross-ply laminates', Composites, Vol. 23, no. 2, 1992, pp. 109-116

122   Heuler, P., Seeger, T., International Journal of Fatigue, no. 4, 1986, pp. 225-230

123   Hinton, M.J., Kaddour, A.S., Soden, P.D., 'A comparison of the predictive capabilities of current failure theories for composites laminates, judged against experimental evidence', Composites Science and Technology, Vol. 62, 2002, pp. 1725-1797

124   Hwang, W., Han, K.S., 'Cumulative Damage Models and Multi-Stress Fatigue Life Prediction', Journal of Composite Materials, Vol. 20, 1986, pp. 125-153

125   Hwang, W., Han, K.S., 'Fatigue of Composites-Fatigue Modulus Concept and Life Prediction', Journal of Composite Materials, Vol. 20, 1986, pp. 154-165

126   Hwang, W., Han, K.S., 'Statistical study of strength and fatigue life of composite materials', Composites, Vol. 18, no. 1, 1987, pp. 47-53

I

127   IEC TS 61400-1, 'Wind turbine generator systems – Part 1: Safety requirements', International Electrotechnical Commission, 2nd edition, 1999

128   IEC, Wind Turbine Generator Systems, Part 13: Measurement of Mechanical Loads, IEC 61400-13 TS, prepared by IEC-TC88, Working Group 11, 1999

129   IEC TS 61400-23, 'Wind turbine generator systems – Part 23: Full-scale structural testing of rotor blades', International Electrotechnical Commission, 1st edition, April 2004

130   Instron, Fast Track 2 Wavemaker and Waverunner, version 7.1.0

131   ISO International Standard, 'Statistical interpretation of test results – Estimation of the mean – Confidence interval', ISO 2602:1980(E), International Organization for Standardization, second edition, Genève, February, 1980

132   ISO International Standard, 'Plastics - Determination of tensile properties - Part 1: General principles', ISO 527-1:1993(E), International Organization for Standardization, Genève, 1993

133   ISO International Standard, 'Fibre-reinforced plastic composites – Determination of compressive properties in the in-plane direction', ISO 14126:1999(E), International Organization for Standardization, Genève, 1999

134   ISO International Standard, 'Fibre-reinforced plastics – Determination of fatigue properties under cyclic loading conditions', ISO 13003:2003, International Organization for Standardization, Genève, December 2003

J

135   Jacobsen, Thorben T.K., 'reference material (OPTIMAT)', OPTIMAT Material specification: OB_SC_R001, doc. no. 10004, LM Glasfiber AG, 2002

136   James, T.K., Appl, F.J., Bert, C.W., 'Low-cycle Fatigue of a Glass-fabric-reinforced plastic Laminate', Experimental Mechanics, 1968, pp. 327-330

137   Jen, M.-H.R., Lee, C.-H., 'Strength and life in thermoplastic composite laminates under static and fatigue loads. Part I: Experimental', International Journal of Fatigue, Vol. 20, no. 9, 1998, pp. 605-615

138   Jen, M.-H.R., Lee, C.-H., 'Strength and life in thermoplastic composite laminates under static and fatigue loads. Part II: Formulation', International Journal of Fatigue, Vol. 20, no. 9, 1998, pp. 617-629

[139] Joneja, S.K., 'Matrix Contribution to Fatigue behavior of Glass Reinforced Polyester Composites', proc. 41st Annual Conference, Reinforced Plastics/Composites Institute, Society of Plastics Industry, Inc., 1986, pp. 10A-1 - 6

[140] Jones, D.L., Whitworth, H.A., 'Determination of the stiffness reduction of $(0,90,\pm45]_s$ graphite/epoxy laminates under cyclic loading', proc. AIAA 84-0863, 1984, pp. 428-435

[141] de Jonge, J.B., 'Fatigue load monitoring of tactical aircraft', National Aerospace Laboratory of the Netherlands report: NLR TR 69063 LI, prepared for presentation at the 29th meeting of the AGARD Structures and Materials Panel, Istanbul, Turkey, 28 September-8 October 1969

[142] de Jonge, J.B., 'The analysis of load-time histories by means of counting methods', in 'Helicopter Fatigue design guide', F. Liard (ed.)., AGARD-AG-292, November 1983

[143] Joffe, R., 'Damage accumulation and stiffness degradation in composite laminates', Ph.D. thesis, nr. LTU-DT-99/27-SE, Luleå Tekniska Universitet, 1999

[144] Joosse, P.A., van Delft, D.R.V., 'Fatigue design curves of fibreglass blade material compared to test data', proc. Wind Energy Conversion 1993, 1993, pp. 275-280

[145] Joosse, P.A., van Delft, D.R.V., Bach, P.W., 'Fatigue Design Curves compared to Test Data of Fiberglass Blade Material', proc. EWEA Conference and Exhibition, 1994, pp. 720-726

[146] Joosse, P.A., van Delft, D.R.V., 'Has fatigue become a wearisome subject? Overview of 12 years of Materials Research in the Netherlands', proc. European Union Wind Energy Conference, 1996, pp. 902-906

[147] Joosse, P.A., van Delft, D.R.V., Nijssen, R.P.L., van Wingerde, A.M., 'Preliminary tests Part 1. Static and fatigue tests of UD and MD laminates', OPTIMAT report: OB_TC_R008, doc. no. 10095, 2003

[148] Joosse, P.A., van Delft, D.R.V., Kensche, Chr., et al., 'Cost effective large blade components by using carbon fibres', proc. AIAA/ASME Wind Energy Symposium, Reno, Nevada, 2002, pp. 9

[149] Joosse, P.A., van Delft, D.R.V., Kensche, Chr., et al., 'Cost effective large blade components by using carbon fibres', Journal of Solar Energy Engineering, Vol. 124, no. 4, 2002, pp. 412-418

K

[150] Kawai, M., Hachinohe, A., 'Two-stress level fatigue of unidirectional fiber-metal hybrid composite: GLARE 2', International Journal of Fatigue, Vol. 24, 2002, pp. 567-580

[151] Kensche, C.W., Seifert, H., 'Wind Turbine Rotor Blades Under Fatigue Loads', 4th European Conference on Composite Materials, 1990, pp. 173-180

[152] Kensche, C.W., 'Environmental effects on Gl-Ep rotor blades', proc. European Wind Energy Conference, 8-12 March, Lübeck-Travemünde, Germany, 1993

[153] Kensche, C.W., 'GFRP Fatigue Data for Certification', proc. EWEA Conference and Exhibition, 1994, pp. 738-742

[154] Kensche, C.W. (ed.), Andersen, S.I., Bach, P.W., Bonnee, W.J.A., Lilholt, H., Lystrup, A., Sys, W., 'Fatigue of materials and components for wind turbine rotor blades', European Commission, Brussels, Luxembourg, 1996, ISBN 92-827-4361-6

[155] Kensche, C. W., 'Fatigue of composites for wind turbines', proc. 3rd International Conference on Fatigue of Composites, 2004

[156] Kiasat, M. S., 'Curing Shrinkage and residual stresses in viscoelastic thermosetting resins and composites', Ph.D. thesis, Delft University of Technology, 2000

[157] Kim, H.C., Ebert, L.J., 'Fatigue life-limiting parameters in fibreglass composites', Journal of Materials Science, Vol. 14, 1979, pp. 2616-2624

[158] Kohout, J., Věchet, S., 'A new function for fatigue curves characterization and its multiple merits', International Journal of Fatigue, no. 23, 2001, pp. 175-183

[159] Konur, O., Matthews, F.L., 'Effects of the properties of the constituents on the fatigue performance of composites: a review', Composites, Vol. 20, no. 4, 1989, pp. 317-328

[160] Krasnikovs, Megnis, M., 'Fatigue damage accumulation in unidirectional composite (UD) under applied cycling tension load', proc. International Conference on Fracture 11, 2005

[161] Krause, O., 'Testing frequency for dynamic tests', OPTIMAT report: OB_TC_003_DLR, doc. no. 10061_001, December 2002

[162] Krause, O., 'Preliminary tests -2 (compression of UD specimens)', OPTIMAT report: OB_TC_N002, doc. no. 10051, 2002

[163] Krause, O., 'Preliminary test results on MD reference material (2nd), influence of gauge length', OPTIMAT report: OB_TC_R007, doc. no. 10055, 2002

[164] Krause, O., Kensche, C.W., Nijssen, R.P.L., et al., 'A Benchmark on lifetime prediction of composite materials under fatigue', proc. European Wind Energy Conference, 2003

[165] Krause, O., Philippidis, T.P., 'General Test Specification', OPTIMAT report: OB_TC_R015, doc. no. 10157, 2005

[166] Krause, O., 'Test specification for load spectra tests', OPTIMAT report: OB_TG1_R021, doc. no. 10280_001, 2005

[167] Kujawski, D., Ellyin F., 'Rate/frequency-dependent behaviour of fibreglass/epoxy laminates in tensile and cyclic loading', Composites, Vol. 26, 1995, pp. 719-723

L

[168] Lange, Clifford H., 'Probabilistic Fatigue Methodology and Wind Turbine Reliability', Sandia National Laboratory report: SAND96-1246, 1996

[169] Langer, B.F., 'Fatigue Failure From Stress Cycles of Varying Amplitude', Journal of Applied Mechanics, Vol. 59, 1937, pp. A160-A162

[170] Lee, L.J., Fu, K.E., Yang, J.N., 'Prediction of fatigue damage and life for composite laminates under service loading spectra', Composites Science and Technology, no. 56, 1996, pp. 635-648

[171] Lee, J., Harris, B., Almond, D.P., et al., 'Fibre composite fatigue-life determination', Composites part A, Vol. 28A, 1997, pp. 5-15

[172] Lee, C.S., Hwang, W., Park, H.C., Han, K.S., 'Failure of carbon/epoxy composite tubes under combined axial and torsional loading 1. Experimental results and prediction of biaxial strength by the use of neural networks', Composites Science and Technology 59, 1999, 1779-1788

173   van Leeuwen, H., van Delft, D., Heijdra, J., et al., 'Comparing Fatigue Strength From Full Scale Blade Tests With Coupon-Based Predictions', Journal of Solar Energy Engineering, Vol. 124, no. 4, 2002, pp. 404-411

174   Lieberman, G.J., 'Tables for One-Sided Statistical Tolerance Limits', Industrial Quality Control, Vol. XIV, No. 10, April 1958

175   Little, R.E., 'Review of Statistical Analyses of Fatigue Life Data Using One-Sided Lower Statistical Tolerance Limits', Statistical Analysis of Fatigue Data, ASTM STP 744, R.E. Little and J.C. Ekvall, Eds., American Society for Testing and Materials, 1981, pp. 3-23

176   Liu, C.C., 'A comparison between the Weibull and Lognormal models used to analyse reliability data', PhD thesis, University of Nottingham, August 1997

M

177   Maekawa, Z., Hamada, H., Lee, K., et al., 'Reliability Evaluation of mechanical properties of AS4/PEEK composites', Composites, Vol. 25, no. 1, 1994, pp. 37-45

178   Madsen, P.H.(ed.), 'Recommended Practices for Wind Turbine Testing and Evaluation - 3: Fatigue Loads', expert group study submitted to Executive Committee of the International Energy Ageny Programme for Research and Development on Wind Energy Conversion Systems, 2nd edition, 1990

179   Mandell, J. F., 'Fatigue Crack Growth in Fiber Reinforced Plastics', Polymer Composites, January 1981, proc. 34th Annual Conference SPI Reinforced Plastics/Composites Institute, 1981, pp. 22-28

180   Mandell, J.F., 'Fatigue behavior of short fiber composite materials', Ch. 7 in 'Fatigue of composite materials', K.L. Reifsnider (Ed.), Elsevier, 1991

181   Mandell, J. F., Reed, R.M., Samborsky, D.D., 'Fatigue of Fiberglass Wind Turbine Blade Materials', Sandia National Laboratory contractor report: SAND92-7005, Montana State University, August 1992

182   Mandell, J.F., Creed, R.F., Jr., , Pan, Qiong R. et al., 'Fatigue of fiberglass generic materials and substructures', SED-Vol. 15, Wind energy, 1994, pp. 7

183   Mandell, J.F., Samborsky, D.D., 'DOE/MSU composite material fatigue database: test methods, materials, and analysis', Sandia National Laboratory report: SAND97-3002, 1997

184   Mandell, J.F., Samborsky, D.D., Combs, D.W., et al., 'Fatigue of Composite Material Beam Elements Representative of Wind Turbine Blade Substructure', NREL/SR-500-24379, 1998

185   Mandell, J.F., Samborsky, D.D., Sutherland, H.J., 'Effects of materials Parameters and Design Details on the Fatigue of Composite Materials for Wind Turbine Blades', proc. European Wind Energy Conference, 1999

186   Mandell, J.F., Samborsky, D.D., Li, M., Orozco, R. 'Selection of fiberglass matrix resins for increased toughness and environmental resistance in wind turbine blades', proc. AIAA/ASME Wind Energy Symposium, paper no. AIAA-2002-0057, Reno, NV, 2000

[187]   Mandell, J.F., Samborsky, D.D., Cairns, D.S., 'Fatigue of composite materials and substructures for wind turbine blades', Sandia National Laboratory report: SAND2002-0771, March 2002

[188]   Mandell, J.F., D. Samborsky, D.D., Wahl, N.K., Sutherland, H.J., 'Testing and Analysis of Low Cost Composite Materials Under Spectrum Loading and High Cycle Fatigue Conditions', proc. 14th International Conference on Composite Materials, paper no. 1811, San Diego, CA, 2003

[189]   Mandell J.F., Samborsky D.D., 'DOE/MSU Composite Material Fatigue Database: test methods, materials, and analysis', Sandia National Laboratories/Montana State University, Sandia National Laboratory report: SAND97-3002, (online via www.sandia.gov/wind, database regularly updated, last update March 2, 2006)

[190]   Marco, S.M., Starkey, W.L., 'A Concept of Fatigue Damage', Transactions of theAmerican Society of Mechanical Engineers, 1954, pp. 627-632

[191]   Marissen, R., 'Two main challenges for the future composites technlogy, costs reduction and strength prediction', proc. 10th European Conference on Composite Materials, 2002

[192]   Martin, J.F., Topper, T.H., Sinclair, G.M., 'Computer Based Simulation of Cyclic Stress-Strain Behavior with Applications to Fatigue', Materials Research and Standards, Vol. 11., no 2, February 1971, pp.23-28, 50

[193]   MIL, 'Polymer matrix composites – Department of defense handbook MIL-HDBK-17-1E working draft', Volume 1-Guidelines for characterization of structural materials, Chapter 8, U.S. Department of Defense, January 23rd, 1997

[194]   Matsuishi, M., Endo, T., 'Fatigue of Metals Subjected to Varying Stress – Fatigue Lives under Random Loading', preliminary proceedings of the Kyushu District Meeting, Japan Society of Mechanical Engineers, March 1968, pp. 37-40

[195]   Matsuishi, M. Master's Thesis, personal communication, 2002

[196]   Megnis, M., Brøndsted, P., 'Preliminary tests -2 (compression of UD specimens)', OPTIMAT report: OB_TG3_R002, doc. no. 10047, 2002

[197]   Megnis, M., Brøndsted, P., Mikkelsen, L.P., 'Damage evolution in laminated composite materials', Materialeopførsel og skadesanalyse. Dansk Metallurgisk Selskabs vintermøde, Kolding, 7-9 Jan 2004. Somers, M.A.J. (eds.), 2004

[198]   Megnis M., Brøndsted, P., Rehman, S.A., et al., 'Characterization of Internal State Variable for fiber fracture in UD Composite', International Conference on Computational and Experimental Engineering Sciences 04, Madeira, Portugal, 26-29 July, 2004

[199]   Megnis, M., Brøndsted, P., 'Life Predictions of long fiber composites in extreme environmental conditions using damage evolution approach', Proceedings (CD-ROM) 11th European conference on composite materials, Rhodes, 2004

[200]   Milborrow, D., Garrad Hassan & Partners, BTM Consult AS, 'Wind Energy - the Facts', 1999

[201]   Milborrow, D., 'Wind Energy Technology, Status Review', Wind Engineering, Vol. 24, no. 2, 2000, pp. 65-72

[202]   Miller, H.R., Reifsnider, K.L., Stinchcomb, W.W., et al., 'Cumulative damage model for advanced composite materials', AFWAL-TR-84-4007, 1984

[203]   Miner, M. A. , 'Cumulative Damage in Fatigue', presented at meeting of Aviation Division, 1945 (june 16-17), pp. A159-A164

204   Mohamadian, H.P., Graham, I.J., 'Fatigue Testing of Unidirectional + Chopped Mat E-glass Fiber/Polyester and Vinylester for Wind Turbine Blades', proc. Windpower '90, 1990, pp. 112-117

205   Mouzakis, F., Morfiadakis, E., Dellaportas, P., 'Fatigue loading parameter identification of a wind turbine operating in complex terrain', Journal of Wind Engineering and Industrial Aerodynamics, no. 82, 1999, pp. 69-88

206   Müller, W., Michaeli, W., 'A statistical Fatigue Rule for Thermoset or thermoplastic Fibre-Reinforced Components under Dynamic Load', Annual technical conference of the Society of Plastics Engineers, 1990 (ANTEC '90), pp. 1320-1325

207   Murakami, Y. (ed.), 'The Rainflow Method in Fatigue – The Tatsuo Endo Memorial Volume', papers presented at Int. Symposium on Fatigue damage measurement ad evaluation under complex loadings, Fukuoka, Japan, July 25-26, 1991, Butterworth-Heinemann, Oxford, 1992, ISBN: 0 7506 0504 9

N

208   Naeem, M., 'Fatigue damage-compliance relationship for GRP', Composites, Vol. 20, no. 6, 1989, pp. 589-592

209   Natrella, M.G.'Experimental Statistics, National Bureau of Standards Handbook 91, U.S. Dept. of Commerce, Washington DC., August 1, 1963

210   NEN, 'Dutch Prestandard NVN 11400-0, Wind turbines -Part 0: Criteria for type-certification - Technical criteria', 1999

211   Nijssen, R.P.L., van Delft, D.R.V., 'Towards alternative fatigue lifetime prediction formulations for variable amplitude loading', proc. 33rd International Sampe Technical Conference, Seattle, Washington, 2001, pp. 11

212   Nijssen, R.P.L., van Delft, D.R.V., van Wingerde, A.M., 'Alternative Fatigue Life Prediction Formulations for Variable Amplitude Loading, proc. AIAA/ASME Wind Energy Symposium, Reno, Nevada, 2002, no. AIAA-2002-0022, pp. 10-18

213   Nijssen, R.P.L., van Delft, D.R.V., van Wingerde, A.M., 'Alternative Fatigue Lifetime Prediction Formulations for Variable-Amplitude Loading', Journal of Solar Energy Engineering, Vol. 124, no. 4, 2002, pp. 396-403

214   Nijssen, R.P.L., van Delft, D.R.V., 'Rainflow counting - history, description and limitations', WMC memorandum KCWMC-2002-30, 2002

215   Nijssen, R.P.L., 'Rainflow counting - Background for rainflow benchmark - memorandum on history, description, limitations', OPTIMAT report: OB_TG1_N001,doc. no. 10069, 2002

216   Nijssen, R.P.L. 'Tolerance bounds for fatigue data', memorandum WMC-2004-06, June 2004

217   Nijssen, R.P.L., van Delft, D.R.V., Joosse, P.A., et al., 'OPTIMAT BLADES -Optimal and reliable use of composite materials for wind turbines-', proc. 14th International Conference on Composite Materials (CD-ROM), San Diego, CA, July 14-18, 2003

218   Nijssen, R.P.L., Krause, O., Philippidis, T.P., 'Benchmark of lifetime prediction methodologies', OPTIMAT report: OB_TG1_R012, doc. no. 10218, September 2004

219 Nijssen, R.P.L., 'Tensile tests on standard OB specimens – effect of strain rate', OPTIMAT report: OB_TG1_R014, doc. no. 10221, October 2004

220 Nijssen, R.P.L., 'Optidat – database reference document', OPTIMAT report: OB_TC_R018, doc. no. 10224, 2006

221 Nijssen, R.P.L., 'OptiDAT – fatigue of wind turbine materials database', via www.kc-wmc.nl/optimat_blades

222 Nijssen, R.P.L., Samborsky, D.D., Mandell, J.F., et al., 'Fatigue and residual strength degradation in wind turbine rotor blade composites', proc. European Wind Energy Conference, 2004

223 Nijssen, R.P.L., Samborsky, D.D., Mandell, J.F., et al., 'Strength degradation and simple load spectrum tests on rotor blade composites', proc. AIAA/ASME Wind Energy Symposium, AIAA-2005-0197, 2005, pp. 28-38

224 Nijssen, R.P.L., Lekou, D., 'OptiDAT data summary -strength and life of standard OB specimens- ',OPTIMAT report: OB_TG1_R022 rev 001, doc. no 10284, 2006

225 Nijssen, R.P.L., van Wingerde, 'Residual Strength Tests -data and analysis-', OPTIMAT report: OB_TG5_R007, doc. no. 10285, 2006

226 Nijssen, R.P.L., Krause, O., Kensche, C., 'Block tests – results and analysis of simple spectrum tests', OPTIMAT report: OB_TG1_R025, doc. no. 10323, 2005

227 Nijssen, R.P.L., '(NEW) WISPER(X) load spectra – test results and analysis', OPTIMAT report: OB_TG1_R024, doc. no. 10313, 2006

228 NIST/SEMATECH e-Handbook of Statistical methods, online via: http://www.itl.nist.gov/div898/handbook/

229 NLR, Genesis 4 Fatigue (CD-Rom), 2001, available on request from: National Aerospace Laboratory NLR, Loads and Fatigue Department, P.O.Box 153, 8300 AD Emmeloord, the Netherlands, e-mail: genesis@nlr.nl, web site: www.nlr.nl

230 Nyman T., 'Composite fatigue design methodology: a simplified approach', Composite Structures, Vol. 35, pp. 183-194, 1996

231 Nyman, T., Ansell, H., Blom, A., 'Effects of truncation and elimination on composite fatigue life', Composite Structures, Vol. 48, 2000, pp. 275-286

O

232 O'Brien, T. K., 'An evaluation of stiffness reduction as a damage parameter and criterion for fatigue failure in composite materials', PhD-thesis, Virginia Polytechnic Institute and State University, 1978

233 Och, F., 'Fatigue testing of composite rotor blades', 51st meeting of the AGARD structures and Materials Panel , 1980, pp. 14

234 Och, F., 'Fatigue Strength', AGARD-AG-292, Helicopter Fatigue design guide, 1983, pp. 109-132

235 Okoli, O.I., Smith, G.F., 'The effect of strain rate and fibre content on the Poisson's ratio of glass/epoxy composites', Composite Structures, no. 48, 2000, pp. 157-161

236 Okoli, O.I., 'The effects of strain rate and failure modes on the failure energy of fibre reinforced composites', Composite Structures, no. 54, 2001, pp. 299-303

237 Oldyrev, P.P., 'Correlation between static and fatigue strength of reinforced plastics', Polymer Mechanics (translated from Mekhanika Polimerov), Vol. 9, no. 3, 1973

238 Owen, D.B., 'A Survey of Properties and Applications of the Noncentral t-Distribution', Technometrics, Vol. 10, no. 3, August 1968, pp. 445-478

239 Owen, D.B., 'Table of Factors for One-Sided Tolerance Limits for a Normal Distribution', Sandia Corporation Monograph SCR-13, April 1958

240 Owen, M.J., Howe, R.J. (1972), J. Phys. D: Appl. Phys., Vol. 5, pp.1637-1649

241 Owen, M.J., 'Fatigue damage in glass-fiber-reinforced plastics', In: Composite materials, Broutman (Ed.), Vol. 5 (Fracture and Fatigue), New York: Academic Press, 1974, pp. 313-340

242 Otani, N., Song, D.-Y, 'Fatigue life prediction of composites under two-stage loading', Journal of Materials Science, Vol. 32, 1997, pp. 755-760

P

243 Palmgren, Arvid, 'Die Lebensdauer von Kugellagern', Zeitschrift des Vereines Deutscher Ingenieure, Vol. 68, 1924, pp. 339-341

244 van Paepegem, W., Degrieck, J., 'Fatigue degradation modelling of plain woven glass/epoxy composites', Composites Part A, Vol. 32, 2001, pp. 1433-1441

245 van Paepegem, W., Degrieck, J., De Baets, P., 'Finite element approach for modelling fatigue damage in fibre-reinforced composite materials', Composites Part B, Vol. 32, 2001, pp. 575-588

246 van Paepegem, W., Degrieck, J., 'A new coupled approach of residual stiffness and strength for fatigue of fibre-reinforced composites', International Journal of Fatigue, Vol. 24, 2002, pp. 747-762

247 van Paepegem, W., Degrieck, J., 'Effects of Load Sequence and Block Loading on the Fatigue Response of Fibre-reinforced Composites', Mechanics of Advanced Materials and Structures, Vol. 9, no. 1, 2002, pp. 19-35

248 van Paepegem, W., Degrieck, J., 'Tensile and compressive damage coupling for fully-reversed bending fatigue of fibre-reinforced composites', Fatigue and Fracture of Engineerging Materials and Structures, Vol. 25, 2002, pp. 547-561

249 Petermann, J., Schulte, K., 'Strain based service time estimation for angle-ply laminates', Composites science and technology, Vol. 62, no. 7-8, 2002, pp. 1043-1050

250 Petermann, J., Plumtree, A., 'A unified fatigue failure criterion for unidirectional laminates', Composites Part A, Vol. 32, 2001, pp. 107-118

251 Phillips, E.P., 'Effects of Truncation of a Predominantly Compression Load Spectrum on the Life of a Notched Graphite/Epoxy Laminate', Fatigue of Fibrous Composite Materials, ASTM STP 723, American Society for Testing and Materials, 1981, pp. 197-212

252 Philippidis, T.P., Vassilopoulos, A.P., 'Fatigue of composite laminates under off-axis loading', International Journal of Fatigue, no. 21, 1999, pp. 253-262

253 Philippidis, T.P., Vassilopoulos, A.P., 'Fatigue design allowables for GRP laminates based on stiffness degradation measurements', Composites Science and Technology, Vol. 60, no. 15, 2000, pp. 2819-2828

254 Philippidis, T.P., Assimakopoulou, T.T., Passipoularidis, V., 'Preliminary test results on UD reference material (2nd round)', OPTIMAT report: OB_TC_R006, doc. no. 10049, 2002

255 Philippidis, T.P., Vassilopoulos, A.P., Assimakopoulou, T.T., et al., 'Preliminary tests, static axial and biaxial tests of UD and MD specimens', OPTIMAT report: OB_TC_R009, doc. no. 10101, 2003

256 Philippidis, T.P., Passipoularidis, V., 'Residual static strength of fibrous composites after fatigue: a literature survey', OPTIMAT report: OB_TG5_R001, 2003

257 Philippidis, T.P., Vassilopoulos, A.P., 'Fatigue strength of composites under variable plane stress', in 'Fatigue of Composites', Bryan Harris (Ed.), 2003, pp. 504-525, ISBN1-85573-608-X/0-8493-1767-3

258 Philippidis, T.P., Vassilopoulos, A.P., 'Life prediction methodology for GRFP laminates under spectrum loading', Composites: Part A, Vol. 35, 2004, pp. 657-666

259 Philippidis, T.P., Assimakopoulou, T.T., Antoniou, A.E., Passipoularidis, V.A., 'Residual strength tests on ISO ±45° coupons', OB_TG5_R008, July 2005

260 Philippidis, T.P., Assimakopoulou, T.T., Antoniou, A.E., Passipoularidis, V.A., 'Residual strength tests on standard OB coupons @ 90°', OB_TG5_R009, July 2005

261 Philippidis, T.P., Passipoularidis, V., 'Validated engineering model for residual strength prediction', OB_TG5_R013, 2006

262 Philippidis, T.P., Passipoularidis, V., Assimakopoulou, T.T., Antoniou, A.E., 'Variable Amplitude Cyclic Tests on Standard OB UD Coupon and ISO [±45]$_s$ performed at UP – Main Test Phases I & II', OB_TG2_R031, April 2006

263 Piggot, M.R., 'The effect of fibre waviness on the mechanical properties of unidirectional fibre composites: a review', Composites Science and Technology, Vol. 53, 1995, pp. 201-205

Q

264 Quarton, D.C., 'The Evolution of Wind Turbine Design Analysis - A Twenty Year Progress Review', Wind Energy, Vol. 1, 1998, pp. 5-24

R

265 Renius, K.Th., 'Last- und Fahrgeschwindigkeitskollektive als Dimensionierungsgrundlagen für die Fahrgetriebe von Ackerschleppern [Load and speed collectives for dimensioning of tractor travel drives]'. Fortschritt-Berichte VDI 1976, Series 1, No. 49, source: http://www.ltm.mw.tum.de/~spaeth/lit/ageng945.html

266 Reifsnider, K.L., 'Fatigue behavior of composite materials', International Journal of Fracture, Vol. 16, no. 6, 1980

267 Reifsnider, K.L., Stinchcomb, W.W., Henneke, E.G., et al., 'Fatigue damage-strength relationships in composite laminates', Vol. 1, 1983

268 Reifsnider, K.L., Schulte, K., Duke, J.C., 'Long-Term Fatigue Behavior of Composite Materials', Long-Term Behavior of Composites, ASTM STP 813, T.K. O'Brien, Ed., American Society for Testing and Materials, 1983, pp. 136-159

[269] Reifsnider, K.L., Case, S., Duthoit, J., 'The mechanics of composite strength evolution', Composites Science and Technology, Vol. 60, 2000, pp. 2539-2546

[270] Rijswijk, K., Joncas, S., Bersee, H.E.N., et al., 'Vacuum Infused Fiber-Reinforced Thermoplastic MW-Size Turbine Blades: A Cost-Effective Innovation?', proc. AIAA/ASME Wind Energy Symposium, Reno, Nevada, January 10-13, 2005

[271] Riziotis, V.A., Voutsinas, S.G., 'Fatigue loads on wind turbines of different control strategies operating in complex terrain', Journal of Wind Engineering and Industrial Aerodynamics, no. 85, 2000, pp. 211-240

[272] Ronold, K.O., Echtermeyer, A.T., 'Estimation of fatigue curves for design of composite laminates', Composites Part A, 27A, 1996, pp. 485-491

[273] Ryder, J.T., Walker, E.K., 'Ascertainment of the effect of compressive loading on the fatigue lifetime of graphite/epoxy laminates for structural applications', AFML-TR-76-241, 1976, pp. 273

S

[274] Saff, Charles R., 'Effect of Load Frequency and Lay-Up on Fatigue Life of Composites', Long-Term Behavior of Composites, ASTM STP 813, T.K. O'Brien, Ed., American Society for Testing and Materials, 1983, pp. 78-91

[275] Samborsky, D.D., Mandell, J.F., 'Fatigue resistant fiberglass laminates for wind turbine blades', published for Wind Energy 1996, ASME, 1996, pp. 46-51

[276] Samborsky, D.D., 'Fatigue of E-glass fiber reinforced composite materials and substructures', M.Sc. report, Montana State University, Bozeman, MT, December 1999

[277] Samborsky, D.D., 'Damage modeling of (0/90)n)s, (0/±45)s and (0/±45/90)s fiberglass composites - Part 1: Material behavior and properties of D155 laminates with a fiber volume fraction of 0.47', Montana State University, (draft version), 2002

[278] Schaff, J.R., Davidson, Barry B.D., 'Life Prediction Methodology for Composite Structures. Part I-Constant Amplitude and Two-Stress Level Fatigue', Journal of Composite Materials, Vol. 31, no. 2, 1997, pp. 128-157

[279] Schaff, J.R., Davidson, Barry B.D., 'Life Prediction Methodology for Composite Structures. Part II-Spectrum Fatigue', Journal of Composite Materials, Vol. 31, no. 2, 1997, pp. 158-181

[280] Schijve, J., 'The Accumulation of Fatigue Damage in Aircraft Materials and Structures', AGARDograph No. 157, 1972

[281] Schijve, J., The Significance of Flight-Simulation Fatigue Tests, Report LR-466, Delft University of Technology, Delft, the Netherlands, June 1985

[282] Schijve, J., 'Fatigue of aircraft materials and structures', Fatigue, Vol. 16, no. 1, 1994, pp. 21-32

[283] Schijve, J., 'Fatigue of Structures and Materials', Kluwer, June 2001, ISBN: 0792370139

[284] Schijve, J., 'Fatigue of materials and structures in the 20th century and the state of the art', International Journal of Fatigue, no. 25, 2003, pp. 679-702

[285] Schön, J., Blom, A., 'Fatigue life prediction and load cycle elimination during spectrum loading of composites', International Journal of Fatigue, Vol. 24, 2002, pp. 361-367

[286] Schön, J., Nyman, T., 'Spectrum fatigue of composite bolted joints', International Journal of Fatigue, Vol. 24, 2002, pp. 273-279

[287] Schulte, K., Nowack, H., Trautmann, H.-F., et al., 'Estimation of the durability of composite materials by means of stiffness reduction under variable loading conditions', 1st European Conference on Composite Materials, 1985, pp. 51-56

[288] Schütz, D. and J.J. Gerharz, Fatigue Strength of a Fibre-Reinforced Material, Composites, 8(4), 1977: 245-250

[289] Schütz, W., 'Standardized Stress-Time Histories - An Overview', Development of Fatigue Loading Spectra, ASTM STP 1006, J.M. Potter and R.T. Watanabe, Eds., American Society for Testing and Materials, Philadelphia, 1989, pp. 3-16

[290] Schütz, W., 'A history of fatigue', Engineering Fracture Mechanics, Vol. 54, no. 2, 1996, pp. 263-300

[291] Sendeckyj, G.P., 'Fitting Models to Composite Materials Fatigue Data', proc. Test Methods and design allowables for fibrous composites, 1979, pp. 245-260

[292] Sendeckyj, G.P., 'Constant life diagrams - a historical review', International Journal of Fatigue, Vol. 23, 2001, pp. 347-353

[293] Shah Khan, M.Z., Simpson, G., Gellert, E.P., 'Resistance of glass-fibre reinforced polymer composites to increasing compressive strain rates and loading rates', Composites, Part A, no. 31, 2000, pp. 57-67

[294] Shan, Y., Liao, K., 'Environmental fatigue behavior and life prediction of unidirectional glass-carbon/epoxy hybrid composites', International Journal of Fatigue, 24, 2002, pp. 847-859

[295] Shen, C.L., Wirsching, P.H., Cashman, G.T., 'Design Curve to Characterize Fatigue Strength', Journal of Engineering Materials and Technology, Vol. 118, October 1996, pp. 535-541

[296] Sims, D.F., Brogdon, V.H., 'Fatigue Behavior of Composites Under Different Loading Modes', ASTM STP 636, 1977, pp. 185-205

[297] Slaughter, W.S., Fleck, N.A., 'Compressive fatigue of fibre composites', J. Mech. Phys. Solids, Vol. 41, no. 8, 1993, pp. 1265-1284

[298] Smissaert, D.C.H., van Beek, C., 'Handleiding BFG', BFG versie 1.39, januari 2001 (in Dutch), WMC-group, 2001

[299] Socie, D. F., 'Fatigue-life Prediction Using Local Stress-Strain Concepts', Experimental Mechanics, Vol. 7, no. 2, 1977, pp. 50-56

[300] Socie, D., Shifflet, G., Berns, H.,'A field recording system with applications to fatigue analysis', International Journal of Fatigue, Vol. 1, No. 2, April 1979, pp. 103-111

[301] Soden, P.D., Hinton, M.J., Kaddour, A.S., 'A comparison of the predictive capabilities of current failure theories for composite laminates', Composites Science and Technology, Vol. 58, 1998, pp. 1225-1254

[302] Soden, P.D., Hinton, M.J., Kaddour, A.S., 'Biaxial test results for strength and deformation of a range of E-glass and carbon fibre reinforced composites laminates: failure exercise benchmark data', Composites Science and Technology 62, 2002, pp. 1489-1514

[303] Söker, H., Kaufeld, N., 'NEW WISPER - Creating a New Load Sequence From Modern Wind Turbine Data', OPTIMAT Publication: OB_TG1_P004, doc. no. 10229, DEWEK

2004 (Deutsche Windenergie Konferenz), 7th German Wind Energy Conference, October 20-21, Wilhelmshaven, Germany, 2004

[304] Solin, J., 'Methods for comparing fatigue lives for spectrum loading', International Journal of Fatigue, Vol. 12, no. 1, 1990, pp. 35-42

[305] Song, D.-Y., Otani, N., 'Fatigue life prediction of cross-ply composite laminates', Materials Science and Engineering A, Vol. 238, no. 2, 1997, pp. 329-335

[306] Song, D.-Y., Otani, N. 'Approximate estimation of fatigue strength of polymer matrix composites by material properties', Materials Science and Engineering A, Vol. 254, no. 1-2, 1998, pp. 200-206

[307] Spindel, J.E. and Haibach, E., 'Some Considerations in the Statistical Determination of the Shape of S-N Curves', Statistical Analysis of Fatigue Data, ASTM STP 744, R.E. Little and J.C. Ekvall, Eds., American Society for Testing and Materials, 1981, pp. 89-113

[308] Subramanian, S., Reifsnider, K.L., Stinchcomb, W.W., 'A cumulative damage model to predict the fatigue life of composite laminates including the effect of a fibre-matrix interphase', International Journal of Fatigue, Vol. 17, no. 5, 1995, pp. 343-351

[309] Sutherland, H.J., 'Analytical Framework for the LIFE2 Computer Code', 1989

[310] Sutherland, H.J., 'Frequency domain analysis of the fatige loads on typical wind turbine blades', Journal of Solar Energy Engineering, Transactions of ASME, Vol. 118, 1996, pp. 204

[311] Sutherland, H.J., 'On the fatigue analysis of wind turbines', Sandia National Laboratories report: SAND99-0089, Albuquerque, New Mexico, June 1999, pp. 10-12

[312] Sutherland, H.J., 'A summary of the fatigue properties of wind turbine materials', Journal of Wind Energy, Vol 3., 2000, pp. 1-34

[313] Sutherland, H.J., 'The development of confidence limits for fatigue strength data', proc. ASME/AIAA Wind Energy Symposium, 2000, 413-423

[314] Sutherland, H.J., Mandell, J.F., 'The Effect of Mean Stress on Damage Predictions for Spectral Loading of Fiberglass Composite Coupons', proc. Special Topic Conference 'Creating Torque from Wind', Delft, 19-21 April, 2004, pp. 546-555

[315] Sutherland, H.J., Mandell, J.F., 'Optimized Goodman diagram for the analysis of fiberglass composites used in wind turbine blades', proc. ASME/AIAA Wind Energy Symposium, paper AIAA-2005-0196, 2005

[316] Svensson, T., 'Prediction uncertainties at variable amplitude fatigue', International Journal of Fatigue, Vol. 19, no. 1, 1997, pp. s295-s302

T

[317] Talreja, R., 'Estimation of Weibull Parameters for Composite material Strength and Fatigue Life Data', ASTM STP 723, 1981, pp. 291-311

[318] Talreja, R., 'Fatigue of composite materials: damage mechanisms and fatigue life diagrams', proc. R. soc. Lond, Vol. A 378, 1981, pp. 461-475

[319] Talreja, R., 'Fatigue of Composite Materials', PhD Thesis, Afdelingen for Faststofmekanik, Danmarks tekniske Højskole, Lyngby, 1985

[320] Talreja, R., 'A Conceptual Framework for the Interpretation of Fatigue Damage Mechanisms in Composite Materials', Journal of Composites Technology and Research, Vol. 7, 1985, pp. 25-29

[321] Tang, R., Guo, Y.-J., Weitsman, Y.J., 'An appropriate stiffness degradation parameter to monitor fatigue damage evolution in composites', International Journal of Fatigue, Vol. 26, 2004

[322] TPI composites, 'Parametric study for large wind turbine blades-windPACT Blade System Design Studies', Sandia National Laboratory report: SAND2002-2519, 2002

[323] Trantina, G.G., 'Statistical Fatigue Failure Analysis', Journal of Testing and Evaluation, Vol. 9, no. 1, 1981, pp. 44-49

U

V

[324] Varna, J., Joffe, R., Talreja, R., 'A synergistic damage-mechanics analysis of transverse cracking in $[\pm\theta/90_4]_s$ laminates', Composites Science and Technology, Vol. 61, 2001, pp. 657-665

[325] Varna, J., Krasnikovs, A., Kumar, R.S., Talreja, R., 'A synergistic damage mechanics approach to viscoelastic response of cracked cross-ply laminates', International Journal of Damage Mechanics, Vol. 13, 2004, pp. 301-334

[326] Veldkamp, H.F., 'Chances in wind energy: A probabilistic approach to wind turbine fatigue design', Ph.D. Thesis, Delft University of Technology, 2006

W

[327] Waddoups, M.E., Committee on life prediction methodologies for composite materials, 'Life Prediction Methodologies for Composite Materials', National Materials Advisory Board National Research Council Washington, DC 20418, 1991

[328] Wahl, N.K., 'Spectrum fatigue lifetime and residual strength for fiberglass laminates', Ph.D. Thesis, Montana State University, Bozeman, 2001

[329] Wahl, N.K., Samborsky, D.D., Mandell, J.F., Cairns, D., 'Spectrum fatigue lifetime and residual strength for fiberglass laminates in tension', proc. ASME/AIAA Wind Energy Symposium, Reno, Nevada, January 2001

[330] Wahl, N.K., Samborsky, D.D., 'Effects of modeling assumptions on the accuracy of spectrum fatigue lifetime predictions for a fiberglass laminate', proc. ASME/AIAA Wind Energy Symposium, Reno, Nevada, paper no. AIAA-2002-0023, January 2002

[331] Wang, S.S., Chim, E.S.-M., 'Fatigue damage and degradation in random short-fibre SMC composite', Journal of Composite Materials, Vol. 17, March 1983, pp. 114-134

[332] Wang, A.S.D., Chou, P.C., Alper, J., 'Effects of Proof Test on the Strength and Fatigue Life of a Unidirectional Composite', Fatigue of Fibrous Composite Materials, ASTM STP 723, 1981, pp. 116-132

333 Wedel-Heinen, J., Tadich, J.K., Brokopf, C., et al. 'Implementation of OPTIMAT in Technical Standards', OPTIMAT report: OB_TG6_R002, doc. no. 10317, 2006

334 Weibull, W., 'A Statistical Distribution Function of Wide Applicability', J.Applied Mechanics, no. 18, 1951, pp. 293-297

335 Weibull, W. 'Fatigue Testing and Analysis of Results', Pergamon Press, New York, 1961

336 Welsh, J.S., Adams, D.F., 'An experimental investigation of the biaxial strength of IM6/3501-6 carbon/epoxy cross-ply laminates using cruciform specimens', Composites: Part A, 33, 2002, pp. 829-839

337 Wetzel, R.M., 'A Method of Fatigue Damage Analysis', Ford Motor Company Metallurgy Department Scientific Research Staff publication, September, 1971

338 Wevers, M., Verpoest, I., Aernoudt, E., et al., 'Fatigue damage development in carbon fiber reinforced epoxy composites: correlation between the stiffness degradation and the growth of different damage types', proc. 6th International Conference on Composite Materials and 2nd European Conference on Composite Materials, 1987, pp. 4.114-4.128

339 Wharmby, A.W., Ellyin, F., Wolodko, J.D., 'Observations on damage development in fibre reinforced polymer laminates under cyclic loading', International Journal of Fatigue, Vol. 25, 2003, pp. 437-446

340 Whitney, J.M., Pagano, N.J., Pipes, R.B., 'Design and Fabrication of Tubular Specimens for Composite Characterization', Composite Materials: Testing and Design (2nd Conference), ASTM STP 497, 1971, pp. 52-67

341 Whitney, J.M., 'Fatigue Characterization of Composite Materials', Fatigue of Fibrous Composite Materials, ASTM STP 723, 1981, pp. 133-151

342 Whitney, J.M., 'Use of the Lognormal Distribution for Characterizing Composite Materials', ASTM STP 787, 1982, pp. 483-497

343 Whitney, J.M., 'A residual strength degradation Model for competing failure modes', Long-Term Behavior of Composites, ASTM STP 813, T.K. O'Brien, Ed., 1983, pp. 225-245

344 Whitworth, H.A., 'A stiffness degradation model for composite laminates under fatigue loading', Composite Structures, Vol. 40, no. 2, 1998, pp. 95-101

345 Whitworth, H.A., 'Evaluation of the residual strength degradation in composite laminates under fatigue loading', Composite Structures, Vol. 48, 2000, pp. 261-264

346 Williams, C.R., Lee, Y.-L., Rilly, J.T., 'A practical method for statistical analysis of strain-life-fatigue data', International Journal of Fatigue, article in press (accepted 1 August 2003), 2003

347 de Winkel, G.D., Rojer, C., 'Focus 5', rotor blade structural analysis software, WMC report: WMC-2005-15/02, 2005

348 van Wingerde, A.M., van Delft, D.R.V., 'Notes on 2D stress patterns in flat, biaxially loaded, plate tests', OPTIMAT report: OB_TG2_N000, rev. 0, September 2002

349 van Wingerde, A.M., van Delft, D.R.V., Janssen, L.G.J., et al., 'OPTIMAT BLADES: Results and Perspectives', proc. European Wind Energy Conference, Athens, February 27th-March 2nd, 2006

350 van Wingerde, 'Presentation of results of WP10, WP11', OPTIMAT report: OB_TG4_O005, doc. no.: 10306 (TG4 Meeting, CRES, September 15th), 2005

351   van Wingerde, A.M., 'Minutes of 7th Technical Committee Meeting', OB minutes OB_TC_M007, doc. no. 10193 (TC meeting at University of Patras, June 2nd, 2004), 2004

352   Wisnom, M.R., 'Size effects in the testing of fibre-composite materials', Composites Science and Technology, Vol. 59, 1999, pp. 1937-1957

353   WMC (Knowledge Centre Wind turbine Materials and Constructions) Web site, www.kc-wmc.nl

X

Y

354   Yang, J.N., 'Fatigue and Residual Strength Degradation for Graphite/Epoxy Composites Under Tension-Compression Cyclic Loadings', Journal of Composite Materials, Vol. 12, 1978, pp. 19-39

355   Yang, J.N., Jones, D.L., 'Statistical fatigue of Graphite/Epoxy Angle-Ply Laminates in Shear', Journal of Composite Materials, Vol. 12, no. 4, 1978, pp. 371-389

356   Yang, J.N., Jones, D.L., 'Effect of Load Sequence on the Statistical Fatigue of Composites', AIAA Journal, Vol. 18, no. 12, 1980, pp. 1525-1531

357   Yang, J.N., Jones, D.L., 'Load Sequence Effects on the Fatigue of Unnotched Composite Materials', Fatigue of Fibrous Composite Materials, ASTM STP 723, 1981, pp. 213-232

358   Yang, J.N., Du, Shanyi, 'An Exploratory Study Into the Fatigue of Composites Under Spectrum Loading', Journal of Composite Materials, Vol. 17, 1983, pp. 511-526

359   Yang, J.N., Jones, D.L., 'Load Sequence Effects on Graphite/Epoxy $[\pm 35]_{2s}$ Laminates', Long-Term Behavior of Composites, ASTM STP 813, T.K. O'Brien, Ed., 1983, pp. 246-262

360   Yao, W.X., Himmel, N., 'A new cumulative fatigue damage model for fibre-reinforced plastics', Composites science and technology, no. 60, 2000, pp. 59-64

Z

361   Zhang, Z., Hartwig, G., 'Relation of damping and fatigue damage of unidirectional fibre composites', International Journal of Fatigue, Vol. 24, 2002, pp. 713-718